THE
PHYSICAL REVIEW
A Journal of Experimental and Theoretical Physics Established by E. L. Nichols in 1893
VOL. 55, NO. 10 MAY 15, 1939 SECOND SERIES

Gamma-Ray Ion Currents in Air at High Pressures and High Gradients at High and Low Temperatures[1]

JAMES W. BROXON AND GEORGE T. MERIDETH
University of Colorado, Boulder, Colorado
(Received February 15, 1939)

Weak gamma-ray ionization currents in air at pressures extending to 193 atmospheres were measured at −76°C and at 96°C. The same apparatus and procedure were used as in the room-temperature measurements, with collecting field intensities from 0.17 to 4500 volts/cm. Under all conditions the current increased with increase of field intensity. At −76°C the current corresponding to a particular intense collecting field has a pronounced maximum in the neighborhood of 60 atmospheres. No such maxima were observed at 96°C. As at room temperature, negative ion currents were found to be greater than the corresponding positives. In their dependence upon temperature and gas density the observed temperature coefficients of the currents agree well with the predictions both of the initial recombination theory and of the columnar theory in the region of low collecting field intensities. They further display the dependence upon field intensity required by the columnar theory. Adopting the assumptions of Gross relative to dependence of the ordinary ion coefficients upon temperature, we modified the coefficient in Zanstra's equation (based upon the Jaffé columnar theory) to correspond to the new temperatures. The result was fairly satisfactory. The theoretical saturation currents so obtained display unexpected relations to gas density. At −76°C the theoretical saturation current has a pronounced maximum at about 90 atmospheres, with some indication of a minimum at about 150 atmospheres. At 96°C the theoretical saturation current values increase very rapidly with increase of pressure at the high pressures.

OUR ion current measurements at high and low temperatures were made according to the same procedure and with the same ionization chamber, Fig. 1, and other equipment employed in our measurements at room temperature.[2] Only the central radium source, S_1, was employed in these measurements, however.

For the low temperature measurements the container B, shown in broken lines, was detached and the chamber submerged in a mixture of alcohol and chopped solid carbon dioxide to a depth which brought the surface of the cooling mixture about 6 cm beneath the bottom of the copper water cooler (heater in this instance) W. The cooling mixture was contained in a large Dewar flask about 44 cm deep. Over the top of this and surrounding the neck of the chamber was placed a thick layer of rock wool. Water from the city mains was kept running to and from W through tubes of glass and rubber several meters long. The resistance of the parallel water columns was about 8 megohms. With all other parts of the apparatus insulated from earth, the water system provided no electrical difficulties.

For the high temperature measurements the container B was attached as shown in Fig. 1. The entire chamber was then inverted from the position shown and B was nearly filled with S.A.E. 60 motor oil. A heating circuit insulated from the chamber was then immersed in the oil

[1] A preliminary report of these measurements was given at the 1937 Denver meeting of the American Physical Society; Phys. Rev. **52**, 252 (1937).
[2] J. W. Broxon and G. T. Merideth, Phys. Rev. **54**, 1 (1938).

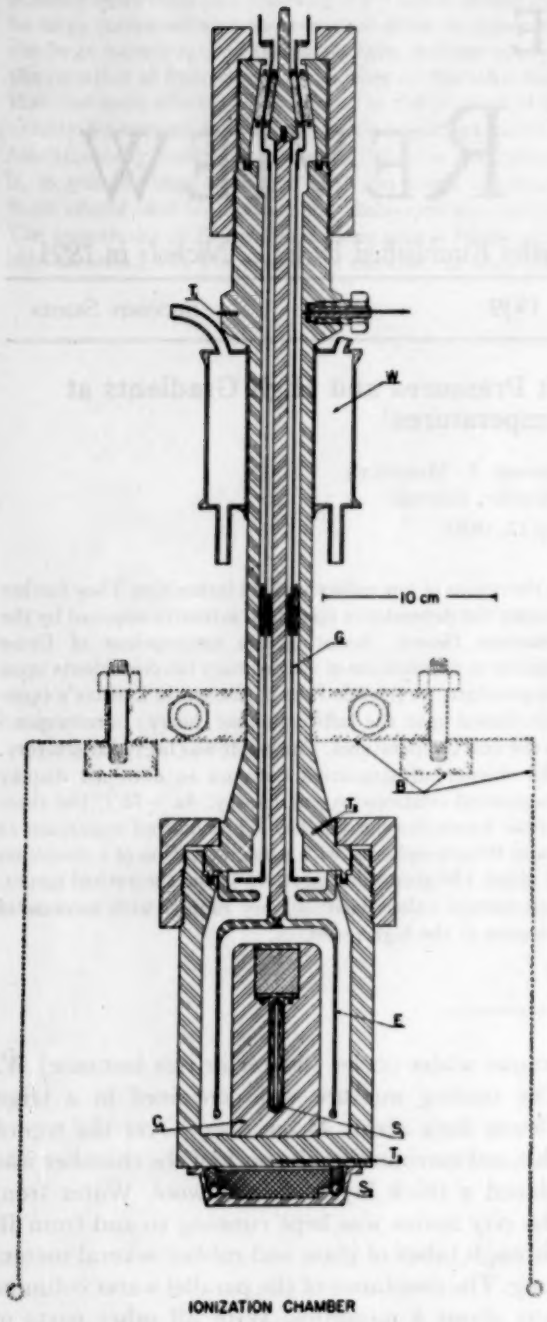

FIG. 1. High pressure ionization chamber.

near the bottom of the container. A motor-driven stirrer provided circulation of the oil. A cover was placed over B and B was entirely surrounded by a thick layer of rock wool.

For both high and low temperature measurements, junctions of three copper-constantan thermocouples were inserted into the chamber walls at T_1, T_2 and T_3. These junctions were electrically insulated from the chamber by very thin-walled glass tubes, and were inserted to the extreme inward ends of the cavities. The constant-temperature junctions were kept immersed in a water-ice mixture in a small Dewar flask. The thermal e.m.f.'s were measured with a Leeds and Northrup type K millivolt potentiometer. The thermocouples were especially calibrated at temperatures in the neighborhood of those used in this investigation.

After cooling the ionization chamber in the carbon dioxide for 25 hours, ion current measurements were begun and continued during the ensuing 5 days. During the observation period the average temperature indicated at the thermojunction T_1 was 18.5°C, that at T_2, −74.7°C, and that at T_3, −77.2°C. The extreme ranges of fluctuations during the observation period were 3.7°C for T_2 and 1°C for T_3. The temperature of the air in the ionization chamber was taken to be −76°C.

Before the high temperature observations were begun the oil bath was heated for 51 hours. Measurements then continued during the succeeding 7 days. The average temperatures observed were 19.7°C at T_1, 91.7°C at T_2, and 98.6°C at T_3. The extreme ranges of temperature variation were 2.5°C at T_2 and 2.1°C at T_3. The temperature of the air in the chamber was taken to be 96°C.

By making high pressure current measurements at room temperature on the identical samples of air used for the low and the high temperature measurements, it was found that the ionization in both these cases was slightly higher than under corresponding conditions obtaining during the extensive measurements[2] with the central source at 28°C. In view of this situation, all currents measured at −76°C and at 96°C were reduced 2 percent to make them correspond with the 28°C measurements. All high and low temperature currents hereinafter recorded or designated in diagrams are values which have been so reduced below measured values in order that the values at the three temperatures may correspond to the same radiation intensity. Because the air was thoroughly aged before admission to the chamber in all cases, it is supposed

that the chamber, itself, may have been variously contaminated on these occasions as the result of rather numerous dismantlings and cleanings. The high and low temperature readings were made during March, April and early May, 1937, and the 28°C readings during late May, 1937. The radium sources were sealed in June, 1934. No correction was applied for the change in volume of the ionization chamber with temperature since it did not vary as much as 0.5 percent from that at room temperature; the same constant was used throughout for converting rate of collection of charge to ions per cc per sec. Application of a correction would decrease our experimental values of β slightly.

In reporting our measurements[2] at room temperature we mentioned the fact that particularly large and apparently erratic conductivity of the air was occasionally observed at the high pressures and gradients. The unusually large current values were not observed with 1000 volts or less over-all P.D. impressed across the set-up. With twice this, however, corresponding to gradients of about 1770 volts/cm mean value in the chamber, large currents were sometimes observed, and the likelihood of such observations appeared to increase rapidly with the field intensity at the high pressures. There appeared to be no difficulty in ascertaining when such conditions had ceased, and the current corresponding to a particular pressure, temperature and gradient was taken, as before, to be the average of four independent values measured under what were considered to be satisfactorily stable conditions.

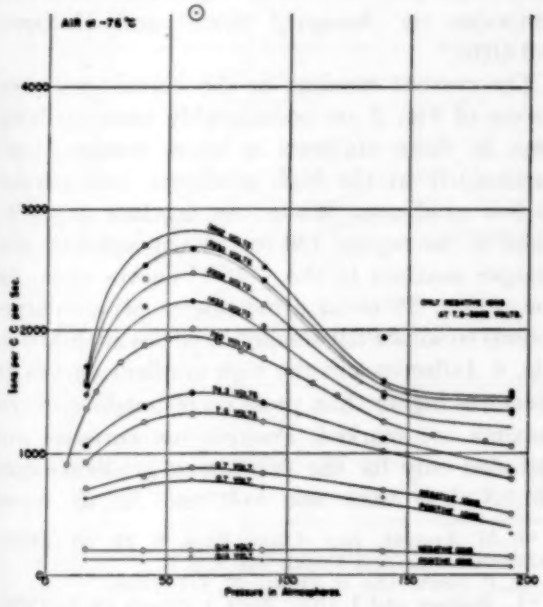

FIG. 2. Pressure ionization current curves at −76°C.

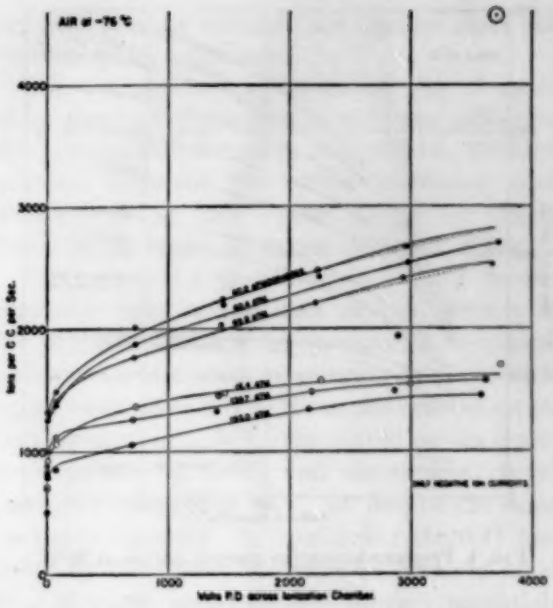

FIG. 3. Voltage ionization current curves at −76°C.

Our experimental values (less 2 percent) for the ionization currents produced by the central-source gamma-radiation in air at −76°C are shown in Figs. 2 and 3. In both diagrams ions per cc per sec. are plotted as ordinates. In Fig. 3 the voltages impressed between the ionization chamber electrodes are plotted as abscissae, and each curve corresponds to a definite designated pressure. In Fig. 2 the pressures in atmospheres are plotted as abscissae, and each curve corresponds to a definite over-all impressed P.D. The average P.D. across the ionization chamber is designated in each instance; the slight effects due to the variation in P.D. across the chamber resulting from variations in the dielectric coefficient of the air with pressure are neglected.

Possibly due in part to the higher gas densities involved and in part to the lack of leisure imposed by the experimental conditions, we do not appear to have minimized the effects of the temporary instabilities at −76°C so well as at 28°C. In this connection we are inclined to suspect there may well be a relation between our

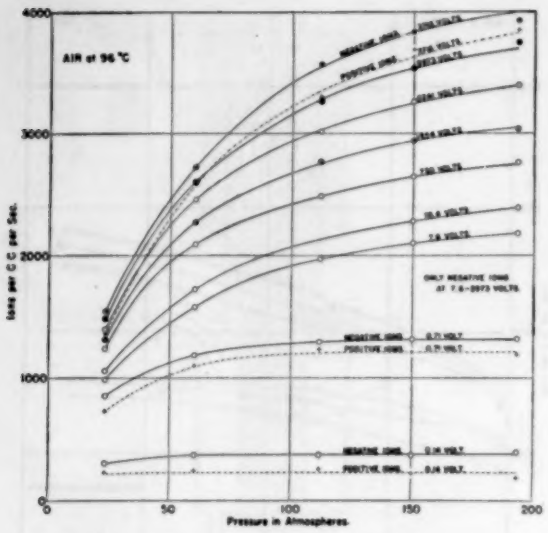

FIG. 4. Pressure ionization current curves at 96°C.

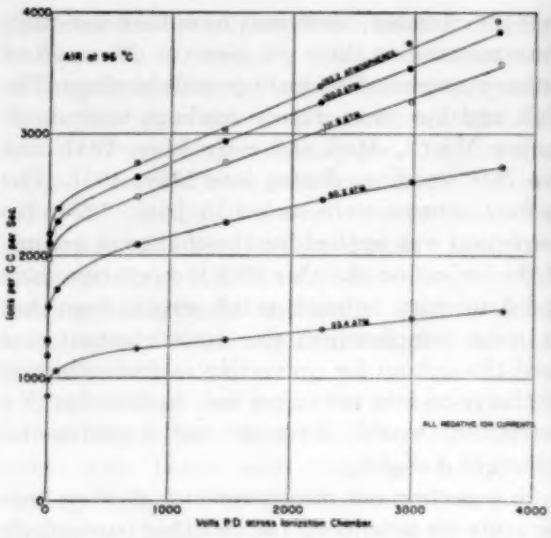

FIG. 5. Voltage ionization current curves at 96°C.

high current observations and those observed by Clay and van Kleef[3] in several gases, but not air, at high pressures and gradients.

Although conditions were not quite ideal, we have a good deal of confidence in the essential correctness of the curves drawn in Figs. 2 and 3. As in the case of the readings at room temperature, in drawing these curves we considered each curve of each of the two families in its relation to the others of its family, and also in relation to the curves of the other family. Also, curves obtained from earlier sets of observations, not given here, agree very well with these except at the two highest gradients and pressures where we were less successful in eliminating instabilities than in the present instance. The full-line curves of Figs. 2 and 3 were drawn from inspection without the benefit of mathematical treatment. The dotted segments were inserted later as a consequence of analysis by the Jaffé-Zanstra theory as will be explained hereinafter.

In Fig. 4 are shown the ionization currents (less 2 percent) measured at 96°C plotted as ordinates against the pressures as abscissae. In Fig. 5 are the currents for 96°C plotted against the potential differences impressed across the ionization chamber. The procedure adopted in plotting the points and drawing the curves was the same as at the other temperatures.

[3] J. Clay and G. van Kleef, Koninklijke Akademie Van Wetenschappen Te Amsterdam **40**, No. 8 (1937).

Figure 6 shows the ionization currents corresponding to each of the three temperatures, −76°C, 28°C and 96°C, and to most of the gradients employed, plotted as ordinates against the specific gravity of the air relative to air at NTP. The gradient designated in each instance was obtained by dividing the mean ionization chamber P.D. by 0.82 cm, which procedure was justified earlier.[2] The specific gravities corresponding to the several pressures and temperatures were obtained from experimental determinations by Amagat,[4] Koch[5] and Holborn and Otto.[6]

The current maxima in the current-pressure curves of Fig. 2 are considerably more striking than in those obtained at room temperature[7] particularly at the high gradients, and persist to low gradients. While the maxima at 28°C occur in the region, 120 to 150 atmospheres, the sharper maxima in the −76°C curves occur in the region, 55 to 65 atmospheres, which corresponds to somewhat smaller densities as shown in Fig. 6. Inflections in the high gradient curves at pressures higher than those corresponding to the maxima are marked. Positive ion currents are included only for the two lowest gradients employed, less than one volt/cm. As at room

[4] E.-H. Amagat, Ann. Chim. Phys. 6, **29**, 68 (1893); *International Critical Tables*, Vol. 3, p. 9.
[5] P. P. Koch, Ann. d. Physik **27**, 311 (1908).
[6] L. Holborn and J. Otto, Zeits. f. Physik **33**, 1 (1925).
[7] Shown in Fig. 3 of reference 2.

temperature, the positive ion currents are seen to be less than the negatives.

The curves of Fig. 3 show that at −76°C as at 28°C saturation was not attained even at the highest gradients employed. Strikingly, the curves representing the relation between current and collecting field intensity at the two highest pressures more nearly resemble that at the lowest pressure than those at the three intermediate pressures. These latter three comprise a group showing a considerably more rapid increase of current with collecting field at the high intensities.

As might have been expected from the trend displayed at the lower temperatures, the 96°C curves of Fig. 4 display no maxima within the pressure range of the investigation. Particularly at the high gradients, the current is seen still to increase considerably with pressure at the highest pressures which correspond, of course, to lower densities than do equal pressures at the lower temperatures. In this instance positive ion currents are included for the strongest collecting field as well as for the very weak fields. Again the positive ion currents are smaller than the corresponding negatives.

The voltage-current curves of Fig. 5 again show the current increasing with the collecting field throughout the range of gradients, the high gradient slope of the curves increasing with pressure. As at 28°C, these curves are nearly linear in the region of strong collecting fields.

The curves of Fig. 6 bring out clearly the dependence upon temperature and air density of the negative ion currents measured with typical collection field intensities selected from the wide range we employed. The continuous curves represent currents at −76°C, the dotted curves represent currents at 28°C, and the broken curves represent currents at 96°C, all due to the same radiation intensity. In considering the 0.17 and 0.87 volt/cm curves, it should be borne in mind that in these measurements contact potentials were not artificially eliminated. Consideration of the positive and negative ion current curves corresponding to the lowest gradients in Figs. 2 and 4 in relation to those for ions of the two signs at higher gradients at these and room temperatures

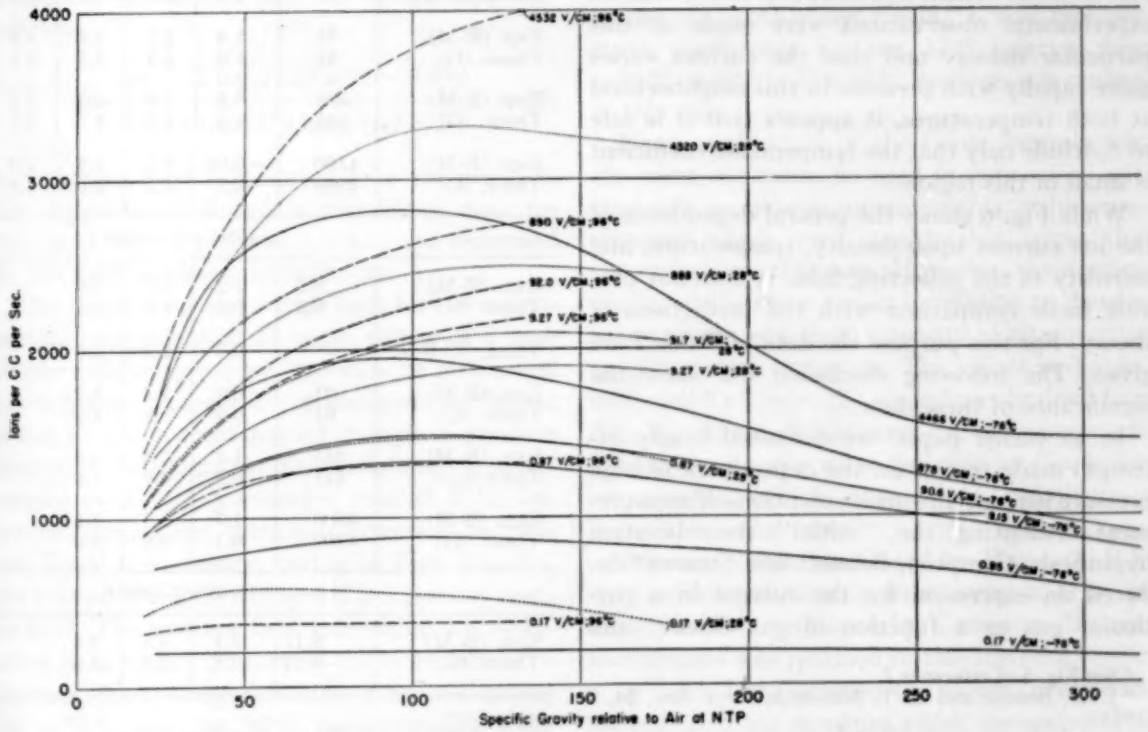

FIG. 6. Density ionization current curves at −76°C, 28°C and 96°C.

provides strong indication that contact potentials must have been very small in the case of the −76°C and the 96°C measurements. Unfortunately, only negative ion currents were measured with the central source at 28°C. However, it has been shown[8] that contact potentials certainly were present in the case of the ring-source measurements at room temperature, and in such a sense as to augment the negative ion currents with the weakest collecting field. While a comparison of the negative ion current in this case with the lowest curve in Fig. 3 of reference 2 indicates that the contact potential effective in the case of the central-source measurements at room temperature must have been considerably less, nevertheless it appears not unlikely that contact potential may account for the positions of the lowest curves for 28°C in Fig. 6 relative to those corresponding to these gradients at the other two temperatures. If the positions of the lowest gradient, room-temperature curves are ruled irregular on this account, then no negative temperature coefficient is indicated except at the highest gradients in the neighborhood of $\sigma=35$, where the 28°C and the −76°C highest gradient curves cross. When, however, it is noted that no experimental observations were made at this particular density and that the current varies quite rapidly with pressure in this neighborhood at both temperatures, it appears that it is safe to conclude only that the temperature coefficient is small in this region.

While Fig. 6 shows the general dependence of the ion current upon density, temperature, and intensity of the collecting field, it does not provide facile comparison with the predictions of theory. For this purpose the data of Table I are given. The following discussion will show the significance of these data.

In an earlier paper[9] we discussed briefly attempts made to explain the dependence of high pressure ion currents upon conditions of measurement. Adopting the "initial" recombination hypothesis, Compton, Bennett and Stearns[10] deduced an expression for the current in a particular gas as a function of gas density and temperature. According to their theory, there is no dependence upon the collecting field intensity within very wide limits. In this connection it may be noted that the strongest field we used at −76°C was about one-fourth as great as the critical field specified by their theory at that temperature. As the temperature coefficient, $\beta=(1/i)(di/dt)$, they derived the expression

$$\beta=\frac{A^2\sigma^2/T^2}{1+A^2\sigma^2/T^2}=\frac{1}{T(1+T^2/A^2\sigma^2)}, \qquad (1)$$

where σ represents the density and T the absolute temperature. To fit Broxon's cosmic-ray data for air, they chose $A=7.1$. Adopting the "columnar" recombination theory of Jaffé,[11] Gross[12] derived an expression for the current in a particular gas as a function of the three variables, pressure (or

TABLE I. *Values of the temperature coefficient β.*

METHOD	E IN V/CM	σ=30	σ=80	σ=130	σ=170
		($10^3\beta$) at $T=249°K$			
Exp. (B-M)	9.2	1.8	2.8	3.5	4.0
Theor. (G)	9.2	1.4	3.1	4.1	4.6
Theor. (C-B-S)	—	1.7	3.4	3.7	3.8
Exp. (B-M)	91	1.6	2.7	3.4	3.8
Theor. (G)	91	1.0	2.5	3.5	4.1
Exp. (B-M)	885	0.8	1.8	2.7	3.5
Theor. (G)	885	0.6	1.8	2.7	3.3
Exp. (B-M)	4500	−0.04	1.1	1.8	2.9
Theor. (G)	4500	0.3	1.2	2.0	2.5
		($10^3\beta$) at $T=335°K$			
Exp. (B-M)	9.2	1.2	1.7	2.0	
Theor. (G)	9.2	0.6	1.6	2.2	
Theor. (C-B-S)	—	0.9	2.2	2.6	
Exp. (B-M)	91	0.9	1.3	1.9	
Theor. (G)	91	0.5	1.3	1.9	
Exp. (B-M)	885	1.2	0.8	1.4	
Theor.(G)	885	0.3	0.9	1.4	
Exp. (B-M)	4500	1.7	1.3	2.8	
Theor. (G)	4500	0.2	0.6	1.0	
		($10^3\beta$) at $T=285°K$			
Exp. (B-M)	0.17	3.1	3.5	3.5	
Theor. (G)	0.17	1.4	2.9	3.8	

[8] See Fig. 5 of reference 2.
[9] J. W. Broxon and G. T. Merideth, Phys. Rev. **54**, 9 (1938).
[10] A. H. Compton, R. D. Bennett and J. C. Stearns, Phys. Rev. **39**, 873 (1932).
[11] G. Jaffé, Ann. d. Physik 4 **42**, 303 (1913).
[12] B. Gross, Zeits. f. Physik **78**, 271 (1932); **80**, 125 (1933).

density), temperature, and intensity of the collecting field. According to this theory, the current obtained under a particular set of conditions depends upon the corresponding values of the ordinary coefficients, namely, α, the coefficient of recombination, D, the coefficient of diffusion, and u, the mobility, and upon certain column parameters, N_0, the specific ionization or number of ions per unit length of a column, and $\langle b \sin \phi \rangle_{Av}$ the mean value of the product of b (which is a constant proportional to the initial radius of a column) and the sine of the angle between the direction of the column and that of the impressed collecting field. Gross apparently considered the density of a gas at constant temperature to be proportional to the pressure. He made assumptions regarding the coefficients which, if we use σ, the specific gravity of the gas relative to air at NTP, in place of the pressure, amounted to setting $\alpha=k_1/(\sigma T)$, $D=k_2T/\sigma$, $u=k_3/\sigma$, $N_0=k_4\sigma$, and $\langle b \sin \phi \rangle_{Av}=k_5/\sigma$ for all densities, temperatures and collecting field intensities, where the k's are constants and T is the absolute temperature. On the basis of these assumptions, indicated by meager experimental evidence, he derived for the temperature coefficient,

$$\beta=\frac{c_2\sigma}{T^3}\,\frac{2\log_{10}(c_3T\sigma/E)-0.434}{1+(c_2\sigma/T^2)\log_{10}(c_3T\sigma/E)}, \qquad (2)$$

in which we have substituted σ for the pressure. To approximate Broxon's cosmic-ray data for air, he chose $c_2=573$ and $c_3=4.1$, and expressed E, the field intensity, in volts/cm.

Our measurements provide only for the experimental determination of mean values of β over rather wide temperature intervals. As mentioned hereinbefore, changes in the dielectric coefficient of the air which accompanied changes in pressure produced variations in the collecting field intensity even with a constant over-all P.D. impressed across the system. Correction for this was found unnecessary, and as in Figs. 2 and 4, the curves of Fig. 6 correspond to constant over-all P.D. The average field intensities are designated in this case. Because of the large difference between the average densities of the air during the -76°C and the 96°C measurements, even these average intensities differ in the two cases by a little more than one percent. By ignoring this difference in the calculation of values of β from the experimental curves, values for the current measured with the same over-all P.D. have been regarded as corresponding to the same field intensity, namely, the average of the field intensities at the extremes of temperature. A mean experimental temperature coefficient for the interval was obtained by setting

$$\beta=\frac{2(i_2-i_1)}{(i_2+i_1)(T_2-T_1)}, \qquad (3)$$

in which i_1 and i_2 represent the currents measured with a certain collecting field intensity and gas density at absolute temperatures T_1 and T_2, respectively. This value was associated with the mean temperature of the interval, $T=(T_1+T_2)/2$, for the purpose of comparison with the theoretical values.

Experimental values obtained by us in this manner are indicated by Exp. (B-M) in Table I. Those listed under 249°K represent mean coefficients for the 104° interval from -76°C to 28°C, those listed under 335°K, for the 68° interval from 28°C to 96°C. The 0.17 volt/cm values are listed under $T=283$°K and represent mean coefficients for the 172° interval from -76°C to 96°C. The 28°C readings are omitted in this case.

Upon application of the Gross formula with the same constants he used in connection with Broxon's cosmic-ray measurements, values were obtained which were considerably larger than the experimental values. However, these values displayed the same trends in relation to density, temperature and field intensity. Consequently, an adjustment was made. The values in Table I indicated by Theor. (G) are values obtained from Eq. (2), after modification of one of its constants. We let $c_3=4.1$, the value assigned by Gross, but set $c_2=132$, which appears to constitute a reasonable adjustment.

Values in Table I indicated by Theor. (C-B-S) were calculated directly from formula (1). The same constant employed by Compton, Bennett and Stearns was retained in this instance.

In Table I are included the values corresponding only to a few densities which are regarded as representative of the range investigated. In

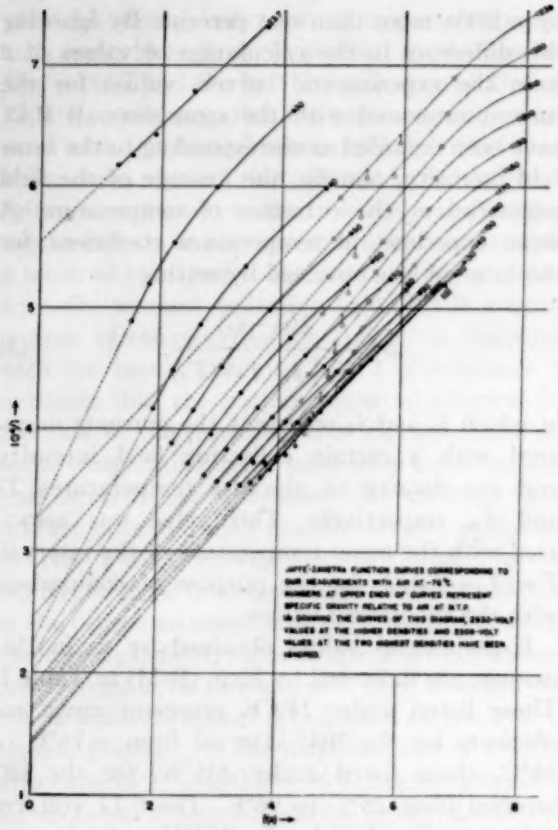

FIG. 7. Jaffé-Zanstra function curves corresponding to our gamma-ray ion current measurements in air at −76°C. Numbers at upper ends of curves represent specific gravity relative to air at NTP.

considering these it should be recalled that the ion current varies rapidly with gas density in the neighborhood of $\sigma=30$ whence values read from the experimental curves at this specific gravity may be a little less reliable than those corresponding to the higher densities.

The Gross theoretical values for the temperature coefficient are seen to agree with the experimental values in displaying an increase with increase of gas density, a decrease with increase of temperature, and a decrease with increase of collecting field intensity. Also, there is very good numerical agreement except at $T=335°K$ where the experimental values at $\sigma=30$ [13] and also at $E=4500$ v/cm are higher than the theoretical. In view of the experimental difficulties involved in the measurements and of the fact that the coefficient is a function of three variables, we are inclined to regard the agreement between experiment and theory as rather surprisingly good, and to consider that the agreement constitutes fair evidence in favor of the columnar theory.

The theoretical values according to Compton, Bennett and Stearns are seen to agree well with the experimental values in the range of field intensities, 9.2–91 volts/cm. This is interesting in connection with the fact that the constant of their formula was chosen by them to fit observations made with collecting field intensities in this same region. This theory, then, may be regarded as successful in predicting the dependence upon density and temperature, of the ionization current measured with a definite field intensity within the range of our observations, but does not show the dependence upon field intensity.

Zanstra's[14] adaptation of the Jaffé[11] columnar theory has been applied[15] to our observations at room temperature. Zanstra made the same assumptions as did Gross regarding the dependence upon gas density of the coefficients involved in the Jaffé theory. However, he did not consider the influence of temperature. In adapting Zanstra's equation[16]

$$1/i=1/I+(q/I)f(x) \qquad (4)$$

to the new temperatures, we have employed the assumptions made by Gross[12] hereinbefore discussed. With the value,[17] 10^{-5}, for the coefficient in $x=10^{-5}(E/\sigma)^2$ taken to be correct for air at 20°C, these assumptions yield $2.2(10)^{-5}$ for the coefficient at −76°C and $6.3(10)^{-6}$ at 96°C. The curves shown in Figs. 7 and 10 have been obtained by using these values for the Jaffé-Zanstra coefficient in the respective cases.

The values plotted in Fig. 7 were obtained from current values read from our experimental curves of Fig. 2 at pressures corresponding to the designated densities. These do not lie precisely

[13] Relative to the relation between experimental and theoretical values for β at low densities and high temperatures, it is interesting that J. W. Hake, University of Kansas Science Bulletin **20**, 183 (1932), found for air in a non-uniform field with $E=8.5$ volts/cm at the outer wall (radial mean $E=33$ volts/cm) at $\sigma=16$ for a 327°C range at a mean $T=370°A$, an experimental variation of natural ionization current yielding $\beta=0.7\times10^{-3}$. Both the Gross formula and the Compton-Bennett-Stearns formula agree in yielding values for $10^3\beta$ between 0.2 and 0.3 under these conditions.

[14] H. Zanstra, Physica **2**, 817 (1935).

[15] J. W. Broxon and G. T. Merideth, Phys. Rev. **54**, 605 (1938); also reference 9.

[16] See reference 9 for a detailed discussion of this equation.

[17] J. Clay and M. Kwieser, Physica **5**, 725 (1938), Fig. 8.

on straight lines as predicted by the theory. Moreover, further reasonable adjustment of the Jaffé-Zanstra coefficient does not appear to improve the situation appreciably. However, if it is assumed that we drew the 2930-volt curve of Fig. 2 a little too high over a considerable section of the range, and that the dotted line represents the actual state of affairs in this region, and that the 2209-volt curve was likewise too high in a very small region as shown by the short dotted line attached to that curve, then the Jaffé-Zanstra curves shown in Fig. 7 are correct for densities up to $\sigma = 230$. If this modification is made in Fig. 2, the curves of Fig. 3 must suffer the slight modifications shown by the dotted lines in that diagram, in the 2930-volt region. The experimental data can hardly be considered to rule out these modifications. In fact, the curves as modified by the dotted sections appear to fit into the ensemble of data rather better than do the full-line curves drawn arbitrarily previous to the theoretical considerations.

With these adjustments of the experimental curves, the corresponding values plotted in Fig. 7 are shifted as indicated by the arrows to the curves as drawn. These curves are very nearly straight lines over the regions corresponding to the three or four highest field intensities at nearly all densities. If our procedure is accepted, then the Jaffé-Zanstra curves are nearly or quite as satisfactory as those obtained with the same source of radiation at room temperature.

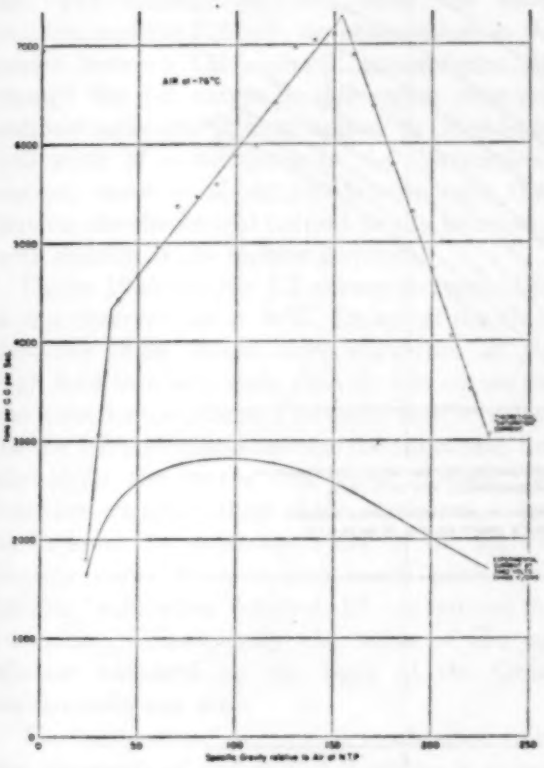

FIG. 8. "Saturation" current curve corresponding to our observations at −76°C, together with experimental curve obtained with strongest collecting field.

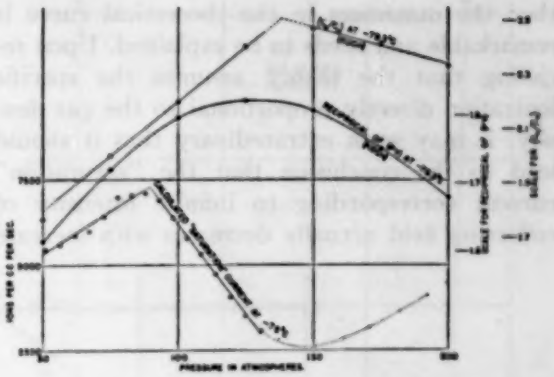

FIG. 9. Curves showing the dependence upon pressure of the theoretical "saturation" current at −76°C, and of the ratio of the specific heats and of the reciprocal of PV for air, both at −79.3°C. The latter two curves are obtained from data by Koch.

By extrapolating the curves as at room temperature, the intercepts and corresponding theoretical "saturation" current values were obtained. For the range from $\sigma = 23.7$ to 230, these are shown in Fig. 8 along with the currents measured at 4466 volts/cm. The most striking feature of the theoretical curve is its indication of a maximum for the "saturation" current, as well as for the experimental currents, the former occurring at a considerably greater density than the latter. It is not to be supposed that an exceedingly sharp maximum is indicated; the straight-line sections are drawn as best representing conditions over considerable regions on either side of the maximum. As at room temperatures, the "saturation" current curve lies everywhere above the highest experimental curve. However, the low-density portion, if extrapolated, would not have a positive intercept on the current axis as was true of the room-temperature curves. Apparently new characteristics would enter in the very low density region.

If the Jaffé-Zanstra theory is regarded as applicable at all in this low-temperature region,

then the maximum in the theoretical curve is remarkable and needs to be explained. Upon recalling that the theory assumes the specific ionization directly proportional to the gas density, it may seem extraordinary that it should lead to the conclusion that the "saturation" current corresponding to infinite intensity of collecting field actually decreases with increase in gas density under any circumstances. However, the theory contains no commitment regarding the rate of production of columns by a particular penetrating radiation under various conditions. If any considerable change were to occur in the normal atomic or molecular conditions in a particular gas, it is perhaps conceivable that an attendant effect might occur at some

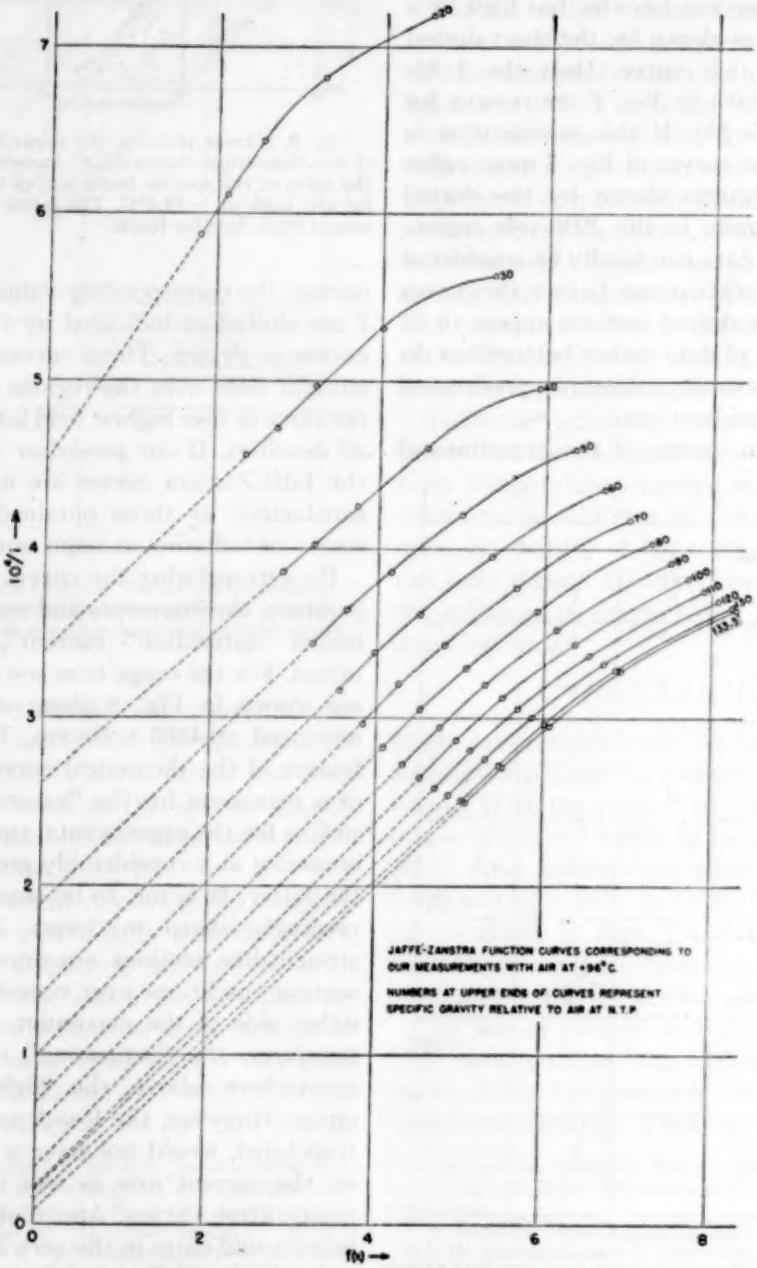

FIG. 10. Jaffé-Zanstra function curves corresponding to our gamma-ray ion current measurements in air at 96°C. Numbers at upper ends of curves represent specific gravity relative to air at NTP.

stage in the ionization process. To remind the reader that some appreciable variation in the condition of air may be supposed to accompany variation in pressure at this low temperature, Fig. 9 has been included. In this the upper curve shows that the ratio of the specific heat at constant pressure to that at constant volume passes through a maximum at about 140 atmospheres at −79.3°C, while the product of pressure by specific volume passes through a minimum at the same temperature at about 125 atmospheres, according to Koch.[5] The full-line section of the "saturation" current curve of Fig. 9 is the same as the corresponding section of the theoretical curve of Fig. 8, but pressure rather than specific gravity is designated by abscissae in Fig. 9. The dotted portion of this curve, corresponding to specific gravities greater than 230, was obtained from Jaffé-Zanstra curves (not shown) which were regarded as less satisfactory than those of Fig. 7. The "saturation" values were based entirely upon the 4466-volt/cm and the 1748-volt/cm observations in the region between 137 and 142 atmospheres, and upon the 4466-volt/cm and the 878-volt/cm observations in the region between 151 and 192 atmospheres. Although the J-Z curves in this region were not entirely satisfactory, they appear to provide an indication of a minimum in the "saturation" current curve at about 150 atmospheres, thus leaving the theoretical current finally increasing with density at the highest densities.

Figure 10 shows the J-Z curves corresponding to our observations at 96°C. Except at the lower densities these retain more curvature at the high field intensity ends than do the curves for the lower temperatures. The use of smaller values for the J-Z coefficients reduces the curvature, but also shifts the curves and tends to lower the intercept values. Values of the coefficient so low as to lower the intercept value of the highest density curve to zero and hence predict an infinite "saturation" current did not remove the curvature. Consequently the value of the coefficient obtained on the basis of the Gross assumptions was used.

The "saturation" current curve obtained from the intercepts of the 96°C J-Z curves is shown in Fig. 11 together with the experimental current curve for $E=4532$ volts/cm at this temperature.

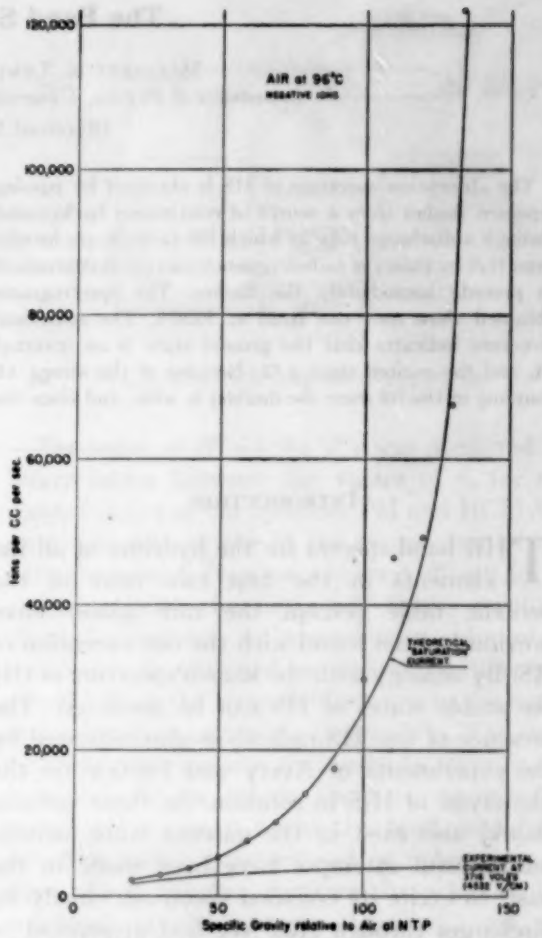

FIG. 11. "Saturation" current curve corresponding to our observations at 96°C, together with experimental curve obtained at strongest collecting field.

The very large scale of ordinates required by the theoretical curve makes the experimental one scarcely recognizable. As at −76°C, the theoretical curve at 96°C is striking. It is difficult to decide just what comment to make regarding it. Among other possibilities, it is possible that higher field intensities should be employed before application of the theory at this temperature, or that the columnar hypothesis does not so well represent conditions at high temperatures, or that a rapid change of ionizing efficiency accompanies change of density of the hot air at high pressures.

We acknowledge the assistance of Mr. Richard L. Burling in making some of the low potential observations while he was employed under the N.Y.A. The oil for the bath was graciously supplied by Miller's University Hill Service Station.

The Band Spectrum of HS

MARGARET N. LEWIS* AND JOHN U. WHITE
Department of Physics, University of California, Berkeley, California

(Received March 17, 1939)

The absorption spectrum of HS is obtained by passing repeated flashes from a source of continuous background through a discharge tube in which HS radicals are formed from H_2S by pulses of radiofrequency current synchronized to precede immediately the flashes. The spectrograms obtained show only one band at 3237A. The rotational structure indicates that the ground state is an inverted $^3\Pi$, and the excited state a $^2\Sigma$. Because of the strong $\Lambda\Sigma$ coupling in the $^3\Pi$ state the doublet is wide, and since the Boltzmann factor greatly favors $^3\Pi_{3/2}$, only the strongest branch, Q_2, from the $^3\Pi_{1/2}$ state is found. From $^3\Pi_{3/2}$ the $^QP_{21}$ and $^RQ_{21}$ satellite branches as well as P_1, Q_1 and R_1 are found. For the $^3\Pi$ ground state the best values of the constants obtained are $B_0''=9.47$; $D_0''=-0.001$ and $A=-378.6$ cm^{-1}. The constants for the excited $^2\Sigma$ state are $B_0'=8.30$; $D_0'=-0.00078$, and $\gamma=0.32$ cm^{-1}. The origin of the 0,0 band is at 30,659.1 cm^{-1}.

INTRODUCTION

THE band spectra for the hydrides of all the elements in the first two rows of the periodic table (except the rare gases) have previously been found with the one exception of HS. By analogy with the known spectrum of OH the stable states of HS can be predicted. The presence of free HS radicals is also indicated by the experiments of Avery and Forbes[1] on the photolysis of H_2S in solution. As these radicals should also exist in the gaseous state, several unsuccessful attempts have been made in the past[2] to excite its emission spectrum, chiefly by discharges through H_2S. We first attempted to excite an emission spectrum of HS by collision of H_2S molecules with resonance excited mercury atoms. No bands caused by HS were found. The reason the spectrum has not been found must be either that the HS radicals react chemically before they radiate, or that their spectrum is masked by that of sulfur. It was found that these difficulties can be avoided by working in absorption using the method described by Oldenberg[3] for studying the OH absorption spectrum.

EXPERIMENTAL

H_2S was made by the reaction of HCl and FeS. The gas was dried with P_2O_5 and $CaCl_2$, and passed into a previously evacuated glass storage reservoir. From here it was flowed continuously during the exposure through the absorption tube and out through the pumps. The pressure was maintained at about 1 mm. The HS molecules were formed in the absorption tube by passing a short pulse of radiofrequency current between two large electrodes above and below the tube. The length of the optical path between the electrodes, where absorption by HS occurred, was 70 cm. As the discharge also formed sulfur vapor that would hide the HS absorption, this had to be removed by flushing the tube completely with H_2S between each flash of the exposure. The duration of the pulse of current was found to be important. Sulfur is chemically stable, and its concentration is proportional to the length of the pulse; HS is relatively short-lived, and its concentration rapidly approaches a limiting value. Thus there must be an optimum duration for the pulse that will produce as much HS as possible without concealing it with sulfur absorption. This was found to be of the order of a hundredth of a second. The mean lifetime of the HS radical must be at most as long as this.

Radiofrequency current was supplied from a power oscillator tube built by Sloan, Thornton and Jenkins.[4] Keying was accomplished by interrupting the d.c. power supply to the filament. The source of continuous background for absorption was the Lyman continuum of a low

* Sarah Berliner Research Fellow, American Association of University Women.

[1] W. H. Avery and G. S. Forbes, J. Am. Chem. Soc. **60**, 1005 (1938).

[2] W. H. Bair, Astrophys. J. **52**, 301 (1920); N. O. Stein, Astrophys. J. **77**, 270 (1933).

[3] O. Oldenberg, J. Chem. Phys. **3**, 266 (1935).

[4] D. H. Sloan, R. L. Thornton and F. A. Jenkins, Rev. Sci. Inst. **6**, 79 (1935).

pressure spark in a quartz capillary. This was used with a 1μf condenser and set off at the desired instant by breaking down a series spark gap with a tickler electrode activated by a Ford ignition coil. To get sufficient resolving power to observe the narrow, rather faint absorption band lines of HS it was necessary to use the new 21-foot, 30,000-line/in. aluminum grating now in the Paschen mounting. The source was bright enough to give a satisfactory exposure in 900 sparks or 5 hours with one spark every 20 seconds. As the position of the spectrum was unknown, a cylindrical lens could not be used to increase the speed of the grating.

The switches for the radiofrequency and source were mounted on two shafts driven by a synchronous motor at 300 and 3 r.p.m., respectively, with a 100 : 1 reduction gear between them. Each circuit had two switches in series, one on each shaft, so that each received a short impulse every 20 seconds. The timing was regulated by the angle between the switches for the two different circuits. On all the plates the time between the end of the discharge and the spark was kept less than a thousandth of a second. No optical shutter was needed to keep the emission spectrum out of the spectrograph, as no such spectrum is known. A schematic diagram of the apparatus is shown in Fig. 1.

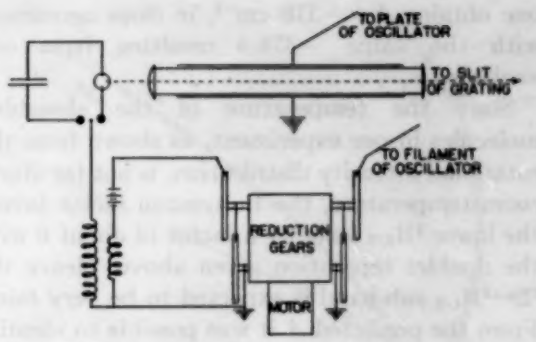

FIG. 1. Schematic diagram of apparatus.

ANALYSIS

The only new band appearing on the plates had its strongest head at 3237A, and was degraded toward long wave-lengths. The wide spacing of the lines made it at once recognizable as a hydride band. Since in homologous series of molecules the corresponding electronic frequencies generally decrease with increasing mass, it was suspected that the observed band was the HS band analogous to the OH band at 3064A. Accordingly, it should represent a transition from an inverted $^2\Pi$ normal state to an excited $^2\Sigma$ state.[5] With this assumption, it was possible to predict the constants of the two states fairly accurately, and the analysis of the band structure confirmed these predictions so well that there remained no doubt as to the correctness of this interpretation.

The value of $B''=h/8\pi^2 I''c$ was predicted by interpolation between the values of r_e for the ground states of the hydrides PH and HCl lying on either side of HS in the second row of the periodic table.[6] Thus we obtained $B''=9.43$, as compared with the value 9.47 finally resulting from the analysis. An approximate value of B' could then be obtained by finding the difference $B'-B''$ from the second differences in the easily recognizable branches P_1, Q_1 and $^QP_{21}$. The combination principle was then used to identify the branches R_1, in which there is considerable blending because it forms the head, and $^RQ_{21}$, which is partly superimposed on other stronger lines. Thus the five strongest branches of the sub-band $^2\Sigma\leftarrow{}^2\Pi_{3/2}$ were identified, and the results are represented in Table I as well as in the Fortrat diagram of Fig. 2.

Two features in which the structure apparently differed radically from that of the corresponding OH band were at first puzzling. The first was the apparent absence of the other sub-band $^2\Sigma\leftarrow{}^2\Pi_{1/2}$, and the second was the very large intensity of the satellite branches $^QP_{21}$ and $^RQ_{21}$ as compared to those in OH. However, it was soon apparent that both of these were a consequence of the much stronger spin-orbit coupling in HS. The coupling coefficient A, which determines the splitting between $^2\Pi_{3/2}$ and $^2\Pi_{1/2}$, can be estimated from the splitting in the normal ^3P state of the sulfur atom.[7] The separation $^3P_0-{}^3P_2$ in S is -572 cm$^{-1}=-3a/2$. Assuming the ratio $A/a=0.97$ as found in HCl^+,

[5] W. Jevons, *Report on Band-Spectra of Diatomic Molecules* (University Press, Cambridge, 1932), p. 164.

[6] R. Mecke, Zeits. f. Elektrochem. **36**, 581 (1930).

[7] R. S. Mulliken, Rev. Mod. Phys. **4**, 1 (1932); R. F. Bacher and S. Goudsmit, *Atomic Energy States* (McGraw-Hill, 1932), p. 397.

one obtains $A=-370$ cm^{-1}, in close agreement with the value -378.6 resulting from our analysis.

Since the temperature of the absorbing molecules in our experiment, as shown from the rotational intensity distribution, is not far above room temperature, the Boltzmann factor favors the lower $^2\Pi_{3/2}$ state by a factor of about 6 with the doublet separation given above. Hence the $^2\Sigma \leftarrow {}^2\Pi_{1/2}$ sub-band is expected to be very faint. From the predicted A it was possible to identify the head and a few lines of the strongest branch, Q_2, of this sub-band, as shown in Table I and Fig. 2.

The unexpectedly large intensities of the satellite branches is now a necessary consequence of the large value of A for HS. The parameter $Y=A/B$ appearing in the intensity formulas[8] is -40 in our case, compared to -7.5 for OH. The observed relative intensities of all of the branches are in good agreement with the theoretical equations for this value of Y.

Constants

The electron configurations of the two states here involved are $3p\sigma^2\ 3p\pi^3\ ^2\Pi$ and $3p\sigma\ 3p\pi^4\ ^2\Sigma$. Since these only differ in the λ value of one electron, the Π and Σ states must stand approximately in the relation of pure precession to each other.other.[9, 10] This simplifies the calculation of constants.

For the $^2\Sigma$ state, the rotational terms are given by

$$F(J)=B_v^*K(K+1)+D_v^*K^2(K+1)^2 +\tfrac{1}{2}\gamma[J(J+1)-K(K+1)-S(S+1)], \quad (1)$$

where

$$B_v^*=B_v-q$$

and

$$q=\frac{2B_v^2l(l+1)}{\nu(\Pi,\Sigma)}. \quad (2)$$

Calculation of q shows that within the experimental error it is negligible, so we may take $B_v^*=B_v$. The spin doubling constant γ may be evaluated directly from the separations $Q_1(K)-{}^qP_{21}(K)=\gamma(K+\frac{1}{2})$. We find $\gamma=0.32$, as compared to the value 0.41 calculated on the assumption of pure precession. That this value is reasonable is seen from comparison with those for the corresponding $^2\Sigma$ states in other hydrides.[10]

[8] E. L. Hill and J. H. Van Vleck, Phys. Rev. **32**, 250 (1928); L. T. Earls, Phys. Rev. **48**, 423 (1935).

[9] J. H. Van Vleck, Phys. Rev. **33**, 467 (1929).

[10] R. S. Mulliken and R. Christy, Phys. Rev. **38**, 87 (1931).

Table I. *Strongest branches of the band* $^2\Sigma \leftarrow {}^2\Pi$.

	R_1 Branch			Q_1 Branch			P_1 Branch		
J	λ	I		λ	I		λ	I	
1.5	3237.099	1*	30882.97	3240.666	7*	30849.00	3242.412	5	30832.37
2.5	3236.765	8*	30886.16	3242.002	5	30836.27	3245.480	6*	30803.23
3.5	3236.600	6*	30887.74	3243.548	5	30821.57	3248.791	5	30771.83
4.5	3236.600	6*	30887.74	3245.304	5	30804.90	3252.294	5	30738.69
5.5	3236.867	8*	30885.19	3247.284	4	30786.11	3256.010	4	30703.61
6.5	3237.269	1	30881.36	3249.465	4	30765.45	3259.928	4	30666.71
7.5	3237.994	1	30874.44	3251.871	5	30742.69	3264.080	3	30627.70
8.5	3238.916	0	30865.65	3254.513	3	30717.74	3268.432	1	30586.92
9.5	3240.092	0	30854.45						
	${}^RQ_{21}$ Branch			${}^QP_{21}$ Branch			Q_2 Branch		
J	λ	I		λ	I		λ	I	
0.5							3279.780	0	30481.10
1.5				3240.666	7*	30849.00	3279.258	4	30485.95
2.5	3236.867	8*	30885.19	3242.055	4	30835.77	3279.121	4*	30487.22
3.5	3236.600	8*	30886.16	3243.664	4	30820.47	3279.121	4*	30487.22
4.5	3236.600	8*	30886.16	3245.480	6*	30803.23	3279.413	5	30484.51
5.5	3237.099	1*	30882.97	3247.459	2	30784.45	3279.908	2	30479.91
6.5	3237.580	2	30878.39	3249.703	00	30763.20	3280.698	1	30472.57
7.5	3238.294	1	30871.58	3252.119	00	30740.35			

* Indicates blend with another identified line.

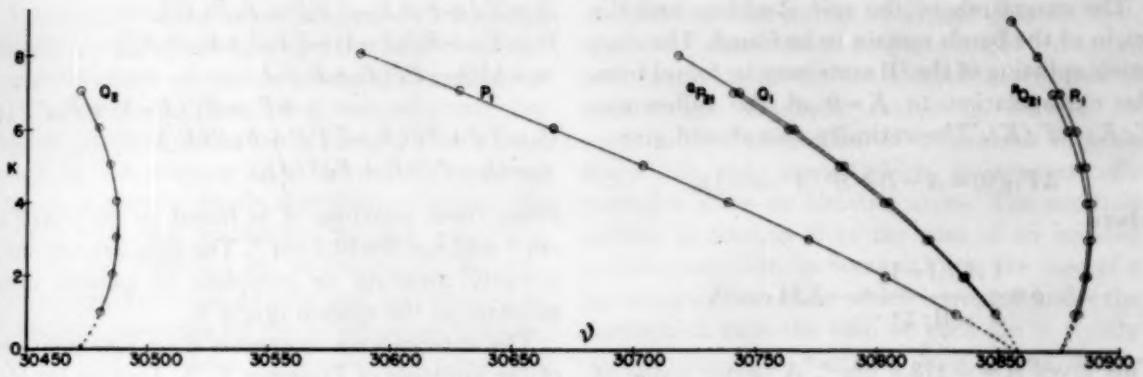

FIG. 2. Fortrat diagram.

To find the values of B_0' and D_0', we have treated the Δ_2F' values obtained from $R(J)-P(J)$ by the usual least-squares method. The results are $B_0'=8.30$ cm^{-1} and $D_0'=-0.00078$ cm^{-1}.

The determination of the constants of the $^2\Pi$ normal state presented more difficulty. This results chiefly from the fact that in the $^2\Sigma\leftarrow{}^2\Pi_{1/2}$ sub-band only one branch, Q_2, is observed, and this yields only one component, T_e, of the Λ-doublets. Since the doubling is largest in $^2\Pi_{1/2}$, it must be taken into account in evaluating the constants.

Since the value of A/B_v is large, it is possible to represent the rotational terms of this $^2\Pi$ state by the case a formula

$$F(J)=\text{Const.}+B_v^*J(J+1)+D_v^*J^2(J+1)^2, \quad (3)$$

where $B_v^*=B_v\pm B_v^2/A$ represents an effective value of B_v for the particular sub-state. The plus and minus signs refer to $^2\Pi_{3/2}$ and $^2\Pi_{1/2}$, respectively. To evaluate B_0^* and D_0^*, the terms T_{1e} were first obtained by subtracting the frequencies of the Q_1 and $^qP_{21}$ lines from the calculated $^2\Sigma$ terms, the terms T_{1d} by subtracting the P_1 lines, and the terms T_{2e} by subtracting the Q_2 lines. From the average of the T_{1e} and T_{1d} levels the constants obtained are $B_0^*(^2\Pi_{3/2})=9.231$ and $D_0^*=-0.00025$ and from the T_{2e} levels, $B_0^*(^2\Pi_{1/2})=9.567$ and $D_0^*=-0.0023$. The value of $B_0^*(^2\Pi_{1/2})$ is now subject to correction for the effect of the Λ-doubling.

For large negative values of A/B_v, expansion of the general energy expression for $^2\Pi$ states intermediate between case a and case b gives the following equations for the Λ-doubling:[10]

$$\Delta T_{1ed}=-(p/y^2+2q/y)(J-\tfrac{1}{2})(J+\tfrac{1}{2})(J+\tfrac{3}{2}), \quad (4)$$

$$\Delta T_{2ed}=p(J+\tfrac{1}{2}). \quad (5)$$

For the $^2\Pi_{3/2}$ state, Eq. (4) gives a very small doubling for low values of J. Experimentally it is only slightly greater than the error of measurement, but as far as can be determined it has the correct sign and magnitude, and follows the theoretical curve. For the $^2\Pi_{1/2}$ state we have no experimental value of ΔT_{2ed}, but it is necessary to know the magnitude of p to obtain the correct value of $B_0^*(^2\Pi_{1/2})$. Assuming pure precession, one obtains $p=0.46$, but this is probably somewhat too large, as in the analogous cases of OH and HCl^+. The observed value of $\gamma=0.32$ should be a better approximation to the true value of p. From this in Eq. (5), it is possible to calculate the average of the terms T_{2e} and T_{2d} in $^2\Pi_{1/2}$.

Treating these average values in the usual way, we then find $B_0^*(^2\Pi_{1/2})=9.60$ and $D_0^*(^2\Pi_{1/2})=-0.0025$. That this B_0^* is very nearly right is shown by calculating B_0 independently from $^2\Pi_{3/2}$ and $^2\Pi_{1/2}$ from the equation

$$B_v^*=B_v\pm B_v^2/A+\tfrac{1}{2}q\pm(p+2q)B_v/2A.$$

Taking the value $A=-378.6$ obtained below, we find $B_0=9.47$ and 9.37 from $^2\Pi_{3/2}$ and $^2\Pi_{1/2}$, respectively. The former of these is adopted as the correct value, since it involves experimental data only. The average value $D_0=-0.0014$ is probably correct only as to order of magnitude.

The magnitude of the spin doubling and the origin of the bands remain to be found. The electronic splitting of the $^2\Pi$ state may be found from the extrapolation to $K=0$ of the differences $T_2(K)-T_1(K)$. Theoretically this should give

$$\Delta T_{12}(0)=A-B+B^2/A-o-\tfrac{1}{2}p,$$

where

$$o=-\frac{1}{4}\frac{A^2l(l+1)}{\nu(\Pi,\Sigma)}=-2.34\ \text{cm}^{-1}.$$

This gives $A=-378.9$ cm^{-1}. A better value of A and of ν_0 may be found from the following considerations. If $T(J)=T_0+F(J)$ then

$$Q_1=T_0'+F_1'(J)-[T_0''+F_{1c}''(J)],$$
$$P_1=T_0'+F_1'(J-1)-[T_0''+F_{1d}''(J)],$$
$$\nu_0=\tfrac{1}{2}\{Q_1-F_1'(J)+F_{1c}''J+P_1-F_1'(J-1)+F_{1d}''J\},$$
$$Q_2=T_0'+F_2'(J)-[T_0''+F_{2c}''(J)],$$
$$\nu_0=Q_2-F_2'(J)+F_{2c}''(J).$$

From these relations A is found to be -378.6 cm^{-1} and $\nu_0=30659.1$ cm^{-1}. The data are not sufficiently accurate or complete to permit any estimate of the system origin ν_e.

The authors wish to express their appreciation of the kindness of Professor F. A. Jenkins for his suggestion of the problem and his help in carrying out the research.

MAY 15, 1939 PHYSICAL REVIEW VOLUME 55

On the Magnetic Scattering of Neutrons

O. HALPERN AND M. H. JOHNSON
New York University, University Heights, New York, New York

(Received December 3, 1938)

In this paper there is contained a full elaboration of two previously published short notes on the subject of magnetic scattering of neutrons together with a comprehensive treatment of certain sides of this problem which have already received some attention from other authors. After presenting the state of the problem in the introduction and discussing in detail our reasons for the choice of an interaction function between neutrons and electrons, and the nonmagnetic interaction between neutrons and nuclei, the various possible cases of coherent and incoherent scattering and depolarization phenomena are treated. Later applications to the theory of ferromagnetic scattering are kept in mind. The general expression for the cross section due to magnetic interaction is obtained and applied to various classes of phenomena (scattering by free, rigidly aligned, and coupled magnetic ions). The influence of the elastic form-factor is treated quantitatively with the aid of a simple model for the current distribution in the ion. Finally a series of performed or suggested experiments is discussed mainly from the point of view whether they will permit theoretical interpretation. Arrangements are described which will allow one to obtain a reliable value for the neutron's magnetic moment and also give insight into the magnetic constitution of the scatterer (ion or crystal) which will exceed the knowledge obtainable from macroscopic magnetic experiments.

I. INTRODUCTION

SOMETIME ago it was suggested[1] that a magnetic moment of the neutron should manifest itself in the scattering of slow neutrons from paramagnetic substances. The magnetic scattering should in some instances be several times as great as the total nuclear scattering if, for the neutron, a magnetic moment of two nuclear magnetons is assumed. This magnetic scattering could therefore be easily isolated by comparing the scattering cross section of the same atoms in different chemical combinations which show a varying magnetic susceptibility. It could also be separated from nuclear scattering by studying the angular distribution of the particles scattered from a single paramagnetic compound. This is due to the fact that magnetic scattering is, under practical conditions, strongly favored in the forward direction, whereas the nuclear scattering is isotropic. If the neutron moment is of the order of magnitude of a nuclear magneton the paramagnetic scattering provides a direct and simple method for its quantitative determination.

[1] O. Halpern and M. H. Johnson, Phys. Rev. **51**, 992; **52**, 52 (1937).

Our suggestions were subsequent to a letter by Bloch[2] in which it was pointed out that the interaction between an assumed magnetic moment of the neutron and that of a ferromagnetic ion should produce observable effects. Bloch supposed in his analysis that the scattering arose from a magnetic dipole distribution within the atom which was unaffected by the scattering process. He confined his attention to the production and detection of polarized neutron beams which are produced by the interference between nuclear and magnetic scattering in a saturated ferromagnetic medium. The appearance of polarization phenomena should make it possible to differentiate between nuclear and magnetic scattering and thereby to determine the magnetic moment of the neutron. Later Schwinger[3] gave a more detailed mathematical treatment of Bloch's idea. He, too, assumed that the scattering system remained unchanged during the scattering process and likewise limited himself to polarization effects in ferromagnetic bodies.

As pointed out in Section IV the physical basis of Bloch's ideas must be enlarged to include changes produced in the scattering system by the scattering process. Since the occurrence of such changes is the rule rather than the exception, results based on stricter assumptions have to be considerably modified. Especially in the case of scattering by a ferromagnetic material several new features appear which greatly increase the difficulty of determining the magnetic moment of the neutron from polarization experiments alone. Such uncertainties which are due to our ignorance of the exact state of the medium do not enter to any large degree into certain cases of paramagnetic scattering.

We intend to present in this paper a comprehensive treatment of the magnetic scattering of neutrons. The various phenomena are analyzed both in their dependence on the magnetic properties of the neutron and on the characteristics of the scatterer. The subject has been divided as follows: In Section II the possible forms of interaction between a neutron and an atomic electron are studied and their essential equivalence for low energy neutrons is demonstrated. In Section III we review the scattering of slow neutrons by nuclei whose spins are free; special emphasis is put on questions of coherence in preparation for the discussion of simultaneous nuclear and magnetic scattering. Section IV contains the deduction of a general formula describing the wave which is magnetically scattered from an isolated atom. The result is applied in Section V to the case of an isolated paramagnetic ion, in Section VI to the case of a ferromagnetic medium which is treated under the assumption that the spin of each ion is rigidly aligned along the magnetic axis of the microcrystals. Some other assumptions are also briefly discussed. Section VII deals with the nature of atomic form factors. Section VIII is devoted to a discussion of coupled scattering systems which are treated as a many-body problem. Here we also consider the influence of external forces acting on the nuclear spin and the modifications in the scattering of para- and ferromagnetic materials due to the forces between the spin vectors of the ions. The final section, IX, treats various experimental arrangements connected with the subject.

We begin with a few general remarks which will aid in fixing a suitable nomenclature. Let the beam of incident neutrons be represented by the wave function

$$\psi_{in}=(2\pi M_0/hk)^{\frac{1}{2}}\exp(i\mathbf{k}\cdot\mathbf{r})\chi_s\Phi_A. \quad (1.0)$$

Here $\mathbf{k}=2\pi\mathbf{P}/h$ is the propagation vector, $\mathbf{r}_n$ the position vector and $\mathbf{P}$ the momentum vector of the incident neutron with a mass M_0. χ_s describes the neutron spin state and Φ_A is the complete wave function for the initial state of the scattering system. We shall use the notation (quantity)$_{av}$ to denote integration and summation of the quantity in parenthesis over all coordinates of the scattering system. For example, the density, I, of incident neutrons is given by

$$I_{in}=(\psi_{in}^*\psi_{in})_{av}=(2\pi M_0/hk)|\chi_s|^2. \quad (1.01)$$

Denoting by $\mathbf{F}$ the differential operator $(h/4\pi M_0 i)\,\mathbf{grad}_n$ we have correspondingly for the flux of the incident neutrons

$$\mathbf{F}_{in}=(\psi_{in}^*\mathbf{F}\psi_{in}-\psi_{in}F\psi_{in}^*)=\mathbf{k}/k|\chi_s|^2. \quad (1.02)$$

Summation over the neutrons spin coordinate shall be denoted by $\sum_{spin}$. Furthermore, by use of

[2] F. Bloch, Phys. Rev. **50**, 259 (1936).
[3] J. Schwinger, Phys. Rev. **51**, 544 (1937).

normalized spin functions, $\sum_{spin}|\chi_s|^2=1$, we have $\sum_{spin}\mathbf{F}_{in}=\mathbf{k}/k$; this means that the incident flux is also normalized to unity. Correspondingly we have for the flux of the scattered wave

$$\mathbf{F}_{sc}=(\psi_{sc}^*\mathbf{F}\psi_{sc}-\psi_{sc}\mathbf{F}\psi_{sc}^*)_{av}. \quad (1.03)$$

The differential cross section $d\Phi$ for scattering into the solid angle subtended by the element of area dA which is perpendicular to $\mathbf{F}_{sc}$ is given by

$$d\Phi=F_{sc}dA. \quad (1.1)$$

Total scattering cross sections are obtained from (1.1) by summing over the neutron spin coordinate and integrating over all scattering angles.

In considering inelastic scattering the neutron density will be used in preference to the flux. This is done in consideration of the fact that all detectors of slow neutrons have cross sections which are inversely proportional to the velocity of the neutrons. The activity of a given detector depends, therefore, apart from geometrical factors, only on the volume density of the neutrons and not directly on the flux. This distinction becomes irrelevant for purely elastic scattering.

If the scattering system consists of two independent parts a and b and if multiple scattering can be neglected, the whole scattered wave

$$\psi_{sc}=\psi_a+\psi_b$$

can be subdivided by writing

$$\psi_a=\psi_a^1+\psi_a^2,$$
$$\psi_b=\psi_b^1+\psi_b^2.$$

In ψ_a^1 and ψ_b^1 the scattering system has remained in its initial state while in ψ_a^2 one of the parts has been changed by the scattering process. Obviously expressions like $(\psi_a^*\mathbf{F}\psi_b^2)_{av}$ vanish because of the orthogonality of the wave functions for the two different states of the scatterer. Substitution into (1.03) gives

$$\mathbf{F}_{sc}=\mathbf{F}_a+\mathbf{F}_b+\mathbf{F}_{ab}+\mathbf{F}_{ba} \quad (1.11)$$

with the simple abbreviations,

$$\mathbf{F}_a=(\psi_a^*\mathbf{F}\psi_a-\psi_a\mathbf{F}\psi_a^*)_{av}, \quad (1.111)$$

$$\mathbf{F}_b=(\psi_b^*\mathbf{F}\psi_b-\psi_b\mathbf{F}\psi_b^*)_{av}, \quad (1.112)$$

$$\mathbf{F}_{ab}=(\psi_a^{1*}\mathbf{F}\psi_b^1-\psi_b^1\mathbf{F}\psi_a^{1*})_{av}, \quad (1.113)$$

$$\mathbf{F}_{ba}=(\psi_b^{1*}\mathbf{F}\psi_a^1-\psi_a^1\mathbf{F}\psi_b^{1*})_{av}. \quad (1.114)$$

The first two terms of (1.11) give the flux produced by each part of the system in the absence of the other part whereas the last two terms describe the interference between the waves scattered by the two parts. The interference terms (1.113) and (1.114) contain only the wave functions ψ^1 which describe an unchanged state of the scatterer. Already at this point we want to emphasize that the amplitudes enter linearly into (1.113) and (1.114). As a consequence, in many cases in which a parameter describing the state of the scattering system is unknown, the interference terms vanish on averaging over the parameter while the terms in (1.111) and (1.112) which involve the squares of the amplitudes do not disappear.

These remarks are easily extended to a scattering system composed of many particles.

II. The Hamiltonian for the Magnetic Interaction

The choice of a proper Hamiltonian representing the magnetic interaction between neutron and electron cannot be made unambiguously since we do not yet possess a satisfactory theory of the structure of the neutron. The question has been the subject of considerable discussion and disagreement.[4] We present in this paragraph our view on the subject which will determine the choice of the Hamiltonian.

By the statement that the neutron carries a magnetic moment we mean to describe the fact that it produces in its neighborhood a field analogous to that of a classical magnetic dipole which owes its existence to a stationary current distribution. Fields that do not satisfy the relation

$$\text{div}\,\mathbf{H}=0 \quad (2.0)$$

may be present inside of the neutron; however, we refuse to recognize them as magnetic fields and prefer to designate them as some sort of spin dependent, short range forces. We know nothing about their existence, which could be detected only experimentally.

The rather trivial remark may be added that real singularities (discontinuities) which cannot be approximated by continuous functions sufficiently well for all physical purposes cannot claim any place in a physical theory.

[4] F. Bloch, Phys. Rev. 51, 994 (1937).

We finally recall the definition of a stationary magnetic moment $\mathbf{m}$ in classical physics as given by the relation

$$\mathbf{i} = c \operatorname{curl} \mathbf{m}. \tag{2.01}$$

As the divergence of $\mathbf{m}$ is still arbitrary, we can impose another condition on $\mathbf{m}$. This condition is usually chosen to make $\mathbf{m}$ disappear in a domain free of current. Since

$$\operatorname{curl} \mathbf{H} = 4\pi \mathbf{i}/c, \tag{2.02}$$

it follows that $\mathbf{m}$ and $\mathbf{H}/4\pi$ have the same curl. Therefore a scalar function ϕ exists such that

$$\mathbf{H} = 4\pi\mathbf{m} + \operatorname{grad} \phi. \tag{2.03}$$

The classical interaction energy can now be written in one of the following equivalent forms

$$W_1 = (1/4\pi) \int \mathbf{H}_n \cdot \mathbf{H}_e d\tau, \tag{2.10}$$

$$W_2 = \int \mathbf{H}_n \cdot \mathbf{m}_e d\tau, \tag{2.11}$$

$$W_3 = \int \mathbf{H}_e \cdot \mathbf{m}_n d\tau. \tag{2.12}$$

These forms follow from each other since

$$\int \mathbf{H} \cdot \operatorname{grad} \phi d\tau = \int \operatorname{div} (\phi \mathbf{H}) d\tau = 0. \tag{2.13}$$

Two other forms can be obtained by introducing the vector potential $\mathbf{A}$ and making use of the well-known relation

$$\mathbf{H} \cdot \mathbf{m} = \mathbf{m} \cdot \operatorname{curl} \mathbf{A} = \mathbf{A} \cdot \operatorname{curl} \mathbf{m} + \operatorname{div} (\mathbf{A} \times \mathbf{m}). \tag{2.14}$$

Thus we obtain

$$W_4 = (1/c) \int \mathbf{A}_n \cdot \mathbf{i}_e d\tau, \tag{2.20}$$

$$W_5 = (1/c) \int \mathbf{A}_e \cdot \mathbf{i}_n d\tau. \tag{2.21}$$

In (2.20) and (2.21) we have dropped the term containing the surface integral which we are always entitled to do if, as mentioned before, we look upon real singularities, etc., as physically meaningless. *It will appear that we thereby do not lose any physical possibilities.*

The terms in the various forms for the interaction energy are determined by the Dirac equation so far as the electron is concerned. The external field of the neutron is given through

$$\mathbf{H}_n(\mathbf{r}) = \frac{-\boldsymbol{\mu}_n}{|\mathbf{r}-\mathbf{r}_n|^3} + 3(\mathbf{r}-\mathbf{r}_n)\frac{\boldsymbol{\mu}_n \cdot (\mathbf{r}-\mathbf{r}_n)}{|\mathbf{r}-\mathbf{r}_n|^5}, \tag{2.30}$$

where $\boldsymbol{\mu}_n = \int \mathbf{m}_n d\tau$ is the neutron's magnetic moment. Obviously this expression cannot be continued up to the origin; it would lead to an indeterminate value for the interaction energy of the form $0 \cdot \log 0$. The forms (2.10) and (2.11) do not give us any hint as to the evaluation of the interaction integral over the interior of the neutron, but as soon as we decide to describe the neutron in the well-known way by a wave equation of the type

$$\left\{ \frac{h^2}{8\pi^2 M_0} \nabla^2 + \gamma \frac{eh}{2\pi M_0 c} \mathbf{s} \cdot \mathbf{H} - E \right\} \psi = 0, \tag{2.40}$$

we are relieved of all difficulties. For we now have for $\mathbf{m}_n$ the expression

$$\mathbf{m}_n = \gamma (eh/2\pi M_0 c) \psi^* \mathbf{s} \psi, \tag{2.50}$$

which, just as $\mathbf{m}_e$ in virtue of the Dirac equation, is not only everywhere regular but for neutrons of sufficiently large wave-length nowhere very large. Quantitatively speaking the integral over the interior of the neutron

$$\int \psi^* \mathbf{s} \psi d\tau$$

can be seen to go to zero for small neutron radius. This determines the previously undetermined form of W and allows us to use any of the expressions (2.10)–(2.12), (2.20), (2.21) according to our convenience.

It will be realized from the preceding discussion that we cannot *a priori* exclude the possibility of short range forces of the type

$$f(\mathbf{r}_e - \mathbf{r}_n, \mathbf{s}_n, \sigma_e, \alpha_e)$$

or of such a current distribution inside the neutron that the integration over the interior gives a considerable contribution to the whole

interaction energy while the outside field is still determined by (2.30). To the first possibility we have to remark that there does not yet exist any evidence for such forces; as to the second, that it will only occur if the interaction between neutron and electron cannot be described by a Hamiltonian in a two-body problem. For this certainly possible complication we also lack at present any physical evidence. We shall therefore proceed with the most convenient classical analog given by (2.10).

III. Scattering by Independent Nuclei

We discuss in this paragraph the scattering of slow neutrons by independent nuclei and place special emphasis upon questions of coherence and polarization. Though quite a few of our results can probably be found in the literature it still seems advisable to offer a comprehensive discussion which will be of great help in the treatment of simultaneous scattering due to nuclear and magnetic forces.

As far as coherence and interference questions are concerned the neutron scattering differs from the analogous x-ray scattering by a wide variability in the intensity of the pattern. The amplitude of the scattered wave varies from one nucleus to another not only as to magnitude but also, unlike most cases of x-ray scattering, may change sign. The points in an interference pattern may show striking difference in intensity depending upon the phase of the waves scattered by the different nuclei. For essentially the same reason the spin degeneracy of nuclear states may cause a much larger diminution of coherence than atomic degeneracies in optical cases do.

In the case of slow neutron scattering only the s wave has to be considered; we can also exclude inelastic collisions since the energy is always too small to excite higher nuclear states. We denote the nuclear spin by $\mathbf{i}$ and the eigenvalues of its component along some arbitrary axis by m_i; the corresponding wave functions shall be Ω_{m_i}. Let m_s denote the eigenvalues of the neutron's spin projection along the same axis. Since we are dealing with s waves, the total spin alone must be conserved in the collision. If the scattering is described by an intermediate state of the system neutron plus nucleus then the magnitude of its total angular momentum, $\mathbf{K}$, must be equal to $i+\frac{1}{2}$ or $i-\frac{1}{2}$.

The incident wave can always be analyzed into wave functions corresponding to total angular momenta $i+\frac{1}{2}$ and $i-\frac{1}{2}$. The probability amplitudes of the scattered wave with the above total angular moments shall be denoted by a_1 and a_0, respectively. Except in the simplest cases we lack complete knowledge even as to the relative sign of a_1 and a_0. Both probability amplitudes are independent of the actual sub level m_k since no distinguished axis has entered into our problem. Denoting the two wave functions of the incident wave by $\psi_{i+\frac{1}{2}}$ and $\psi_{i-\frac{1}{2}}$ we have for the complete wave the expression

$$\chi_s\Omega_N = c_0\psi_{i-\frac{1}{2}} + c_1\psi_{i+\frac{1}{2}} \tag{3.0}$$

with arbitrary complex constants. The scattered wave can then be written in the form

$$\psi_n = \left(\frac{2\pi M_0}{hk}\right)^{\frac{1}{2}} \frac{e^{ikr}}{r}(a_0c_0\psi_{i-\frac{1}{2}} + a_1c_1\psi_{i+\frac{1}{2}}). \tag{3.1}$$

To analyze the initial state into functions with definite total angular momentum it is convenient to use two operators η_0 and η_1 defined as follows:

$$\eta_0\psi_{i-\frac{1}{2}} = \psi_{i-\frac{1}{2}}, \tag{3.11}$$

$$\eta_0\psi_{i+\frac{1}{2}} = 0, \tag{3.12}$$

$$\eta_1\psi_{i+\frac{1}{2}} = \psi_{i+\frac{1}{2}}, \tag{3.13}$$

$$\eta_1\psi_{i-\frac{1}{2}} = 0. \tag{3.14}$$

From these definitions we now have

$$\eta_0\chi_s\Omega_N = c_0\psi_{i-\frac{1}{2}}, \tag{3.15}$$

$$\eta_1\chi_s\Omega_N = c_1\psi_{i+\frac{1}{2}}, \tag{3.16}$$

and for the scattered wave

$$\psi_n = \left(\frac{2\pi M_0}{hk}\right)^{\frac{1}{2}} \frac{e^{ikr}}{r}(a_0\eta_0 + a_1\eta_1)\chi_s\Omega_N. \tag{3.2}$$

Operators satisfying (3.11) to (3.14) are easily found to be given by

$$\eta_0 = (2i+1)^{-1}(i - 2\mathbf{i}\cdot\mathbf{s}), \tag{3.21}$$

$$\eta_1 = (2i+1)^{-1}(i+1+2\mathbf{i}\cdot\mathbf{s}). \tag{3.22}$$

We shall hereafter use the abbreviation

$$\eta = a_0\eta_0 + a_1\eta_1.$$

If several isotopes are present, our knowledge of the scattering nucleus is described by a wave function which corresponds to the simultaneous presence of all the isotopes weighted in the ratio of their abundance. If $\Omega_N{}^P$ describes the spin state of the Pth isotope the total spin wave function is given by

$$\Omega_N=\sum_P \Omega_N{}^P b_P, \quad \sum |b_P|^2=1. \tag{3.23}$$

The term $|b_P|^2$ is determined by the relative abundance of the Pth isotope, while b_P contains an undetermined phase. Quantities obtained from (3.23) must be averaged over the arbitrary phase occurring in each b_P. The previous result for the scattered wave is easily generalized. The scattered wave is still given by (3.2) if we understand by $\eta\Omega_N$ the expression

$$\eta\Omega_N=\sum_P b_P\eta_P\Omega_N{}^P, \tag{3.24}$$

where
$$\eta_P=a_0{}^P\eta_0{}^P+a_1{}^P\eta_1{}^P,$$
$$\eta_0{}^P=(2i_P+1)^{-1}(i_P-2\mathbf{i}_P\cdot\mathbf{s}),$$
$$\eta_1{}^P=(2i_P+1)^{-1}(i_P+1+2\mathbf{i}_P\cdot\mathbf{s}).$$

To illustrate coherence properties by a simple example, the interference between the scattering of two identical nuclei a and b shall be discussed. The positions of the two nuclei are assumed to be precisely known and multiple scattering shall be neglected. If the total scattered wave is analyzed according to different spin states of the nucleus, we find for that part of the wave in which the nuclear state is unchanged the expression

$$\psi_{sa}{}^1=\left(\frac{2\pi M_0}{hk}\right)^{\frac{1}{2}}\frac{\exp\,(ik|\mathbf{r}-\mathbf{r}_a|+i\mathbf{k}\cdot\mathbf{r}_a)}{|\mathbf{r}-\mathbf{r}_a|}\times(N|\eta|N)_a\chi_s. \tag{3.30}$$

A similar expression holds for the nucleus b. This part of the wave suffices for the discussion of coherent properties; we have from (1.11) for the interference terms.

$$F_{ab}+F_{ba}=\frac{1}{r^2}\cos\{k|\mathbf{r}-\mathbf{r}_a|-k|\mathbf{r}-\mathbf{r}_b| +\mathbf{k}\cdot(\mathbf{r}_a-\mathbf{r}_b)\}\{[(N|\eta|N)_a{}^*\chi_s{}^*]\times[(N|\eta|N)_b\chi_s]+\text{conj.}\}. \tag{3.31}$$

Through η the vector $\mathbf{i}$ enters into (3.30); the amount of coherent scattering therefore depends upon the nuclear spin state through the matrix element $(N|\mathbf{i}|N)_a\cdot\mathbf{s}\chi_s{}^*$ etc. In practical cases the nuclear spin has no preferred axis which makes $(N|\mathbf{i}|N)=0$. Eq. (3.31) simplifies thereby to

$$F_{ab}+F_{ba}=2/r^2\cos\{k|\mathbf{r}-\mathbf{r}_a|-k|\mathbf{r}-\mathbf{r}_b| +\mathbf{k}\cdot(\mathbf{r}_a-\mathbf{r}_b)\}\left\{\frac{ia_0+(i+1)a_1}{2i+1}\right\}^2\chi_s{}^*\chi_s. \tag{3.32}$$

The first factor in (3.32) arises from the path difference between the two nuclei. The last factor $\chi_s{}^*\chi_s$ shows that the spin of the neutron is unchanged in the interference term. The middle factor makes it clear that the coherence depends upon a linear combination of a_0 and a_1 which even may be of opposite sign. We shall see that the total scattering depends only upon $a_0{}^2$ and $a_1{}^2$ so that even for large total scattering the spin degeneracy may completely destroy all interference effects. Such a case is approximately realized in ${}_1H^1$; it may be expected that hydrogen in a crystal lattice will not appreciably contribute to the formation of a diffraction pattern.

In the presence of several isotopes the results are easily generalized. By use of (3.23) and (3.24) and analogous reasoning, one obtains, after averaging over the arbitrary phases in the coefficients b_P, the expression

$$F_{ab}+F_{ba}=2/r^2\cos[k|\mathbf{r}-\mathbf{r}_a| -k|\mathbf{r}-\mathbf{r}_b|+\mathbf{k}\cdot(\mathbf{r}_a-\mathbf{r}_b)]\times\left\{\sum_P|b_P|^2\frac{i_Pa_0{}^P+(i_P+1)a_1{}^P}{2i_P+1}\right\}^2\chi_s{}^*\chi_s. \tag{3.33}$$

The bracket { } indicates that the amplitudes of all the isotopes enter a linear combination. Hence coherence may be reduced not only by opposite signs of a_0 and a_1 for a single isotope, but also by the cancellation of the amplitude for one isotope against that of another. Whereas a combination of two measurements (total scattering and interference) is sufficient for experimental determination of the amplitudes a_0 and a_1 in the case of a single isotope, this is no longer true in the case of several isotopes. Only in the case of a single isotope with no spin ($a_1=a_0$) does a scattering

measurement allow predictions of interference phenomena.

In practice the thermal agitation prohibits a precise knowledge of the nuclear position in a crystal. Its position is then described by a spatial wave function $\theta(\mathbf{r}_N)$ whose extension is determined by the amplitude of the thermal oscillations. For the discussion of elastic scattering each point of the distribution $|\theta(\mathbf{r}_N)|^2$ can be considered the origin of a secondary wavelet. Thus the elastically scattered wave becomes

$$\psi_m=\left(\frac{2\pi M_0}{hk}\right)^{\frac{1}{2}}\frac{e^{ikr}}{r}F_N{}^{\frac{1}{2}}\eta\chi_s\Omega_N, \tag{3.4}$$

$$F_N{}^{\frac{1}{2}}=\int \exp\left(i(\mathbf{k}-\mathbf{k}')\cdot\mathbf{r}_N\right)|\theta(\mathbf{r}_N)|^2 d\tau_N, \tag{3.41}$$

where $\mathbf{k}'$ is the propagation vector of the scattered neutron. The coherent scattering is reduced by the factor F_N, which is called the form factor of the nuclear distribution.

To obtain the scattering from a single nucleus one has to insert the expression for the scattered wave (3.30) into (1.03) which gives the outgoing flux. One finds

$$F_{\mathfrak{N}}=r^{-2}[(\eta^*\chi_s^*\Omega_N^*)(\eta\chi_s\Omega_N)]_{\mathrm{av}}, \tag{3.5}$$

which can be transformed on account of the Hermitian character of η into

$$F_N=r^{-2}(N|(\eta'\chi_s)(\eta\chi_s)|N),$$
$$\eta'=(2i+1)^{-1}[ia_0+(i+1)a_1+2(a_1-a_0)\mathbf{i}\cdot\mathbf{s}^*]. \tag{3.51}$$

After expansion of the product, the terms linear in the spin component can again be dropped since the nuclear spin has no preferred direction. We have for the same reason the relation

$$(N|i_xi_x|N)=(N|i_yi_y|N)$$
$$=(N|i_zi_z|N)=\tfrac{1}{3}i(i+1). \tag{3.6}$$

It is also clear that terms like $(N|i_xi_y|N)$ have to disappear. This can be seen as follows; if $\mathbf{A}$ is a real vector the average value of $(\mathbf{A}\cdot\mathbf{i})^2$ i.e., $(N|(\mathbf{i}\cdot\mathbf{A})(\mathbf{i}\cdot\mathbf{A})|N)$ must be expressible in terms of the scalar A^2 when $\mathbf{i}$ has no preferred direction. This requires that terms like $(N|i_xi_y|N)$ vanish.

We thus arrive at the expression

$$F_n=r^{-2}(2i+1)^{-2}\{[ia_0+(i+1)a_1]^2|\chi_s|^2$$
$$+(4/3)i(i+1)(a_1-a_0)^2(\mathbf{s}^*\chi_s^*)\cdot(\mathbf{s}\chi_s)\}. \tag{3.7}$$

The total scattering is found by summing (3.7) over the spin coordinate of the neutron. Again on account of the Hermitian character of $\mathbf{s}$ we can write

$$\sum_{\text{spin}}\cdot(\mathbf{s}^*\chi_s^*)\cdot s\chi_s=\sum_{\text{spin}}\chi_s^*\mathbf{s}\cdot\mathbf{s}\chi_s$$
$$=\tfrac{3}{4}\sum_{\text{spin}}|\chi_s|^2=\tfrac{3}{4} \tag{3.7}$$

and so obtain finally for the total outgoing flux

$$\sum_{\text{spin}}F_n=r^{-2}(2i+1)^{-1}[ia_0^2+(i+1)a_1^2]. \tag{3.80}$$

From (3.80) there follows for the differential cross section for scattering into the solid angle $d\Omega$ the expression

$$d\Phi_n=(2i+1)^{-1}[ia_0^2+(i+1)a_1^2]d\Omega, \tag{3.81}$$

and since the scattered wave is an s wave we have a total cross section

$$\sigma_n=4\pi(2i+1)^{-1}[ia_0^2+(i+1)a_1^2]. \tag{3.82}$$

Equation (3.82) contains the important result that the total scattering is independent of the initial spin state of the neutron and involves only the absolute magnitude of a_0 and a_1. In the presence of isotopes the Eqs. (3.81) and (3.82) must be averaged over the isotopes; each isotope is weighted in the degree of its abundance. It is important to realize the totally different behavior that the expressions for the interference terms (representing the coherent scattering) and that for the total scattering exhibit as far as the dependence on sign and relative magnitude of the probability amplitudes is concerned.

The relation (3.5) also determines the change produced by the scattering in the spin state of the neutron. Let α and β be two orthogonal and normalized spin functions representing the spin parallel and antiparallel to the z axis, respectively. The spin coordinate of the neutron also taken along the z axis can have the values $\pm\frac{1}{2}$. We have with these coordinates

$$\alpha(\tfrac{1}{2})=1, \quad \beta(\tfrac{1}{2})=0,$$
$$\alpha(-\tfrac{1}{2})=0, \quad \beta(-\tfrac{1}{2})=1. \tag{3.90}$$

The spin vector is then represented by the well-known relations

$$\begin{aligned} S_x\alpha &= (\tfrac{1}{2})\alpha, \qquad S_y\alpha = (i/2)\beta, \\ S_x\beta &= -(\tfrac{1}{2})\beta, \quad S_y\beta = -(i/2)\alpha, \\ S_z\alpha &= (\tfrac{1}{2})\beta, \\ S_z\beta &= (\tfrac{1}{2})\alpha. \end{aligned} \tag{3.901}$$

The initial spin state of the neutron can be written as follows:

$$\chi_s = a\alpha + b\beta, \quad |a|^2 + |b|^2 = 1, \quad a^* - a = 0, \tag{3.91}$$

where the last relation is used only to eliminate a trivial phase factor. The initial state is polarized in a direction whose polar angles are given by

$$\cot(\theta/2) = |a/b|, \tag{3.911}$$

$$\tan\phi = (b - b^*)/i(b + b^*). \tag{3.912}$$

As a measure of the polarization relative to the z axis, we take a quantity P_0 defined by

$$P_0 = |a|^2 - |b|^2. \tag{3.92}$$

If the initial state is unpolarized, all results which contain χ_s must be averaged over the angles θ and ϕ. The relation (3.7) now becomes

$$\begin{aligned} F_n = r^{-2}(2i+1)^{-2}\{&[(ia_0 + (i+1)a_1)^2 \\ &+ \tfrac{1}{3}(a_1 - a_0)^2 i(i+1)](|a|^2\alpha^*\alpha + |b|^2\beta^*\beta) \\ &+ \tfrac{2}{3}i(i+1)(a_1 - a_0)^2(|b|^2\alpha^*\alpha + |a|^2\beta^*\beta\}. \end{aligned} \tag{3.93}$$

With the abbreviation

$$Q = \tfrac{2}{3}(2i+1)^{-1}i(i+1)\frac{(a_1 - a_0)^2}{ia_0^2 + (i+1)a_1^2} \tag{3.94}$$

we can now write (3.93) in the form

$$\begin{aligned} F_n = r^{-2}\{&[(1-Q)|a|^2 + Q|b|^2]\alpha^*\alpha \\ &+ [(1-Q)|b|^2 + Q|a|^2]\beta^*\beta\} \\ &\times [ia_0^2 + (i+1)a_1^2](2i+1)^{-1}. \end{aligned} \tag{3.95}$$

Constructing a quantity P for the scattered wave as we did in (3.92) for the incident wave, we find for the polarization of the scattered wave the expression

$$P = (1-2Q)(|a|^2 - |b|^2) = (1-2Q)P_0. \tag{3.96}$$

Since the z axis is arbitrary, we learn from (3.96) that the polarization of the incident beam relative to any axis is changed through the scattering process by a factor $1-2Q$. Large polarization changes will occur if a_0 and a_1 show opposite signs; in that case Eq. (3.33) leads to small interference effects.

In the presence of isotopes the quantity Q must be averaged as before.

IV. Magnetic Scattering of an Isolated Ion

To place in evidence the uniqueness of result as discussed in Section II, we shall use the fundamental form (2.00) for the interaction between electron and neutron, which must be summed over all the electrons of the atom. By taking the nucleus as the origin of coordinates and designating by Ψ_A the wave function of the electrons in the state A, the Born method in first approximation gives for the scattered wave at large distances from the ion, the expression

$$\begin{aligned} \psi_n = (2\pi M_0/h^2)(2\pi M_0/hk)^{\frac{1}{2}} &\sum_{s'A'} r^{-1}e^{ik'r} \\ &\times \chi_{s'}\Psi_{A'}(\mathbf{k}', s', A'|V|\mathbf{k}, s, A), \end{aligned} \tag{4.00}$$

where the primes indicate final states. The propagation vector of the neutron, $\mathbf{k}$, satisfied the energy condition

$$(h^2/8\pi^2 M_0)(k^2 - k'^2) = E_{A'} - E_A, \tag{4.01}$$

where E refers to the energy of the atomic electrons. The matrix elements in (4.00) when written out in full are

$$\begin{aligned} (\mathbf{k}'s'A'|V|\mathbf{k}sA) = -(4\pi)^{-1}\int \sum_l \mathbf{H}(\mathbf{r}_l)\cdot\mathbf{curl}_l \\ \times\left[\int \exp(i(\mathbf{k}-\mathbf{k}')\cdot\mathbf{r})\frac{(s'|\boldsymbol{\mu}|s)\times(\mathbf{r}-\mathbf{r}_l)}{|\mathbf{r}-\mathbf{r}_l|^3}d\tau\right]d\tau_{\text{atom}} \end{aligned} \tag{4.02}$$

when $d\tau_{\text{atom}}$ is the volume element for all the internal coordinates of the atom and $d\tau$ is the volume element for the space coordinate of the neutron. $\mathbf{H}(\mathbf{r}_l)$ is the magnetic field due to the current distribution of the l'th electron while $\mathbf{curl}_l$ is the indicated operation for the coordinates of the lth electron. $(s'|\boldsymbol{\mu}|s)$ are the matrix elements of the neutron's magnetic moment

referred to the initial and final spin states, s and s'. Inasmuch as the magnetic field of the electrons is nowhere discontinuous or singular, we may integrate by parts over the electron coordinates and safely discard the surface integrals that result. The expression $\mathbf{curl}_l \mathbf{H}(\mathbf{r}_l)$ which results may then be replaced by $4\pi\mathbf{i}_l/c$ where $\mathbf{i}_l$ is the current density of the l'th electron. Thus we find

$$(\mathbf{k}'s'A'|V|\mathbf{k}sA)=\int\sum_l \Psi_{A'}{}^*c\boldsymbol{\alpha}_l\Psi_A \cdot\frac{(s'|\boldsymbol{\mu}|s)\times(\mathbf{r}-\mathbf{r}_l)}{|\mathbf{r}-\mathbf{r}_l|^3}\cdot\exp(i(\mathbf{k}-\mathbf{k}')\cdot\mathbf{r})d\tau_{\text{atom}}d\tau. \tag{4.03}$$

The current density of the electrons[5] can be written up to the order v^2/c^2 in the following form

$$\mathbf{i}_l=\mathbf{i}_l{}^{(0)}+\mathbf{i}_l{}^{(1)}, \tag{4.04}$$

$$\mathbf{i}_l{}^{(0)}=\frac{eh}{4\pi mi}[\Psi^*\,\mathbf{grad}_l\,\Psi-\Psi\,\mathbf{grad}_l\,\Psi^*], \tag{4.041}$$

$$i_l{}^{(1)}=\frac{eh}{2\pi mc}\,\mathbf{curl}_l\,(\Psi^*\mathbf{s}_l\Psi), \tag{4.042}$$

where $\mathbf{s}_l$ is the spin of the l'th electron, $\mathbf{i}_l{}^{(0)}$ its orbital current, and $\mathbf{i}_l{}^{(1)}$ its spin current. In all cases of practical interest (ion in crystals) the orbital current is either absent (s state) or quenched. The magnetic properties of the ion are almost wholly due to the electron spins. We shall therefore in what follows use $\mathbf{i}_l{}^{(1)}$ for the electron current. Inserting it into (4.03), changing the origin of coordinates for the integration over the space of the neutron to $\mathbf{r}_l$, and integrating by parts over the electron coordinates we obtain

$$(\mathbf{k}'s'A'|V|\mathbf{k}sA)=-i\left(\frac{eh}{2\pi mc}\right)\int\exp(i(\mathbf{k}-\mathbf{k}')\cdot\mathbf{r}) \times\frac{(s'|\boldsymbol{\mu}|s)\times\mathbf{r}}{|\mathbf{r}|^3}\cdot\left[(\mathbf{k}-\mathbf{k}')\times\sum_l\int\Psi_{A'}{}^* \exp(i(\mathbf{k}-\mathbf{k}')\cdot\mathbf{r}_l)\mathbf{s}_l\Psi_A d\tau_{\text{atom}}\right]d\tau. \tag{4.05}$$

The integration over $\mathbf{r}$ is now easily carried out with the result

$$(\mathbf{k}'s'A'|V|\mathbf{k}sA)=4\pi\left(\frac{eh}{2\pi mc}\right)\left(\frac{eh\gamma}{2\pi M_0c}\right) \times[(s'|\mathbf{s}|s)\times\mathbf{e}]\cdot[\mathbf{e}\times(A'|\mathbf{P}|A)], \tag{4.06}$$

$$\mathbf{e}=\frac{\mathbf{k}-\mathbf{k}'}{|\mathbf{k}-\mathbf{k}'|}, \tag{4.07}$$

$$\mathbf{P}=\sum_l\exp(i(\mathbf{k}-\mathbf{k}')\cdot\mathbf{r}_l)\mathbf{s}_l, \tag{4.08}$$

where $\mathbf{s}$ stands for the spin of the neutron and γ for its moment in nuclear magnetons. In the limit of long wave-lengths the exponential in (4.08) can be replaced by unity. $\mathbf{P}$ then becomes the total spin of the ion. Substitution of the matrix element into the wave function (4.00) gives the result

$$\psi_m=\left(\frac{2\pi M_0}{hk}\right)^{\frac{1}{2}}\left(\frac{2e^2\gamma}{mc^2}\right)\sum_{s'A'}\frac{e^{ik'r}}{r}\chi_{s'}\Psi_{A'} \times(s'A'|(\mathbf{e}\cdot\mathbf{s})(\mathbf{e}\cdot\mathbf{P})-\mathbf{P}\cdot\mathbf{s}|sA). \tag{4.1}$$

If the ground state of the ion is alone involved in the collision the expression (4.1) may be further simplified. Let Ω_M be the spin wave function describing the orientation of the spin $\mathbf{S}$ of the ground state and let B stand for the remaining atomic quantum numbers so that M and B replace the totality of quantum numbers A in (4.1). We then have by a well-known result in the algebra of vector coupling[6]

$$(M'B|\mathbf{P}|MB)=(M'|\mathbf{S}|M)\cdot F^{\frac{1}{2}},$$

$$F^{\frac{1}{2}}=\left(B\left|\frac{\mathbf{P}\cdot\mathbf{S}}{S(S+1)}\right|B\right) =\left(B\left|\sum_l\exp(i(\mathbf{k}-\mathbf{k}')\cdot\mathbf{r}_l)\frac{\mathbf{s}_l\cdot\mathbf{S}}{S(S+1)}\right|B\right). \tag{4.2}$$

We have with the aid of (4.2) obtained an expression for $(A|\mathbf{P}|A)$ as a product of two factors, one of which refers to the spin coordinates only, while the other deals with the remaining coordinates. The quantity F which now refers to all the electrons in the atom can be

[5] W. Pauli, article on quantum mechanics in Springer's *Handbuch der Physik*, Vol. 24-A, p. 238.

[6] E. U. Condon and G. H. Shortley, *The Theory of Atomic Spectra* (Cambridge University Press, 1935), p. 59.

called the atomic form factor. It reduces to unity if $\lambda/2\pi$ is large compared to the linear size of the electron distribution. This condition is in practical cases not even satisfied by liquid-air neutrons. For elastic transitions $k'=k$ and F then becomes unity in the forward direction and decreases to its smallest value for scattering under 180° ($\mathbf{k}'=-\mathbf{k}$). Since, under the last made assumptions, the atomic system can only change its spin state M during collision, we may omit the part of the wave function referring to the other internal coordinates and can write (4.1) in the form

$$\psi_m=\left(\frac{2\pi M_0}{hk}\right)^{\frac{1}{2}}\left(\frac{2e^2\gamma}{mc^2}\right)\sum_{s'M'}\frac{e^{ik'r}}{r}\chi_{s'}\Omega_{M'}\times(s'M'|\mathfrak{M}|sM)F^{\frac{1}{2}} \quad (4.3)$$

$$\mathfrak{M}=(\mathbf{e}\cdot\mathbf{s})(\mathbf{e}\cdot\mathbf{S})-\mathbf{s}\cdot\mathbf{S}. \quad (4.4)$$

If all collisions are elastic so that $F^{\frac{1}{2}}$ is the same for every term under the summation sign, (4.3) can be written

$$\psi_m=\left(\frac{2\pi M_0}{hk}\right)^{\frac{1}{2}}\left(\frac{2e^2\gamma F^{\frac{1}{2}}}{mc^2}\right)\frac{e^{ikr}}{r}\mathfrak{M}\chi_s\Omega_M. \quad (4.5)$$

V. Scattering From Independent Paramagnetic Ions

The formulae for magnetic scattering as derived in the last paragraph are far too general to permit a direct physical discussion. We shall investigate in this and the following sections a number of special cases which allow a more explicit evaluation as well as a direct physical interpretation. These special cases will also form the theoretical basis for various groups of experiments. Unfortunately we can proceed quantitatively only in selected circumstances and have to limit ourselves frequently to qualitative discussions.

Beginning with the treatment of paramagnetic substances especially salts containing magnetically active ions, we remember that, in the solid state, the levels of the ions are as a rule strongly affected by interionic forces. If e.g. the ground state of an ion forms a multiplet having an orbital angular momentum $\mathbf{L}$ and a spin angular momentum $\mathbf{S}$, then the crystalline field will, as a rule, decouple $\mathbf{L}$ and $\mathbf{S}$ and quench the orbital currents. This is the reason why we retained in (4.05) the spin current only. In most cases the states associated with different orientations of $\mathbf{L}$ are split and differ from each other by energies large compared to kT. The ion then will be normally found in the lowest of these levels. Since energetic considerations make it impossible for a thermal neutron to transfer the ion to higher states, only the ground state will be active during the collision. We shall in this section assume throughout that the ionic spin is uninfluenced by forces due to the neighboring atoms; also we shall, at first, suppose that the spin is completely free from internal forces. The ground state of the magnetic ion is then degenerate and Eq. (4.4) can be applied directly.

To illustrate coherence we treat the interference between the magnetic scattering by two ions a and b which are situated at the points $\mathbf{r}_a$ and $\mathbf{r}_b$. According to (3.30) it is for the interference questions only necessary to consider that part of the scattered wave $\psi_m{}^1$ in which the ionic spin is unchanged. By expanding $\psi_m{}^1$ in terms of the spin states M of the ion, we find for the part of the wave in which the spin state is unchanged by the scattering process the expression

$$\psi_{ma}{}'=\left(\frac{2\pi M_0}{kk}\right)^{\frac{1}{2}}\left(\frac{2e^2\gamma F^{\frac{1}{2}}}{mc^2}\right)|r-r_a|^{-1}\times\exp\,(ik|\mathbf{r}-\mathbf{r}_a|+i\mathbf{k}\cdot\mathbf{r}_a)\times(M|\mathfrak{M}|M)_a\chi_s\Omega_M{}^*. \quad (5.0)$$

Since the ionic spin has no preferred direction in space, we obtain

$$(M|\mathbf{S}|M)_a=0, \quad (5.01)$$

$$\psi_{ma}{}^1=0. \quad (5.02)$$

The result (5.01) is valid as long as the medium is far from magnetic saturation. In accordance with (5.02) the interference terms are zero and all the magnetic scattering is incoherent. There is no interference between the scattering from two ions in a lattice or between the magnetic and nuclear scattering of the same ion. The consequent additivity of nuclear and magnetic scattering from paramagnetic substances forms the basis for the method of separating the two effects as mentioned in the introduction.

The scattering by a single ion is determined by (4.05) and (1.03). We obtain

$$F_m=r^2\left(\frac{2e^2\gamma F}{mc^2}\right)^2[(\mathfrak{M}\chi_s\Omega_M)^*(\mathfrak{M}\chi_s\Omega_M)]_{\rm av}. \quad (5.1)$$

By use of the Hermitian property of **S**, (5.1) becomes

$$F_m=r^2\left(\frac{2e^2\gamma F}{mc^2}\right)^2(M|(\mathfrak{M}'\chi_s)^*(\mathfrak{M}\chi_s)|M), \quad (5.2)$$

$$\mathfrak{M}'=(\mathbf{e}\cdot\mathbf{s})(\mathbf{e}\cdot\mathbf{S})^*-\mathbf{s}\cdot\mathbf{S}^*. \quad (5.21)$$

Just as in the case of the nuclear spin, the random orientation of **S** implies

$$(M|S_xS_x|M)=\tfrac{1}{3}S(S+1), \quad (5.22)$$

$$(M|S_xS_y|M)=0, \text{ etc.} \quad (5.23)$$

Eq. (5.2) now becomes

$$F_m=\tfrac{1}{3}S(S+1)r^2\left(\frac{2e^2\gamma F}{mc^2}\right)^2 \times[\mathbf{s}^*\chi_s^*\cdot\mathbf{s}\chi_s-(\mathbf{e}\cdot\mathbf{s})^*\chi_s^*(\mathbf{e}\cdot\mathbf{s})\chi_s]. \quad (5.3)$$

The total scattering is found from (5.3) by summing over the spin coordinates of the neutron. Again the Hermitian character of **s** gives

$$\sum_{\rm spin}\mathbf{s}^*\chi_s\cdot\mathbf{s}\chi_s=\tfrac{3}{4}, \quad (5.31)$$

$$\sum_{\rm spin}(\mathbf{e}\cdot\mathbf{s})^*\chi_s^*(\mathbf{e}\cdot\mathbf{s})\chi_s=\sum_{\rm spin}\chi_s^*(\mathbf{e}\cdot\mathbf{s})(\mathbf{e}\cdot\mathbf{s})\chi_s=\tfrac{1}{4}. \quad (5.32)$$

Eq. (5.3) then becomes

$$\sum_{\rm spin}F_m=r^2\left(\frac{e^2\gamma F}{mc^2}\right)^2\tfrac{2}{3}S(S+1). \quad (5.4)$$

We finally have for the differential cross section for scattering into the solid angle $d\Omega$ the expression

$$d\Phi_m=\tfrac{2}{3}S(S+1)\left(\frac{e^2\gamma F}{mc^2}\right)^2d\Omega. \quad (5.41)$$

This cross section depends on the angle of scattering only in virtue of the form factor and is independent of the initial spin state of the neutron. In the limit of long wave-lengths the form factor F approaches one and we obtain for the integrated cross section the simple expression

$$\sigma_m=\frac{8\pi}{3}S(S+1)\left(\frac{e^2\gamma}{mc^2}\right)^2, \quad (5.5)$$

which may be large in comparison with nuclear cross sections.

Equation (5.3) also allows a study of the change in polarization produced by the scattering process. Placing (3.91) for the spin state of the incident neutron into the expression (5.3) we find, for the scattered flux

$$F_m=\tfrac{1}{3}S(S+1)\left(\frac{e^2\gamma F}{mc^2}\right)^2\{[(1-e_z^2)|a|^2 +(1+e_z^2)|b|^2-K]\alpha^*\alpha+[(1-e_z^2)|b|^2 +(1+e_z^2)|a|^2+K]\beta^*\beta\}, \quad (5.60)$$

$$K=e_z[a^*b(e_x-ie_y)+ab^*(e_x+ie_y)]. \quad (5.61)$$

If we now express a and b in terms of the angles θ, ϕ, we have

$$K=2\cos\theta/2\sin(\theta/2)e_z(e_x\cos\varphi+e_y\sin\varphi) =(\mathbf{e}\cdot\boldsymbol{\lambda}-e_z\lambda_z)e_z. \quad (5.62)$$

Here $\boldsymbol{\lambda}$ is a unit vector in the direction of polarization of the incident neutrons. By remembering the relations

$$|b|^2-|a|^2=\sin^2\theta/2-\cos^2\theta/2 =-\cos\theta=-\lambda_z, \quad (5.63)$$

we can write (5.60) in the form

$$F_m=\tfrac{1}{3}S(S+1)r^2\left(\frac{e^2\gamma F}{mc^2}\right)^2 \times\{[1-e_z(\mathbf{e}\cdot\boldsymbol{\lambda})]\alpha^*\alpha+[1+e_z(\mathbf{e}\cdot\boldsymbol{\lambda})]\beta^*\beta\}. \quad (5.7)$$

If we designate by $\boldsymbol{\lambda}'$ the direction along which the scattered beam is analyzed, we find for its polarization P the value

$$P=-(\mathbf{e}\cdot\boldsymbol{\lambda})(\mathbf{e}\cdot\boldsymbol{\lambda}'). \quad (5.8)$$

Eq. (5.8) allows a simple interpretation: the part of the original polarization which is parallel to **e** is reversed in the scattered beam while the

part which is perpendicular to **e** is completely depolarized.

Let us next examine in a general manner the modification of these results required by the presence of internal forces acting on the ionic spin. Such forces are present for all ions of the ion group except Fe^{+++} and Mn^{++} which are in an S state; they arise from the incomplete decoupling of the spin **S** and the orbital angular momentum; their interaction normally causes the separation of the multiplet states formed from **L** and **S**. This incomplete decoupling can produce an energy separation of the orientation states of the spin which may result in a more or less complete quenching of the spin currents also. Since anomalies in the magnetic susceptibility frequently begin around 70°K, the separations are of the order of magnitude of $50k$. Consequently a part of the neutron scattering will be inelastic and involve energy changes of a similar amount.

For the reason indicated in Section I we use the neutron density I in dealing with inelastic collisions. The density of scattered neutrons is constructed by summing $|\psi_m|^2$ over the spin variables of the ion and the neutron and dividing by the density of incident neutrons, i.e., $2\pi M_0/\hbar k$. We find

$$\frac{I_{sc}}{I_{in}}=r^2\left(\frac{2e^2\gamma}{mc^2}\right)^2\sum_{s'M'}|(s'M'|\mathfrak{M}|sM)F|^2. \quad (5.90)$$

The form factor F has been included under the summation sign as it depends on the energy change in each transition and is to be taken zero for those conditions which are energetically impossible. The quantity (5.90) must be averaged over the orientation states of the ionic spin in accordance with the Boltzmann distribution law. If the wave-length of the neutron suffers a small change on scattering, F is nearly the same for all transitions and the summation yields our former result for the total scattering. If the scattering becomes inelastic, the influence of this loss of energy varies with the scattering angle. The forward scattering is diminished from that given by (5.41) because $\mathbf{k}-\mathbf{k}'$ is no longer zero when **k** and **k'** are parallel, and this leads to a decrease in the value for F. Transitions in which the neutron gains energy $k'>k$ decrease in frequency. for all scattering angles while transitions in which the neutron loses energy, $k'<k$ are more frequent in the case of backward scattering.

It is of interest to see how much of the scattering given by (5.90) is elastic. Summing over the spin variable of the neutron in that term of (5.90) for which $M=M'$, one obtains

$$I_{sc}(\text{elastic})/I_{in}=r^2\left(\frac{2e^2\gamma F}{mc^2}\right)^2\tfrac{1}{4}[(M|\mathbf{S}|M)\cdot(M|\mathbf{S}|M)-(M|\mathbf{e}\cdot\mathbf{S}|M)]. \quad (5.91)$$

The expression (5.91) again must be averaged over the temperature distribution of the ions among their orientation states. If the spins are fully quenched in all these states, we have

$$(M|\mathbf{S}|M)=0, \quad (M|S_x|M)^2=0, \quad (5.92)$$

which means that all the scattering is inelastic. The greatest decrease will be shown for scattering through small angles and particularly so if the neutron energy becomes smaller than the energy difference between the orientation states. In this latter case only hyperelastic collisions could occur which are made less frequent if these higher orientation states are less populated because of a lowering of the temperature. If the quenching of the spin current is incomplete, intermediary results have to be expected. This brief discussion is sufficient to show the great complexity which even in absence of a coupling between the spins of different ions must be expected in the scattering of very slow neutrons unless the ion is originally in an S state.

VI. Scattering by an Individual Ion in a Ferromagnetic Material

A ferromagnetic material below the Curie point consists of microcrystals each of which shows an alignment of the spins of its ions along a definite but arbitrary axis. We shall assume as basis of our discussions that each spin in the microcrystal is parallel to the axis, the direction of which shall be designated by the unit vector κ. In addition, it shall be supposed that the spins are rigidly aligned so that the initial kinetic energy of the neutron is insufficient to change the

orientation of an ionic spin. Elastic collisions in which the ionic spin state is unchanged are then alone possible for energetic reasons. The condition that the scattering system remains unchanged during the scattering process underlies the previous discussions by Bloch and Schwinger.

If the ferromagnetic medium is magnetized to saturation the vectors, κ, of all microcrystals become parallel while in the unmagnetized state they are oriented at random. The discussion of a change in the spin orientation of a whole microcrystal will be taken up later.

Let us designate by C the amplitude of the coherent nuclear scattering

$$C=\sum_P |b_P|^2(2i_P+1)^{-1}[i_P a_0{}^P+(i_P+1)a_1{}^P]. \quad (6.0)$$

If E^2 be the quantity

$$E^2=\sum_P |b_P|^2(2i_P+1)^{-1} \times i_P(i_P+1)(a_1{}^P-a_0{}^P)^2, \quad (6.01)$$

which is proportional to the intensity of incoherent scattering, then the total nuclear scattering is given by E^2+C^2. Here we have neglected the possible effect of the nuclear form factor F_N of (3.4) as it is probably not very large, at least for the forward scattering and sufficiently heavy nuclei.

For the magnetic scattering the relation (4.5) is here applicable. The spin function Ω_M of the initial state of the ion must represent the ionic spin parallel to the axis κ. Since transitions to other ionic spin states do not enter, we may write

$$\mathbf{S}\Omega_M=\mathbf{S}\kappa\Omega_M. \quad (6.10)$$

The spin function Ω_M may therefore be omitted in the incident and scattered wave. The magnetically scattered wave is now given by

$$\psi_m=\left(\frac{2\pi M_0}{h\mathbf{k}}\right)^{\frac{1}{2}} 2Dr^{-1}e^{i\mathbf{k}r}\mathbf{q}\cdot\mathbf{s}\chi_s \quad (6.20)$$

with the abbreviations

$$D=\frac{e^2\gamma S}{mc^2}F, \quad (6.21)$$

$$\mathbf{q}=\mathbf{e}(\mathbf{e}\cdot\kappa)-\kappa. \quad (6.22)$$

The sum of the coherent nuclear and magnetically scattered wave now becomes

$$\psi_{sc}=\left(\frac{2\pi M_0}{h\mathbf{k}}\right)^{\frac{1}{2}} r^{-1}e^{i\mathbf{k}r}(C+2D\mathbf{q}\cdot\mathbf{s})\chi_s. \quad (6.30)$$

The vector $\mathbf{q}$ is *not* a unit vector but has the magnitude

$$q=[1-(\mathbf{e}\cdot\kappa)^2]^{\frac{1}{2}}. \quad (6.31)$$

It is perpendicular to $\mathbf{e}$ and has a projection on κ equal to $q^2\leqq 1$.

The scattering by a single ion is now described by considering the flux associated with the wave function. Thus

$$\mathbf{F}_{sc}=r^{-2}[(C+2D\mathbf{q}\cdot\mathbf{s})^*\chi_s^*] \times[(C+2D\mathbf{q}\cdot\mathbf{s})\chi_s]. \quad (6.32)$$

To obtain the total scattering cross section, (6.32) must be summed over the neutron spin coordinate. Using the hermitian property of $\mathbf{s}$ and the relation

$$(\mathbf{q}\cdot\mathbf{s})(\mathbf{q}\cdot\mathbf{s})=\tfrac{1}{4}q^2 \quad (6.321)$$

we find

$$\sum_{\text{spin}} \mathbf{F}_{sc}=r^{-2}[C^2+q^2D^2+\sum_{\text{spin}} \chi_s^*4CD\mathbf{q}\cdot\mathbf{s}\chi_s]. \quad (6.33)$$

The corresponding differential cross section for scattering into a solid angle $d\Omega$ is then

$$d\Phi=[C^2+D^2q^2+\sum_{\text{spin}} 4CD\chi_s^*\mathbf{q}\cdot\mathbf{s}\chi_s]d\Omega. \quad (6.34)$$

Here, for the first time, the scattering in a given direction depends upon the initial spin state of a neutron. It is remarkable that the distinguished direction is not characterized by the direction of the ionic spin alone, but rather by the vector $\mathbf{q}$ as defined by (6.22).

For an unpolarized incident beam the spin of the neutron has no preferred axis. The last term on the right side of (6.34) which involves the matrix elements $(s|\mathbf{s}|s)$ linearly, therefore vanishes and the differential cross section becomes

$$d\Phi=(C^2+D^2q^2)d\Omega. \quad (6.40)$$

Eq. (6.40) expresses the fact that as far as the total scattering is concerned nuclear and magnetic scattering of an unpolarized beam superpose their intensity.

For an *unmagnetized* medium we must average (6.32) and (6.34) over all directions of $\varkappa$ which gives

$$q_{av}^2=\tfrac{2}{3}. \tag{6.41}$$

If we pass from an unmagnetized to a completely magnetized state of the medium, the differential cross section $d\Phi$ given by (6.34) will increase or decrease from its average value

$$(C^2+\tfrac{2}{3}D^2)d\Omega, \tag{6.42}$$

depending upon the direction of scattering. It will become a maximum for $q=1$, i.e., $\mathbf{e}$ perpendicular to $\varkappa$. It will be a minimum for $q=0$, i.e., $\mathbf{e}$ parallel to $\varkappa$. The vector $\mathbf{e}$ lies in the plane defined by the directions of incidence and scattering, $\mathbf{k}$ and $\mathbf{k}'$, and is perpendicular to $\mathbf{k}$ for scattering through small angles. Thus, the first case can be realized for small angle scattering if the medium is magnetized transversely, perpendicular to the plane defined by $\mathbf{k}'$ and $\mathbf{k}$; the second case if the medium is transversely magnetized in the plane of $\mathbf{k}'$ and $\mathbf{k}$.

If the incident beam is completely polarized in an arbitrary direction defined by a unit vector $\boldsymbol{\lambda}$ we have to proceed as follows. We use the spin wave functions which characterize states with a neutron spin parallel to $\boldsymbol{\lambda}$ and obtain

$$2\sum_{\text{spin}}\chi_s^*(\mathbf{s})\chi_s=2(s|\mathbf{s}|s)=\boldsymbol{\lambda}. \tag{6.43}$$

This result is, of course, independent of the direction along which we analyze the spin. Eq. (6.34) now takes on the form

$$d\Phi=[C^2+D^2q^2+2CD\mathbf{q}\cdot\boldsymbol{\lambda}]d\Omega. \tag{6.5}$$

When $\mathbf{q}$ is kept fixed, the cross section obviously becomes a maximum for $\boldsymbol{\lambda}$ parallel to $\mathbf{q}$ if the amplitudes C and D have the same sign, and a minimum if $\boldsymbol{\lambda}$ is antiparallel to $\mathbf{q}$. If C and D have opposite signs, the behavior is just reversed. In the first case discussed in the previous paragraph, $\mathbf{e}\cdot\boldsymbol{\varkappa}=0$ $\mathbf{q}=-\boldsymbol{\varkappa}$ and so is antiparallel to $\varkappa$ and of absolute magnitude unity. In this case the greatest difference of scattering from the parallel and antiparallel polarization states is obtained. The second case mentioned above $\mathbf{e}\cdot\boldsymbol{\varkappa}=1$, leads to $q=0$ and therefore to the absence of any magnetic scattering. All polarization states of the neutron are then of course scattered alike. It must be kept in mind that according to its definition $\mathbf{q}$ depends upon the scattering angle and *the azimuth*. It does not therefore represent a fixed direction even for a constant scattering angle. Relations between $\mathbf{q}$ and $\boldsymbol{\varkappa}$ therefore hold true only for special scattering angle and azimuth. If, for example the direction of polarization lies along $\mathbf{q}$, $d\Phi$ becomes a perfect square, $d\Phi=(C\pm Dq)^2d\Omega$ in agreement with Bloch's result. But this special expression for the differential cross section cannot be integrated over all angles of scattering for which purpose recourse must be had to the generally valid relation (6.34).

It is interesting to observe that the form factor which becomes important when $d\Phi$ is integrated over all angles has a double influence. On one hand it reduces the total scattering, and on the other it changes the influence of magnetization on the total scattering. Taking for example, as a crude approximation for illustrative purposes, $F=1$ inside a cone of scattering directions making an angle θ_0 with the incident direction, and $F=0$ outside this cone, one obtains for the integrated cross section for an unpolarized beam the expression

$$\sigma=4\pi C^2+\pi D^2\eta[2+\eta-\varkappa_z^2(3\eta-2)]. \tag{6.51}$$

Here the direction of incidence is taken as the z axis and η stands for $\sin^2(\theta_0/2)$. The cross section for an unmagnetized medium is obtained by averaging over $\varkappa$

$$\sigma_{\text{unmag}}=4\pi C^2+8\pi D^2\eta/3. \tag{6.52}$$

The change in scattering, due to magnetization of the medium is given by

$$\sigma-\sigma_{\text{unmag}}=\pi D^2\eta(3\eta-2)(\tfrac{1}{3}-\varkappa_z^2). \tag{6.53}$$

Equation (6.32) allows us to determine the polarization of the scattered neutrons. Using the spin functions of Eq. (3.91) along an arbitrarily chosen z axis we find by substitution into (6.32) that

$$\begin{aligned}\mathbf{F}_{sc}=r^{-2}\{&[(C+Dq_z)^2|a|^2\\&+D^2(q^2-q_z^2)|b|^2+D(C+Dq_z)\\&\times(a^*b(q_x-iq_y)+ab^*(q_x+iq_y))]\alpha^*\alpha\\&+[(C-Dq_z)^2|b|^2+D^2(q^2-q_z^2)|a|^2\\&+D(C-Dq_z)(a^*b(q_x-iq_y)\\&+ab^*(q_x+iq_y)]\beta^*\beta\}.\end{aligned} \tag{6.60}$$

If we express a and b in terms of the polarization angles θ, ϕ and let $\boldsymbol{\lambda}$ be a unit vector along the direction of polarization, we find

$$a^*b(q_x-iq_y)+ab^*(q_x+iq_y)$$
$$=2\cos\theta/2\sin\theta/2(q_x\cos\phi+q_y\sin\phi)$$
$$=\boldsymbol{\lambda}\cdot\mathbf{q}-q_z(|a|^2-|b|^2). \quad (6.61)$$

The coefficients of $\alpha^*\alpha$ and $\beta^*\beta$ become

$$N_\alpha=r^{-2}[C^2|a|^2+D^2q^2|b|^2$$
$$+CDq_z+D(C+Dq_z)\boldsymbol{\lambda}\cdot\mathbf{q}], \quad (6.62)$$
$$N_\beta=r^{-2}[C^2|b|^2+D^2q^2|a|^2$$
$$-CDq_z+D(C-Dq_z)\boldsymbol{\lambda}\cdot\mathbf{q}]. \quad (6.63)$$

The sum $N_\alpha+N_\beta$ leads at once to (6.5). The polarization of a scattered beam defined by

$$P=(N_\alpha-N_\beta)(N_\alpha+N_\beta)^{-1} \quad (6.64)$$

now becomes equal to

$$P_{\lambda'}=\frac{(C^2-D^2q^2)\boldsymbol{\lambda}\cdot\boldsymbol{\lambda}'+2CD\boldsymbol{\lambda}'\cdot\mathbf{q}+2D^2(\boldsymbol{\lambda}\cdot\mathbf{q})(\boldsymbol{\lambda}'\cdot\mathbf{q})}{C^2+D^2q^2+2CD\boldsymbol{\lambda}\cdot\mathbf{q}}, \quad (6.65)$$

where $\boldsymbol{\lambda}'$ denotes the axis along which the spin is analyzed. If the original polarization is parallel to $\mathbf{q}$, $P_{\lambda'}$ becomes equal to $\boldsymbol{\lambda}\cdot\boldsymbol{\lambda}'$ which shows that the scattering *in this exceptional case* leaves the polarization unaltered. In all other cases the direction and amount of polarization are altered. Of special interest is the case of an initially unpolarized beam. Here it is necessary to average N_α and N_β over the incident polarization direction

$$(N_\alpha)_{av}=r^{-2}[\tfrac{1}{2}(C^2+D^2q^2)+CD\boldsymbol{\lambda}'\cdot\mathbf{q}],$$
$$(N_\beta)_{av}=r^{-2}[\tfrac{1}{2}(C^2+D^2q^2)-CD\boldsymbol{\lambda}'\cdot\mathbf{q}]. \quad (6.66)$$

Thus

$$(P_{\lambda'})_{av}=\frac{2CD\boldsymbol{\lambda}'\cdot q}{C^2+D^2q^2}=\frac{2\boldsymbol{\lambda}'\cdot\mathbf{q}}{q}\left[\frac{C}{Dq}+\frac{Dq}{C}\right]^{-1}. \quad (6.67)$$

The polarization can be complete only if $C=Dq$. It is a symmetrical function of the ratios C/Dq and Dq/C and becomes small whenever either of these quantities is large.

If we want to study intensity and polarization of a transmitted beam, we must average (6.60) and (6.67) over all angles of scattering. The results would consist of so lengthy formulae that we limit ourselves to the discussion of the cross section in the special case of a transverse field, i.e., $\mathbf{k}\cdot\boldsymbol{\kappa}=0$. From the previously mentioned crude approximation for F^1, we find

$$\sigma_{\lambda'}=\pi\{\tfrac{1}{2}[4C^2+D^2\eta(2+\eta)]$$
$$+\tfrac{1}{2}[4C^2-D^2\eta(2+\eta)]\boldsymbol{\lambda}\cdot\boldsymbol{\lambda}'$$
$$-CD\eta(2+\eta)(\boldsymbol{\lambda}+\boldsymbol{\lambda}')\cdot\boldsymbol{\kappa}$$
$$+D^2\eta[(1+\eta+\tfrac{1}{3}\eta^2)(\boldsymbol{\lambda}\cdot\boldsymbol{\kappa})(\boldsymbol{\lambda}'\cdot\boldsymbol{\kappa})$$
$$+\tfrac{1}{2}(-1+\eta+\tfrac{1}{3}\eta^2)\boldsymbol{\lambda}\cdot\boldsymbol{\lambda}'+\tfrac{1}{2}(-1+3\eta-5\eta^2/3)$$
$$\times(\boldsymbol{\lambda}\cdot\mathbf{k}/k)(\boldsymbol{\lambda}'\cdot\mathbf{k}/k)]\}. \quad (6.71)$$

The total cross section for scattering into both polarization states $\boldsymbol{\lambda}'$ and $-\boldsymbol{\lambda}'$ is obtained by adding $\sigma_{\lambda'}$ and $\sigma_{-\lambda'}$

$$\sigma=\sigma_{\lambda'}+\sigma_{-\lambda'}=\pi[4C^2+D^2\eta(2+\eta)$$
$$-2CD\eta(2+\eta)\boldsymbol{\lambda}\cdot\boldsymbol{\kappa}]. \quad (6.72)$$

The result (6.72) can also be obtained by integrating (6.5) over all angles of scattering.

So far our attention has been confined to single scattering processes. The treatment of double (or multiple) scattering is only possible for very restricted cases. It is easily seen that large polarization effects may be expected in two successive single scattering processes. If the first scattering occurs under the small forward angle and such an azimuth that $\mathbf{e}\cdot\boldsymbol{\kappa}=0$, the scattered beam according to (6.65) is almost completely polarized if we assume for illustrative purposes and probably as an approximation to the case of Fe that $C=2D$. If $\mathbf{e}\cdot\boldsymbol{\kappa}=0$ for the second scattering also and if the polarization is parallel or antiparallel to the magnetic field at the second scatterer, the cross sections become

$$d\Phi=(C+D)^2d\Omega \quad (6.731)$$

or

$$d\Phi=(C-D)^2d\Omega, \quad (6.732)$$

respectively; consequently reversal of the polarization state relative to the magnetic field of the second scatterer can cause the intensity to change by a factor of 9 in our assumed case.

To obtain a precise estimate it is necessary to treat the double scattering *without averaging* over the initial polarization state until the end ("interference of amplitudes"). By omitting factors referring to the space coordinates the spin wave function of a twice scattered neutron becomes

$$\psi_{sc}=(C+2D\mathbf{q}_1\cdot\mathbf{s})(C+2D\mathbf{q}_2\cdot\mathbf{s})\chi_s. \quad (6.74)$$

Constructing then the flux as before, we find for an initially unpolarized beam

$$\sum_{spin} F_{sc}=\text{constant}\times[C^4+D^4q_1^2q_2^2 + C^2D^2(2\mathbf{q}_1\cdot\mathbf{q}_2+|\mathbf{q}_1+\mathbf{q}_2|^2)]. \quad (6.75)$$

For the conditions mentioned above $q_1=q_2=1$ and q_1 is parallel or antiparallel to q_2. The ratio of intensities then becomes 41 : 9.

In his treatment of double scattering Schwinger[3] used the conditions $\mathbf{e}_1\cdot\boldsymbol{\kappa}_1=\mathbf{e}_2\cdot\boldsymbol{\kappa}_2=0$ to simplify his formulae and added the remark that they describe a convenient set of experimental conditions. It deserves mentioning that these conditions give rise to the maximum effect as the magnetic scattering is then greatest. Furthermore it should be noted that the theoretical treatment is strictly correct only under these same conditions. In all other cases the scattered neutrons are not polarized parallel to the magnetic field, and there results a precession of the spin about the direction of the field as the neutron passes from the first to the second scatterer. Only the component of the spin parallel to the field is preserved; the perpendicular components average to zero because of the varying neutron velocities and different distances between points in the two scatterers. The polarization at the second scatterer is thereby reduced. In our discussion of polarization and double scattering these precessions must be taken into account, a task to which we now address ourselves.

The wave equation of a neutron moving in a constant magnetic field is

$$\left\{-\frac{h^2}{8\pi^2M_0}\nabla^2+\gamma\frac{eh}{2\pi M_0c}\mathbf{s}\cdot\mathbf{H}-E\right\}\psi=0. \quad (6.80)$$

By use of spin functions α and β representing states of spin parallel and antiparallel $\mathbf{H}$, this equation has the general solution

$$\psi=\exp(i\mathbf{k}\cdot\mathbf{r})\left\{a\alpha\exp\left[\frac{i\omega}{2v}\left(\frac{\mathbf{k}\cdot\mathbf{r}}{k}\right)\right] + b\beta\exp\left[-\frac{i\omega}{2v}\left(\frac{\mathbf{k}\cdot\mathbf{r}}{k}\right)\right]\right\}, \quad (6.81)$$

$$\omega=\gamma(eH/M_0c). \quad (6.811)$$

Here $\mathbf{H}$ is the homogeneous magnetic field in the ferromagnet which we have omitted from our previous considerations since the scattering is caused entirely by the atomic fields. We assume the field to be either constant or to change so abruptly that the passage of the neutrons through the regions of inhomogeneity can be treated as a quasi-instantaneous process.

According to (6.81) the two components of the spin function of the neutron

$$\chi_s=a\alpha+b\beta \quad (6.812)$$

have phase factors which vary from point to point along the trajectory of the neutron. This result can be put into a more convenient form by means of the operators $\frac{1}{2}(1+2\boldsymbol{\kappa}\cdot\mathbf{s})$ where $\boldsymbol{\kappa}$ is, as usual, a unit vector parallel to $\mathbf{H}$. These operators obviously have the following properties

$$\begin{aligned}&\tfrac{1}{2}(1+2\boldsymbol{\kappa}\cdot\mathbf{s})\alpha=\alpha, \quad \tfrac{1}{2}(1-2\boldsymbol{\kappa}\cdot\mathbf{s})\beta=\beta,\\ &\tfrac{1}{2}(1+2\boldsymbol{\kappa}\cdot\mathbf{s})\beta=0, \quad \tfrac{1}{2}(1-2\boldsymbol{\kappa}\cdot\mathbf{s})\alpha=0.\end{aligned} \quad (6.82)$$

Hence

$$\psi=\exp(i\mathbf{k}\cdot\mathbf{r})\left\{\tfrac{1}{2}(1+2\boldsymbol{\kappa}\cdot\mathbf{s})\exp\left[\frac{i\omega}{2v}\left(\frac{\mathbf{k}\cdot\mathbf{r}}{k}\right)\right] \times\tfrac{1}{2}(1-2\boldsymbol{\kappa}\cdot\mathbf{s})\exp\left[-\frac{i\omega}{2v}\left(\frac{\mathbf{k}\cdot\mathbf{r}}{k}\right)\right]\right\}(a\alpha+b\beta). \quad (6.83)$$

If χ_s' is the spin function of the neutron at the point $\mathbf{r}_1$ of its trajectory and χ_s its spin function in another point $\mathbf{r}_2$ then

$$\chi_s'=\left[\cos\frac{\omega r}{2v}+2i\boldsymbol{\kappa}\cdot\mathbf{s}\sin\frac{\omega r}{2v}\right]\chi_s, \quad (6.84)$$

where r denotes the distance along the trajectory between the points $\mathbf{r}_1$ and $\mathbf{r}_2$.

If now χ_s denotes the spin function of the incident neutron at the location of the scatterer,

the scattered wave is given by

$$\psi_{sc}=\left(\frac{2\pi M_0}{hk}\right)^{\frac{1}{2}}\frac{e^{ikr}}{r}\left[\cos\frac{\omega r}{2v}+2i\boldsymbol{\kappa}\cdot\mathbf{s}\sin\frac{\omega r}{2v}\right]\times(C+2D\mathbf{q}\cdot\mathbf{s})\chi_s. \quad (6.85)$$

The polarization of the scattered wave can be studied exactly as before; the general result is of course considerably more complicated than (6.65). Because the neutrons have traveled over varying distances with varying velocities, it is permissible to put

$$\cos^2\omega r/2v=\sin^2\omega r/2v=\tfrac{1}{2}, \quad (6.851)$$

$$\cos\omega r/2v\cdot\sin\omega r/2v=0. \quad (6.852)$$

By taking the important special case $\mathbf{e}\cdot\boldsymbol{\kappa}=0$, the general equation for the polarization reduces to

$$P_{\lambda'}=\boldsymbol{\lambda}'\cdot\boldsymbol{\kappa}\frac{(C^2+D^2)\boldsymbol{\lambda}\cdot\boldsymbol{\kappa}-2CD}{C^2+D^2+2CD\boldsymbol{\lambda}\cdot\boldsymbol{\kappa}}. \quad (6.86)$$

The polarization $(P_{\lambda'})_{av}$ for an initially unpolarized beam is then still given by (6.67) with $\mathbf{q}=-\boldsymbol{\kappa}$; this agrees with our expectation that the polarization is unaffected if it is parallel to $\mathbf{H}$.

In the double-scattering problem only the effect of the magnetic field on the neutron as it traverses the distance r between the scatterers is of importance because we are interested in the total flux originating from the second scatterer. Hence we may write for the spin function of the doubly scattered wave,

$$\psi_{sc}=\text{const.}\times[C+2D\mathbf{q}_2\cdot\mathbf{s}]\times[\cos(\omega r/2v)+2i\boldsymbol{\kappa}\cdot\mathbf{s}\sin(\omega r/2v)\times[C+2D\mathbf{q}_1\cdot\mathbf{s}]\chi_s. \quad (6.90)$$

The flux is now computed in the familiar way. Again we find that the result in the important case described by $\mathbf{e}_1\cdot\boldsymbol{\kappa}_1=\mathbf{e}_2\cdot\boldsymbol{\kappa}_2=0$ reduces to that previously given.

Only a few words need to be said about the modifications which are introduced if the ionic spin can change its orientation during the collision. Such transitions are very unlikely in Fe, Co, or Ni since the work required to change the spin state is approximately equal to zJ where J is the well-known exchange integral and z the number of neighbors of every ion. The value of zJ lies for the substances mentioned in the neighborhood of a fraction of a volt. Only in a medium with a very low Curie temperature can such transitions be of importance. To treat this problem we construct the density of scattered neutrons $|\psi_{in}|^2$ from (4.4). Dividing the result by the density of incident neutrons and omitting the term corresponding to elastic scattering, $M'=M$, we have

$$I(\text{inelastic})/I_{in}=(2e^2\gamma/mc^2)^2\times\sum_{s'}|(M's'|\mathfrak{M}|Ms)F'|^2. \quad (6.91)$$

As the ion is initially parallel to field, $M=S$ and $M'=S-1$. The matrix element of $\mathbf{S}$ for this transition is given by the well-known formulae

$$\begin{aligned}(S-1|S_x+iS_y|S)&=0,\\(S-1|S_x-iS_y|S)&=(2S)^{\frac{1}{2}},\\(S-1|S_z|S)&=0.\end{aligned} \quad (6.92)$$

By use of (4.4), and substitution of (6.92) into (6.91) we obtain

$$\begin{aligned}&I(\text{inelastic})/I_{in}\\&=(e^2\gamma F'/mc^2)^2 2S\sum_{s'}|(s'|(\mathbf{e}\cdot\mathbf{s})(e_x+ie_y)-s_x-is_y|s)|^2\\&=(e^2\gamma F'/mc^2)2S\sum_{spin}\chi_s^*|(\mathbf{e}\cdot\mathbf{s})(e_x+ie_y)-s_x-is_y|^2\chi_s.\end{aligned} \quad (6.93)$$

By using the familiar commutation relations, $\mathbf{s}\times\mathbf{s}=i/2\mathbf{s}$, and the fact $s_x^2=s_y^2=s_z^2=\frac{1}{4}$, this reduces to

$$I(\text{inelastic})/I_{in}=\left(\frac{e^2\gamma F'}{mc^2}\right)^2\frac{S}{2}\{1+(\mathbf{e}\cdot\boldsymbol{\kappa})^2-2\sum_{spin}\chi_s^*(\mathbf{e}\cdot\boldsymbol{\kappa})(\mathbf{e}\cdot\mathbf{s})\chi_s\}. \quad (6.94)$$

If the incident beam is unpolarized, the sum in (6.94) vanishes. The intensity becomes a maximum for $\mathbf{e}\cdot\boldsymbol{\kappa}=1$; this condition implies that the elastic magnetic scattering treated previously becomes zero (cf. p. 911). If the incident beam is completely polarized along the direction $\boldsymbol{\lambda}$, the term under summation becomes $-(\mathbf{e}\cdot\boldsymbol{\kappa})(\mathbf{e}\cdot\boldsymbol{\lambda})$.

Consequently states which are polarized antiparallel to **e** will be scattered most; the scattered neutrons will therefore be partially polarized in this direction. The details of the state of polarization can be determined analogously to the cases discussed before.

In dealing with ferromagnetic media, it should finally be remembered that we do not possess a satisfactory theory of the magnetic moment of the metals below the Curie point. The magnetic moments obtained through saturation at low temperatures do not agree at all with the magnetic moments above the Curie point or with the spin which has to be ascribed to the ion for the purpose of accounting theoretically for the saturation curve. These discrepancies have led to the well-known attempts to explain the behavior of the ferromagnetic metal by ascribing several states to the atom (ion) in the metal. The discrepancy becomes the more important since, in no case, does the magnetic moment of metallic Fe approach that of the ions Fe^{+++} or Fe^{++} as observed in salts. It appears therefore that the model for a ferromagnetic medium so far used in the case of neutron scattering may well require drastic modifications. This can affect the neutron scattering principally in two ways. The atomic domain giving rise to the magnetic moment may not be confined to the *d* shell which would reduce the scattering on account of the form factor. There may also be several ionic levels of different spins involved which would permit inelastic scattering of the neutron. Finally there may occur a considerable amount of quenching of the spin current which is indicated by the experimental fact that the gyromagnetic ratio lies only close to two but differs from it measurably.

VII. The Form Factor for Elastic Collisions

We have seen in IV that the matrix element which determines the transition in the scattering process is essentially defined

$$\mathbf{P}=\sum_e \exp\left[i\mathbf{r}\cdot(\mathbf{k}-\mathbf{k}')\right]\mathbf{s}_e. \qquad (4.08)$$

To evaluate (4.08) we have to know the energy change in the transition as well as the spin density distribution in the initial and final state.

We shall be concerned in this paragraph with elastic scattering only. The numerous difficulties arising in the case of inelastic transitions are qualitatively discussed in Section VIII.

Assuming therefore the same spin distribution for the initial and final state we have to make more or less arbitrary assumptions about the spin density. It is reasonable to take the spin density proportional to the charge density of the outer electrons (cf. 4.042). The charge density on the other hand can be estimated either from semi-theoretical expressions given by the Hartree distribution or with the aid of simple assumptions treating the problem as quasi-hydrogenic.

In the case of greatest interest (Mn^{++}, Fe^{+++}; $j=S=5/2$) we know that the five extra electrons are in a $3d$-state and that the whole distribution is spherically symmetrical. It therefore does not seem to be without interest to represent the charge distribution with the aid of the hydrogenic wave function

$$\psi=Cr^2e^{-\alpha r}, \qquad (7.0)$$

where α is in a simple way connected with the effective nuclear charge Z_{eff} or the ionization potential. The most probable radius r_0 is defined by

$$(d/dr)(r^6e^{-2\alpha r})=0, \qquad (7.01)$$

$$\alpha=3/r_0. \qquad (7.02)$$

It can also be expressed in the form

$$\alpha=Z_{eff}/3a_0, \qquad (7.03)$$

where $a_0=0.52$A stands for the Bohr radius of the ground state of hydrogen. Since for room-temperature neutrons the wave-length λ is approximately 1.45A, the influence of the form factor will be considerable since Z_{eff} will lie between 3 and 6 and $2\pi r_0/\lambda$ therefore will be of the order of magnitude of one.

To find the differential form factor, i.e., the factor with which the cross section for scattering under the angle ϑ has to be multiplied we have to evaluate the integral

$$F^1_{diff}=A\int\int \exp\left[i(\mathbf{k}-\mathbf{k}')\cdot\mathbf{r}-2\alpha r\right] \times r^6\sin\theta\, dr\, d\theta \qquad (7.1)$$

and to normalize the constant A in such a form

that F_{diff} approaches unity for very small values of k. F_{diff} is a function of the scattering angle ϑ alone. Choosing the polar axis along the direction of $\mathbf{k}'-\mathbf{k}$ and introducing spherical coordinates we find for F_{diff} the form

$$F^{\frac{1}{2}}_{diff}=\int_0^\infty r^6 e^{-2\alpha r}dr \times\int_0^\pi \exp\left[2ik\sin\tfrac{1}{2}\vartheta r\cos\theta\right]\sin\theta d\theta, \quad (7.2)$$

which can be immediately evaluated. We so obtain

$$F_{diff}(\vartheta)=\frac{\left[1-\frac{10}{3}\left(\frac{k\sin\frac{1}{2}\vartheta}{\alpha}\right)^2+\left(\frac{k\sin\frac{1}{2}\vartheta}{\alpha}\right)^4\right]^2}{\left[1+\left(\frac{k\sin\frac{1}{2}\vartheta}{\alpha}\right)^2\right]^{12}}. \quad (7.3)$$

The integral form factor F_{int} follows from (7.3) by integration over ϑ. A trivial but lengthy procedure leads to

$$F_{int}=I_0+I_1+I_2+I_3+I_4+I_5, \quad (7.40)$$

$$I_0=\frac{4}{77}\left(\frac{\alpha}{k}\right)^2, \quad (7.41)$$

$$I_1=-\left(\frac{\alpha}{k}\right)^2\frac{1-\frac{20}{3}\left(\frac{k}{\alpha}\right)^2+\left(\frac{118}{9}\right)\left(\frac{k}{\alpha}\right)^4-\frac{20}{3}\left(\frac{k}{\alpha}\right)^6+\left(\frac{k}{\alpha}\right)^8}{11\cdot\left[1+\frac{k^2}{\alpha^2}\right]^{11}}, \quad (7.42)$$

$$I_2=\frac{\alpha^2}{k^2}\frac{\frac{20}{3}-\frac{236}{9}\left(\frac{k}{\alpha}\right)^2+20\left(\frac{k}{\alpha}\right)^4-4\left(\frac{k}{\alpha}\right)^6}{11\cdot 10\left[1+\left(\frac{k}{\alpha}\right)^2\right]^{10}}, \quad (7.43)$$

$$I_3=-\frac{\alpha^2}{k^2}\frac{\frac{236}{9}-40\left(\frac{k}{\alpha}\right)^2+12\left(\frac{k}{\alpha}\right)^4}{11\cdot 10\cdot 9\left[1+\left(\frac{k}{\alpha}\right)^2\right]^9}, \quad (7.44)$$

$$I_4=\frac{\alpha^2}{k^2}\frac{40-24(k/\alpha)^2}{11\cdot 10\cdot 9\cdot 8[1+(k/\alpha)^2]^8}, \quad (7.45)$$

$$I_5=-\frac{\alpha^2}{k^2}\frac{24}{11\cdot 10\cdot 9\cdot 8\cdot 7[1+(k/\alpha)^2]^7}. \quad (7.46)$$

It seems noteworthy that the differential form factor F_{diff} is not a monotonic function of the angle; it has two zeros which are due to the diffraction from the spherical spin distribution and which are located at the two angles

$$\sin\tfrac{1}{2}\vartheta_1=\alpha/k3^{\frac{1}{2}}, \quad (7.51)$$

$$\sin\tfrac{1}{2}\vartheta_2=3^{\frac{1}{2}}\alpha/k. \quad (7.52)$$

The first zero ϑ_1 makes the expression

$$k\sin\tfrac{1}{2}\vartheta/\alpha$$

equal to $3^{\frac{1}{2}}/3$. The denominator in (7.3) has not yet grown too large so that this zero is of physical interest. The second zero if reached at all, is without significance since the form factor is already unobservably small. The zeros shift with increasing wave-length towards larger angles; their presence is of particular importance for comparatively short wave-length since it then diminishes the scattering under small angles which otherwise is of greatest importance. It is also clear by inspection that for any value of Z_{eff} between 3 and 6, the scattering of room temperature neutrons, is negligible for angles larger than say, 60°.

In the expression for the integral form factor only the term I_0 which does not contain denominators contributes in most cases of practical interest. We see from (7.40) that the total scattering is inversely proportional to the absolute neutron temperature provided that α/k does not become so large that the terms with the denominators in (7.42–7.46) must be taken into account. But even for $\alpha/k\sim 2$ these terms would give only a small correction. Furthermore, we see that in our model the integral form factor becomes proportional to Z_{eff}^2. We assume for the purpose of illustration that Z_{eff} equals 6 which probably overrates the screening effect of equivalent electrons and obtain for F_{int} with $\lambda\sim 1.45$A

$$F_{int}\sim 1/23.$$

The exact numerical value of the integral form factor as well as the occurrence of diffraction

zeros in the differential form factor are of course dependent upon the special model we have chosen; it seems plausible on the other hand that the general features of the angular dependence as well as the big reduction in total scattering is not too badly represented by these calculations. They also allow us to understand why in the case of backwards scattering of neutrons from MnS Whitaker[7] was unable to find any indication of additional magnetic scattering.

VIII. Coupled Scattering Systems

The treatment of neutron-scattering by coupled systems can be carried out quantitatively only in a few special cases. The solution of the more general problem appears to be extremely laborious due to great mathematical difficulties.

Coupling may occur between the spins of the individual ions, between the electronic and nuclear spins of an atom or between spins of the nuclei in a homonuclear molecule. Since the nuclear coupling is most easily considered, we discuss it first.

The coherent part of nuclear scattering (cf. Section III) arises from the terms in (3.51) which do not contain the nuclear spin. It is therefore always present and remains coherent independently of the coupling between the nuclear spin states. Furthermore, in all attainable experimental arrangements the nuclear spin will have no preferred axis; our previous arguments therefore show that this term will give the entire coherent scattering. The additional scattering will be inelastic because of the energy separations introduced by the coupling. If the coupling is due to atomic electrons (hyperfine structure), then the energy separations are, in every case, very small as compared with the neutron energy. The energy change will therefore have no appreciable effect on the atomic form factor. For the same reason, the different states of the scattering system will be equally populated. An obvious application of the principle of spectroscopic stability shows us that the total scattering is under these conditions unaltered by the coupling. Similarly in the homonuclear molecules, the coupling forces are in general too small to have any influence on the scattering. The only important exception to this rule can be found in the case of parahydrogen to which Teller[8] was the first to call attention. Here the coupling energy equals the energy separation of the neighboring rotational states of the molecule. If the neutron energy is less than the energy necessary to excite the first rotational state, then inelastic collisions with parahydrogen in its ground state become energetically impossible. Since the ground state is nondegenerate, only the coherent scattering remains. The striking transparency of parahydrogen for very slow neutrons thus illustrates the marked effect previously mentioned (cf. Section III) which the spin degeneracy may have upon coherent nuclear scattering.

The problem of the spin coupling of neighboring ions in a salt presents difficulties of a different order of magnitude essentially for two reasons: the energy changes due to the exchange forces are very much larger than those due to nuclear coupling; furthermore, the problem becomes a many-body problem since the spins of all ions have to be taken into account simultaneously. It is customary to write for the interaction function between the spins the expression[9]

$$H = -2J\sum \mathbf{s}_P \cdot \mathbf{s}_q, \tag{8.0}$$

where J is the Heisenberg exchange integral and $\mathbf{s}_P$ is the spin of the P'th ion. The summation extends as a rule, over all neighboring ion pairs. If J is positive, then states of large resultant spin of the crystal are most stable (ferromagnetic case) whereas a negative value of J makes states of small resultant spin energetically most stable (antiferromagnetic case). The resultant crystalline spin $\mathbf{S}'$ can be used as one quantum number to describe the stationary states of lattice since it commutes with the interaction function H.

The discussion branches now along two ways. The ferromagnetic case below the Curie point has been treated before. The ferromagnetic case above the Curie point and the antiferromagnetic case can be treated together for our present purposes.

The presence of the spin exchange forces had manifested itself previously in the deviation of the paramagnetic susceptibility of most salts of

[7] M. D. Whitaker, Phys. Rev. **52**, 384 (1937).

[8] E. Teller, Phys. Rev. **49**, 421 (1936).

[9] J. H. Van Vleck, *Theory of Electricity and Magnetic Susceptibilities*, p. 328.

the iron group from the simple Curie law. To determine theoretically the paramagnetic permeability it is necessary to know the energies of the $(2S+1)^f$ states into which the originally $(2S+1)^f$ times degenerate state of the crystal of f ions splits up in virtue of the spin coupling forces. It is, of course, still possible and will actually be the case that some of these states still retain their energy degeneracy. We encounter here a problem which is well known from the theory of ferromagnetism and is at present anything but solved. We have to be satisfied to know for the moment the number of states $\omega(S')$ which belong to a total resultant spin vector $\mathbf{S}'$ and to possess some information about the *average* energy values $\bar{W}(S')$ for levels belonging to a total resultant spin S. We quote the following well-known relations[9]

$$\bar{W}(S')=\frac{-zJ}{f-1}[S'(S'+1)-fS'(S'+1)], \quad (8.01)$$

$$\langle[W(S')-\bar{W}(S')]^2\rangle_{\text{av}} = zJ^2\frac{(f^2-4S'^2)(3f^2-4S'^2)}{f^3} \quad (8.02)$$

(z = number of neighbors per atom.)

It is clear from (8.01) that the average energy for small values of the resultant spin is small and the difference between the average energies of two groups of levels with neighboring resultant spins is quite negligible for $W(S')-W(S'-1)=(2zJ/(f-1))S'$. On the other hand the "spread in energy" even of the levels belonging to $S'=0$ is considerable; namely, of the order of magnitude fJ.

For the purpose of calculating paramagnetic susceptibilities, it is customary and has been found to be a sufficient approximation, to ascribe to the levels of total spin S' a weight as determined by simple permutations and the energy $-(zJ/f)S'^2$. With these approximations one obtains for the magnetic susceptibility the following expressions

$$\chi=\left(\frac{eh}{4\pi mc}\right)^2\frac{4S(S+1)}{3k(T-T_c)}, \quad (8.11)$$

$$T_c=2zJS(S+1)/3k. \quad (8.12)$$

Here z denotes the number of neighbors possessed by each ion. It is clear that this statistical procedure is not at all rigorous; it seems to work for the determination of susceptibilities because in the presence of even weak magnetic fields the resultant spin is of the order αfS where α is a small number depending upon the external conditions. Still αfS is almost always very much larger than $f^{\frac{1}{2}}S$ which is a measure of the spin in the absence of an external magnetic field. We can sum up by stating that paramagnetic investigations do not lead very far in the study of the levels of a spin lattice.

Returning now to the scattering of neutrons in a spin lattice, we may write from equation

$$\psi_m^{(P)}=\left(\frac{2\pi M_0}{hk}\right)^{\frac{1}{2}}\left(\frac{2e^2\gamma}{mc^2}\right)\sum_{s'M'}\frac{e^{ik'r}}{r}\chi_{s'}\Omega_{M'}^{(P)} \times e^{i\delta_P}(s'M'|\mathfrak{M}|sM)_P F\times\Pi_l'\Omega_M^{(l)} \quad (8.20)$$

for the wave scattered from the P'th lattice point. Here the P'th atom is located at the position $\mathbf{r}_P$, which is contained in δ_P, the phase difference for waves scattered from this point. The Π_l' means a product of the spin functions of all the atoms but the P'th. The entire wave scattered by the lattice is then

$$\psi_m^{(P)}=\left(\frac{2\pi M_0}{hk}\right)^{\frac{1}{2}}\left(\frac{2e^2\gamma}{mc^2}\right)\sum_{Ps'}\frac{e^{ik'r}}{r}\chi_{s'}e^{i\delta_P} \times\sum_{MP'}(s'M'|\mathfrak{M}|sM)_P F^{\frac{1}{2}}\Pi\Omega_M^{(l)}\cdots \times\Omega_{M_{P-1}}^{(P-1)}\cdot\Omega_{M_P'}^{(P)}\cdot\Omega_{M_{P+1}}^{(P+1)}\cdots. \quad (8.21)$$

If we let L stand for the totality of lattice quantum numbers, thus replacing $M_1\cdots M_P\cdots$ by L and write Ω_L for the spin wave function of the entire lattice, we have

$$\psi_m=\left(\frac{2\pi M_0}{hk}\right)^{\frac{1}{2}}\left(\frac{2e^2\gamma}{mc^2}\right)\sum_{s'L'}\frac{e^{ik'r}}{r}\chi_{s'}\Omega_{L'} \times(s'L'/\sum_P e^{i\delta_P}\mathfrak{M}_P|sL)F^{\frac{1}{2}}. \quad (8.22)$$

Summing the density of scattered neutrons, $|\psi_m|^2$, over all spin variables and dividing the

result by the incident density, we have

$$I/I_{in}=r^{-2}(2e^2\gamma/mc^2)^2 \sum_{s'L'}|(s'L'|\sum_P e^{i\delta_P}\mathfrak{M}_P|sL)F^1|^2. \quad (8.30)$$

To obtain the complete result, we must average (8.30) over the temperature distribution among the lattice states.

If now the energy changes in all transitions were small so that the atomic form factors were the same for all transitions, then expression (8.30) becomes

$$I/I_{in}=r^{-2}(2e^2\gamma F^1/mc^2) \times(sL|\sum_{PP'} e^{i(\delta_P-\delta_{P'})}\mathfrak{M}_{P'}{}^*\mathfrak{M}_P|sL). \quad (8.31)$$

Here the interference between different ions can be neglected. We can furthermore put $(L|s_{xP}s_{yP}|L)=0$ since the total crystalline spin S' is always small compared with fS in paramagnetic substances. Eq. (8.31) thereby reduces to our previous result (5.2). Changes in the scattering formula can therefore only occur if in virtue of the spin coupling the transitions in the lattice are accompanied by energy changes large enough to alter substantially the form factor F. It should be remembered that almost all of the scattering is, strictly speaking, inelastic; the elastic transitions, $L=L'$ in (8.31) are proportional to terms of the type $|(L|s_z|L)|^2$. This expression is very small since the total crystalline spin lies in the neighborhood of zero.

If we now employ the approximation which we describe as being useful for the treatment of susceptibilities, then it can easily be seen that the scattering is uninfluenced by the spin coupling. This is due to the fact that as we learn from

$$W(S')-W(S'-1)=(2zJ/(f-1))S'\sim(2zJS/f^1)$$

whenever the crystalline spin is small. But only such transitions can occur in (8.31) because $\sum_P e^{i\delta_P}\mathfrak{M}_P$ has nonvanishing matrix components only between states for which $\Delta S'=\pm1, 0$. The energy change during the scattering process would thus be completely unobservable; the scattering from the crystal would be therefore, the same as that from an equal number of free ions.

Unfortunately we are not justified *a priori* to use the approximation as sketched. The splitting of the levels of low spin is in general so wide that energy differences which are quite comparable with the neutron energy must be expected to occur. There does not exist therefore any direct connection between the theory of magnetic susceptibilities and that for neutron scattering.

Relation (8.31) allows a further simplification if we neglect for a moment the interference terms which are without interest for us at the present stage of the discussion. Dropping the phase factors $e^{i(\delta_P-\delta_{P'})}$ we find

$$I_{sc}/I_{in}=r^{-2}(2e^2\gamma/mc^2)^2 \times\sum_{Ps'L'}|(s'L'|\mathfrak{M}_P|sL)F^1|^2. \quad (8.40)$$

Since now the spins are no longer distinguished by their position, we can write instead of

$$I_{sc}/I_{in}=r^{-2}(2e^2\gamma/mc^2)^2f \times\sum_{s'L'}|(s'L'|\mathfrak{M}_0|sL)F^1|^2. \quad (8.41)$$

Here $\mathfrak{M}_0$ refers to any of the ions in the lattice. If we now use the abbreviation

$$P(LL')=|(s'L'|\mathfrak{M}_0|sL)|^2 \div\sum_{L'}|(s'L'|\mathfrak{M}_0|sL)|^2, \quad (8.42)$$

then $P(LL')$ gives us, apart from the form factor, the probability that due to the collision, the lattice will change from the state L to the state L'. The problem of neutron scattering by lattice therefore consists in the determination of the matrix elements $P(LL')$ as a function of the energy difference between the initial and the final crystalline state. The form factor belonging to the transition $L\rightarrow L'$ may then be constructed and the distribution of energy changes for each collision determined. The simplification now achieved consists in the fact that (8.42) contains the spin coordinates of one ion only in the operator. Mathematical difficulties seem to us to prevent an immediate and direct attack even on the simplified problem.

The conditions in a saturated ferromagnetic medium which we have treated before are quite different. If the medium is close to saturation, the

elastic term, $L'=L$, in (8.22) gives the coherent scattering treated in Section VI. Since this scattering equals the fraction $S/(S+1)$ of the total scattering which is to be expected from a free ion of equal spin, the remaining terms cannot contribute more than the fraction S^{-1} of the coherent scattering. It is possible that a considerable amount of this scattering appears in transitions between states of the lattice having the same resultant spin. It would probably exhibit polarization phenomena which are similar to those discussed in Section VI. Quantitative estimates of this scattering face exactly the same difficulties as those outlined in the previous paragraph.

If the spin coupling should actually lead to considerable splitting of crystalline levels having equal total spin, then a remarkable phenomenon should become observable at the Curie point of ferromagnetic bodies. Since below the Curie point the ferromagnet should show the scattering given by (6.40) which is large and coherent, a marked decrease is to be expected if the ferromagnet becomes paramagnetic. Since the Curie temperatures of all ferromagnets lie appreciable above room temperature (exchange integral large), the energy changes in the paramagnetic state would become very appreciable and the accompanying form factors would cut down the scattering to a large extent. Particularly the scattering into forward angles should be strongly diminished. Absence of the effect just described should be interpreted in our opinion as information that the transitions occur mostly between levels of small energy difference, and that the wide fluctuation in the energy of levels with equal spin as given by (8.02) is due to a comparatively small number of levels with energies vastly different from the average.

IX. Experiments

The considerations of the last sections obviously suggest a number of experiments in the field. The purpose of such experiments can essentially be twofold. They can be arranged with the aim of obtaining information about the magnetic moment of the neutron, or they can be used to explore the magnetic structure of the scattering system provided that the magnetic moment of the neutron is known. Quantitative information about it therefore seems to be of paramount importance.

The determination of the magnetic moment of the neutron can be carried out by scattering experiments alone or by a combination of scattering experiments with outside fields which act upon the polarization state of neutron beams. The last type of experiment is the one carried out by Frisch, Von Halban and Koch.[10] In these experiments a beam of neutrons was partially polarized by allowing it to pass through a magnetized piece of iron. Upon leaving the ferromagnet the neutrons were exposed to a magnetic field which could be varied in magnitude and direction, and which changed the state of polarization by an amount dependent on the neutron's magnetic moment during the passage from the first ferromagnet to a second. To determine the angle through which the individual spins rotate it is necessary to know the time of passage, i.e., the velocity of the neutrons. The scattering by, or the transmission through, the second ferromagnet will show a maximum (minimum) for definite directions of polarization of the incident beam. It is obvious that by assuming a certain knowledge about the velocity of the neutron, the variation of the strength of the magnetic field will permit a change from maximum to minimum transmission and thereby obtain information about the magnetic moment of the neutron. The authors gave as the most probable value two nuclear magnetons for the magnitude of the magnetic moment of the neutron.

Unfortunately the effect observed is very small, though, according to the authors, beyond the experimental error. It seems that iron is as poor a polarizer as it is an analyzer since the change in scattering (transmission intensity) remains a fraction of a percent. Furthermore, we do not seem to be able to determine the neutron velocity with too great an accuracy which also has a detrimental influence on the quantitative reliability of the method described.

Turning now to pure scattering and transmission experiments, it may, perhaps, be pointed

[10] Frisch, Von Halban and Koch, Phys. Rev. **53**, 719 (1938).

out that the treatment of the scattering of a neutron by a *free* paramagnetic ion involves no uncertainties with the possible exception that the interaction between neutron and electron may not be wholly magnetic in origin. Furthermore, the scattering effects which are to be expected if the magnetic moment of the neutron is of the order of magnitude of one nuclear magneton can be very large (cf. (5.5)). Therefore, as previously stated, the simplest and most direct method of determining the neutron's moment seems, in our opinion, to be a scattering experiment with an appropriate paramagnetic salt. The salt selected should have a large magnetic moment, a condition which is well satisfied by the salts of divalent manganese and trivalent iron, and to a lesser extent by salts of several other ions in the iron group. (The rare earths are not very suitable for experiments of that type since they cannot be freed from highly absorbing members of their group). A particular salt must then be chosen which approximates as closely as possible the condition of a free ion. The ion will be called free if there is no appreciable effect from quenched orbital currents, from the spin-orbit coupling and from the spin-spin coupling between different ions. There is convincing evidence that divalent manganese and trivalent iron ions are in an S state so that the first two conditions are well satisfied. If we finally choose a salt which shows the full molar magnetic susceptibility as calculated on the assumption of a free spin (T_c in (8.12) small), we may be fairly certain to have also avoided difficulties arising from spin-spin coupling. Several salts whose susceptibility has been studied over a wide range of temperature satisfy (8.11) with a constant T_c considerably less than 100°K (e.g. $MnSO_4$). After selection of the salts as described, scattering experiments with slow neutrons should be carried out under several angles up to a minimum deflection chosen as small as the experimental arrangement will permit. These scattering measurements should be made relative to some standard which is nonmagnetic and shows only isotropic nuclear scattering; thereby geometric uncertainties can be avoided. The scattering data can then be fitted to the curve corresponding to a form factor (cf. Section VII) by an appropriate choice of the size of the scattering domain. Even without such theoretical assistance the measurement of the scattering at several angles should permit a satisfactory extrapolation to very small forward angles where the form factor becomes unity. The experiments can then be evaluated by the use of (5.9).

The various formulae of Section VI offer in principle a basis for the determination of the magnetic moment of the neutron through experiments with ferromagnets. By far the simplest method can be deduced from (6.40). It consists in an observation of the beam scattered by a magnetized body under a constant angle of scattering θ and at two different azimuths so chosen that $\mathbf{e}\cdot\boldsymbol{\varkappa}=1$ and $\mathbf{e}\cdot\boldsymbol{\varkappa}=0$. The difference in scattering then amounts to the ***total magnetic scattering*** independent of the amplitude and phase of the nuclear scattering. The disadvantages of this arrangement are several: It is necessary to delimit the scattered beam to a fraction of the azimuthal circumference which weakens the intensity by a factor of 2π approximately. It is furthermore essential to have single scattering since otherwise additional neutrons will be scattered into the chosen angle and also the assumption of a primarily unpolarized beam would no longer be justified. Apart from these not unsurmountable technical difficulties there remain certain theoretical ambiguities of perhaps greater importance. It would of course also be necessary, as in the paramagnetic case discussed before, to carry out observations at different angles θ to obtain information about the form factor. Even for the case of elastic scattering the form factor for ferromagnetic bodies will probably be of greater importance than in the case of paramagnetic scattering from free ions since it is likely that the outer shells will also be somewhat coupled and that there has occurred a noncalculable but probably large amount of spin quenching. A considerable contribution from incoherent magnetic scattering must also be expected to be present which will probably strongly diminish the otherwise marked azimuthal effect.

It should also be mentioned that the relative effect, even in the absence of all the difficulties mentioned above is rather unfavorable in the case of iron, since the nuclear cross section is large, $d\Phi_n=10^{-24}d\Omega$, while the elastic magnetic scattering amounts to $d\Phi_n\sim 2.5\times10^{-25}d\Omega$ if we

use for γ the empirically determined magnetic moment ~ 2 Bohr magnetons.

Originally it had been suggested[2] and an attempt[11] made to determine the magnetic moment with the aid of polarization experiments based upon the interference between nuclear and magnetic scattering. The two types of experiments mostly discussed are the double scattering and transmission arrangements which we mentioned in Section VI. Here too there exist in our opinion grave difficulties if one attempts to evaluate the experiments quantitatively for the purpose of determining the neutron moment. Section III dealt with the problem how far the coherent scattering of a nucleus can be determined from observation of the total nuclear cross section. We found that in the presence of isotopes and the nuclear spin it is almost impossible to draw quantitatively reliable conclusions. It must be admitted that the case of iron is favorable insofar as the dominant isotope has an atomic weight of 56 and therefore, probably no spin. It nevertheless does not seem feasible to determine the amplitude of coherent scattering quantitatively; we must be satisfied to enclose it within certain not improbable limits. There must, in addition, be considered a background due to inelastic nuclear scattering which arises from the coupling with the lattice. Since this coupling need not be the same for nuclear and magnetic scattering there arise inaccuracies which cannot be removed at our present state of knowledge. The inelastic scattering which is due to the strong spin coupling forces will, in the case of a saturated ferromagnet also show polarization effects of an unpredictable magnitude. The difficulty of obtaining sufficient intensity in a neutron beam for the purpose of carrying out a double scattering experiment has already been pointed out in the literature.

That all these factors mentioned are of considerable influence on the actual state of polarization of a beam passing through iron follows in our opinion from the minuteness of the effect which has been observed in the experiments by Frisch, von Halban and Koch. A rough estimate on the basis of (6.30) etc. would indicate that iron is by far a better polarizer (and analyzer) than the actual observations indicate. We consider these experiments as offering direct support for our contention as to the complexity of scattering processes in ferromagnetic bodies.

Similar difficulties enter into the quantitative evaluation of experiments concerned with the attenuation of an incident unpolarized neutron beam. Since it is the *total* and not the *differential* cross section that here becomes of importance, we are not able to study independently the form factor as function of the scattering angle. This form factor enters (cf. e.g. (6.53)) in a decisive but complex manner into the absorption cross section; without knowing the form factor no conclusions can be drawn as to the magnitude of the magnetic moment. If there is an appreciable amount of incoherent nuclear scattering present, the beam will be depolarized as it passes through the ferromagnet. Care must also be taken that in the case of a highly attenuated primary beam no secondary neutrons shall be scattered into the forward direction. Previous evaluations have also neglected the purely magnetic coherent and incoherent scattering as well as the effect of the precession of the neutron spin during the passage through the ferromagnet.[12] The combined weight of all these variable factors seems, in our opinion, sufficient to make a quantitative evaluation of transmission experiments appear rather improbable.

Assuming a quantitative knowledge of the magnetic moment of the neutron which, as we have shown, can probably be obtained with fewest ambiguities from observations of paramagnetic scattering, we are able to outline a series of experiments from which much information can be gained as to the magnetic structure of the scatterer. As previously pointed out, we find ourselves now on less satisfactory ground as far as the theory is concerned, and we think that the most promising attack can be made from the experimental side. The difficulties to which we

[11] Cf. e.g. Hoffman, Livingstone and Bethe, Phys. Rev. **51**, 214 (1937); several notes by J. Dunning and collaborators in Phys. Rev. **51**, (1937).

[12] *Note added in proof.*—The problem of magnetic scattering of neutrons has been further treated together with related questions in two notes which will appear shortly. Abstracts have been presented to the meetings of the American Physical Society in Washington (cf. a paper by O. Halpern and Th. Holstein presented in December, 1938; Phys. Rev. **55**, 601 (1939); and a paper by Halpern, Hammermesh and Johnson presented in April, 1939; Abstract No. 73 in Am. Phys. Soc. Bull. **14**, No. 2, April 12, 1939).

are referring are mainly our lack of knowledge concerning the elastic and even more important, the inelastic form factors. The complications which we encounter in attempting to estimate the energy change per collision due to the presence of spin coupling forces have been discussed fully in Section VIII. We there realized the impossibility of drawing reliable conclusions from the mean square fluctuation of the energy which, in our opinion, does not at all determine the actual energy change per collision. Ceding this group of problems to experimental investigation, we have learned in the meantime by letter and personal communication that Professor Van Vleck has become interested in the theoretical side of this problem and is attempting to derive information about the energy changes from considerations about energy fluctuations. His results[13] show that from such considerations the average energy change is of the order of the exchange integral.

Leaving these theoretical considerations aside for the moment we may point out that there exists a very simple type of experiment which will show if it is justified to predict energy changes of the order of magnitude of the exchange integral J. For this purpose it is only necessary to determine the integral cross section of various salts containing the same paramagnetic ion (Mn^{++} or Fe^{+++}). Since these salts show widely varying susceptibilities and exchange integrals (Curie temperatures between 100° and 1000°K), we should expect large changes in the integral cross section. If, for example, we choose a salt like MnS which does not show an appreciable magnetic scattering in the backward direction, then we should expect according to the hypothesis mentioned a vanishingly small total magnetic cross section, since the inelastic form factor will almost completely eliminate the forward scattering also. If, on the other hand, the small backward scattering is due to the influence of the elastic form factor which (cf. (7.30)) is small enough to make it unobservable, then a sizable magnetic cross section should be measured which would be due to a large amount of forward scattering. All these discussions presuppose of course, the existence of a magnetic moment of the neutron which is not much smaller than one nuclear magneton.

Experimenting with quasi-free magnetic ions we can use the angular dependence of the magnetic scattering to obtain information on the magnetically active size of the ion. Similarly observations on the angular dependence of scattering can be used to obtain information about the probability $P(L, L')$. For this purpose it seems advisable to carry out observations at various neutron energies, and for a series of salts of variable "magnetic dilution." Since the magnitude of spin coupling is known from susceptibility data, one can thus obtain experimentally a relationship between spin coupling and neutron scattering. Again the salts of divalent manganese and trivalent iron are especially suitable because of the absence of orbital currents. It will also prove interesting to investigate the scattering from paramagnetic metals. Susceptibility data are here difficult to interpret because of the erratic temperature dependence which may well be connected with a large spin coupling in these magnetically concentrated materials. This spin coupling will in the antiferromagnetic case operate to quench the ionic spins in the presence of an external magnetic field. After one has determined the general effect of spin coupling with the aid of observations on ions of known magnetic structure, the neutron scattering from metals should present information as to the actual ionic moment and hence, the ionic state in the metal.

We have already pointed out that the presence of spin coupling forces could give rise to marked phenomena if the scattering by ferromagnets is observed above and below the Curie point. If the energy changes should really turn out to be of the order of magnitude of the exchange integral, then we would expect that the scattering above the Curie point is practically absent on account of the large inelastic form factor. An experiment of such a kind should give us information similar to that obtained from observations on the total cross sections of paramagnetic salts.

[13] See following paper.

On The Theory of the Forward Scattering of Neutrons by Paramagnetic Media

J. H. VAN VLECK
Harvard University, Cambridge, Massachusetts

(Received September 6, 1938)

Experiments on the scattering of neutrons by paramagnetic media may have two possible goals: (*a*) determination of the magnetic moment of the neutron, and (*b*) investigation of exchange forces. In (*a*), materials of negligible exchange coupling should be used, while in (*b*) the reverse is true. The present paper is concerned with (*b*). It is shown that the exchange interaction between the paramagnetic ions tends to make the scattering inelastic, and reduces the form factor for forward scattering, so that it is no longer unity. An attempt is made to calculate the amount of this reduction. The distribution of energy changes in the inelastic processes is estimated by calculating the mean square and mean fourth power absorption frequencies, as well as the exact frequency distribution spectrum for an over-simplified "cluster" model. A Gaussian distribution appears to be the best feasible approximation. If this is used, it is estimated that in MnS, a typical material with appreciable exchange coupling, the form factor reduces the scattering of monochromatic liquid-air and room-temperature neutrons near the forward direction by about 75 and 50 percent, respectively.

1. INTRODUCTION

BLOCH[1] has noted that the cross section due to interaction between the magnetic moment of a neutron and that of a ferromagnetic ion is by no means negligible compared with that due to the usual short range nuclear forces. Halpern and Johnson[2] have shown that instead of performing experiments on double scattering by ferromagnetic media which involves polarization effects, magnetic scattering should be detectable by comparing the cross section of a paramagnetic compound with the sum of the cross sections of the uncombined ingredients. For instance, in pure Mn, or in pure S, there should presumably be no appreciable magnetic scattering since Mn is only weakly magnetic, while S is diamagnetic. On the other hand, in the paramagnetic compound, MnS, the Mn^{++} ion has a spin 5/2, and so MnS should exhibit strong magnetic scattering. If one neglects the form factor, one calculates that the total scattering cross section for MnS should be about six times greater than that for Mn+S. The present paper is concerned entirely with scattering of the paramagnetic, or Halpern-Johnson type, rather than the Bloch-Schwinger ferromagnetic polarization effects. Experiments on the latter have already furnished evidence on the magnetic moment of the neutron,[3] but Whitaker's[4] measurements aimed at detecting paramagnetic scattering have as yet been unsuccessful. In comparing Mn+S with MnS, he finds no deviation from additivity within the experimental error (about four percent of the expected effect.) However, as Halpern and Johnson now show in detail,[5] the difficulty is that Whitaker measured the scattering mostly rather near the backward direction. Here the influence of the form factor is very important. Halpern and Johnson calculate that this factor makes the scattering in Whitaker's experiments only about 1/35 as great as otherwise, and so is probably adequate to explain the negative results. In the forward direction, where measurements are now in progress,[5a] a positive outcome is presumably to be expected. The forward form factor is unity if the collisions are treated as perfectly elastic. However, in a great many paramagnetic materials, e.g. those so far used by Whitaker, there is a very considerable exchange coupling between the spins of the various atoms in the scattering medium, and this has the effect of making the scattering dominantly inelastic

[1] F. Bloch, Phys. Rev. **50**, 259 (1936); J. S. Schwinger, Phys. Rev. **51**, 544 (1937).
[2] O. Halpern and M. H. Johnson, Jr., Phys. Rev. **52**, 53 1937).
[3] Hoffman, Livingston and Bethe, Phys. Rev. **51**, 214 (1937); J. R. Dunning and collaborators, Phys. Rev. **51**, 51, 371, 382, 1022 (1937); Frisch, von Halban and Kogh, Nature **139**, 756 (1937).
[4] M. D. Whitaker, Phys. Rev. **52**, 384 (1937).
[5] O. Halpern and M. H. Johnson, Phys. Rev. **55**, 818 (1938).
[5a] *Note added in proof:* Such experiments, which definitely show the existence of paramagnetic scattering, have just been performed by M. D. Whitaker, H. G. Beyer, and J. R. Dunning, Phys. Rev. **54**, 771 (1938).

rather than elastic. So the influence of the form factor persists even in the forward direction. It is the purpose of the present paper to attempt an estimate of how great is the resulting reduction in forward scattering.

Uncertainties caused by inelastic effects can, however, be avoided by using scattering materials in which the exchange coupling is of inconsequential size. The compounds possessing this property are presumably those which have a negligible Δ in the Weiss-Curie formula $C/(T+\Delta)$ for the susceptibility, as Δ is more or less proportional to the exchange integral. Two examples of substances meeting this criterion are $MnCl_2$ and $MnSO_4$, but the large absorption of neutrons by the chlorine nucleus makes $MnCl_2$ not very suitable. Magnetically dilute materials with a large amount of water of coordination, such as the hydrated sulphates, have small values of Δ, but are not feasible, for the large nuclear scattering by the numerous nonmagnetic ingredients tends to mask the paramagnetic effect.

The substances with negligible Δ are obviously those which should be used if the paramagnetic scattering is used to determine the magnetic moment of the neutron, because then the difficulties caused by exchange coupling do not enter. Since such substances are available, the question naturally arises as to what is the use of the calculations of the present paper, wherein we treat the influence of exchange on the form factor. The answer is that experiments on paramagnetic scattering may yield information not only on the magnetic moment of the neutron, but also on the details of the exchange forces in the solid state, serving as a valuable supplement to the usual determinations of magnetic susceptibility.

In materials with an appreciable Δ, the effect of the exchange perturbations is such as to prevent any spatial component of spin of a given atom from being a "good quantum number," or in other words, to make the spin matrix elements of a given atom consist primarily of off-diagonal matrix elements involving appreciable energy changes. Nondiagonal matrix elements correspond classically to periodic rather than time-constant force centers, and give rise to inelastic rather than elastic scattering. If $h\nu$ denotes the energy change involved in the inelastic process, and if E denotes the energy of the incident neutron, conservation of energy does not allow the excitation of the atom if $h\nu > E$. Because of the atomic Boltzmann factor, the converse type of collision in which the atom is de-excited and imparts energy to the neutron is unlikely if $h\nu > kT$. Even when $h\nu$ is not large enough to make these energetic considerations operative, the inelastic character of the collisions may sufficiently influence the form factor to reduce the cross section appreciably. It is thus of interest to calculate about how large are the energy changes involved in most of the collision processes. An attempt is made in the next section to do this by calculating the mean square energy change, also the mean fourth power. It appears that in the case of MnS, a typical material, the energy changes are not sufficient to make most of the collisions energetically impossible even with liquid-air neutrons, but still all told probably influence the form factor enough to make the scattering in the forward direction about one-fourth as large as one would calculate for purely elastic scattering. Because of the tremendous complexity of the exchange secular problem, too much quantitative accuracy should not be attributed to the results.

II. Mathematical Details—Calculation of the Mean Square and Mean Fourth Power of the Frequency

To compute the influence of the exchange interaction, it does not suffice to resort to the usual artifice of representing this coupling by means of a Weiss molecular field, as the latter vanishes for an unmagnetized paramagnetic body. However, if the exchange integral J is large enough, there are appreciable distortions because of local fluctuations in the alignment of the spins, or in other words, local order effects even though there is no long distance order in the spin. The following type of calculation shows this.

Let H_0 be the Hamiltonian function of the crystal without the impinging neutron. Then $h\nu$ is the difference between two characteristic values W of H_0. Let U be the perturbing or scattering potential due to atom i. The specific

forms of H_0, U are

$$H_0=\text{const.}-2J\sum_{j>i}\mathbf{S}_i\cdot\mathbf{S}_j, \quad (1)$$

$$U=g\beta[r_{iN}^{-3}\boldsymbol{\mu}\cdot\mathbf{S}_i-3r_{iN}^{-5}(\mathbf{r}_{iN}\cdot\mathbf{S}_i)(\boldsymbol{\mu}\cdot\mathbf{r}_{iN})], \quad (2)$$

where J is the exchange integral connecting neighboring paramagnetic atoms, β is the Bohr magneton $he/4\pi mc$, $\mathbf{S}_i$ is the spin vector of atom i, measured in multiples of $h/2\pi$, and $\boldsymbol{\mu}$ is the magnetic moment of the neutron. The distance between the neutron and the spin of the ith atom is denoted by r_{iN}. We make the usual assumption that the exchange integral can be neglected except between the paramagnetic atoms which are nearest to each other. The fashion (1) of writing the exchange energy is that furnished by the Dirac vector model.[6]

A root mean square energy change, which is sufficient for qualitative purposes, may be defined by

$$h\nu_{\text{rms}}=[\textstyle\sum_{mn}(W_n-W_m)^2U_{mn}^2/\sum_{mn}U_{mn}^2]^{\frac{1}{2}} \quad (3)$$

inasmuch as, except for the form factor, the probability of a collision is proportional to the square of the corresponding matrix element U_{mn} of the scattering potential. The effect of the form factor corrections is, of course, to suppress scattering due to the higher frequencies and so lower ν_{rms}, but this fact is irrelevant to the present calculation. We are first of all interested in seeing whether $h\nu_{\text{rms}}$ is large enough to be important.

The expression (3) may be written[7]

$$h\nu_{\text{rms}}=[\overline{(H_0U-UH_0)^2}/\overline{U^2}]^{\frac{1}{2}}, \quad (4)$$

where the bars denote the usual quantum-mechanical average, proportional to the "spur" or diagonal sum. In virtue of the invariance of the latter, this average may be calculated in any system of representation,—most conveniently that in which each atom is separately space quantized. Eq. (4) shows that if U and H_0 commuted, $h\nu_{\text{rms}}$ would be zero. Actually, U and H_0 do not commute, inasmuch as

$$S_{xi}S_{yj}-S_{yj}S_{xi}=\delta_j{}^iS_{zi}, \quad \text{etc.} \quad (5a)$$

On the other hand

$$S_{xi}\mu_y-\mu_yS_{xi}=0. \quad (5b)$$

On utilizing (5a), (5b) and the familiar relations

$$\overline{S_{xi}{}^2}=\tfrac{1}{3}S(S+1), \quad \overline{S_{xi}S_{yi}}=0, \quad \overline{S_{xi}}=0; \quad (6)$$

$$\overline{\mu_x{}^2}=\overline{\mu_y{}^2}=\overline{\mu_z{}^2}; \quad \overline{\mu_x\mu_y}=0, \quad \text{etc.}$$

it is found that (4) becomes

$$h\nu_{\text{rms}}=2[\tfrac{3}{8}zS(S+1)J^2]^{\frac{1}{2}}, \quad (7)$$

where z is the number of neighbors possessed by an atom. We shall henceforth take $z=6$, as very likely the paramagnetic atoms have a simple cubic spacing, and anyway, a precise knowledge of z is not important for our qualitative purposes.

To estimate the exchange integral J, we use the susceptibility formula

$$\chi=4NS(S+1)\beta^2/3k(T+\Delta), \quad (8)$$

where Δ is usually positive in paramagnetic media since the ordinary type of chemical bonding involves a J of negative sign and hence leads to antiferromagnetic coupling. According to the usual, first-order approximation of the Heisenberg theory[8]

$$\Delta=-\tfrac{3}{8}zJS(S+1)/k. \quad (9)$$

This approximation is surely adequate for our needs, and Eq. (8) works empirically surprisingly well, although mathematically the underlying convergence of the series development is still a mystery. Combination of (7) and (9) gives

$$h\nu_{\text{rms}}/k=[6\Delta^2/z(S^2+S)]^{\frac{1}{2}}. \quad (10)$$

The materials used by Whitaker all have positive

TABLE I. *Calculated root mean square frequencies.*

	MnS	MnO	MnO_2	Fe_2O_3
$\chi\times10^6$	44	67	14–38	21
Δ	827	512	277–1250	1023°K
$h\nu_{\text{rms}}/k$	280	173	95–420	350°K
ν_{rms}/c	196	121	66–293	245 cm^{-1}

[6] P. A. M. Dirac, *The Principles of Quantum Mechanics*, Chap. XI. For application to ferromagnetism, see Chap. XII of my *Electric and Magnetic Susceptibilities*.

[7] An analogous calculation of the root mean square frequency is made by Waller in connection with paramagnetic relaxation (Zeits. f. Physik **79**, 370 (1933)). There is, however, the difference that he has dipole-dipole rather than exchange coupling between the paramagnetic ions.

[8] Cf., for instance, J. H. Van Vleck, reference 6, p. 332.

values of Δ, as shown in Table I. The experimental values of the susceptibility χ per unit mass from which Δ is calculated by means of (8) are also included.[9] The two bottom lines of the table give the values of $h\nu_{rms}$ computed from Δ by means of (10). For convenience, $h\nu_{rms}$ is expressed both in degrees and in cm^{-1}.[10]

The objection against the preceding calculation has been raised that it is misleading because the total spread in the energy levels of a crystal composed of N atoms is of the order NJ, obviously an enormously large quantity. Hence some of the matrix components of spin of a given atom can occasionally involve energy transitions which are very large, of a much greater order of magnitude than J, and hence than $h\nu_{rms}$. Obviously the presence of a few abnormally high frequencies, even though not especially abundant, may conceivably materially raise the mean square average so that the latter is not typical. Actually, this is not the case, as is shown by our subsequent calculation of the mean fourth power of the frequency, which turns out not to differ too widely from ν_{rms}^4. Further evidence that ν_{rms} is not appreciably influenced by the great spread in eigenvalues for the whole crystal is furnished by the fact that ν_{rms} has exactly the same value for a central atom surrounded by its z nearest neighbors as for an atom embedded in an infinite crystal. This agreement is, of course, because the spin of the central atom commutes in multiplication with all terms in the coupling energy (1) except those which involve this atom. (The mean fourth power of the frequency involves, however, the next to nearest as well as nearest atoms (cf. later remarks after Eq. (12)).

Nevertheless, it would not be right to calculate the form factor on the assumption that every collision involves the same energy change $h\nu_{rms}$, since an appreciable fraction of the collisions may involve such small energy changes that they are effectively elastic. Clearly the information which we really need is a distribution curve for the frequencies, but to obtain this is far too difficult a mathematical problem. Some idea of the dispersion in frequencies can be obtained by calculating the mean value of the fourth power of the frequency, and examining how much its fourth root, which we will denote by ν_4, differs from ν_{rms}. The formula for ν_4 is[11]

$$\nu_4^4 = \overline{(\Phi H_0 - H_0\Phi)^2}/\overline{U^2}, \tag{11}$$

where $\Phi = H_0U - UH_0$. On making the requisite calculations we find that

$$\nu_4^4 = 16J^4[4z(3x^2 - \tfrac{1}{4}x) + 14z(z-1)x^2], \tag{12}$$

where $x = \frac{1}{3}S(S+1)$. For $z=6$, $S=5/2$, the ratio ν_4/ν_{rms} is 1.36. A Gaussian distribution function $q^{\frac{1}{2}}\pi^{-\frac{1}{2}}e^{-q^2}$ would give $\nu_4/\nu_{rms} = 1.32$. If ν_4 were calculated for a model consisting only of the central atom and its z nearest neighbors, without including an additional zone of atoms, the factor 14 in (12) becomes 10, and $\nu_4/\nu_{rms} = 1.27$.

Of course the mere fact that ν_4/ν_{rms} is about the same as for a Gaussian spread by no means shows that the actual distribution at all approaches the Gaussian form. However, the Gaussian assumption is doubtless a far better approximation than assuming all energy changes are identical, and our examination in Section III of a particular, over-specialized model, "the local cluster," gives us, as we shall show, some reason for believing that it is in not too violent contradiction to the actual physical situation. Hence we shall proceed to estimate the form factor on the basis of a Gaussian distribution of frequencies.[11a]

In general the form factor for scattering is

$$f = \left[\int\int\int \psi^2 \exp i\mathbf{k}\cdot\mathbf{r}\, dv\right]^2 \tag{13}$$

where $\mathbf{k}/2\pi$ is the vector difference between the de Broglie wave numbers of the incident and scattered neutron. For the atomic wave function

[9] The experimental determinations of χ used in Table I are from the following sources: MnS, low MnO_2 value, Wedekind and Horst, Ber. Chem. Ges. **45**, 262 (1912); **48**, 105 (1915); high MnO_2, FeO, Honda and Sone, Sci. Rep. Tohoku Univ. **2**, 1, 25 (1913); MnO, Theodorides, Arch. Sci. Phys. **3**, 161 (1921).

[10] Do not confuse these wave numbers, which relate to energy, with the de Broglie wave numbers, which relate to momentum and which are of the order 10^8 cm^{-1}.

[11] See I. Waller, reference 7. His paper gives the details of the matrix algebra in the calculation of ν_4 for a formally somewhat related problem.

[11a] *Note added in proof:* It is interesting to remark that in studying the effect of dipole-dipole interaction on magnetic susceptibilities at radiofrequencies, Kronig and Bouwkamp have very recently assumed a Gaussian distribution of internal fields, which is entirely analogous to the present procedure. See Physica **5**, 521 (1938).

ψ we shall choose the simple analytical form

$$\psi = Ar^2 e^{-cr/2}. \tag{14}$$

The absence of a θ, φ factor in ψ is justified because Mn^{++} and Fe^{+++} are normally in ^6S states, and also because interatomic forces, anyway, would tend to blur out any angular dependence. The ionization potential for Mn^{++} is not known, but extrapolation indicates that it is probably very nearly twice the Rydberg constant. Hence we shall take $c = 2\sqrt{2}/a_0$ where $a_0 = h^2/4\pi^2 e^2 m$. With use of (14), Eq. (13) becomes

$$f = [\tfrac{1}{3}(3c^{12} - 10c^{10}k^2 + 3c^8 k^4)/(c^2+k^2)^6]^2. \tag{15}$$

We must now integrate (15) over a Gaussian distribution of frequencies. The resultant reduction in intensity in scattering because of the form factor is then

$$F = \pi^{-\frac{1}{2}} q^{\frac{1}{2}} \int_{-E/h}^{\infty} f e^{-q\nu^2} d\nu \tag{16}$$

with $q = 1/2\nu_{rms}^2$ and

$$k = (8\pi^2 m/h^2)^{\frac{1}{2}}[(E+h\nu) - 2\cos\theta E^{\frac{1}{2}}(E+h\nu)^{\frac{1}{2}} + E]^{\frac{1}{2}}. \tag{17}$$

Here E is the energy of the incident neutrons and θ is the angle between the incident and scattered beam. The lower limit of integration in (16) is $-E/h$ rather than infinite because the neutron cannot emerge with less than zero energy. In (16) we have neglected the influence of the Boltzmann factor on the distribution of frequencies, but the calculation to be made in Section III shows that this is probably not a major item except in ferromagnetic or nearly ferromagnetic media.

With $\nu_{rms}/k = 196$ cm^{-1} the value appropriate to MnS, and with $E = \frac{3}{2}k \cdot 86$, i.e., monochromatic liquid-air neutrons, we find on evaluating the integral in (15) numerically that F is about 1/3.1 for forward scattering ($\theta = 0$). If, on the other hand, we lumped all the frequencies at ν_{rms}, i.e., used (15) with $\nu = \pm\nu_{rms}$ in (17), the value[12] of $\frac{1}{2}(f_+ + f_-)$ is 0.045. The Gaussian approximation doubtless comes closer to reality than that of a universal frequency ν_{rms}, but one reason why our estimate 1/3.1 may be a little high is that our charge distribution (14) may not be quite diffuse enough. This is particularly true because MnS doubtless does not have the ideal structure $Mn^{++}S^{--}$, but also some admixture of $Mn^{+}S^{-}$ and MnS. In other words some of the spin probably occasionally wanders to the S atoms. So we contented ourselves with saying in Section I that F is about 0.25. Future experiments on forward scattering should be valuable in determining F, and hence give us an idea of how great the wandering tendency really is.

If room-temperature rather than liquid-air neutrons are used, the influence of the form factor on forward scattering becomes somewhat less important. On the basis of our Gaussian distribution, F becomes about 0.55, while $\frac{1}{2}(f_+ + f_-) = 0.25$ if all frequencies are concentrated at ν_{rms}.

The form factor is, of course, much larger, i.e., closer to unity, for forward than for backward scattering. With the wave functions (14), one calculates that the form factors for the backward scattering of monochromatic liquid-air and room-temperature neutrons are only 10^{-3} and 10^{-7} if the collisions are treated as elastic.[13] It is to be noted that raising the energy of the incident neutrons increases the forward form factor, but diminishes the backward one. This is because (17) yields $dk/dE < 0$ if $\theta = 0$, whereas $dk/dE > 0$ if $\theta = \pi$.

It is to be cautioned that the numerical values of f which we have quoted all relate to monochromatic neutrons with a uniform velocity given by $mv^2 = 3kT$. In actual experiments, the neutrons will have a Maxwellian distribution $Av^2 e^{-mv^2/kT}$. The presence of some very low velocity electrons in the latter will tend to make the influence of inelastic effects on the form factor somewhat greater than that which we calculate on the basis of a common velocity.

The recent experiments of Whitaker, Beyer, and Dunning,[5a] though they have given real evidence of the existence of paramagnetic

[12] In this connection we assume that the temperature is high enough so that the matrix elements of the atom are distributed equally between absorption and emission. The corresponding form factors are denoted by f_+ and f_-. With liquid-air, but not with room-temperature neutrons, the expression (17) becomes imaginary when $\nu = -\nu_{rms}$, $\theta = 0$, or in other words, absorption becomes energetically impossible, so that $f_- = 0$.

[13] Do not confuse these estimates with the larger ones quoted in Section I in connection with Whitaker's early experiments. The latter involve a complicated distribution in angle largely but by no means entirely backwards.

scattering, unfortunately do not as yet seem to throw any light on the inelastic form factor. In fact, unless an unreasonably high value for the magnetic moment of the neutron is assumed, they give greater scattering than that to be expected even on the basis of an elastic form factor. Professor Dunning informs the writer that the difficulty is probably that, due to interference effects, the nuclear cross sections are not really additive, so that the quantitative value of the residue to be attributed to the magnetic process is in doubt.

III. Detailed Calculation of Frequency Spectrum for a Local Cluster

We have seen above that ν_{rms} has the same value when the given atom is surrounded merely by its z nearest neighbors, as when the atom is embedded, as it is actually, in the entire crystal. It is therefore tempting to calculate the frequencies in detail for the soluble "cluster" model of a central atom surrounded by z atoms, which are not coupled to the rest of the crystal. Such a procedure obviously shows a certain amount of analogy to the well-known Bethe-Peirls approximation scheme in superlattices. Too much significance should not be attached to the resulting distribution curve, but the correction for the interaction with the remainder of the crystal is probably mainly to smooth out the curve. In this idealized model we can neglect the interaction of the z atoms surrounding the central atom with each other, and imagine them coupled only to the central atom. This is allowable since in a simple cubic or body-centered lattice the atoms which are nearest neighbors of a given central atom are never nearest neighbors to each other. The Dirac vector-model theory shows that the collective spin of the z corner atoms is then a good quantum number S', which can assume the values 0, $\cdots zS$, where S is the spin of an individual atom. The exchange energy of our cluster is[14]

$$W(S', S_c) = -2J\mathbf{S}'\cdot\mathbf{S} = -J[S_c(S_c+1) - S'(S'+1) - S(S+1)] \tag{18}$$

where S_c, the total spin of the cluster, is the resultant of S' and the spin of the central atom, and so takes on quantized values between $|S'-S|$ and $S'+S$. The spin S of the central atom is diagonal in S', and we have effectively only a two-vector problem. One can easily convince oneself that for our purposes the scattering potential can be taken to be S_z, or any other component of $\mathbf{S}$, rather than (2), as, because of (6), the substitution of S_z for (2) merely influences the absolute magnitude of the scattering probability without changing its distribution among frequencies. Our problem is that of finding the size of the matrix elements of the spin of the central atom connecting the various eigenvalues of the cluster, and is thus similar to that of finding the "line-strength," in Condon and Shortley's terminology,[15] for a two-vector problem. For our purposes, the word "line-strength," which we henceforth paraphrase as "scattering-strength," means the square of the matrix component of spin angular momentum, summed over the various Zeeman components of the initial and final states, i.e., over the various quantized orientations of S_c. This strength is thus proportional to the scattering probability associated with a given transition or frequency change, except for modulations due to the form factor. Condon and Shortley's Eqs. (2b) are immediately adaptable to our purposes by substituting S, S', S_c for their L, S, J, respectively, and taking their γ-factor equal to unity. The fraction of scattering-strength associated with zero energy changes is

$$\tfrac{1}{4}B\textstyle\sum_{S'}\, s_c(2S_c+1)(S_c^2+S_c)^{-1}[S_c(S_c+1) - S'(S'+1) - S(S+1)]\omega_{S'}e^{-W(S',\, S_c)/kT}$$

Table II. *Degree of degeneracy* $\omega_{S'}$.

$S'=$	0	1	2	3	4	5	6	7	8	9	10	11	12	13	14	15
$\omega_{S'}=$	111	315	475	575	609	581	505	405	300	204	126	70	35	15	5	1

[14] See reference 6 or more specifically, J. H. Van Vleck, Phys. Rev. **45**, 413, item II (1934).
[15] E. U. Condon and G. H. Shortley, *The Theory of Atomic Spectra* (Cambridge, 1935), Chap. IX, especially Eqs. (2b), p. 238.

TABLE III. *Distribution of scattering-strength I among different frequencies.*

$h\nu/J=$	0	3	5	7	9	11	13	15	17	19	21	23	25	27	29	31	33	35
(*a*) $I=39.4$	1.0	2.6	4.7	6.7	7.8	8.4	7.8	6.9	5.4	3.9	2.6	1.4	0.8	0.4	0.1	0.04	0.01%
(*b*) $I=50.4$	0.1	0.3	0.6	0.8	1.0	1.1	1.1	1.0	0.8	0.6	0.4	0.2	0.1	—	—	—	— %
(*c*) $I=$ —	0.2	0.6	1.3	2.2	3.3	4.4	5.4	5.9	5.9	5.1	3.9	2.3	0.9	0.1	—	—	— %

(*a*) Percentage of scattering-strength associated with various energy changes when $J/kT=0$. (*b*) Percentages of these strengths associated with excitation of atom when $J/kT=-0.1$. (*c*) Corresponding strengths associated with de-excitation of atom when $J/kT=-0.1$. When $J/kT=0$ the excitative and de-excitative strengths are equal and have been combined together. Thus (*a*) is to be compared with the sum of (*b*) and (*c*).

and that with a transition S', $S_e \rightarrow S'$, $S_e \pm 1$

$$\tfrac{1}{4}B[S_e+\tfrac{1}{2}\pm\tfrac{1}{2}]^{-1}[(S_e+\tfrac{1}{2}\pm\tfrac{1}{2})^2-(S'-S)^2][(S+S'+1)^2-(S_e+\tfrac{1}{2}\pm\tfrac{1}{2})^2]\omega_{S'}e^{-W(S',\,S_e)/kT},$$

where

$$1/B=S(S+1)\textstyle\sum_{S_e,\,S'}\omega_{S'}e^{-W(S',\,S_e)/kT}.$$

Here $\omega_{S'}$ is the statistical weight of a given value of S' (exclusive of the Zeeman factor $2S'+1$). It may be found by repeated application of the branching rule[16] to the successive compounding of z vectors of equal magnitude S. We will make our calculations for the case $z=6$, $S=5/2$. Then one finds that the values of $\omega_{S'}$ are as given in Table II. The computed distribution of strength is shown in Table III. Here we have combined all strengths associated with the same frequency even though they originate in different initial states. Because of the atomic Boltzmann factor, it is necessary to specify the temperature T of the scattering material in obtaining the latter's distribution of frequencies. Our previous calculations of ν_{rms}, ν_4 in Section II assumed that each state had a weight proportional to its *a priori* probability, and tacitly assumed infinite temperature. The present computations are obviously superior in this respect. In fact one reason we have made them is to examine whether the Boltzmann factor has a very pronounced influence on the frequency distribution. Actually this influence is seen to be relatively unimportant, although it has some trend towards accentuating the elastic or low frequency scattering. If $T=293°$, the value -0.1 of J/kT employed in connection with (*b*) and (*c*) of Table III corresponds according to formula (9) to $\Delta=1030°\text{K}$, about the order of Δ in the materials used by Whittaker (cf. Table I). As a check on the mathematical accuracy of the calculations, it may be noted that the value of ν_{rms} computed numerically from the distribution given in (*a*) of Table III agrees with that yielded by Eq. (7); and that ν_4/ν_{rms} has the value 1.27 demanded by the proper modification of Eq. (12).

According to Table III, almost 50 percent of the collisions should be elastic in character. However, this result is because of the over-simplified character of the model, whereby all states of the same S' have the same energy, with a high degree of degeneracy as shown in Table II. Actually the interaction of our cluster of $z+1$ atoms with the next group of the crystal will lift the degeneracy and "smear out" these states, presumably superposing additional splittings very similar to those exhibited in the table. When the influence of still more remote atoms is considered, doubtless the remaining degenerate states will be again split, so that finally the distribution curve for ν will acquire a smooth shape, which is probably not too remote from a Gaussian one, since Table III suggests that the peak is probably at $\nu=0$.

In closing it should be noted that our use of the Gaussian distribution of frequencies for the moment matrix of a single atom in neutron scattering should not be confused with the employment of a Gaussian distribution for the energy levels of the whole crystal in connection with the susceptibility. The latter is known to be an exceedingly poor approximation, but this fact has no bearing on our work, as the susceptibility calculations, unlike those on scattering, are exceedingly sensitive to the exact nature of the tailing out of the distribution curve,[17] and to its variation with slight changes of the total crystalline spin. The Gaussian assumption probably introduces less error in our calculations than does the choice (14) of the atomic wave function.

The writer is indebted to Dr. John R. Stehn for calling his attention to the subject of paramagnetic neutron scattering, and to Professors Halpern and Johnson for instructive discussions.

[16] Cf., for instance, J. H. Van Vleck and A. Sherman, Rev. Mod. Phys. **7**, 192 (1935).
[17] See D. R. Inglis, Phys. Rev. **42**, 442 (1932).

Intercalibration and Comparison in Two Laboratories of Measurements Incident to the Determination of the Geological Ages of Rocks

R. D. Evans,* Clark Goodman,* N. B. Keevil,† A. C. Lane‡ and W. D. Urry**
Massachusetts Institute of Technology, Cambridge, Massachusetts

(Received February 6, 1939)

In an effort to extend the scope of geological age measurements based on the accumulation of helium in igneous rocks, researches were initiated which indicated disagreement when compared with previously published results from the same geological horizons. Cooperative investigations, undertaken by the authors, show that the radium determinations used in formulating the previous helium time scale are incorrect by more than a factor of two. The magnitude of the necessary downward revision of ages varies, depending upon the Th/U ratio of the individual rock specimens. Helium age determinations have been made on a number of igneous rocks by two entirely different techniques, the alpha-helium method and the radon-thorium-helium method. The alpha-helium method is independent of radioactive standards, and its results are in agreement with the new measurements by the radon-thorium-helium method. These researches also represent the first comparison of helium age measurements on the same specimens by two or more observers. While the helium ages of many individual geological horizons are lowered by these new results, the total span of geological time remains unreduced. Precision radium standards in the region of 10^{-12} gram have been verified.

I. Introduction

THE ultimate aim of the historical geologist is the accurate reconstruction of the consecutive geographies of the past. The fundamental criteria used in delimiting geologic periods are: (1) index fossils, (2) unconformities and, (3) cycles of sedimentation. Within recent years a fourth criterion, based upon the accumulation of the decay products of radioactivity, has been added. This method is particularly applicable to igneous rocks and minerals, which invariably contain at least measurable traces of the slowly decaying parent elements uranium, actino-uranium, and thorium. The three earlier criteria cannot be applied directly to igneous rocks, which constitute about 95 percent of the earth's crust.[1] Hence the radioactive method promises to be an extremely valuable aid in solving geochronological problems.

During the last quarter-century a fairly complete time scale, extending over most of the recognized range of geological time, has been built up from radioactivity measurements. The apparent agreement between ages based upon the accumulated radiogenic lead in radioactive minerals[2] and those obtained from the helium method applied to close grained igneous rocks[3–7] was the most convincing evidence for the validity of both methods.[5, 7] In an effort to extend the scope of this work, researches were initiated to develop a direct, physical method (Evans and Goodman[8]), and to test the applicability of the helium method to coarse grained igneous rocks which are predominant in the earth's crust (Keevil).[9] These researches indicated a serious disagreement in ages when compared with published results from the same geological horizons. A cooperative investigation, with two independent methods of measurement, was undertaken to determine the source and magnitude of these differences. As a result there is now complete agreement between the alpha-helium method and the radon-thoron-helium method but all radium determinations published by Urry since July, 1934,[4–6] are low by a factor of over two. Between 30 and 40 per-

* George Eastman Research Laboratory of Physics.
† Fellow, Royal Society of Canada, 1936–1937. Now Research Associate, Massachusetts Institute of Technology.
‡ Professor Emeritus, Tufts College.
** Department of Geology. Now Geophysical Laboratory, Carnegie Institution of Washington, Washington, D. C.

[1] F. H. Grout, *Petrography and Petrology* (McGraw-Hill Book Co., 1932).
[2] National Research Council Bull. 80, "Age of the Earth" (1931).
[3] W. D. Urry, Chem. Rev. **13**, 305–343 (1933).
[4] A. C. Lane and W. D. Urry, Bull. Geol. Soc. Am. **46**, 1101–1120 (1935).
[5] W. D. Urry, Bull. Geol. Soc. Am. **47**, 1217–1233 (1936).
[6] W. D. Urry, J. Chem. Phys. **4**, 34–48 (1936).
[7] A. Holmes, *The Age of the Earth* (Thos. Nelson & Sons Ltd., 1937), p. 178.
[8] R. D. Evans and C. Goodman, Phys. Rev. **51**, 595A (1937).
[9] N. B. Keevil, Trans. Roy. Soc. Can. Sec. **4** (1938).

cent of this difference is explicable by radium standard differences and the remaining source of discrepancy, although not definitely ascertained, is possibly due to the use of very dilute standard solutions.

With a constant thorium to uranium ratio in rocks, the use of the revised radium calibrations would lower evenly all the published results.[4–7] But this ratio varies and causes an uneven decrease in the present helium time scale. An even more important difficulty is the apparent disagreement of the revised helium ages with the accepted lead ages[7] for minerals supposedly from the same geological period. In addition certain experimental evidence[10] supporting the lack of leakage of helium from close-grained rocks is invalidated as a result of this revision of the radium content of the rocks measured. Thus it is seen that while the techniques used for helium age measurements have been improved and their reliability established, the geological significance of the results is still to be evaluated.

The present paper has as its fivefold purpose: (1) to describe discrepancies in past work, (2) to show the accuracy and validity of the new techniques, (3) to indicate the concurrence of various workers, (4) to give a critical consideration of age measurements and (5) to serve as a basis for sounder age determinations by radioactive methods.

II. Radioactivity Measurements

A. Importance

Wide variations, even in order of magnitude, in the determination of the radium and thorium contents of rocks have been obtained by different workers in the past. These differences emphasize the need for the international intercalibration between the various workers which has recently been initiated.[11]

The Rn-Tn-He method of age analysis, as the name implies, depends upon the measurement of the emanation products in assumed equilibrium with the parent elements in a known amount of rock sample. Calibrations are made with standard radium and thorium solutions. The rates at which helium is being produced by the two radioactive series are then determined by use of the appropriate decay constants. A distinct advantage of this method, particularly for very inhomogeneous rocks, is that all measurements are made on the same portion of the sample. The alpha-helium method[12] involves a measurement of the helium content of the rock and a direct electrical count of the total rate of alpha-emission, which equals the rate of production of helium.

Separate radium and thorium determinations are not necessary in ascertaining the age of young rocks by the alpha-helium method.[12] But in all age analyses by this method, the radium content has been determined by the direct-fusion technique as routine procedure. This additional determination affords (1) a rough check on the alpha-count, (2) the correction factor[13] for the decay of parent elements which is applied to old rocks (over 400 million years), (3) a means of more direct comparison of results by other methods, as for example the radon-thoron-helium method, and (4) a measurement of the actual amounts of the three radioactive series present in terrestrial materials, which is of value in geophysics.

At a Th/U ratio of 3.7, the rates at which helium is being generated by the thorium and uranium series are equal. Averages of previous determinations of this ratio range between 2 and 3 for igneous rocks[2] and a value of 7 is reported for 2 suites of rocks,[14, 15] but results on a larger number of specimens indicate that a lower value, between 3 and 4, is more representative.[16, 17] Hence for most terrestrial materials, the thorium and uranium series are of about equal importance as sources of helium and lead, and in the generation of heat within the earth's crust.

B. Methods for radon measurements

Largely because of its medical importance, the quantitative relationship between radium and

[10] Reference 4, p. 1115.
[11] R. D. Evans and C. Goodman, Phys. Rev. **53**, 916A (1938).
[12] C. Goodman and R. D. Evans, Phys. Rev. **53**, 916A (1938).
[13] This correction is less than 10 percent for most rocks.
[14] R. D. Evans, G. D. Finney, A. F. Kip and R. Mugele, Phys. Rev. **47**, 791 (1935).
[15] R. D. Evans and R. W. Raitt, Phys. Rev. **48**, 171–176 (1935).
[16] N. B. Keevil, Econ. Geol. **33**, 685–696 (1938).
[17] A. O. Nier, J. Am. Chem. Soc. **60**, 1571 (1938).

radon has been well established. The determination of the radon in rocks gives a direct and accurate measure of the radium with which it is in equilibrium. These radium determinations involve two problems, first, removal of radon from the material being tested, and second, the accurate measurement of this radon by means of its alpha-ray ionization.

(1) Release of radon

When heated without flux, Evans[18] has demonstrated the necessity for complete fusion in order to insure 100 percent release of radon. Some investigators use the carbonate-fusion method, in which the finely ground rock is fluxed with alkali carbonates. In the direct-fusion method the equilibrium amount of radon in the rock is measured directly, while in the carbonate-fusion method the radon has usually been allowed to escape during fusion and subsequently reaccumulated and removed for measurement by boiling an acid solution of the flux. A recent improvement involves collection of the rock radon, together with the CO_2 released during fluxing, in a liquid-nitrogen trap.[19]

The results in Section C indicate that the direct-fusion and carbonate-fusion-solution methods are in good agreement on a variety of different kinds of rocks and hence that both methods are accurate for quantitative release of radon.

While the carbonate-fusion-solution method and the procedures to circumvent previously just criticisms have been described,[3, 6] it might be well to mention briefly these possible sources of error and indicate the procedures used to avoid them. A complete description including recent improvements is appearing elsewhere.[20] The chemical treatment used in preparation for the emanation measurements commences with the fluxing of the rock with Na_2CO_3 plus $Ba(OH)_2$.[6] The soda ash was obtained free of any activity, but it was necessary to recrystallize the $Ba(OH)_2$ in order to free it from radium contamination. Ordinary distilled water contains sufficient radioactivity to introduce error when such small concentrations, as occur in rocks, are to be measured. Consequently, all the water used in the chemical procedure, as well as that used in the standard solutions, must be redistilled. Even with these precautions, it is advisable to make blank runs, in which similar amounts of water and chemicals are taken as in the usual procedure for rocks. In this way a slight correction may be made if necessary and any unknown source of contamination revealed.

Aside from the possible loss of active elements during the chemical manipulations, there are two other effects which may cause low results. The emanations may be adsorbed by precipitated silica; hence cloudiness of the solutions used for emanation measurements should be avoided. Also the emanating power of sulfates has been shown to be low. The addition of an excess of barium, avoids the difficulty of sulfate formation by the radioactive elements, because any sulfate ions present have about an equal affinity for the much more abundant barium.

(2) Detection apparatus

The double ionization-chamber method has been developed independently by Evans[21, 22] for alpha-rays and by Steinke[23] and Schindler[24] for cosmic rays, who later suggested the similar apparatus for radon measurements used in Paneth's laboratory. The use of this method in conjunction with a Compton electrometer arranged for visual observation has been described by Urry.[6] This apparatus has been used for intercalibration and comparison with Evans's string-electrometer, photographic recording instrument.[22] The advantages of the automatic sensitivity calibration and photographic recording have been clearly emphasized when analyses by the two methods were made on the same samples. No significant changes in apparatus or technique have been found necessary in over 10,000 hours of almost continuous performance of the Evans a.c.-operated instrument.

(3) Calibration

The principal purpose of calibration is to enable the results to be expressed on an absolute basis. In addition, the standard solutions used

[18] R. D. Evans, Rev. Sci. Inst. **4**, 223–230 (1933).
[19] N. B. Keevil, Am. J. Sci. **36**, 304–309 (1938).
[20] N. B. Keevil, (in preparation).
[21] R. D. Evans, Phys. Rev. **39**, 1014L (1932).
[22] R. D. Evans, Rev. Sci. Inst. **6**, 99–112 (1935).
[23] E. Steinke, Physik. Zeits. **31**, 1019 (1930).
[24] H. Schindler, Zeits. f. Physik **72**, 625 (1931).

for such calibrations offer the most convenient means of intercomparison between different investigators. Even more important is the check on the proper operation of the apparatus afforded by frequent calibration. Both Evans and Urry have used standard solutions, kindly supplied by Professor S. C. Lind, as primary standards of calibration. Because these standards were of different concentration and received different treatment, for purposes of differentiation, the original solutions as received from Lind will be designated as the L-E (Lind-Evans) and the L-U (Lind-Urry) standards, respectively.

(*a*) *L-E standard.*—In December, 1932 one liter of solution containing 1.573×10^{-11} gram of Ra per cc (as of the date of separation 1919) plus 2 percent $BaCl_2$ and 2 percent HCl sealed in a Pyrex flask was received by Evans from Lind. This solution was prepared in Lind's laboratory by a 100-fold dilution of the original final standard solution prepared in 1919 by Lind and Roberts.[25] In preparing subdilutions of this standard, the extended tip of the flask has been open only long enough to allow two small portions for rinsing and one full portion of the solution to be withdrawn in a delivery pipette. Immediately following this operation the flask has been carefully sealed. No dilution of the original solution has occurred and possibilities of contamination and evaporation have been reduced to a minimum.

TABLE I. *Early radium calibrations by Urry with L-U standard. The apparent increase in calibration constant with decreasing radon in the ionization chamber was interpreted as a real effect. The apparent agreement between the higher values of K_U and that computed from the Duane-Laborde equation* led to the use of 0.00945 v/hr.·10^{-13} curie† prior to the discovery of the discrepancy in this value, Table II.*

DATE	Ra CONTENT (10^{-13} G)	Rn ACCUMULATED (10^{-13} CURIE)	**K_U OBSERVED (V/HR.·10^{-13} CURIE)
4/18/34	0.50	0.48	††0.0102 0.00867
5/ 8/34	0.50	0.48	0.00941 ††0.00951
6/ 6/34	0.50	0.50	0.00945
2/ 4/35	0.50	0.50	0.00944
4/20/34	1.25	1.21	0.00741
3/29/34	6.25	3.26	0.00827
3/29/34	31.3	15.9	0.00665

* Reference 26.
† Reference 6, p. 44.
** Collecting potential, 180 volts.
†† Determined by the null method (reference 6, p. 45).

(*b*) *L-U standard.*—In February, 1934 about 25 cc of the original Lind and Roberts final standard solution,[25] containing 1.573×10^{-9} gram Ra per cc (1919) with $Ba/Ra=7.1\times10^{+6}$ and about 2 percent HCl sealed in a Pyrex flask were received by Urry from Lind. The entire solution was then diluted by weight to contain 6.25×10^{-10} gram Ra per cc (corrected to 1934) and sealed in a manner similar to the L-E standard.

(*c*) *Earlier calibrations.*—Seven calibrations to obtain the conversion constant for Urry's apparatus K_U, in volts per 10^{-13} gram of radium, were made in 1934–35 by using subdilutions of the L-U diluted standard, and various quantities of radon in the ionization chamber. These values are given in Table I. The average $K_U=0.00945$ was used for all published radium determinations after July, 1935,[4, 5, 6] with a few exceptions as explained below. In Table I the value of K_U diminishes with increasing radon concentration in the chamber. Urry believed this to be caused by a dependence of the ionization current with respect to the saturation current, i/S, on the total number of ions present. Such a case is treated by Meyer and Schweidler[27] and by substitution the two last values in Table I gave a value of $K_U=0.0090\pm0.0005$ for 0.3×10^{-12} curie of radon compared with $K_U=0.00945$ as found for the very dilute standard solutions.[28] Consequently for a few cases of analysis with high electrometer charging rates, the appropriate value of K_U was read off a curve from the values in Table I.

(*d*) *Recent results.*—Discrepancies began to appear about two years ago between the helium ages obtained on the same hand samples by different investigators. With the geologically inferred ages used as a basis for comparison, the ages obtained by the alpha-helium method were consistent among themselves but considerably

[25] S. C. Lind and L. D. Roberts, J. Am. Chem. Soc. **42**, 1170 (1920).
[26] Duane and Laborde, Comptes rendus **1**, 1421 (1910).
[27] S. Meyer and E. v. Schweidler, *Radioaktivität* (Teubner, Berlin, 1927), p. 183.
[28] Reference 6, page 44.

lower than the corresponding published ages. At first it was suspected that there might be contamination of the thin rock film as deposited in the alpha-helium method, but numerous blank runs indicated no appreciable error from this source. The possibility of unknown alpha-emitters in terrestrial materials was considered, but subsequent work has reduced this to a low probability.

In the summer of 1937, Keevil, working in Urry's laboratory, while the latter was in Europe, found differences in the age results and obtained different apparatus constants from those used by Urry. In order to ascertain the source and magnitude of these differences, a cooperative program of intercalibration and comparison of results was undertaken. The primary source of discrepancy was found to be in the calibration of the radium apparatus. These results are described in detail in the next section.

(*4*) *Intercalibration*

Table II presents the calibration constants obtained by the two sets of apparatus on separate portions of the same standard solutions. It indicates no variation in the value of the calibration constant with radon concentration down to concentrations of about 1×10^{-12} curie in the ionization chamber. Below this concentration Urry thinks there may be an increase because of a small extraneous source of radon having no measurable effect at the higher concentrations but of the same order of magnitude as the very low concentrations. Others think these effects are spurious and caused by contamination or to the increased experimental error at low concentrations.

(*5*) *Selection of standard*

At the time this research was undertaken, no facilities were available for direct comparison of less than a milligram of radium with the National Radium Standard. However, the National Bureau of Standards will shortly have standard solutions covering the range from 10^{-11} to 10^{-5} gram of radium which should fill a serious need in the field of radioactivity.

When the above differences were found in supposedly reliable standards, it was necessary to evaluate the probable accuracy of various standards. The method of standardization of the Physikalisch Technische Reichsanstalt solutions, which were available, was not known, and the manipulation of the ampoule in which the solution is contained, during dilution introduces a possible source of error. Hence, the selection was between the L-E and the L-U standards mentioned above which had both been prepared from the original solution prepared in 1919 by Lind, using 206.7 mg of 100 percent radium chloride (equivalent to 157.3 mg of elemental radium by calculation and confirmed by gamma-ray comparison of the National Bureau of Standards against the National Radium Standard in 1920).

That the L-E Standard is the more reliable of the two Lind standards and within a small probable error is correct on an absolute basis may be inferred from the following:

(1) The solution obtained from Lind has not been diluted or transferred from the original flask.

(2) The solution as received from Lind contained 2 percent $BaCl_2$ and 2 percent HCl to prevent possible precipitation of the Ra as sulfate. No other chemicals have been added.

(3) Because of the extremely low concentration of Ra in the standards, ordinary contamination would tend to increase the Ra content. Precipitation as sulfate would produce the opposite effect; however, in correctly protected solutions one would favor the solution giving the lower value.

(4) One of the best known characteristics of radium is the rate of alpha-particle emission, which affords an independent and accurate means of standardization. The results of alpha-counts on de-emanated portions of these standards are given in Table III. Thus it is seen that the L-E standard is nearest to the recent determination of Gleditsch and Foyn[29, 30] in which the value, 3.50×10^{10} alphas per sec. per gram of Ra, was obtained.

(5) The L-E standard is in complete agreement with the theoretically predicted ionization[32] produced by its Rn, Ra A, and Ra C′ alpha-rays in a cylindrical ionization chamber of accurately known geometrical and electrical characteristics. Urry's selection of the higher values of K_U in

[29] E. Gleditsch and E. Foyn, Am. J. Sci. **24**, 387 (1932).
[30] E. Foyn, Arch. Math. Natur. **41**, No. 4 (1935).

Table I was largely based on the rough agreement with the calibration constant predicted by the Duane-Laborde equation.[26] This criterion is invalid, as Evans[31] has pointed out the inapplicability of this empirical formula for plain ionization chambers. It is even less reliable when applied to chambers containing nets, such as those used by Urry.

(6) Subsequent to the selection of L-E as the primary standard, we were fortunate in securing, through Dr. L. F. Curtiss, four ampoules of Ra solution prepared as subdilutions of an accurately known amount of $RaCl_2$, determined both gravimetrically and by gamma-ray comparison with the National Radium Standard by the National Bureau of Standards. These ampoules contained 2.00, 2.00, 1.00 and 1.00 micrograms of Ra, respectively, as shown by gamma-ray comparison with one another in which the counting-rate meter circuit gamma-ray apparatus[32, 33] equipped with a continuous photographic recorder was used. Accurate dilutions of one of the 1.00-microgram ampoules were compared with the L-E standard by the emanation

[31] R. D. Evans, Phys. Rev. **48**, 177–186 (1935).

[32] N. S. Gingrich, R. D. Evans and H. E. Edgerton, Rev. Sci. Inst. **7**, 450–456 (1936).

[33] L. I. Schiff and R. D. Evans, Rev. Sci. Inst. **7**, 456–462 (1936).

TABLE II. *Calibration constants of radium apparatus with various standards. In the determination of radium by the emanation method, in which an electrometer is used for the ionization measurements, it is necessary to calibrate the instrument with a solution of known* Ra *content in order to reduce the observations to an absolute basis. Such solutions also afford a convenient means of intercomparison between two apparatus as in the present case. Four different standard solutions were used, the L-E and the L-U (diluted), as defined in* **B**(*3*), *and two prepared from Physikalisch Technische Reichsanstalt ampoules (PTR-1 and PTR-2). For the nine reasons presented in* **B**(*5*), *the L-E standard has been selected as the most reliable and has been adopted as our primary reference standard. In the last column of the table, the ratio of the average calibration constants observed for the other standards are referred to that found for the L-E. On this basis the PTR standards appear to be slightly higher than their labeled value and the L-U (diluted) substantially higher by a factor of 1.32 as an average for the two instruments. These values are in good agreement with those found by the alpha-counts, Table III. The high* Ra *content of the L-U (diluted) standard only partially explains the difference between the former Urry calibration constant, 0.00945,* and the present accepted value of 0.00444±0.0005, the ratio in this order being 2.13. Because of this discrepancy, all of Urry's measurements in which the higher constant was used are subject to revision.† The calibration constant, K_E, of the Evans' apparatus with the L-E standard is somewhat higher than was formerly used†† on the basis of the same standard, because the installation of drying trays and a new type of head on the ionization chambers has increased the capacity by about 10 percent.*

DATE	OBSERVER	STANDARD	Ra CONTENT IN 10^{-12} G	Rn ACCUMULATED IN 10^{-12} CURIE	COLLECTING VOLTAGE	CALIBRATION CONSTANT	RATIO TO L-E
	URRY'S COMPTON ELECTROMETER APPARATUS					K_U** IN V/HR. $\cdot 10^{-12}$ CURIE	
9/ 6/37	Keevil	PTR-1	10.08	7.67	315	0.0048	
9/17/37	Keevil	PTR-1	10.08	6.52	315	0.0045	
9/28/37	Keevil	PTR-2	10.08	6.02	315	0.0048	
10/ 2/37	Keevil	PTR-2	10.08	3.10	315	0.0045	
					Average	0.00465±0.00006	1.05
9/20/37	Keevil	L-E	19.50	8.43	315	0.0043	
9/27/37	Keevil	L-E	19.50	12.50	315	0.0041	
1/27/38	Keevil	L-E	19.50	0.80	315	0.0041	
1/18/38	Urry	L-E	19.50	7.93	315	0.0043	
1/14/38	Urry	L-E	19.50	5.77	315	0.0043	
1/15/38	Urry	L-E	19.50	2.80	315	0.0046	
1/21/38	K & U	L-E	19.50	0.69	180	0.0043	
1/24/38	K & U	L-E	19.50	0.59	180	0.0050	
1/24/38	K & U	L-E	19.50	1.11	180	0.0050	
			Average (corrected to 315 volts collection)			0.00444±0.0005	1.00
10/27/37	K & U	L-U (dil.)	31.3	4.02	315	0.0053	
12/ 1/37	Urry	L-U (dil.)	6.26	0.56	180	0.00694	
11/30/37	Urry	L-U (dil.)	6.26	0.72	180	0.00799	
11/23/37	Urry	L-U (dil.)	6.26	0.88	180	0.00560	
11/26/37	Urry	L-U (dil.)	6.26	1.74	180	0.00666	
12/ 4/37	Urry	L-U (dil.)	6.26	3.19	180	0.00577	
11/19/37	Urry	L-U (dil.)	6.26	5.91	180	0.00547	
12/30/37	Urry	L-U (dil.)	6.26	6.05	180	0.00534	
			Average (corrected to 315 volts collection)			0.0061±0.0003	1.38

TABLE II. (*Continued.*)

DATE	OBSERVER	STANDARD	Ra CONTENT IN 10^{-12} G	Rn ACCUMULATED IN 10^{-12} CURIE	COLLECTING VOLTAGE	CALIBRATION CONSTANT	RATIO TO L-E
EVANS' STRING ELECTROMETER PHOTOGRAPHIC-RECORDING APPARATUS						Kg‡ IN 10^{-12} CURIE·HR./V	
12/18/35	Cooper	L-E	19.52	3.30	300	3.75	
3/ 9/36	Cooper	L-E	19.52	19.52	300	3.96	
3/30/36	Cooper	L-E	19.52	6.70	300	3.95	
5/26/36	Goodman	L-E	19.51	4.80	300	4.03	
6/20/36	Goodman	L-E	19.51	19.50	300	3.97	
9/ 3/36	Goodman	L-E	19.51	13.0	300	3.88	
10/30/36	Goodman	L-E	19.51	18.0	300	4.10	
9/20/37	Goodman	L-E	19.50	7.70	300	4.04	
10/ 1/37	Goodman	L-E	19.50	17.0	300	3.90	
10/10/37	Goodman	L-E	19.50	16.0	300	3.80	
10/13/37	Goodman	L-E	19.50	8.6	300	3.95	
12/ 8/37	Goodman	L-E	19.50	0.94	300	3.65	
3/ 5/38	Goodman	L-E	19.50	19.50	300	3.93	
3/ 7/38	Goodman	L-E	19.50	6.10	300	3.77	
3/12/38	Goodman	L-E	19.50	11.80	300	3.74	
					Average	3.89±0.02	1.00
9/ 7/37	Goodman	PTR-1	10.08	1.18	300	3.69	
9/26/37	Goodman	PTR-2	10.08	3.75	300	3.67	
10/12/37	Goodman	PTR-2	10.08	9.60	300	3.80	
					Average	3.72±0.03	1.04
10/15/37	Goodman	L-U (dil.)-1	12.50	1.46	300	3.20	
10/16/37	Goodman	L-U (dil.)-1	12.50	2.50	300	3.14	
12/18/37	Goodman	L-U (dil.)-2	12.50	2.25	300	2.90	
12/20/37	Goodman	L-U (dil.)-2	12.50	5.20	300	3.20	
					Average	3.07±0.05	1.26

* Reference 28. † References 4–6. †† Reference 34.
‡ All values of Kg are referred to zero sensitivity of the electrometer. Note that Kg is expressed in the reciprocal manner to K_U.
** The ionization current, and therefore, the calibration constant is dependent upon the collecting voltage. For comparison purposes, the average values of K_U have been computed to 315 volts collecting potential.

method, and found to be in agreement within the probable observation uncertainty of ±1.5 percent.

(7) A new portion of Lind's solution having 100 times the Ra concentration of the L-E standard has recently been supplied by Professor Lind. Comparison of this solution with the L-E standard (both undiluted) by the emanation method indicates agreement within ±1 percent.

TABLE III. *Alpha-counts on standard radium solutions. The rates of alpha-particle emission from de-emanated portions of standard radium solutions are given. These values were obtained from a plot of observed counts against time, extrapolated back to the time at the end of the de-emanation, in order to obtain the alpha-emission from the radium alone.* The theoretically expected counts are based on Gleditsch and Foyn's latest measurement of the curie as 3.48×10^{10} alphas per second per gram of radium. Their published value of 3.50×10^{10} has been corrected for the now generally accepted change in the Avogadro number to 6.03×10^{23} atoms per gram atomic weight. A 4-percent correction for the presence of* Po *has been included in the tabulated results. The magnitude of this correction was determined by deposition on nickel of the* Po *from the radium solution with subsequent measurement of the surface alpha-activity.*

STANDARD	Ra CONTENT IN G $\times10^{12}$	ALPHA COUNT OBSERVED	ALPHA COUNT THEORETICAL	RATIO MEASURED TO THEORETICAL
L-E	1.56	95±3	97.5	0.975±0.03
PTR-2	0.806	51±2	48.7	1.05 ±0.04
L-U (dil.)	1.25 (label)	109±3	78.0	**1.40 ±0.04
	†1.70 (meas.)		106.0	1.03 ±0.03

* References 30 and 31.
** This ratio of 1.40 is approximately equal to the average value 1.32 found from emanation measurements, Table II. Thus the alpha-activity confirms the inaccuracy of the labeled value of the radium content of the L-U (dil.) standard after dilution.
† Radium content based upon emanation measurements.

[34] R. D. Evans, Ph.D. Thesis, California Institute of Technology (1932).

TABLE IV. *Comparison of radium determinations on rocks by two methods. In addition to calibrations of the two radium apparatus with the same standard solutions (Table II), divided portions of granulated rock samples were measured by both the carbonate-fusion and the direct-fusion methods. Since the average ratio of the results is very close to unity (1.02), no consistent difference between the two techniques is indicated.*

Sample	Ra in 10^{-12} g/g of Rock		Ratio: Carbonate-Fusion to Direct-Fusion
	Carbonate-Fusion	Direct-Fusion	
RF[1]	1.95 ±0.06	2.14±0.07	0.91
[2]		1.96±0.06	
[2]		2.81±0.10	
RG[3]	1.88 ±0.05	1.80±0.06	1.04
M-6[3]	1.29 ±0.04	1.24±0.03	1.02
	1.24 ±0.05		
FG[3]	0.78 ±0.03	0.88±0.03	0.89
HOR-2[3]	0.72 ±0.02	0.68±0.03	1.06
No-3[3]	0.51 ±0.03	0.46±0.03	1.11
C-1[3]	0.47 ±0.03	0.57±0.04	0.83
HOK-2[3]	0.40 ±0.025	0.32±0.02	1.25
8b[2]	0.495±0.03	0.47±0.04	1.05
7[2]	0.46 ±0.02	0.46±0.04	1.00
C-10-A[1]	0.265±0.04	0.24±0.04	1.10
		0.33±0.05	
O[2]	0.23 ±0.015	0.25±0.01	1.09
		0.16±0.02	
37[2]	0.14 ±0.03	0.16±0.02	0.88
15b[2]	0.135±0.02	0.14±0.02	1.08
		0.11±0.03	
		Average	1.02

[1] Acid solution of carbonate fluxed rock.
[2] Separate portions of same hand specimen.
[3] Quartered portions of granulated rock used for both methods.

(8) The activity index measurements indicated in Section D afford an independent confirmation of the accuracy of the L-E standard to within the experimental uncertainty of ±9 percent.

(9) Finally, the age agreement, to be described later, between the radon-thoron-helium and the alpha-helium methods represents another independent confirmation of the L-E standard.

C. Comparison of radium determinations on rocks

From apparatus constants based on the L-E standard, a number of radium determinations on rock samples were made by the two techniques, the direct-fusion and the carbonate-fusion methods. These results are tabulated in Table IV. Because of the inherent inhomogeneity of rocks and the probable error of the measurements, some variation between the results by the two methods is to be expected. Thus the agreement is quite good, particularly on samples of higher than average radium content and in those cases where divided portions of the same prepared rock sample were used. The differences which do exist have a random distribution in sign, with an algebraic average of only 2 percent which indicates no systematic disagreement between the two methods when correct constants are used.

TABLE V. *Thorium calibration constants. The calibration of the constant streaming thoron apparatus was made by three* observers using thorium X solutions prepared from minerals of accurately analyzed thorium content.†*

Date	Observer	Apparatus**	Standard g Th×10^{8}	Constant α/hr.·10^{-4} g Th
5/16/33	Urry	I	3.4	2.80
5/17/33	Urry	I	6.9	2.86
5/17/33	Urry	I	13.7	2.72
5/18/33	Urry	I	27.4	2.68
11/21/33	Urry	I	5.2	2.69
11/22/33	Urry	I	10.4	2.88
11/23/33	Urry	I	20.8	2.73
11/24/33	Urry	I	19.8	2.64
11/25/33	Urry	I	29.7	2.75
			Mean	2.75±0.01
5/13/35	Urry	II	10.2	2.91
5/13/35	Urry	II	20.4	2.94
			Mean	2.93±0.02
4/27/37	Urry	III	10.3	2.99
4/27/37	Urry	III	20.6	2.94
			Mean	2.97±0.02
8/ 8/37	Keevil	IV	10.3	3.07
8/ 8/37	Keevil	IV	20.6	3.05
8/27/37	Keevil	IV	20.6	3.00
			Mean	3.04±0.02
9/19/37	Keevil	V	20.9	3.10
9/19/37	Keevil	V	20.9	3.08
			Mean	3.09±0.02

* Some of the calibrations were made with the assistance of Mrs. N. B. Keevil.
† References 36 and 37.
** I. Apparatus as originally constructed in 1933. II. New chamber, constant as computed on basis of previous value: 2.94. III. New chamber, about same volume as II but dead space decreased. IV. Rotameter rebuilt, new dead-spare tubing. V. Cleaned chamber and replaced dead-space tubing.

D. Thorium measurements

(1) *Detection apparatus*

As in the case of the uranium series, for the minute concentrations found in rocks, the gaseous product in the thorium series is the most convenient member to measure. Because of the short half-life of thoron ($T=54.5$ sec.), however, it is not feasible to follow the method used for radon ($T=3.82$ days). The streaming method first used by Strutt[35] has been adopted by Urry[6] for direct alpha-counting on the thoron itself, instead of ionization measurements on the thoron active deposit which would require several hours to build up. The source of thoron is a solution containing Th X, derived from the carbonate flux of the rock. The efficiency of the thoron counting, and its dependence on apparatus geometry and gas flow rate has been given elsewhere by Evans,[32] and by Urry.[6]

(2) *Calibration*

The apparatus constant used to convert the observed number of alpha-particles per hour into the equivalent amount of thorium is obtained from measurements on standard thorium solutions. These standards are more readily obtained than those of radium, because the concentrations involved allow convenient quantities of accurately analyzed thorium minerals[36, 37] to be fluxed with carbonate and the equilibrium amount of Th X separated out to form a solution of known content. Table V indicates the constants obtained from solutions of various concentrations. All of the constants obtained are in good agreement when the changes in apparatus indicated are taken into consideration.

(3) *Thorium determinations on rocks*

In Urry's previous thorium determinations, de-emanated air was streamed through the Th X solutions to act as a carrier for the Th emanating from the solutions. Because the activities to be observed are so small, background runs must be made to determine the natural alpha-count coming from the ionization chamber materials. Urry[38] sometimes shut off the chamber from the rest of the system during background observations. In this way it is possible* that higher counts would be obtained for the backgrounds than actually occur during a rock determination.

This possible error was circumvented in all the present work by the simple expedient of streaming de-emanated air through the system and chamber at the same rate for both the background and rock determination. Backgrounds were observed before or after every run.

TABLE VI. *Rate of helium production in igneous rocks. In the alpha-helium method the rate of helium production is observed as the number of alpha-particles (helium nuclei) per hour per milligram of rock, which we define as the "activity index." This quantity is determined indirectly in the radon-thoron-helium method from the measured* Ra *content (in 10^{-12} gram per gram of rock) and* Th *content (in 10^{-6} gram per gram of rock). The multiplicative factors involved are obtained as follows:*

$\lambda_{Ra}=4.68\times10^{-6}$ *hr.*$^{-1}$; $\lambda_{Th}=5.69\times10^{-15}$ *hr.*$^{-1}$

Activity Ratio (AcU *series to* UI *series):*

$$=\frac{\lambda_{AcU}N_{AcU}}{\lambda_{Ra}N_{Ra}}=0.046\pm0.002.^{*}$$

$$\begin{aligned}\textit{Activity Index}&=8\lambda_{Ra}N_{Ra}+7\lambda_{AcU}N_{AcU}+6\lambda_{Th}N_{Th}\\&=8.32\lambda_{Ra}N_{Ra}+6\lambda_{Th}N_{Th}\\&=1.04\text{Ra}+0.0886\text{Th}.\end{aligned}$$

Sample	Activity Index (1.04 Ra +0.0886 Th) (1)	Alphas/hr. mg (2)	Ratio (2)/(1)
RF	4.00±0.14	3.94±0.10	0.99
HOR-2	1.14±0.07	1.26±0.08	1.11
8b	0.88±0.06	0.67±0.06	0.76
No-3	0.72±0.05	0.64±0.08	0.89
HOK-2	0.725±0.07	0.62±0.08	0.86
C-10-A	0.46±0.03	0.34±0.06	0.74
O	0.44±0.02	0.42±0.03	0.96
15b	0.28±0.03	0.22×0.03	0.79
		Average	0.89

* Reference 39.

[35] R. J. Strutt, Proc. Roy. Soc. London **A76**, 88 (1905).
[36] Reference 6, page 39.
[37] Reference 22, page 111.
[38] Reference 6, pp. 35–36.
[39] A. O. Nier, Phys. Rev. **55**, 150–153 (1939).

* The authors are not in entire agreement as to the effects of different methods of streaming the carrier gas in the flow method of thoron measurement. Dr. Urry explains the effect as follows: In an incompletely tight system laboratory air infiltration produces, with no streaming, a continuously rising background which, however, quickly drops to a constant background on streaming as in the actual rock runs. A tight system shows no difference with or without streaming. To obviate this possible source of error in obtaining background counts higher than actually occur in the rock runs and to circumvent the necessity for periodic control of the background with and without streaming, it is advisable to reproduce always the same streaming conditions for both run and background. With Apparatus II (Table V) only, was the chamber shut off for background runs but the agreement of the constant for Apparatus II indicates a correct background.

Since no separate thorium determinations are made in the alpha-helium method, the thorium measurements cannot be compared directly on the rocks analyzed. However, a very significant comparison can be made on the basis of the "*activity index*," herein defined as *the total number of alpha-particles emitted per hour by the radioactive material contained in one milligram of rock.* This quantity is observed directly in the alpha-helium method but is calculated in the radon-thoron-helium method, from the decay constants of the parent elements. Table VI contains a comparison of the activities observed by the two methods on separate portions of the same rock sample.

Three conclusions can be drawn from the agreement in activities observed by these two, entirely independent methods of measurement:

(1) There are no unknown strong alpha-emitting radioactive elements in ordinary terrestrial materials.[40]

(2) The accepted decay constants of the parent elements thorium and uranium are correct to within the experimental accuracy of our measurements (±5 to 10 percent).

(3) The radon-thoron-helium method modified as indicated above, yields radioactivity measurements in agreement with the alpha-helium method.

III. Helium Measurements

A. Importance

Only in radioactive *minerals* is the content of active elements sufficient to produce gravimetrically measurable quantities of radiogenic lead during geologic time. In *ordinary* terrestrial materials the minute amounts of the parent radioactive elements produce so little lead that even for the oldest rocks the radiogenic lead content is extremely low, and is usually greatly exceeded by the common lead present. Hence helium affords the only readily observable evidence of the number of radioactive atoms which have decayed since the formation of the rock. Helium, being gaseous and inert chemically, may escape to some extent during geological changes such as metamorphism, weathering, and recrystallization, but theoretical considerations of the size of the helium atom, and the interatomic forces in rocks[41] show that the tendency to escape from perfect crystal structures of common rock minerals during geological time is negligible. The presence of relatively large amounts of helium in certain rocks also attests to its retention over hundreds of millions of years.

What was previously considered the most convincing experimental evidence[10] for helium retention in fine grained basic igneous rocks has been invalidated by the revision of those data as shown in this paper. There is some evidence that helium may escape from highly altered feldspars, but is retained in quartz and certain ferromagnesian minerals.[42, 43] Further studies on this important question of helium retention are now in progress.

The number of atoms of helium can be readily calculated from a measured volume of the gas at a known pressure. When divided by the rate of generation, such a determination affords a direct measure of the length of time required to accumulate the helium found in the sample. Hence, in both the alpha-helium method and the radon-thoron-helium method, the calculated age is directly proportional to the observed volume of helium in the rock. If no leakage of helium has occurred since solidification of the magma, and no important amount was originally present, the ratio thus obtained represents the true age of the igneous rock.

B. Methods of helium measurement

Similar to the radioactivity measurements, the determination of the helium content of rocks can conveniently be divided into two operations, (1) the release of the gas from the rock and (2) the measurement of its volume. It is necessary to separate the minute quantity of the inert helium from the relatively large volume of other gases released during the fusion of the rock. Since helium is not adsorbed to any appreciable extent, all the other gases can be completely removed, with the exception of the last traces of hydrogen, by adsorption on charcoal at liquid-air temperatures. The apparatus, purification procedure, and

[40] R. D. Evans and R. W. Raitt (see reference 15, p. 174) have previously shown that there are no strong unknown gamma-ray emitters in terrestrial materials.

[41] N. B. Keevil, Proc. Am. Acad. Arts and Sci. (in press)
[42] N. B. Keevil, Am. J. Sci. **36**, 406–416 (1938).
[43] N. B. Keevil, Nature **143**, 32A (1939).

methods of measurement have been described in detail in a series of papers by Paneth and his co-workers[44] and only the factors concerning comparative determinations will be considered here.

(1) *Apparatus for release of helium*

The carbonate-fusion vacuum furnace has been applied successfully by Paneth and his co-workers[45, 46] for stony meteorites, tektites, and igneous rocks and was modified by Petersen and Urry. Recently Paneth[47] has employed a vacuum induction furnace on South African rocks and minerals and compared the results on samples from lump to fine powder, and with and without various fluxes.

The difficulties in this method, which generally can be made small compared to the experimental uncertainty, are the necessity of using finely ground samples leading to possible loss of helium in grinding and during evacuation of the furnace, and the use of chemicals which must be examined for possible radioactive contamination, or preferably used in blank runs. One might also mention the low temperatures which are sufficient for carbonate fusion, but which might not liberate all of the helium from insoluble grains in some

TABLE VII. *Calibration factors for helium apparatus. In the helium determinations the McLeod gauge used, for measuring the volume of helium at a known pressure, contains a certain fraction of the total helium released from a weighed quantity of rock. We have chosen the reciprocal of this fraction to represent the calibration factor C of the apparatus. C is defined as the ratio of the effective total volume of the apparatus to the volume of the McLeod. C is most easily determined following an ordinary measurement by retaining the rock helium in the McLeod gauge while the remainder of the apparatus is flushed out with oxygen and evacuated. By allowing the helium in the McLeod to be redistributed throughout the system and following the regular adsorption procedure, the ratio of the effective volumes can be determined.*

DATE	OBSERVER	CALIBRATION FACTOR C	MEAN C
		Rn-Tn-He Apparatus	
3/ 5/34	Urry	2.263	
4/10/34	Urry	2.278	
4/25/34	Urry	2.281	2.274±0.004
7/18/37	New McLeod Gauge Installed		
7/20/37	Urry	*2.268	2.268±0.010
8/21/37	Keevil	1.96	
8/26/37	Keevil	1.93	
9/13/37	Keevil	1.94	
10/ 1/37	Keevil	2.00	
10/ 5/37	Keevil	1.95	1.956±0.008
11/ 8/37	Urry	2.022	
11/ 9/37	Urry	1.997	
11/ 9/37	Urry	2.052	
11/10/37	Urry	†2.064	2.024±0.011
		Direct-Fusion Apparatus	
11/ 1/36	Goodman	‡1.89	
5/17/37	Goodman	1.72	
5/17/37	Goodman	1.78	
9/13/37	Goodman	1.72	
1/13/38	Goodman	1.72	
2/25/38	Goodman	1.69	1.726±0.01

* Hydrogen present, reburned over Pd and adsorbed over-night.
† Hydrogen present, not included in the mean value.
‡ Determined with He and Ne from air; this value is high due to the greater adsorption of Ne relative to He, and is therefore not included in the mean value.

[44] For complete list of references: F. Paneth and W. D. Urry, Zeits. f. physik. Chemie **152**, 110 (1931).

TABLE VIII. *Comparison of helium determinations by two methods. Helium determinations on rocks of various types were made by Keevil and Goodman who used the carbonate-fusion and the direct-fusion methods, respectively. The conversion factors given in Table VII were used. With the exception of sample "O" (Oldwick basalt), in which case separate portions of the same hand specimen were used, quartered portions of granulated rock were used as samples, and the measurements were made concurrently on the two apparatus. Sample RG is excluded from the average ratio because of insufficient heating in the direct-fusion measurement. Sample No-3A was not measured by the direct-fusion method until 3 days after granulation; the lower result is attributed to loss of helium during this time and was not included in the average ratio.*

SAMPLE	HELIUM CONTENT IN 10^{-6} CC/G OF ROCK		RATIO: CARBONATE-FUSION TO DIRECT-FUSION
	CARBONATE-FUSION	DIRECT-FUSION	
15b	18.0	17.1	1.06
C-10-A	14.7	15.6	0.94
RF	11.6	11.2	1.04
RG	10.5	7.9	—
8b	6.6	7.9	0.84
7	6.8	7.7	0.88
No-3A	5.7	3.9	—
FG	3.5	2.6	1.34
HOK-2	1.7	1.8	0.95
O	0.85	0.80	
		0.71	
		0.77	1.14
		0.68	
		Average	1.02

[45] F. Paneth, H. Gehlen and K. Peters, Zeits. f. Anorg. Chemie **175**, 363 (1928).
[46] F. Paneth, H. Gehlen and P. Günther, Zeits. f. Elektrochem. **34**, 645 (1928).
[47] A. Holmes and F. Paneth, Proc. Roy. Soc. London **A154**, 385 (1936).

instances, and the time required in the operations. The important advantage is the measurement of helium on the same portion of rock sample used for the subsequent radioactivity measurements.

As indicated elsewhere[8] the direct-fusion method avoids these difficulties and gives a very rapid method for release of the helium from rock by directly boiling the sample in a graphite crucible at about 2000°C. However, it is necessary to use separate portions of the sample for the helium and alpha-ray measurements. This disadvantage might in some cases necessitate several determinations in order to obtain a reliable average value for the sample. The use of the radon condensation method[19] in conjunction with the helium determination, serves to minimize such errors. Test series already made, and the agreement between the alpha-helium and the radon-thoron-helium ages indicate that the inhomogeneity of most rock samples is not important enough to make this difficulty serious.

(2) Purification and measurement of helium

(a) Removal of other gases.—One of the main problems is the complete removal of the last traces of hydrogen before an accurate volumetric determination of the helium can be made. The direct-fusion method generates somewhat more hydrogen than the carbonate-fusion method, probably because of the reducing atmosphere and the higher temperatures reached. The addition of a small auxiliary charcoal trap and the inclusion of spongy palladium in the last trap adequately take care of this extra hydrogen.

(b) Measurement of helium.—For most determinations about five grams of rock are used, although several times this amount can conveniently be used in the direct-fusion method. Ordinary rocks have helium contents between 10^{-6} and 10^{-4} cc (referred to 0°C and 760 mm Hg) per gram. The volume of the system in which this gas is distributed during purification is about one liter, of which the McLeod gauge represents about one-half. The accurately determined ratio of the volume of the entire system to that of the McLeod constitutes the helium apparatus constant *C*. Determinations of this constant for the two apparatus are included in Table VII.

(c) Comparative determinations.—In order to test the extent of agreement between the two sets of apparatus for release and measurement of helium, analyses of duplicate samples were

TABLE IX. *Comparison of helium re-determinations with previous results. In seeking the cause of the difference in ages observed by Goodman and Keevil on the same hand specimens analyzed by Urry (Table XI), a limited number of these rocks were re-determined for helium by Urry, and the results are presented in column 3. No consistent ratio can be inferred from the comparison with the earlier measurements, although the fluctuations show the inhomogeneity present in some rocks.*

Sample	Helium in 10^{-6} cc per Gram of Rock		Ratio 1938 to 1934–1937
	1934–37	1938	
No-3A	6.40	6.28	0.98
No-3B	6.34 6.34	5.56	0.88
HOK-2	3.31	—	—
HOK-1	2.84	2.3 2.2	0.79
HOR-2	8.86	6.3	0.71
HOR-1	6.91	6.6	0.96
Kew 11	6.82	7.1	1.04
Kew 26	5.36	4.4	0.82
G 1	6.50	6.7	1.03
			Mean: 0.90

TABLE X. *Comparison of age measurements by two methods. The ages indicated were obtained by substitution of the helium content (Table VIII) and the measured "activity index" (Table VI) in the simplified age equation:*

$$\text{Age in million years} = K\frac{\text{Helium in } 10^{-6} \text{ cc/g of rock}}{\text{Activity Index (in } \alpha/\text{hr}\cdot\text{mg})} = 30.8\ \text{He}/I,$$

where I = activity index, He = helium content. For ages greater than 400 million years (C-10-A *and* 15b) *an old-age correction*[13, 43] *for the decay of the parent elements* UI, AcU *and* Th *has been included. With the single exception of specimen 8b, the agreement between the two sets of results is well within the experimental uncertainty of the measurements. There is no reason to suspect either determination of 8b, hence this sample was included in the average ratio. With 8b excluded the average ratio is 1.02.*

Sample	Age in Million Years		Ratio: Alpha-Helium to Rn-Th-He
	Alpha-Helium Goodman	Rn-Th-He Keevil	
O	54± 2	59± 3	0.92
HOK-2	89± 8	77± 7	1.16
RF	88± 5	89± 3	0.99
RG	110± 6	95± 4	1.16
HOR-2	100± 6	109± 6	0.92
No-3A	255± 18	242± 15	1.05
8b	350± 25	226± 15	1.55
C-10-A	820± 110	890± 50	0.92
15b	1850± 300	1800± 200	1.03
			Mean: 1.08

TABLE XI. *Re-determination of previously published ages. An attempt has been made to reconcile some of Urry's previous age measurements*[4–6] *with the newer values of Goodman and Keevil by recalculating (column 7) the former results (column 3) with the revised radium calibration of Table II. Although this correction does account for a good share of the difference, a serious lack of agreement is still evident by comparing column 7 with columns 4 and 5. Repeat measurements were made by Urry (column 6) in an effort to determine the cause of this remaining difference. Urry believes the lower 1938 values to be due to helium leakage from the hand specimens depending upon the nature of the rock.*

Sample	Geological Horizon	Age in Million Years				
		Urry 1933–36	Goodman 1937	Keevil 1937	Urry 1938	Urry (col. 3 recomputed)
O	Triassic	—	54± 2	59± 3	—	—
H 1	Triassic	180±11	—	—	—	104± 7
HOK-2	Post-Devonian	215± 8	89± 8	80± 7	—	140± 9
HOK-1	Post-Devonian	215± 8	—	—	110± 8 115± 9	140±10
HOR-2	Post-Devonian	220± 4	100± 6	109± 6	120± 5	140± 7
HOR-1	Post-Devonian	200± 5	—	—	130± 7	125±10
No-1	Keweenawan	485±20	—	—	—	335±15
No-3A	Keweenawan	525±25	255±18	242±15	260±14	365±15
No-3B	Keweenawan	520±25	—	—	290±15	365±18
Kew 11	Keweenawan	490±20	—	—	205±10	270±15
Kew 26	Keweenawan	555±25	—	—	355±13	365±15
G 1	Late Huronian?	515±25	—	—	290±11	320±16
G 1A	Late Huronian?	550±25	—	—	300±12	285±13

undertaken concurrently. The results presented in Table VIII indicate good agreement. The algebraic mean deviation between the two methods is only about 2 percent, which indicates no systematic difference. The variation observed is largely due to the inhomogeneous distribution of helium in the sample, because the probable error of the actual measurement is quite low as shown by the consistency of the measured values of C (Table VII).

Part of the search for the cause of age differences consisted of a re-determination of helium on a number of rocks. In Table IX Keevil and Goodman find consistently lower helium contents than Urry's published values. Urry's re-determinations are also in general lower than the early results for the same hand specimens. Some of the differences observed may be due to inhomogeneity of the specimens, but the possible leakage of helium during the intervening time is suggested. A better comparison is that of the ages, given in the following section, which should be independent of any such inhomogeneity.

IV. Age Measurements

The age of a rock calculated from the individual He, Ra, and Th determinations should agree with that obtained from measurements of the rate of alpha-particle emission from rocks and the helium content. The ages obtained from these independent methods are in very good agreement, as indicated in Table X. The alpha-ray counting method is a direct determination of the rate of production of helium in the rock, and age results by this method are therefore entirely independent of all radioactive standards. Except for the second-order correction on very old rocks;[13, 48] alpha-helium ages do not depend in any way on standard radium or thorium solutions, nor upon the decay constants of thorium, uranium or actino-uranium.

The agreement of the radon-thoron-helium method (with the new calibration constants described above) with the direct alpha-helium method is cogent evidence for the validity of these revised calibration constants. It also strengthens the radioactive concepts upon which the helium age methods are based.

Because of emphasis on quantity of results from the numerous geological periods in order to obtain a broad view of the value of ages based on radioactivity, very little comparative work has

[48] Reference 7, page 153, N. B. Keevil, Am. Jour. Sci. **237**, 195–214 (1939).

TABLE XII. *Age data on radioactive minerals by the lead method. Of the many radioactive minerals which have been examined by the lead method, four have been selected as most nearly fulfilling the three criteria for lead ages. Thus far no direct comparison of the lead and helium age methods has been made, so that it is impossible to say with certainty that the two techniques yield ages which are in disagreement.*

MINERAL	LOCALITY	GEOLOGICAL AGE	LEAD AGE IN MILLION YRS.	METHODS	REMARKS
Samarskite[50, 51]	Spinelli Quarry, Glastonbury, Conn.	Pre-Triassic	270±75	Pb/U and Pb/Th ratios	No determination of isotopic constitution
Pitchblende[39, 52, 53]	Jachymov, Bohemia	Late-Paleozoic	220±40	Pb^{207}/Pb^{206} Pb/U and Pb/Th ratios, atomic wt. and isotopic analyses	No accurate geological data
Thorite[39, 53, 54]	Brevig, Norway	Permian (?)	230±30	ditto	Geological age somewhat uncertain
Kolm[39, 53, 54]	Güllhögen, Sweden	Upper Cambrian	450±75	ditto	Accurately dated geologically; sample somewhat porous and loss of emanations possible

heretofore been done in this field. In fact, so far as we are aware the present age results constitute the first agreement between two observers working on the same geological specimens. The importance of such intercomparisons in the early stages of development of such a technique should be emphasized.

The above ages found by both methods are lower by approximately a factor of two or more than Urry's time scale. When these relatively low ages were obtained, the question naturally arose as to whether the discrepancy was partially due to the particular geological specimens being investigated. Hence, a limited number of rocks previously analyzed by Urry were redetermined by the two methods. The results are summarized in Table XI and indicate that the previous ages are too high by about the same amount found in the determinations on the other rocks. The data for Urry's early radium determinations (1933-36) have been recomputed with the corrected radium calibration constant, and result in the ages given in the last column of Table XI. These recomputed values are still somewhat higher than the redeterminations of Goodman, Keevil and Urry, and suggest that some unknown source of error exists in Urry's previous age measurements, which, however, might be partially or completely accounted for by a leakage of helium from the hand specimens in the 3–5 years intervening between measurements.

Until a large number of existing problems have been settled and many more rocks analyzed, it does not seem advisable to prepare a revised helium time scale in which the geologic periods are delimited. However, some benefit derives from a presentation of the ages obtained, together with their most likely geological horizons, in order to show the relative values and the wide extent of time represented. It will be noted (Table X) that the range of ages is from 5 to 1800 million years, which is equivalent to the previous helium and lead age scales. In fact, if the oldest age of 1800 million years were based on the previous calibration constants used by Urry, the age would be considerably in excess of any found by the lead method.[49]

Thus the revised helium ages do not indicate any decrease in the generally accepted total span of geologic time, popularly called the "Age of the Earth," but only suggest *a redistribution of this time among the various geologic periods.*

V. LEAD AGES

In Holmes' recent publication[7] the ages calculated from lead ratios and from Urry's radon-thoron-helium measurements have been compared. It is thus concluded that "it is remarkable how consistently the age estimates fall into appropriate positions. That this stringent test of internal consistency is satisfactorily met must be

[49] Reference 7, page 207.
[50] R. C. Wells, National Research Council Report of the Committee on Geological Time, p. 76 (1935).
[51] Reference 7, p. 165.
[52] Reference 7, p. 159.
[53] Rose and Stranathan, Phys. Rev. **50**, 792 (1936).
[54] Reference 7, pp. 176, 178.
[55] Reference 2, pp. 6, 7, 101 and 210.
[56] Reference 7, pp. 161–163, 172.

regarded as the final proof that the ages calculated from the lead- and helium-ratios are at least of the right order and that no serious error is anywhere involved." At the time this statement was being written, the first observations were being made which revealed the unfounded optimism of Holmes' conclusion. Since the apparent agreement between the two radioactive methods of age measurements has been emphasized as such strong evidence for the accuracy of both methods, it is only natural to inquire into the actual extent of this apparent agreement and the fundamental principles underlying the lead method, now that the previous helium ages have been definitely invalidated.

In many radioactive minerals an easily measurable amount of lead has accumulated since crystallization. By use of the so-called lead ratio,[2] and the appropriate decay constants, the length of time required for the production of this amount of lead by the parent radioactive element can be determined readily. However, any common lead present in the mineral would increase the observed ratio resulting in an inordinately high age.

Recent developments in accurate isotopic abundance[39] and atomic weight determinations enable the exact proportions of the isotopes in the mineral lead to be ascertained. These measurements dictate the required correction in the lead ratio and yield reliable ages, provided other criteria are fulfilled. Because ages were obtained on a large number of minerals prior to the realization of the importance of common lead as a contaminant, the workers in this field are reluctant to discard these results, particularly where agreement with the newer ages exists. The result of this inclusion of earlier measurements is to present an almost solid front of what at first sight appears to be indisputable evidence for the absolute validity of lead ages. Upon further investigation, however, uncertainties begin to appear and individual consideration of each measurement must be made before the results can be properly weighted.

While independent geologic evidence for the horizon of either minerals or rocks cannot be obtained for every sample analyzed, nevertheless, for the formulation of a time scale it seems desirable that specimens should have their positions determined with an accuracy comparable to that of the analysis. This is even more important when there is uncertainty as to the agreement between two methods of measurement. Anomalous rock and mineral analyses should not be discarded, but the reasons for variations from what might be expected should be investigated.

Among the large number of lead ages on radioactive minerals, only four[39, 50–56] have been definitely established which are (1) free from alteration, (2) of well-established geological horizon, and (3) based on isotopic abundance or atomic weight determination of the lead. The important age data on these four minerals are summarized in Table XII. Even in these specimens the span of possible horizons is so great that no sharp disagreement exists between the corresponding helium ages found for rocks (See Table X.) The most important result to be drawn from this critical consideration of the lead time scale is the obvious necessity for further age measurements on well-authenticated minerals and rocks, preferably from neighboring formations with unquestioned relative ages.

VI. Geologic Notes for Rock Specimens

O—Lat. 40°40′N, Lon. 40°45′W. Specimen collected from a basalt flow by A. C. Hawkins in 1936, fifty feet from the surface in a working quarry at Oldwick, N. J. The top of the flow has been removed by erosion, and the bottom is not visible. Similar flows in the area of slightly different periods of eruptivity have been identified as being of Triassic age from fossils in adjacent sedimentary beds (red shales and sandstones).[57] Age: Probably Triassic.

HOK 1 and 2, and HOR 1 and 2. Lat. 55°45′N, Lon. 5°3′W. Monchiquite dike specimens sent by Arthur Holmes in 1936 from Kilchattan and Riasg Buidhe on the Island of Colonsay, Scotland. Geological relations nowhere provide evidence of their age beyond the fact that they cut formations regarded as Torridonian.[58] Age: Post-Devonian.

RG—Lat. 42°40′N, Lon. 70°35′W. Granite collected by N. B. Keevil August 18, 1937 from freshly quarried block from the Upper Pigeon Hill Quarry, Cape Ann, Mass. Intrudes Salem gabbro diorite, which in turn cuts Pre-Cambrian rocks and is possibly of Devonian Age. It is cut by diabase dikes which are generally considered to be related to similar dikes interbedded with Triassic sedimentary beds at Deerfield and Mt. Holyoke, Mass.[59] Age: Probably Pre-Triassic and Post-Cambrian.

[57] J. V. Lewis and H. B. Kümmel, Bull. 14, Geol. Survey of New Jersey, pp. 62, 95 (1915).

[58] Arthur Holmes, private communication.

[59] B. K. Emerson, U.S.G.S. Bull. **597**, 188 (1917). C. H. Clapp, U.S.G.S. Bull. **704**, 25–26 (1921). T. N. Dale, U.S.G.S. Bull. **738**, 293 (1923). C. H. Warren and

RF—Fine-grained cognate xenolith from the same large hand specimen as RG.

7 and 8b—Lat. 44°56½'N, Lon. 109°29½'W elev. 9800 ft. Trap rocks collected by A. C. Lane in July, 1937 from the center and two feet from the margin, respectively, of a 100-ft. dike at Long Lake, Wyoming. The specimens were taken from a small working quarry for road metal. The dikes of this series are intrusive into the early pre-Cambrian complex (Stillwater series), and appear to be older than the middle-Cambrian rocks of Bear Tooth Butte, but the exact relations are obliterated by overburden for a considerable distance.[60] Age: Possibly Pre-Middle Cambrian, and post early Pre-Cambrian (younger than 15b).

No-3 and No-3A—Lat. 43°15'N, Lon. 79°2'W. Diabase specimen collected by P. Price three feet from the chilled contact of a north-south dike at the 17th level (1975 ft.) of the Horne Mine at Noranda, Quebec. The dikes of this set are unaltered and cut all the other rocks of the region, including the Cobalt series of the late Pre-Cambrian.[61] Age: Post-Cobalt.

C10A—Lat. 48°14'N, Lon. 77°54'W. Hornblende granodiorite collected by W. C. Güssow in 1936 from a specimen freshly blasted from a road cut ten feet from the surface. The granodiorite is intrusive into a sedimentary complex of Keewatin or possibly earlier age, and is thought to be older than the diabase dikes in the area, and the Cobalt series to the southwest.[62] Age: Probably Pre-Cobalt and Post-Keewatin.

L15—Lat. 45°1'N, Lon. 109°25'W. Norite from the metamorphosed Stillwater complex collected in July 1937 by A. C. Lane from Quad Creek, Montana, one mile north of the state line. The Stillwater complex is bordered by a Cambrian conglomerate at an erosional contact,[63] and is cut by granite and basic dikes. Age: Probably early Pre-Cambrian.

The authors are indebted to Mrs. N. B. Keevil for her assistance in most of the thorium determinations. These researches have been supported in part by grants-in-aid to A. C. Lane from the Penrose Fund of the Geological Society of America, and an award by the Carnegie Fellowships Board of the Royal Society of Canada to N. B. Keevil.

H. E. McInstry, Proc. Am. Acad. Arts and Sci. **59**, 315 (1924). L. LaForge, U.S.G.S. Bull. **839**, 31–33 (1932).

[60] E. C. H. Lammers, private communication.

[61] Specimen from Loc. 14, Map 241, Can. Inst. of Min. and Met.; P. Price, Can. Min. Inst., March (1934); M. E. Wilson, Can. Min. Inst., pp. 389-390, August (1934).

[62] W. C. Güssow, Trans. Roy. Soc. Canada, Sec. IV, **31**, 130, 150 (1937).

[63] J. W. Peoples, Rept. of XVI Int. Geol. Congress, Washington, 1933. Reprint issue, pp. 353–360, October (1936).

MAY 15, 1939 PHYSICAL REVIEW VOLUME 55

Conditions for Producing Intense Ionic Beams

LLOYD P. SMITH AND G. W. SCOTT, JR.
Cornell University, Ithaca, New York

(Received September 6, 1938)

Conditions for the optimum production of positive ions and their complete removal from the ionization region to form a beam are developed. The calculations take into account the variation in ionization cross section as a function of electron energy. The mechanism of proton production is considered and the efficiency of arc type sources is discussed.

I. INTRODUCTION

ALONG with the development of the field of nuclear physics it has become increasingly important to have a device capable of supplying large numbers of ions, especially protons, deuterons and alpha-particles. In response to the demand a number of ion sources have been built, most of which are modifications of the arc type in which use is made of the positive ion current to the wall surrounding the arc plasma. It was by no means certain that the greatest number of ions could be produced and delivered as a beam with this type of source. Consequently a systematic study of the whole problem was undertaken to determine the best method for producing an ion beam of a prescribed intensity. The results of the study are set forth below, wherein it will be seen that in principle it is possible to produce beams of extremely high intensity.

Before discussing in detail the various factors involved in the formation of ion beams it will be well to note what characteristics are generally desirable in a good ion source. In the first place the source should deliver an approximately

parallel beam. As will be shown later it is possible to construct a source in which the beam remains of constant cross section in the ionization region but it is very difficult to maintain a small delivered beam of high intensity unless the ions are rapidly accelerated. Secondly the ion current should be steady over rather long periods and at the same time it should be possible to vary the ion current over a wide range and still maintain a high degree of stability. This may be accomplished provided the intensity of the bombarding electron beam, the gas pressure, the ion extracting potential and the intensity of the ion beam are not complicated functions of one another but independently controllable. A third item of considerable importance is the ratio of useful ions to neutral atoms in the beam. It is obvious that this ratio should be as high as possible in order to avoid removing large quantities of gas from the accelerating apparatus by fast pumps. This can only be accomplished by having a large number of bombarding electrons and making the most efficient use of them as ionizing projectiles. When the ions desired are protons, it is usually very important that the ratio of protons to hydrogen molecular ions be as high as possible. As will be pointed out later the conditions for attaining this are intimately connected with several modes of production of protons and atomic recombination but, in so far as these are understood at present, high proton yields require large numbers of bombarding electrons.

Other convenient features of a source would be homogeneity of the ion beam with regard to ion velocity, low input power and relatively low ion extracting voltage. These are not always important for certain applications and indeed not all obtainable in a given type of source.

II. Ionization Processes

The most efficient method available for ionizing atoms is by bombardment with electrons of suitable energy. In this section the ionization of hydrogen will be discussed specifically but the discussion applies generally to ionization of other atoms as well.

The likelihood that an electron will ionize an atom when directed toward that atom is quantitatively expressed in terms of the ionization cross section. This cross section σ is a function of the energy of the electron, increasing sharply for energies above the ionization potential to a maximum for an energy roughly three to four times the ionization potential and decreasing with increasing energy and for large energies varying approximately inversely with the energy. The ionization cross section[1] for hydrogen for relatively low energies is shown in curve *a*, Fig. 2. The ordinates on the left-hand side represent the number of positive ions formed per incident electron per centimeter path at a pressure of one mm Hg at 0°C.

Since the probability of formation of a proton by direct electron impact with the hydrogen molecule H_2 appears to be very small,[2] this process deserves special consideration in order to determine necessary conditions for a large ratio of H_1^+ to H_2^+. Existing evidence points to the conclusion that the formation of H_1^+ is a secondary or tertiary process. The primary process is that of first producing H_1 in the following ways:

$$H_2+e\rightarrow H_1+H_1, \tag{1}$$

$$H_2+e\rightarrow H_2^++2e;\quad H_2^++H_2\rightarrow H_3^++H_1, \tag{2a}$$

$$\rightarrow H_1^++H_1+H_2. \tag{2b}$$

The first process in (2) is the normal ionization process with cross section σ. The cross section for the process (1) has been calculated by Massey and Mohr[3] and although the calculations are admittedly not very accurate the maximum value which occurs at about 15 volts is $6\pi a_0^2$. This is roughly six times the maximum cross section for the formation of H_2^+. Even though this cross section decreases rapidly with increasing electron energy at 50 volts it is still of the order of magnitude of that for the formation of H_2^+. It seems likely that at low pressures and low electron energies the process (1) is important for the production of H_1.

A further process which could be important at higher pressures is the collision of an H_2^+ after acceleration with a neutral molecule H_2 according to the reactions (2a) and (2b). The detection of the H_3^+ ion shows that (2a) occurs to some extent.

[1] P. T. Smith and J. T. Tate, Phys. Rev. **39**, 270 (1932).
[2] H. D. Smyth, Rev. Mod. Phys. **3**, 348 (1931).
[3] N. Massey and F. Mohr, Proc. Roy. Soc. **A135**, 258 (1932).

If the production of protons first requires the production of H_1 atoms according to one of the processes mentioned above, then the rate of proton production depends on the equilibrium concentration n_1 of H_1 atoms. Aside from the primary rate of production of H_1 atoms denoted by r, the equilibrium concentration n_1 will depend on the loss of H_1 atoms by formation of protons and recombination of H_1 atoms. The latter may take place in the gas chamber or at the walls. Ordinarily the recombination at the wall is considerably greater than in the space because an atom striking the wall may on the average remain there a certain time before reevaporation so that there is considerable chance of another H_1 atom striking near enough to recombine with it, the excess energy being taken up by the wall. This rate of disappearance of H_1 may be represented by an_1 where a is a kind of accommodation coefficient which depends on the nature of the enclosing walls and the mean velocity of approach of the H_1 atoms etc. In proton sources special precautions are usually taken to keep the accommodation coefficient small. This may be done by maintaining the ionization chamber walls at high temperature or coat the walls with P_2O_5 or subject the walls to considerable electron bombardment. The rate of loss of H_1 within the walls may be represented by αn_1^2 where α is a recombination coefficient. Consequently the rate of increase of n_1 would be given by

$$dn_1/dt = r - an_1 - \sigma_1^+ I_- n_1 - \alpha n_1^2,$$

where the term $\sigma_1^+ I_- n_1$ represents the rate of decrease of n_1 because of ionization and will henceforth be neglected. If the interior recombination is the more important the equilibrium concentration will be approximately

$$n_1 \cong (r/\alpha)^{\frac{1}{2}}. \tag{3a}$$

If, on the other hand, the recombination at the walls is the more important then

$$n_1 \cong r/a. \tag{3b}$$

Considering the reaction (1), $r = \sigma_2^1 I_- n_2$ and it is readily seen that the ratio of proton to molecular ion current is

$$\frac{I_1^+}{I_2^+} = \frac{\sigma_1^+}{\sigma_2^+}\left(\frac{\sigma_2^1 I_-}{\alpha n_2}\right)^{\frac{1}{2}} \quad \text{for case (3a)} \tag{4a}$$

$$= \frac{\sigma_1^+}{\sigma_2^+}\frac{\sigma_2^1 I_-}{a} \quad \text{for case (3b).} \tag{4b}$$

If the H_1's were produced by either of the reactions (2a) or (2b) the two corresponding yield ratios would be

$$I_1^+/I_2^+ = \sigma_1^+(\kappa_2^1 I_-/\alpha\sigma_2^+)^{\frac{1}{2}} \tag{5a}$$

$$= \kappa_2^1 \sigma_1^+ I_- n_2/a. \tag{5b}$$

From data presented in the following paper, on an actual ion source, it appears that the proton yield ratio is always high for low H_2 pressures and at these low pressures the yield varies approximately as the square root of the electron current in agreement with (4a). For higher pressures the yield materially decreased and was thereafter not very sensitive to changes in electron bombarding current or pressure which is not in accord with (4b) and (5b) and very likely (5a). The formation of H_1^+ according to (2b) gives rise to the yield ratio $\kappa_2^{1+} n_2$ which is independent of I_- and increases linearly with the pressure; a result not found in our experiments.

The constancy of the yield ratio as regards electron current and pressure at high pressures is not to be accounted for by the indirect processes considered so far. In order to obtain a constant yield ratio it is necessary that the proton be produced directly by an electron collision with an H_2 molecule. The direct process

$$H_2 + e \rightarrow H_1^+ + H_1 + 2e$$

is a possible one and should take place for electron energies greater than about 30 electron volts. The yield ratio is $\sigma_2^{1+}/\sigma_2^{2+}$. It is thought therefore that this is important at high pressures. Thus the maximum yield occurs at low pressures and for high electron bombarding current. Since this appears to be brought about by the reaction (1) the velocity of the electrons should be made as close as practical to that corresponding to the maximum cross section for the process which according to the calculations already referred to[3] corresponds to about 15 electron volts. It will rarely be possible to attain this low velocity and still be able to draw all of the ions out of the

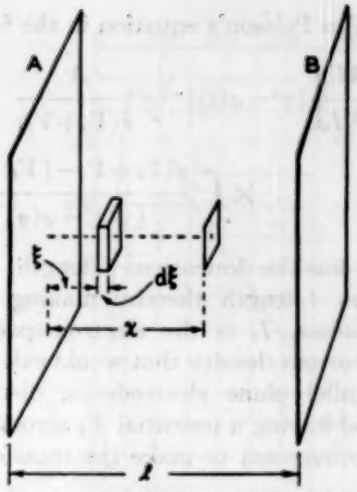

FIG. 1.

ionization chamber as will be pointed out in the next section.

III. REQUIREMENTS FOR OPTIMUM TOTAL ION YIELDS

When the desired number of ions is produced in the ionization chamber by electron impact in accordance with the considerations of the preceding section, they must not be wasted but all ions must be removed from the chamber and made to contribute to the useful beam current. The two most important factors which prevent the recovery of all of the ions formed are the positive ion space charge in the ionization chamber and the divergence of the ion beam caused by the mutual electrostatic interaction of the ions in the beam. The space charge problem can be solved for an electrode arrangement and ionizing conditions close enough to practical conditions to afford a satisfactory guide in design and application of proper electrode potentials. It will suffice for an understanding of the space charge problem to consider the ionization chamber bounded by two parallel plane electrodes as shown in Fig. 1.

The ions are produced by electron collisions with gas atoms or molecules between the plates A and B, the electrons entering the chamber with a certain initial velocity either at the plate A or B. If they enter the chamber at plate B, they will be accelerated and in accordance with Figs. 1 and 2 their ionizing efficiency will decrease as they approach plate A. The potential distribution between plates A and B will be the same for electrons entering at B with a velocity corresponding to the potential V_b and then accelerated by the potential difference V_l between the plates as for electrons entering at A with an initial velocity corresponding to V_b+V_l. Consequently it will suffice to discuss the case where electrons are introduced at B.

The number of ions produced per unit volume in the neighborhood of ξ will be proportional to the number of electrons traversing unit area there. The ion pairs produced near ξ tend to increase the number of electrons in the beam to the left of ξ, but the contribution of these electrons to the beam will be negligibly small unless the mean free path for ionization is short compared to the distance between plates which means $1/\sigma p \ll l$ where p is the gas pressure in mm Hg. On the other hand, this increase will, in part, be compensated for by the electrons removed from the beam by scattering so that it will be assumed that the same number of electrons traverse every unit area between A and B.

The problem at hand is to determine the conditions which must obtain in order that all ions produced shall flow toward the plate B and eventually through a hole to form the ion beam. This requires that the potential distribution between the plates have the property that dV/dx does not vanish at any point between A and B except at the plate A where $x=0$. The potential distribution may be found by solving Poisson's equation

$$d^2V/dx^2=4\pi(\rho_- - \rho_+), \tag{6}$$

subject to the condition that $V=dV/dx=0$ at $x=0$. The potential to the right of plate A, i.e., for $x>0$ will be negative and the potential difference between the plates be denoted by V_l.

If $N(\xi)$ is the number of ions formed per unit time per unit volume in the neighborhood of the point ξ, the contribution of the ions formed in the element of volume $d\xi$ to the ion space charge density at x will be

$$d\rho_+ = dI_+/v_{x\xi} = eN(\xi)d\xi/v_{x\xi}, \tag{7}$$

where I_+ is the positive ion current density and $v_{x\xi}$ is the velocity that the ion produced at ξ will have upon arrival at x. It is readily seen that

$$v_{x\xi}=[2e\{V(\xi)-V(x)\}/M]^{\frac{1}{2}}.$$

The total ion space charge density at x will then be

$$\rho_+ = (eM/2)^{\frac{1}{2}} \int_0^x \frac{N(\xi)d\xi}{[V(\xi)-V(x)]^{\frac{1}{2}}}. \quad (8)$$

The electron space charge density is given by the expression

$$\rho_- = I_-[m/2l(V_b - V_l - V(x))]^{\frac{1}{2}}. \quad (9)$$

$N(\xi)$ in Eq. (7) may be expressed in terms of the ionization cross section defined in Section 2 so that

$$N(\xi) = (I/e) - p\sigma(V_b - V_l + V(\xi)). \quad (10)$$

If these expressions are substituted in Eq. (6) and the following changes are made in the independent and dependent variables, namely

$$s = \alpha x; \quad \alpha = (M/m)^{\frac{1}{2}} p\sigma(V_b + V_l);$$

$$\varphi(s) = -V(s/\alpha)/|V_l|; \quad \gamma^2 = 1 + V_0/V_l$$

and

$$I_0 = (2e/m)^{\frac{1}{2}} V_l^{\frac{1}{2}} \alpha^2/9\pi \quad (11)$$

one obtains Poisson's equation in the form

$$\frac{d^2\varphi}{ds^2} = -\frac{4I_-}{9I_0}\left[|\gamma^2 - \varphi(s)|^{-\frac{1}{2}} - \frac{1}{\sigma(V_b+V_l)} \times \int_0^s \frac{\sigma(V_b+V_l-|V_l|\varphi(\eta))}{[\varphi(s)-\varphi(\eta)]^{\frac{1}{2}}} d\eta\right].$$

Since $p\sigma$ has the dimensions 1/length, α has the dimension 1/length thereby making s and φ dimensionless. I_0 is the electron-space-charge-limited current density that would exist between two parallel plane electrodes a distance $1/\alpha$ apart and having a potential V_l across them.

It is convenient to make the transformations

$$\varphi(s) = \rho^2(s) \quad \text{and} \quad \rho(\eta) = \rho(s)\sin\theta$$

in the above equation and regard s as a function of ρ which makes it possible to carry out one integration with respect to ρ subject to the condition $d\varphi/ds = 2\rho/ds/d\rho = 0$ at $s=0$. This yields the equation

$$\rho = -\frac{2I_-}{9I_0}\frac{ds}{d\rho}\left[\int_0^\rho |\gamma^2 - \rho^2(s)|^{-\frac{1}{2}}\frac{ds}{d\rho}d\rho - \int_0^\rho \frac{ds}{d\rho}d\rho \int_0^{\pi/2} \frac{\sigma(V_b+V_l-|V_l|\rho^2(s)\sin^2\theta)(d\eta/d\rho)d\theta}{\sigma(V_b+V_l)}\right]. \quad (12)$$

The solution of this equation may be sought by expressing s as a power series in ρ of the form

$$s = c_1\rho + c_2\rho^2 + c_3\rho^3 + \cdots \quad (13)$$

This fulfills the boundary conditions that $\varphi = \rho^2 = 0$ at $s=0$ and $d\varphi/ds = 0$ at $s=0$. Substituting (13) in Eq. (12), expanding the integrands as power series in ρ, which may be done since $\gamma > 1$ and $\rho \leq 1$, and evaluating the integrals, one obtains a power series in ρ on the right-hand side. Equating the coefficients of like powers of ρ on each side, one obtains the following equations for the determination of the unknown coefficients:

$$c_1^3 - 2c_1^2/\pi\gamma - 9I_0/\pi I_- = 0, \quad (14a)$$

$$c_2 = 0,$$

$$\left(\frac{4}{c_1} - \frac{9\pi\gamma}{4}\right)c_3 + \left(\frac{d\log\sigma(E)}{d\log E}\right)_{E=V_b+V_l}\frac{\pi c_1}{12\gamma} + \frac{1}{6\gamma^2} = 0 \quad (14b)$$

$$c_4 = 0.$$

By means of elementary algebraic methods, it is easily seen that the above cubic equation has only one positive real root which is

$$c_1 = (2/3\pi\gamma)[1 + u^{-\frac{1}{3}}F(u) + u^{\frac{1}{3}}F(u)^{-1}],$$

where

$$u = (2/3\pi\gamma)^3\pi I_-/9I_0 \quad (15)$$

and

$$F(u) = [1 + 2u + (1+4u)^{\frac{1}{2}}]^{\frac{1}{3}}\cdot 2^{-\frac{1}{3}}.$$

An inspection of the above expression for c_1 shows that as u traverses the range $\infty \geq u \geq 0$ of physical interest, c_1 traverses the region $1 \leq \pi\gamma c_1/2 \leq \infty$.

In order to see whether the potential distribution between the plates remains monotomic to the approximation under consideration, it is necessary to determine the conditions for which $d\varphi/dx$ remains positive for all x. Since

$$d\varphi/dx = (dx/d\varphi)^{-1} = 2\alpha\varphi^{\frac{1}{2}}/c_1 + 3c_3\varphi, \quad (16)$$

$d\varphi/dx$ will remain positive provided $-\frac{1}{3} < c_3/c_1$. The value of c_3/c_1 may be found by writing Eq. (14b) in the form

$$c_3/c_1 = (1+Dv)/[3\gamma^2(9v-8)], \quad 1 \leq v \leq \infty, \quad (17)$$

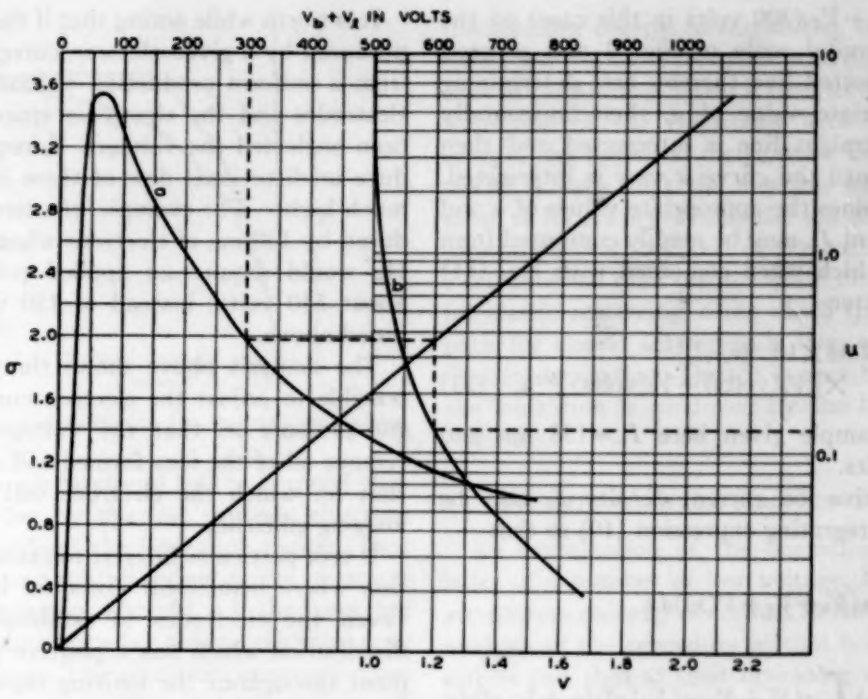

FIG. 2. Curve a is the ionization cross section in cm²/cm³ units for hydrogen at 1 mm Hg pressure and 0°C. Curve b is a plot of the function $v(u)$ defined by Eq. (5), (15) and (18). The straight line represents Eq. (23) and has slope

$$\frac{2}{\pi\gamma pl}\left(\frac{m}{M}\right)^{\frac{1}{2}}=1.64.$$

where $$v=\pi\gamma c_1/2 \tag{18}$$

and $$D=\left(\frac{d\log\sigma(E)}{d\log E}\right)_{E=V_b+V_l}.$$

An examination of Eq. (17) shows that c_3/c_1 can become less than $-\frac{1}{3}$ only when $D<-(1+\gamma^2)$. From the quantum theory of collisions it can be shown that for all ionization functions $-1\leq D$, so that $d\varphi/dx$ does not change signs between the plates when the ions are produced by electron collisions with atoms.

In order to facilitate the calculations, v has been plotted as a function of u in curve b, Fig. 2. The coefficients c_1 and c_3 are then easily found from Eqs. (17) and (18). When V_b+V_l corresponds to an energy well beyond the maximum of the ionization cross section, D is very nearly -1 and c_3 may usually be neglected in comparison to c_1.

With the coefficients c_1 and c_3 determined, the voltage distribution is given by $\alpha x=c_1\varphi^{\frac{1}{2}}+c_3\varphi^{\frac{1}{4}}$. The minimum potential which must be applied across the electrodes in order that all ions will be removed may be found from the above relation by substituting the boundary values $x=l$ and $\varphi=1$ so that

$$\alpha l=c_1+c_3. \tag{19}$$

Neglecting c_3, we obtain as a first approximation

$$\sigma(V_b+V_l)=(m/M)^{\frac{1}{2}}2v/\pi\gamma pl. \tag{20}$$

This equation serves to determine V_l close enough for most practical purposes. If greater accuracy is desired one may go to a second approximation by making use of Eqs. (17) and (19). In order to determine the proper bombarding current density I_- for which all the ions will be removed for an applied V_l and given values of p, l and γ it is most convenient to proceed as follows. It is to be noted that Eq. (20) is satisfied by values of σ lying on the straight line through $v=0$ of Fig. 2 with the slope $(m/M)^{\frac{1}{2}}2/\pi\gamma pl$. Consequently this line is drawn as shown in Fig. 2. (The one actually drawn is for hydrogen molecular ions when $\gamma^2=2$, $l=1$, $p=0.0045$ mm Hg.) First select a

value of V_b+V_l (300 volts in this case) on the upper horizontal scale of Fig. 2 and proceed along the dotted line thereby first determining the appropriate value of σ, then horizontally until the straight line is intersected and then vertically until the curve u vs v is intersected. This determines the appropriate values of u and v. The current I_- may be readily computed from Eq. (15), which when combined with Eq. (11) may be written

$$I_-(\text{amp.})=2.83\times10^{-4}(v/\gamma l)^2 \times[V_b(\text{volts})+V_l(\text{volts})]^{3/2}u. \quad (21)$$

For the example given here $I_-=138$ ma and $V_l=150$ volts.

The positive ion current density I_+ may be found by integrating expression (10) so that

$$I_+=I_-p\int_0^l \sigma(V_b+V_l+V(x))dx$$

$$=(I_-p/\alpha)\int_0^1 \sigma(V_b+V_l-|V_l|\rho^2)(c_1+3c_3\rho^2)d\rho,$$

since $\alpha dx=(c_1+3c_3\rho^2)d\rho$. If the integrand is expanded in a power series in ρ and the terms in ρ^3 and higher powers are neglected then

$$I_+/I_-=(m/M)^{\frac{1}{2}}(2v/\pi\gamma) \times\{1-D/3\gamma+(1+Dv)/[3\gamma^2(9v-8)]\}. \quad (22)$$

For the special case considered above it is readily found that $D=-0.72$ at $(V_b+V_l)=300$ and the above expression becomes

$$I_+/I_-=8.9\times10^{-3}[1+0.169-0.0083] =1.03\times10^{-2}. \quad (23)$$

The small term in the brackets in Eq. (23) is the value of c_3/c_1 so that neglecting it in Eq. (20) was justified.

It should be noted that I_+/I_- does not depend explicitly on the distance apart of the electrodes and that throughout the important range of values of I_-, v is a slowly varying function of the order unity so that I_+/I_- is nearly constant for the potential distribution under consideration.

The curves of Fig. 2 make it possible to see clearly the effect of changes in bombarding electron current, gas pressure etc., on the minimum allowable applied potential difference V_l.

It is worth while noting that if the ion currents produced by a given electron current had arisen from a uniform production of ions between the electrodes and the electronic space charge had been neglected the voltages V_l required to produce unidirectional flow of these ions would be much higher. For example, the ion current produced by 138 ma of electrons when $p=0.01$ mm Hg would require an applied potential V_l of about 540 volts; instead of 150 volts as computed above.

The analysis above shows that it is always possible to adjust the electron current and the gas pressure so that the voltage required to remove all of the ions formed will correspond to that for which the electrons will have a high ionizing efficiency.

It is of particular interest to examine the situation where insufficient potential is applied between the electrodes to establish a potential distribution which has a positive potential gradient throughout the ionizing region, because a number of ion sources to be mentioned later operate under these conditions. This situation has been discussed briefly by Langmuir[4] for a special case.

If for a given electron current entering the ionization chamber, the applied potential is adjusted so that unidirectional ion flow occurs for a given pressure and the pressure is then increased, more ions will be formed and the potential distribution will tend to pass from that shown in Fig. 3a to b. When this occurs it is obvious that all of the ions produced will no longer flow in one direction. The potential distribution b is never realized, however, because the low energy electrons ejected from the atoms during the process of ionization will be trapped and tend to reduce the positive space charge. The final steady-state condition will be that approximately shown by curve c. Throughout the region where the potential gradient is small, the number of trapped electrons per unit volume is nearly equal to the number of positive ions per unit volume. This is the condition usually associated with a plasma; but it should be pointed out that the steady-state condition is not one where an appreciable number of the ions

[4] I. Langmuir, Phys. Rev. 33, 954 (1929).

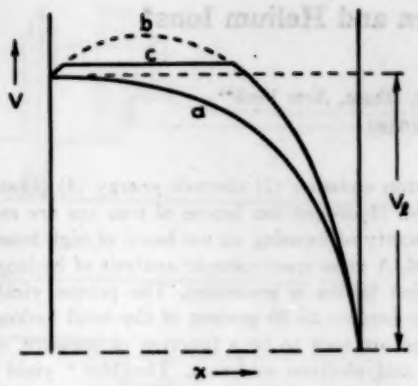

FIG. 3. Potential distribution in non-arcs and arc sources.

in the plasma are produced by the trapped electrons but rather by the fast primary electrons entering one side of the ionization region. That no steady-state condition exists at the pressures under consideration wherein all the ions are produced by the trapped or plasma electrons may be seen as follows. The maximum measured cross section for the ionization of hydrogen is 3.5 cm^2/cm^3 at a pressure of 1 mm Hg. Consequently the shortest mean free path for ionization will be $l_+ = 1/3.5p$, where p is the pressure in mm Hg. The range of pressures actually used is from 10^{-2} to 10^{-1} mm Hg. The corresponding range for l_+ is 2.9 to 29 cm. The actual l_+ would be somewhat greater than this because the ionizing electrons do not usually have the energy corresponding to the maximum ionization cross section.

It is clear that the ionization is not mainly done by the slow trapped electrons when the distance between electrodes is comparable with l_+ since many electrons would arrive at the anode without having produced an ion and many electrons having only produced one ion. Of course it may be argued that the inter-electrode distance is not the actual distance traversed by an electron because it undergoes other types of collision and therefore follows a devious trajectory. This is unlikely in hydrogen because the cross section for all types of inelastic collisions combined is of the order of magnitude of the ionization cross section. The minimum mean free path l_i for elastic scattering is 0.8 cm for $p = 10^{-1}$ mm Hg when the electron energy is near zero, while at the electron energy corresponding to maximum ionization the mean free path is already 3.8 times that for ionization. Even if the electrons started from one of the electrodes with nearly zero energy, the potential distribution between electrodes is such that the electron would receive most of its energy within the ion sheath in the immediate neighborhood of the cathode, i.e., in a distance less than the minimum mean free path for elastic scattering, after which the mean free path for elastic scattering is long compared to that for ionization. Thus it is seen that most of the ionization is produced by the fast primary electrons.

IV. Low Voltage Arc Ion Sources

An examination of the operating characteristics of a number of low voltage, low pressure arc sources recently described in the light of the analysis of the preceding section brings out the salient fact that at their operating voltages and pressures the mean free path for ionization is of the order of magnitude of the cathode anode distance, making them fall into a class to which the preceding analysis may be applied. Calculations show that, in general, the cathode to anode potentials in these sources are insufficient to produce unidirectional ion flow, so that the potential distribution between cathode and anode is of the type shown in Fig. 3c. In most of these sources the arc is confined to a small cylinder and since there is only a small potential gradient along the arc a radial potential gradient is set up as described by Langmuir and Tonks,[5] such that the ions produced flow to the wall in all radial directions. Since the ions are extracted through a small hole in the wall only a very small fraction of the ions produced can contribute to a useful beam current.

With the analysis presented above as a guide, several ion sources have been constructed, the description and operation characteristics of which are given in the following paper. Also a method of holding an intense ion beam together will be given in a later paper.

[5] I. Langmuir and L. Tonks, Phys. Rev. **34**, 876 (1929).

Focused Beam Source of Hydrogen and Helium Ions*

G. W. Scott, Jr.
*Department of Physics, Cornell University, Ithaca, New York***

(Received September 6, 1938)

An ion source of high intensity is described in which the ions are produced by bombarding a region of gas by a focused beam of electrons. This ion source is universal in that it may be used with any gas that may be ionized by electron impact. A theoretical expression for the emission from the ring-shaped cathode used in this source is given, and the emission *vs.* voltage curve calculated from this expression is compared with experimental emission curves. Electron beams as intense as 2.2 amp./cm² are reported. Curves of total ion yield from the source plotted against (1) electron emission (2) electron energy (3) pressure are presented. Hydrogen ion beams of four ma are reported. The difficulty of focusing an ion beam of high intensity is discussed. A mass spectroscopic analysis of hydrogen and helium ion beams is presented. The proton yields vary from five percent to 80 percent of the total hydrogen ion beam and are seen to be a function of pressure, electron energy, and electron emission. The He^{++} yield in the helium ion beam is of the order of five percent of the total beam current.

1. Introduction

IN the ion source described in this paper, the ions are produced by bombarding gas atoms with a focused beam of electrons. With the guidance of the analysis of Smith and Scott,[1] which specifies the minimum potential required for complete removal of the ions formed by electron impact, this type of ion source offers a good opportunity to obtain conveniently intense beams of a wide variety of ions. Several ion sources of this type[2, 3] have been built, and, the source to be described represents the simplest and most convenient modification to date.

2. Description of Ion Source and Auxiliary Apparatus

The constructional details of the ion source are drawn to scale in Fig. 1. The ionization chamber assembly *G* is made from a copper rod one inch in diameter. The actual chamber is a cylindrical hole $\frac{1}{4}''$ in diameter and $\frac{3}{8}''$ deep in the end of the copper rod. Gas is introduced into and directed toward the back of the ionization chamber by means of two 13-mil holes shown in Fig. 1.

The flow is regulated by a gas leak described by Fowler,[4] placed between the ionization gauge and the Hoke reducing valve attached to the tank containing the gas to be ionized. The entire ionization chamber assembly is water cooled by a pipe which introduces water into the central portion of the copper rod and by another pipe surrounding and coaxial with the first, which removes it.

The cathode *D* is of 15-mil oxide-coated, protruded nickel, cylindrically shaped, mounted coaxial with the ionization chamber and $\frac{1}{16}''$ from it. It is spot-welded to 15-mil nickel strips which are attached to the lead-ins as shown in Fig. 1. The cathode is coated with type 50 oxide spray coating, manufactured by Callite Products Company, Union City, New Jersey.

Figure 2 is a diagram of the electrical connections. The pumping system is an all metal, three-stage, self-purifying, condensation pump, employing Eastman's octoil as the pumping medium. The details of construction and important characteristics of this pump are described by Malter and Marcuvitz.[5] According to Malter and Marcuvitz, the speed of this pump varies from 35 to 40 liters/sec. over a pressure range from 10^{-3} to 10^{-6} mm Hg. From measurements made in this work, it was found that to maintain a pressure of 5×10^{-5} mm Hg at the ionization gauge, a gas flow of approximately eight cc/hour, measured at atmospheric pressure,

* Part of a thesis submitted by G. W. Scott, Jr., in partial fulfillment of the requirements for the Ph.D. degree in the graduate school of Cornell University.
** Now at Massachusetts Institute of Technology.
[1] L. P. Smith and G. W. Scott, Jr., preceding paper.
[2] L. P. Smith and G. W. Scott, Jr., Phys. Rev. **51**, 1025(A) (1937).
[3] L. P. Smith and G. W. Scott, Jr., Phys. Rev. **53**, 677(A) (1938).
[4] R. D. Fowler, Rev. Sci. Inst. **6**, 26 (1935).
[5] L. Malter and W. Marcuvitz, Rev. Sci. Inst. **9**, 92 (1938).

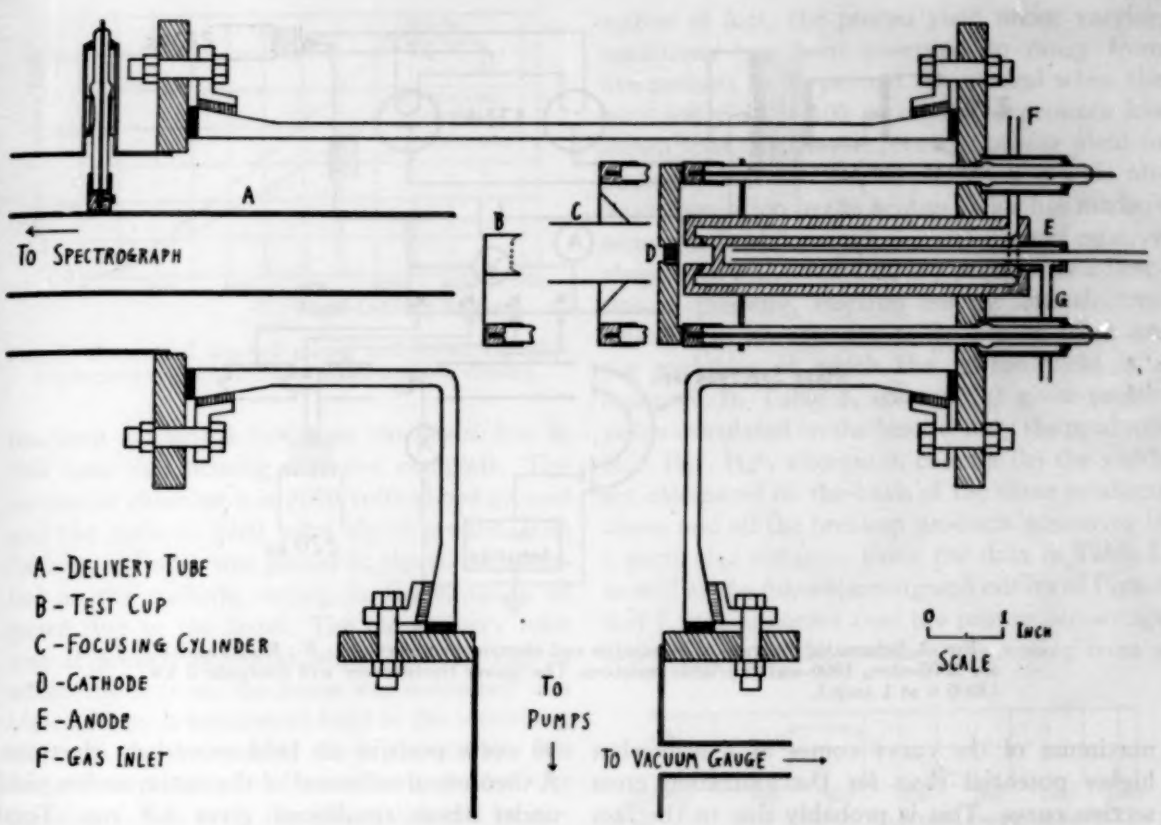

FIG. 1. Ion source assembly. *A*-copper focusing cylinder, *B*-test cup mounted so that it may be turned into or out of the ion beam. A willemite screen makes the ion beam visible. *C*-nickel focusing cylinder, *D*-cylindrical cathode $\frac{1}{4}''$ in diameter and $5/32''$ wide coaxial with beam, *E*-copper-anode assembly with ionization chamber, gas inlet *F*, and water cooling *G*.

is required; whereas to maintain a pressure of 5×10^{-4} mm Hg at the ionization gauge a gas flow of approximately 57 cc/hour, measured at atmospheric pressure, is required.

3. Electron Production

Necessarily a very important feature of the type of ion source being discussed is the production of intense beams of electrons. The cathode construction and coating have already been described.

In Fig. 3 are plotted the currents between anode and cathode for two pressures of hydrogen as functions of anode-cathode voltage. The dashed curve is a plot of $i=Ci_0^{\frac{1}{2}}V^{3/4}$ (i is cathode emission, i_0 is saturation current density, C is a constant) which an approximate theoretical calculation gives for the thermionic emission of this type of cathode when the positive ion space charge is neglected. The effect of the positive ion space charge is clearly evident. Cathodes of satisfactorily long life have produced electron beams of 600 ma (2.2 amp./cm^2) with not more than 800 volts anode-cathode potential and 12 to 13 amperes heating current.

4. Total Ion Yields

The positive ion yield as a function of electron emission current for constant electron energy and hydrogen pressure is shown in Fig. 4. Since under these circumstances the ionization produced by an electron beam is directly proportional to the number of electrons in the beam the points of this curve should fall on a straight line as they do. In Fig. 4 is also shown the way in which the ion current varies with electron energy when the emission and pressure are kept constant. This curve has the general shape to be expected from the variation of cross section for ionization with electron energy. However, the

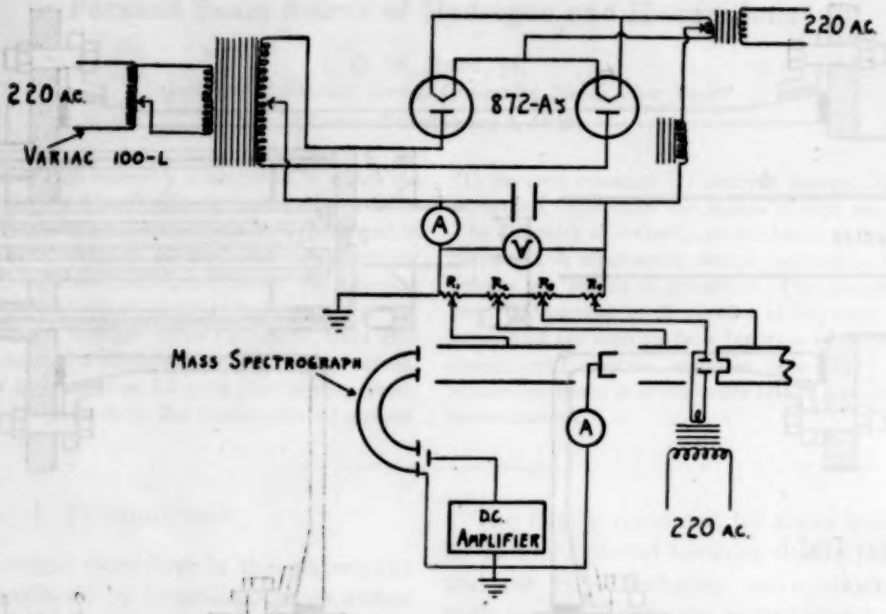

FIG. 2. Schematic diagram of apparatus and electrical connections. R_1, R_2, R_3 and R_4 are 2000-ohm, 1000-watt variable resistors. The power transformer will dissipate 3 kw (3000 v at 1 amp.).

maximum of the curve comes at a somewhat higher potential than for the ionization cross section curve. This is probably due to the fact that not all the positive ions are drawn out of the ionization chamber at the lower potentials. The variation of the total ion current with pressure at constant electron emission and energy is shown in the curve of Fig. 5. This curve has a point of inflection whose interpretation is interesting. As the pressure is increased the ion current would be expected to increase somewhat faster than a first power law because of the contribution of multiple collisions and secondary electrons. This is observed to be the case. However, after the point of inflection, it increases slower than a first power law. Such a change of slope may be attributed to the fact that after the pressure has reached a particular value, more ions are formed than the potential available will remove and so a part of them necessarily flow to the walls of the ionization chamber.

Focused ion beams as high as four ma have been measured to the test cup. For a four-ma hydrogen ion beam, the hydrogen pressure at the ionization gauge was 3×10^{-4} mm Hg, the electron emission 500 ma, and the test cup biased 90 volts positive to hold secondary electrons. A theoretical estimate[1] of the optimum ion yield under these conditions gives 4.8 ma. Total helium ion yields are somewhat less, since the ionization cross section for helium is less than that for hydrogen.

5. FOCUSING OF THE ION BEAM

In this source, the focusing of ion and electron beams is accomplished by the electrostatic fields between configurations of coaxial cylinders. At the higher intensities the focusing is made more difficult by the positive space charge in the beam which tends to make it diverge.

For total ion intensities up to 100 μa the ion beam responded readily to the focusing fields. In a typical instance the ionization chamber was 1250 volts above ground, the cathode 750 volts, and the auxiliary focusing cylinder at ground. The ion current was measured to a cup biased positively to hold in secondary electrons, enclosed in a grounded shield box with a $\frac{3}{8}$" opening. The current to the cup responded to variations in the potential on the focusing cylinder, indicating that the beam reaching the cup was a focused beam.

The highest ion beam focused to the test cup

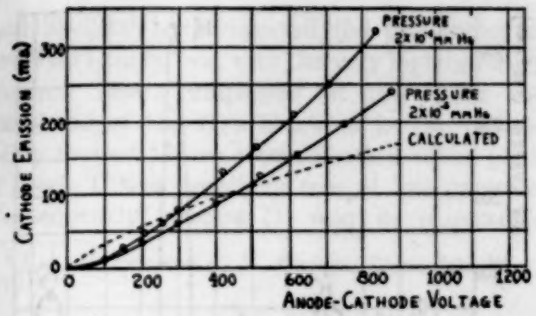

FIG. 3. Theoretical (dashed curve) and actual cathode-anode current as a function of anode-cathode voltage.

has been a four-ma hydrogen ion beam, but in this case the focusing was not complete. The ionization chamber was 3000 volts above ground and the cathode 2200 volts above ground. The focusing cylinder was placed at the same potential as the cathode, acting in the capacity of guard ring to the latter. The ion delivery tube was at ground potential, while the test cup to which the four-ma ion beam was measured was biased 90 volts positive to hold in the secondary electrons. In the case of the high intensity ion beams it is possible to observe how complete the focusing action is by the glow produced by the ion beam.

6. Mass Spectroscopic Analysis of the Ion Beam

Figures 6 and 7 give mass-spectrograph curves of the ion beam for hydrogen pressures (1) 1×10^{-5} mm Hg and (2) 8×10^{-5} mm Hg, which show the variation of the beam content as a function of pressure. It is to be emphasized that the pressure reading is always at the ionization gauge, whose location may be seen from Fig. 1, and not in the ionization chamber. The beam in Fig. 6 is seen to be composed entirely of H_1^+ and H_2^+, the proton yield being 48.5 percent of the total beam current. The beam in Fig. 7 contains not only H_1^+ and H_2^+ but also H_3^+ and all of the breakup products[6] H_{3-1}^+, H_{3-2}^+, H_{2-1}^+. The proton yield in this instance is 13.1 percent.

It will be concluded from the above date that the proton percentage in the hydrogen ion beam is definitely a function of the pressure. As a matter of fact, the proton yield under varying conditions has been observed to range from five percent to 80 percent. In general when the total ion yield is 100 μa or less, experience has shown that one may expect the proton yield to be approximately 50 percent. Such a wide observed variation in the proton yields has made it seem worth while to take a careful set of relative abundance measurements in hydrogen as a function of pressure, electron energy and electron emission in an attempt to determine what are the variables of which the proton yield is a function. In Table I, column (a) gives proton yields calculated on the basis of only the products H_1^+, H_2^+, H_3^+, whereas in column (b) the yields are calculated on the basis of the three products above and all the breakup products appearing in a particular instance. From the data in Table I, as well as the mass-spectrograph curves of Figs. 6 and 7, it is apparent that the proton percentage is a function of the pressure, decreasing from a

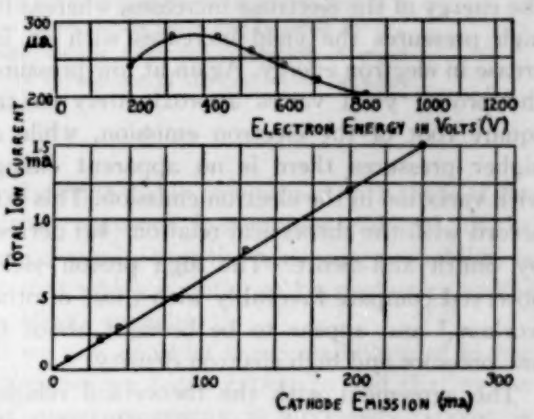

FIG. 4. Total hydrogen ion current as a function of bombarding electron current and variation of total ion current with energy of bombarding electrons with pressure constant.

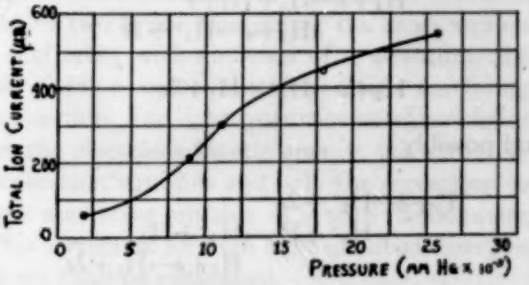

FIG. 5. Variation in total ion current with hydrogen pressure-electron current constant.

[6] H. D. Smyth, J. Frank. Inst. **198**, 795 (1924).

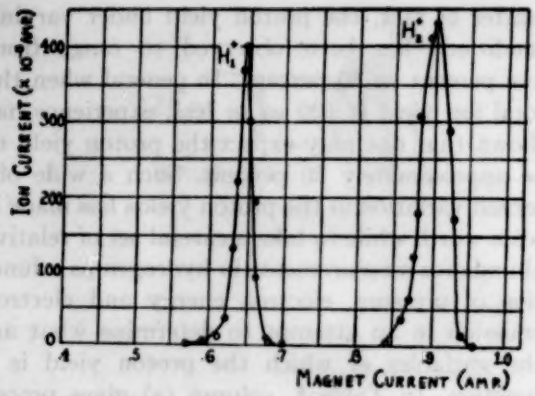

FIG. 6. Mass-spectrographic analysis of ion beam for $p=1\times10^{-4}$ mm Hg.

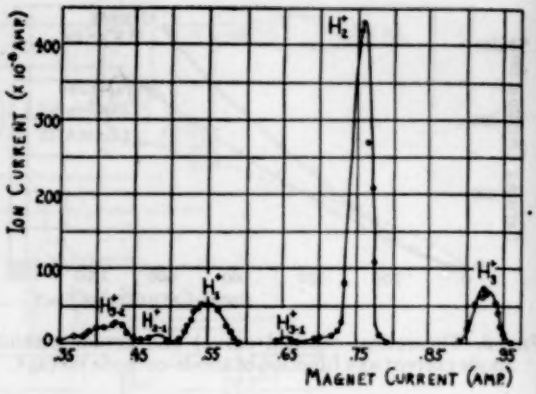

FIG. 7. Mass-spectrographic analysis of ion beam for $p=8\times10^{-4}$ mm Hg.

high value at low pressure to as low as five percent for high pressure. Although the variation is not as obvious as in the case of the pressure, the proton yield is seen to be a function of both the electron energy and the electron emission. For low pressures, the proton yield decreases as the energy of the electrons increases, whereas for high pressures the yield increases with an increase in electron energy. Again at low pressures the proton yield varies approximately as the square root of the electron emission, while at higher pressures there is no apparent change with variation in the electron emission. This is in accord with the theoretical relation (4a) derived by Smith and Scott.[1] The high proton yields observed compare favorably with those of other workers,[7] and appear to be brought about by low pressure and high electron density.

The agreement with the theoretical relation mentioned above leads one to believe that the important processes involved in the formation of protons in the sources under consideration are

$$\begin{aligned} H_2+e&\rightarrow H_1+H_1+e \\ H_1+e&\rightarrow H_1^++2e \end{aligned} \qquad (1)$$

$$H_2+e\rightarrow H_1^++H_1+2e \qquad (2)$$

and possibly

$$\begin{aligned} H_2+e&\rightarrow H_2^++2e \\ H_2^++H_2&\rightarrow H_3^++H_1 \\ H_1+e&\rightarrow H_1+2e. \end{aligned} \qquad (3)$$

These processes have all been observed experimentally by other workers.[8] Although Hughes

TABLE I. *Proton yields.*

Hydrogen Pressure (mm Hg)	Electron Energy (volts)	Electron Current (ma)	(a) Proton Yield Without Breakup Products	(b) Proton Yield With Breakup Products
1×10^{-4}	400	125	61.2%	53.8%
	500		58.0	52.0
	600		57.3	52.7
	400	90	56.1	48.6
	500		51.8	45.8
	600		50.9	46.2
	400	60	47.6	47.6
	500		48.4	43.4
	600		58.5	54.2
3×10^{-4}	400	125	12.1	15.7
	500		14.1	16.7
	600		17.3	20.0
	400	90	14.1	16.7
	500		13.9	16.9
	600		16.0	18.1
	400	60	14.1	16.7
	500		17.5	19.5
	600		26.1	27.7
7×10^{-4}	400	125	5.7	10.4
	500		5.2	10.8
	600		12.4	15.9
	400	90	6.1	10.2
	500		6.1	9.15
	600		10.2	13.4
	400	60	4.9	9.4
	500		6.0	9.9
	600		9.8	13.5

[7] E. S. Lamar, W. W. Beuchner and K. T. Compton, Phys. Rev. 51, 936 (1937).

[8] N. F. Mott and H. S. W. Massey, *Theory of Atomic Collisions* (Oxford University Press, 1933), p. 215.

and Skellett[9] have reported the probability of process (1) to be low, with the very high intensity electron beams employed in this work the likelihood of the H_1's liberated in the process being ionized before recombination takes place is good. This is especially true at low pressure. Consequently, process (1) may be responsible for the observed high proton yields at low pressure and high electron intensity.

An analysis of the helium ion beam with the mass spectrograph showed the yield of He^{++} to be of the order of five percent of the total ion beam.

The author wishes to acknowledge the assistance he has received in this work from Professor L. P. Smith and Dr. P. L. Hartman.

[9] A. L. Hughes and A. M. Skellett, Phys. Rev. **30**, 11 (1927).

MAY 15, 1939 PHYSICAL REVIEW VOLUME 55

On Radiative Corrections for Electron Scattering

S. M. DANCOFF
University of California, Berkeley, California

(Received March 27, 1939)

A relativistic treatment of the radiative correction of order $e^2/\hbar c$ to the elastic scattering cross section leads to the following results: (a) For the scattering in an electrostatic field of a particle described by the Pauli-Weisskopf theory, the correction is finite and is given by (3). (b) For the scattering of a Dirac electron in an electrostatic field, the correction diverges logarithmically and is positive. (c) The convergence or divergence of the correction depends critically on the type of scattering potential considered.

THE customary quantum-mechanical treatment of the scattering of electrons in a field of force involves the assumption that radiative reaction may be considered a small correction. However, when one attempts to calculate the contribution of radiative effects to the scattering cross section, certain characteristic difficulties are encountered.[1] Making an expansion in powers of $\alpha=e^2/\hbar c$, one finds that the probability of scattering with emission of a single quantum with frequency between q and $q+dq$ behaves as dq/q at low frequencies, resulting in an infinite cross section. This "infrared catastrophe" has been shown to arise from the illegitimate neglect, implied in the expansion, of processes involving the simultaneous emission of many light quanta. By taking these into account, and considering only frequencies so low that the light quantum energy and momentum may be neglected in comparison with those of the electron, one finds, in complete analogy with the classical result, that the scattering probability is just that which is obtained by neglecting radiative effects entirely.

If we now consider the contribution of higher frequencies we might expect to find that as the light quantum energy is increased, a point is reached beyond which the expansion in powers of α is legitimate; this would imply the convergence at high frequencies of the successive terms in the expansion. The first-order terms in α are of two types, one giving the cross section for scattering with emission of a quantum, the other giving a correction to the elastic scattering cross section. For light quantum energies higher than the electron's kinetic energy, the radiative cross section vanishes and only the correction to elastic scattering remains. It is with the behavior of this correction for high light quantum energies that we shall be concerned.

According to Braunbek and Weinmann, if one takes a point charge for the electron and neglects

[1] N. F. Mott, Proc. Camb. Phil. Soc. **27**, 255 (1931); F. Bloch and A. Nordsieck, Phys. Rev. **52**, 54 (1937); W. Braunbek and E. Weinmann, Zeits. f. Physik **110**, 360 (1938); W. Pauli and M. Fierz, Nuovo Cim. xv, 3, 1 (1938).

all relativistic effects, this (negative) correction of order α diverges logarithmically at high frequencies. If this result were right it would again show that the expansion in powers of α could not be valid. This is the point of view adopted by Pauli and Fierz who, making a nonrelativistic calculation not involving the expansion in powers of α, show that with this treatment the effect of the high frequencies is actually to make the total cross section vanish. Pauli and Fierz see in this paradoxical result another illustration of the inadequacies of the quantum electrodynamics.

We want now to investigate to what extent the inclusion of relativistic effects modifies the conclusions of Pauli and Fierz. In the absence of a complete relativistic method not involving the expansion in powers of α, only the first-order terms in α are considered in the range $q>T$ (the kinetic energy of the electron) where one would expect relativity to be important.

A simple argument will illustrate why one would expect the relativistic treatment to be essential even when the electron velocity is not comparable with that of light. The emission of a high frequency quantum by the electron causes a recoil which may be large even compared to mc. The transverse momentum, on the other hand, is unaltered. Hence, the relativistic mass increase will reduce the transverse velocity, to which the coupling is proportional. One may therefore expect to obtain convergence at high frequencies in terms which, if calculated nonrelativistically, would diverge logarithmically.

The calculations have been carried through both for a Dirac electron and for a particle of charge e and mass m described by the scalar relativistic wave equation of Pauli and Weisskopf. In each case, the procedure is as follows: one calculates the probability of transition from a state $\Psi(\mathbf{k})$ to a state $\Psi(\mathbf{p})$, where $k^2=p^2$, induced by an electrostatic potential, V. Ψ represents a stationary state of a free particle interacting with its own radiation field; as the interaction (or charge on the particle) is permitted to vanish, Ψ approaches a free particle wave function u_0 with vanishing light quantum numbers. Higher terms in the expansion of Ψ in powers of e represent states with one or more quanta in the field and with an electron and, in general, some pairs present. "Renormalization terms," the first of which occur in order e^2, give the depletion of the state u_0.

The matrix element of V between states $u_0(\mathbf{k})$ and $u_0(\mathbf{p})$—called V_{pk}—leads to the elastic scattering cross section. We then pick out the terms in $\Psi(\mathbf{k})$ and $\Psi(\mathbf{p})$ which combine, through the scattering, pair production, or pair annihilation parts of V, to give corrections to V_{pk} of order e^2. This results in a correction to the elastic scattering cross section, $\delta\sigma/\sigma$, of order α.

We will make the following grouping of terms: (A) Those representing a relativistic modification of terms occurring in the nonrelativistic theory. (B) Those involving pairs in initial and final wave functions, but scattering of electron or positron by the scattering potential (even in V). (C) Those involving pair production and annihilation by the scattering potential (odd in V). Terms involving matrix elements of the square of the vector potential may appear in (C) but not in (A) or (B).

Terms (A)

The effect of the relativistic mass increase is most immediately evident on the Pauli-Weisskopf theory. Here we obtain:

$$\left(\frac{\delta\sigma}{\sigma}\right)_A=\frac{\alpha}{4\pi^2E_k}\int_{q\geq T}\frac{d\mathbf{q}}{q^3}\times\left\{\frac{(E_{k-q}+E_{p-q})(\mathbf{k}\times\mathbf{q})\cdot(\mathbf{p}\times\mathbf{q})}{E_{k-q}E_{p-q}\Delta^+(\mathbf{k})\Delta^+(\mathbf{p})}-\frac{|\mathbf{k}\times\mathbf{q}|^2}{E_{k-q}|\Delta^+(\mathbf{k})|^2}-\frac{|\mathbf{p}\times\mathbf{q}|^2}{E_{p-q}|\Delta^+(\mathbf{p})|^2}\right\}. \quad (1)$$

Here $\hbar$, m and c are chosen unity, $E_k=(1+k^2)^{\frac{1}{2}}$, and $\Delta^+(\mathbf{p})=E_p-E_{p-q}-q$. The lower limit of q, the propagation vector of the quantum, can be taken in the neighborhood of the particle's kinetic energy, T.

The first term in the bracket comes from terms linear in e in $\Psi(\mathbf{k})$ and $\Psi(\mathbf{p})$. The second and third are the corresponding renormalization terms.

We note that when q is large E_{k-q}, E_{p-q}, $\Delta^+(\mathbf{p})$, and $\Delta^+(\mathbf{k})$ are all proportional to q; hence each

of the three terms converges at high light quantum energy.

If we now take k, $p \ll 1$, we see that the nonrelativistic formula differs from this only in having $(1+q^2)^{\frac{1}{2}}$ replaced everywhere by 1. This is particularly important in the matrix elements of the radiative coupling corresponding to the emission and absorption of light of momentum $\mathbf{q}$ in scattering, in the one case from $\mathbf{k}$ to $\mathbf{k}-\mathbf{q}$, in the other from $\mathbf{p}-\mathbf{q}$ to $\mathbf{p}$. Such matrix elements have the form $e(1+q^2)^{-\frac{1}{2}}(\mathbf{k}\times\mathbf{q})/q$ on the present theory and simply $e(\mathbf{k}\times\mathbf{q})/q$ nonrelativistically. The presence of the factor $(1+q^2)^{-\frac{1}{2}}$ corresponds to the use for the effective mass of the particle the harmonic mean of its mass before and after recoil.[2] It is to this circumstance that convergence is due.

Corresponding to (1), we have for a Dirac electron:

$$\left(\frac{\delta\sigma}{\sigma}\right)_A = \frac{\alpha}{4\pi^2}\int_{q\geq T}\frac{d\mathbf{q}}{q^3} \times\left\{\frac{2Tr[\lambda_p{}^+\lambda_k{}^+(\boldsymbol{\alpha}\times\mathbf{q})\cdot\lambda^+{}_{k-q}\lambda^+{}_{p-q}(\boldsymbol{\alpha}\times\mathbf{q})]}{Tr[\lambda_p{}^+\lambda_k{}^+]\Delta^+(\mathbf{k})\Delta^+(\mathbf{p})} -\frac{1}{2}\frac{Tr[\lambda^+{}_{k-q}(\boldsymbol{\alpha}\times\mathbf{q})\cdot\lambda_k{}^+(\boldsymbol{\alpha}\times\mathbf{q})]}{|\Delta^+(\mathbf{k})|^2} -\frac{1}{2}\frac{Tr[\lambda^+{}_{p-q}(\boldsymbol{\alpha}\times\mathbf{q})\cdot\lambda_p{}^+(\boldsymbol{\alpha}\times\mathbf{q})]}{|\Delta^+(\mathbf{p})|^2}\right\}. \quad (2)$$

Here λ is the projection operator,

$$\lambda_k{}^{\pm} = \tfrac{1}{2}[1\pm(\boldsymbol{\alpha}\cdot\mathbf{k}+\beta)/E_k]$$

and $\boldsymbol{\alpha}$ and β are the customary Dirac matrices.

In contrast to (1), the three terms in (2) are separately divergent, converging only upon combination. Expanding each term in powers of p/q and k/q, the leading integrals, of form $\int dq/q$ subtract out. In the limit of low k and p, (2) can be approximately evaluated, and yields

$$\left(\frac{\delta\sigma}{\sigma}\right)_A = -\frac{2\alpha}{3\pi}(\mathbf{p}-\mathbf{k})^2\ln g/T, \quad (3)$$

where g is a number of order unity. This result is identical with that obtained from the Pauli-Weisskopf treatment in the same limit.[3]

Terms (B)

The terms (B) arise from first-order corrections in $\Psi(\mathbf{k})$ and $\Psi(\mathbf{p})$ involving pairs, and from the corresponding renormalization terms. Here only the scattering (even) parts of the force field are involved. The terms may be combined and expressed as follows.

For the Pauli-Weisskopf particle: the resulting formula is the negative of (1), if in that formula the Δ^+ are replaced by Δ^-, where $\Delta^-(\mathbf{k}) = E_k + E_{k-q} + q$.

For the Dirac electron: the resulting formula is equal to (2), if there $\lambda^+{}_{p-q}$ and $\lambda^+{}_{k-q}$ are replaced by $\lambda^-{}_{p-q}$ and $\lambda^-{}_{k-q}$, respectively, and if the Δ^+ are replaced by Δ^-.

As in terms (A), these terms converge independently in the P-W case and converge only upon combination in the Dirac case. However, the occurrence of the Δ^- replacing the Δ^+ renders them negligible in comparison for low particle velocities, since then the q integral builds up logarithmically with decreasing T for terms (A), but not for terms (B).

Terms (C)

There are twelve terms which involve pair production and annihilation by the scattering potential; the first two, (a) and (a') below, combine corrections of order e in $\Psi(\mathbf{k})$ and $\Psi(\mathbf{p})$ while the remainder combine corrections of order e^2 in one Ψ with the uncorrected u_0 in the other. (f) and (f') below result from the corrections of order e^2 arising from the terms in the Hamiltonian in the square of the vector potential; (f) and (f') will occur in the P-W treatment, but not in the Dirac.

The terms are indicated by the following transition schemes:

[2] It may be remarked that the effect of the $(1+q^2)^{-\frac{1}{2}}$ in the above matrix elements of the current is *formally* equivalent to the introduction, into a nonrelativistic calculation, of an extended current distribution of the form

$$\frac{e\mathbf{k}}{8\pi^3}\int d\mathbf{x}(1+x^2)^{-\frac{1}{2}}\exp(i\mathbf{x}\cdot\mathbf{r})$$

with $\mathbf{r}$ the distance from the particle in units $\hbar/mc$.

[3] These proofs of the convergence of terms (A) are due to Professors Bloch and Oppenheimer who, because of these results, suggested the remainder of this investigation.

$$
\begin{aligned}
&E(\mathbf{k}\to\mathbf{l}\mathbf{q})\cdot V(\mathbf{l}\mathbf{q}\to\mathbf{l}\mathbf{q}\mathbf{p}\mathfrak{p})\cdot A(\mathbf{p}\mathbf{q}\mathfrak{p}\to\mathbf{p}), && (a)\\
&E(\mathbf{k}\to\mathbf{k}\mathfrak{l}\mathfrak{p}\mathbf{q})\cdot V(\mathbf{l}\mathbf{q}\mathbf{k}\mathfrak{p}\to\mathbf{l}\mathbf{q})\cdot A(\mathbf{l}\mathbf{q}\to\mathbf{p}), && (a')\\
&E(\mathbf{k}\to\mathbf{l}\mathbf{q})\cdot A(\mathbf{l}\mathbf{q}\to\mathbf{l}\mathbf{p}\mathfrak{p})\cdot V(\mathbf{p}\mathfrak{l}\mathfrak{p}\to\mathbf{p}), && (b)\\
&V(\mathbf{k}\to\mathbf{k}\mathfrak{l}\mathfrak{p})\cdot E(\mathbf{l}\mathbf{k}\mathfrak{p}\to\mathbf{l}\mathbf{q})\cdot A(\mathbf{l}\mathbf{q}\to\mathbf{p}), && (b')\\
&E(\mathbf{k}\to\mathbf{k}\mathbf{p}\mathfrak{p}\mathbf{q})\cdot A(\mathbf{p}\mathfrak{p}\mathbf{k}\mathbf{q}\to\mathbf{p}\mathfrak{p}\mathfrak{l})\cdot V(\mathbf{p}\mathfrak{l}\mathfrak{p}\to\mathbf{p}), && (c)\\
&V(\mathbf{k}\to\mathbf{k}\mathfrak{l}\mathfrak{p})\cdot E(\mathbf{k}\mathfrak{p}\mathfrak{l}\to\mathbf{k}\mathfrak{p}\mathbf{p}\mathbf{q})\cdot A(\mathbf{p}\mathbf{k}\mathfrak{p}\mathbf{q}\to\mathbf{p}), && (c')\\
&E(\mathbf{k}\to\mathbf{k}\mathfrak{l}\mathfrak{p}\mathbf{q})\cdot A(\mathbf{k}\mathfrak{p}\mathfrak{l}\mathbf{q}\to\mathbf{k}\mathfrak{p}\mathbf{p})\cdot V(\mathbf{p}\mathbf{k}\mathfrak{p}\to\mathbf{p}), && (d)\\
&V(\mathbf{k}\to\mathbf{k}\mathbf{p}\mathfrak{p})\cdot E(\mathbf{p}\mathfrak{p}\mathbf{k}\to\mathbf{p}\mathfrak{p}\mathfrak{l}\mathbf{q})\cdot A(\mathbf{p}\mathfrak{l}\mathfrak{p}\mathbf{q}\to\mathbf{p}), && (d')\\
&E(\mathbf{k}\to\mathbf{k}\mathbf{p}\mathfrak{p}\mathbf{q})\cdot A(\mathbf{k}\mathbf{p}\mathfrak{p}\mathbf{q}\to\mathbf{k}\mathbf{p}\mathbf{v})\cdot V(\mathbf{p}\mathbf{k}\mathbf{v}\to\mathbf{p}), && (e)\\
&V(\mathbf{k}\to\mathbf{k}\mathbf{p}\mathfrak{p})\cdot E(\mathbf{k}\mathbf{p}\mathfrak{p}\to\mathbf{k}\mathbf{p}\mathbf{v}\mathbf{q})\cdot A(\mathbf{p}\mathbf{k}\mathbf{v}\mathbf{q}\to\mathbf{p}), && (e')\\
&\mathbf{A}^2(\mathbf{k}\to\mathbf{k}\mathbf{p}\mathfrak{p})\cdot V(\mathbf{p}\mathbf{k}\mathfrak{p}\to\mathbf{p}), && (f)\\
&V(\mathbf{k}\to\mathbf{k}\mathbf{p}\mathfrak{p})\cdot\mathbf{A}^2(\mathbf{p}\mathbf{k}\mathfrak{p}\to\mathbf{p}). && (f')
\end{aligned}
\tag{4}
$$

The propagation vectors of the pair particles (e.g., electrons and positrons) are here indicated by Latin and Greek letters, respectively. E and A represent the matrix elements of the current-vector potential coupling for emission and absorption, respectively, of a quantum $\mathbf{q}$. V indicates the matrix element of the scattering potential (odd for all terms (C)).

One reads (b), for example, as follows: in $\Psi(\mathbf{k})$ we consider the term through which $\mathbf{k}$ is scattered to $\mathbf{l}$ with emission of a quantum $\mathbf{q}$, then $\mathbf{q}$ is absorbed by the creation of the pair $\mathbf{p}$ and $\mathfrak{p}$, $\mathbf{l}$ remaining in the field; this combines, by means of the term in the scattering potential annihilating $\mathbf{l}$ and $\mathfrak{p}$ with $u_0(\mathbf{p})$ in $\Psi(\mathbf{p})$.

Inserting the matrix elements and energy denominators corresponding to the above schemes, we see that the primed terms are the $(\mathbf{k},\mathbf{p})$ interchange of the unprimed.

The values of $\mathbf{l}$, $\mathfrak{p}$, $\mathbf{v}$ above, the propagation vectors for intermediate states, are determined by conservation of momentum in each process involving the vector potential. For example in (b), $\mathbf{l}=\mathbf{k}-\mathbf{q}$; $\mathfrak{p}=\mathbf{p}-\mathbf{q}$.

Pauli-Weisskopf Particle

We consider first the P-W case. We note that for terms (a), (d), (e), and their primes, as well as for the terms (f) and (f') in the square of the vector potential, the scattering potential V is involved through creation or annihilation of a pair both of whose members have the same energy. Consequently these terms vanish, since the matrix elements for pair creation or annihilation by an electrostatic potential are here proportional to $(E_\mathbf{l}-E_\mathfrak{p})(E_\mathbf{l}E_\mathfrak{p})^{-\frac{1}{2}}$, where $\mathbf{l}$ and $\mathfrak{p}$ are the propagation vectors of the pair members.

There remain (b), (c), and their primes. These prove to be much more rapidly convergent at high q and of higher order in v/c than either terms (A) or (B), and are therefore of little interest.

This concludes the proof that the radiative corrections of order α for elastic scattering of a P-W particle by an electrostatic potential are finite.

Dirac Electron

Terms (a), (b), (c), and their primes are found to converge separately and to be of order $(\Delta\mathbf{v}^2/c)^2$. They give a smaller contribution for low particle velocities than terms (A) because of the less singular behavior of their energy denominators for low q.

Terms (d) and (e) are as follows:

$$
\left(\frac{\delta\sigma}{\sigma}\right)_{4d}=-\frac{\alpha}{4\pi^2E_\mathbf{k}}\int_{q\geq T}\frac{d\mathbf{q}}{q^3}\times\frac{Tr[\lambda_\mathbf{p}{}^+\lambda_\mathbf{k}{}^+\lambda_\mathbf{p}{}^-(\boldsymbol{\alpha}\times\mathbf{q})\cdot\lambda^+{}_{\mathbf{p}-\mathbf{q}}(\boldsymbol{\alpha}\times\mathbf{q})]}{Tr[\lambda_\mathbf{p}{}^+\lambda_\mathbf{k}{}^+]\Delta^-(\mathbf{p})},\tag{4d}
$$

$$
\left(\frac{\delta\sigma}{\sigma}\right)_{4e}=+\frac{\alpha}{4\pi^2E_\mathbf{k}}\int_{q\geq T}\frac{d\mathbf{q}}{q^3}\times\frac{Tr[\lambda_\mathbf{p}{}^+\lambda_\mathbf{k}{}^+\lambda_\mathbf{p}{}^-(\boldsymbol{\alpha}\times\mathbf{q})\cdot\lambda^-{}_{\mathbf{p}-\mathbf{q}}(\boldsymbol{\alpha}\times\mathbf{q})]}{Tr[\lambda_\mathbf{p}{}^+\lambda_\mathbf{k}{}^+]\Delta^-(\mathbf{p})}.\tag{4e}
$$

From $\lambda^-{}_{\mathbf{p}-\mathbf{q}}=1-\lambda^+{}_{\mathbf{p}-\mathbf{q}}$, it follows that (d) and (e) are equal. Performing the spin sums, we find that for low p and k the sum of (d), (e), and their primes is simply

$$
\left(\frac{\delta\sigma}{\sigma}\right)_C=\frac{2\alpha}{3\pi}(\mathbf{p}-\mathbf{k})^2\int^\infty dq/q,\tag{5}
$$

a positive logarithmic divergence, indicating an infinite cross section.*

* Dr. R. Serber has pointed out that corrections to the scattering cross section of order α resulting from the Coulomb interaction with the virtual pairs in the field of the scattering potential should properly be considered here. A typical term is represented by the scheme $V(\mathbf{k}\to\mathbf{k}\mathfrak{l}\mathfrak{p})\cdot C(\mathfrak{l}\mathfrak{p},\ \mathbf{k}\to\mathbf{p})$, where C indicates the Coulomb matrix element for annihilation of $\mathbf{l}$ and $\mathfrak{p}$ and scattering of $\mathbf{k}$ to $\mathbf{p}$. While not a "radiative" process, the above will give corrections of the same structure and magnitude as those already considered.

Calculation of the above term plus its prime (in the sense of (4)) yields, for low velocities, on either theory: (a) a divergent term, $-2\alpha/3\pi\int^\infty dl/l$, and (b) convergent terms vanishing with $(\Delta\mathbf{v}/c)^2$ and comparable in magnitude with the terms (B). These results also follow directly from formulae for the "polarization of the vacuum." The logarithmic divergence occurs in zero order of $\Delta\mathbf{v}/c$, and may be removed by a suitable renormalization of charge density.

There are also two exchange terms (which do not

Conclusion

If the P-W theory is applied to the calculation of the radiative correction of order α to the elastic scattering cross section in an electrostatic field, a finite negative result is obtained, given for low particle velocities by (3). This corresponds to the fact that logarithmically divergent integrals which occur in the nonrelativistic treatment are reduced by factors which spring from the relativistic mass variation. New terms of order α (terms (B) and (C)) involving pair creation and annihilation give contributions small compared to (3) in the low velocity limit.

For a Dirac electron, on the other hand, while terms (A) converge and lead to (3), terms (C) contribute a *positive* logarithmic divergence, (5); it is to be remembered that nonrelativistically the divergence was negative, indicating an infinite cross section.

The convergence or divergence of these results could not have been predicted on the basis of the nonrelativistic treatment alone. The somewhat unexpected result that the radiative correction of order α diverges for the Dirac theory, but not for the P-W[4] is due to features of the expressions for charge and current which have no classical analog. One cannot therefore draw too close an analogy between these convergence questions and those which arise in the classical theory of radiation reaction for a point charge and vanishing collision time.

One gets a striking example of the fortuitous nature of the results by considering, instead of the electrostatic, a world scalar scattering potential (a potential invariant under Lorentz transformations). If one now examines terms (C) on the P-W theory, one finds that (4*a*), (4*d*), (4*e*), (4*f*), and their primes no longer vanish. On the contrary, they must be included, and the terms in A^2, (4*f*) and (4*f'*), in particular diverge as $\int^{\infty} q dq$. For the Dirac treatment, on the other hand, convergence arguments are essentially unaltered by the substitution of such a potential. Again, if we consider a purely even scattering potential, the correction is finite for both kinds of particles.

The results obtained are valid only to order e^2 in the radiative correction. It seems certain that calculations to order e^4 and higher would diverge on either theory. It is uncertain whether corrections of order e^3, even when convergent, can be consistently included, and whether they will provide the correct prediction for the result of a given scattering experiment.

The author wishes to express his gratitude for the guidance of Professor J. R. Oppenheimer. Thanks are also due Professor F. Bloch and Mr. Hartland Snyder for fruitful discussions.

follow from the customary polarization calculation where the pair producing charge is not an electron), namely $V(\mathbf{k}\to\mathbf{k}\mu)\cdot C(\mathbf{k}\mu, \mathbf{l}\to\mathbf{p})$ and its prime. This calculation leads again to a convergent correction, vanishing with $(\Delta v/c)^2$ and comparable with the terms (*B*).

It follows that the conclusions drawn below are unaffected by the presence of the Coulomb interaction.

[4] In calculations of the proper energy, etc., where divergences appear, they are usually more extreme on the P-W theory than on the Dirac.

MAY 15, 1939 PHYSICAL REVIEW VOLUME 55

The Liquid-Drop Model and Nuclear Moments

Katharine Way*
Bryn Mawr College, Bryn Mawr, Pennsylvania

(Received March 25, 1939)

The magnetic and electric quadrupole moments of charged spinning drops have been compared with experimental nuclear moments and the agreement found to be very poor.

Discussion of Problem and Results

In view of the renewed interest in the liquid-drop model aroused by the recent fission experiments, it seems worth while to compare experimental nuclear moments, magnetic and electric quadrupole moments, with those of a uniformly charged spinning drop. Such a drop,

*Helen Schaeffer Huff Research Fellow.

if assigned classical properties, will have a magnetic moment on account of the rotation of the charges, and a quadrupole moment if any bulging is caused by the spinning.

In direct contrast to the drop model is the picture in which the nuclear moments are attributed entirely to a single extra neutron or proton moving outside a central momentless core. The outside particle is a neutron or proton according to whether the nucleus contains an odd number of neutrons or of protons. No element with an even number of both neutrons and protons has been found to possess moments. This model, which will be called the odd-particle model, has been shown by Schmidt[1] to give good qualitative agreement with experiment for the magnetic moment. The charge distribution in this model is, however, either spherical or pancake-like so that the cigar-like distributions required by most of the experimental quadrupole moments cannot be accounted for without additional assumptions.

The calculations reported below show that the magnetic moments of spinning drops are of the same order of magnitude as experimental ones and as those of the odd-particle model, but the drop model cannot account for negative magnetic moments as the odd-particle model can. Moreover, the charge distributions in the drop are always pancake-like and give rise to quadrupole moments much smaller than experimental ones and smaller also than those due to the motion of an odd proton around a core. More details about the moment of drops are given below.

The poor agreement of the droplet model with experiment is undoubtedly caused by the fact that for small values of the nuclear spin quantum number, I, the spin cannot be associated with rotation of the drop as a whole. In fact Teller and Wheeler[2] have found that for heavy nuclei the value of I for which the rotational energies approach those of a rigid body is about 36. So even the largest nuclear spin, 9/2, is much too small to justify identification with rotation as a whole.

To sum up one can say that in an attempt to account for nuclear moments, the result of identifying the spin with the nucleus as a whole is less successful than that of identifying it with only one particle. The agreement in order of magnitude of the magnetic moments on the two pictures is to be expected since the magnetic moments due to orbital motion, or rotating charge, are of the same order of magnitude, as the intrinsic moments of the elementary particles. Nevertheless, neither extreme model is particularly promising especially as regards quadrupole moments. Attempts to combine the two treatments in a purely empirical way give no more success.

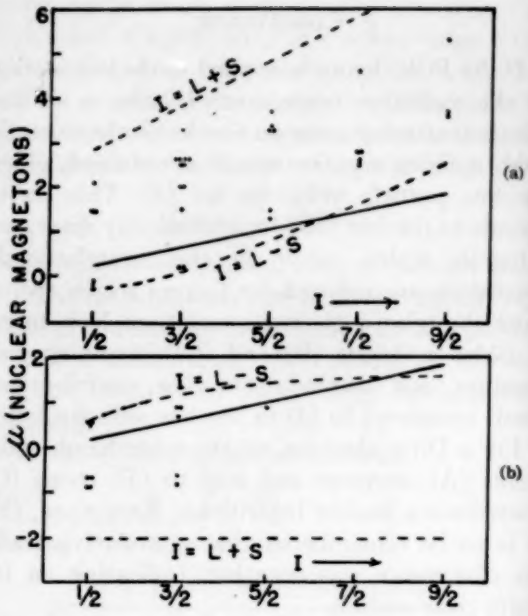

FIG. 1. The dots represent experimental nuclear magnetic moments, the dotted lines magnetic moments of the odd-particle model, and the full line magnetic moments of the liquid-drop model for $Z/A = 50/119 = 0.42$. (a), odd proton, (b), odd neutron.

As a by-product of the investigation, various expressions for the energy of a liquid drop were worked out which may be used in treatments of the stability of heavy nuclei against fission.

MAGNETIC MOMENTS OF DROPS

If the spinning drop is spherical and the charge density uniform, the magnetic moment, μ, is

$$\pi\rho\int r^4 \sin^3\theta dr d\theta = ZI/A$$

nuclear magnetons, where Z is the number of protons, A the mass number, I the value of the spin in units of $\hbar$, and ρ the charge density.

[1] Th. Schmidt, Zeits. f. Physik **106**, 308 (1937).
[2] E. Teller and J. A. Wheeler, Phys. Rev. **53**, 778 (1938).

Figure 1 (a) and (b) show the experimental magnetic moments plotted against spin for nuclei with odd numbers of neutrons and protons, respectively. The dotted lines indicate the moments of the odd-particle model, the top line of (a) and the bottom line of (b) being for $I=L+S$ and the others for $I=L-S$. The full line represents moments of a spinning drop for $Z/A=50/119=0.42$. The same line appears on both graphs since on this model there is little difference between nuclei with an odd number of protons and those with an odd number of neutrons.

Quadrupole Moments of Drops

The electric quadrupole moment, q, is defined as the average over the charge distribution of $3z^2-r^2$ where z is the distance along the axis of symmetry. For a cigar-like distribution q is positive and for a pancake-like one negative. The experimental values[3] of q range from -0.40×10^{-24} cm^2 to 5.90×10^{-24} cm^2. It is remarkable that most of them are positive indicating the cigar-like shape.

The equilibrium shape of a charged spinning drop can be calculated approximately if it is assumed that the drop is an ellipsoid of revolution. Let b be the length of the axis in the spin direction and a the length of the two axes perpendicular to this, and let $x=a/b$. The energy of the drop as a function of x is then the sum of the following expressions:

$$\text{Kinetic energy}=\frac{5I^2}{4A^{5/3}x^{2/3}}\frac{\hbar^2}{Mr_0^2},$$

$$\text{Surface energy}=\frac{\gamma A^{\frac{2}{3}}x^{\frac{1}{3}}}{2}\left[1+\frac{\sin^{-1}(1-x^2)^{\frac{1}{2}}}{x(1-x^2)^{\frac{1}{2}}}\right],$$

$$\text{Electrostatic energy}^4=\frac{1}{8\pi}\int E^2d\tau$$

$$=\frac{3Z^2e^2x^{\frac{1}{3}}}{5r_0}\frac{\tanh^{-1}(1-x^2)^{\frac{1}{2}}}{(1-x^2)^{\frac{1}{2}}},$$

$$\text{Magnetic energy}=\frac{1}{8\pi}\int H^2d\tau$$

$$=\frac{15}{28}\frac{I^2Z^2}{A^3}\frac{e^2\hbar^2}{M^2c^2r_0^3}\frac{1}{1-x^2}\left[1-\frac{x^2\tanh^{-1}(1-x^2)^{\frac{1}{2}}}{(1-x^2)^{\frac{1}{2}}}\right].$$

M is the mass and r_0 the radius of an elementary particle. E and H were found from the potentials V and $\mathbf{A}$ which are the solutions of the equations of Laplace and Poisson expressed in elliptic coordinates. $\gamma=4\pi r_0^2T$ where T is the surface tension.

The value of x for which the energy is a minimum gives the equilibrium shape of the drop. The above expressions were differentiated and the values of x for which the sum of the derivatives vanished were determined graphically for $_{49}In^{115}$ and $_{83}Bi^{209}$. Both of these nuclei have spins of 9/2, the largest known nuclear spin value. For $_{49}In^{115}$, x turned out to be 1.003 and for $_{83}Bi^{209}$, 1.000. The quadrupole moment q was then calculated from the relation

$$q=2ZA^{\frac{1}{3}}r_0^2(1-x^2)/5x^{4/3}.$$

If r_0 is taken equal to 1.48×10^{-13} cm, one then finds $q(_{49}In^{115})=-0.06\times10^{-24}$ cm^2 and $q(_{83}Bi^{209})=0.00\times10^{-24}$ cm^2. The experimental values are 0.80 and -0.40×10^{-24} cm^2, respectively. In both calculations γ in the surface energy term was taken equal to 13.2 Mev.

From the signs of the different terms it is clear that for any values of Z, A, r_0 and γ, a positive q, or cigar-like shape, will never be obtained from the drop model if the drop has any angular momentum. The case of zero spin has already been discussed by Weizsäcker.[4] In this case when the energy of the drop is plotted against x it is found that for values of $5r_0\gamma A/3Z^2e^2$ between 0.565 and 0.5 the energy has a minimum for a cigar-like shape as well as for the spherical one. Although the cigar-like shape is stable against distortion into other ellipsoids, it has not been shown whether it is stable against arbitrary distortions.

[3] For a recent table see Schuler, Roig and Korsching, Zeits. f. Physik 111, 165 (1938).

[4] The electrostatic and surface energy expressions have also been given by Weizsäcker, Naturwiss. 8, 133 (1939).

The Detection of Single Positive Ions, Electrons and Photons by a Secondary Electron Multiplier

JAMES S. ALLEN
Department of Physics, University of Minnesota, Minneapolis, Minnesota
(Received April 1, 1939)

A secondary electron multiplier tube has been developed and used successfully for counting single positive ions, electrons and photons. This tube has twelve electrodes covered with a thin layer of beryllium. Tests have shown that with 330 volts per stage this tube will multiply the primary current by a factor of 10^6. The use of guard ring insulation and electrostatic shielding for the final collecting electrode has reduced the background current to an extremely low value. The last electrode was connected to the grid of the first tube in a linear amplifier. In order to count single positive ions or electrons the tube was waxed to the end of a simple magnetic spectrograph. Ions having energies from 50 to 20,000 electron volts and masses from one to 32 were detected. By increasing the gain of the thermionic amplifier electrons could be counted. With still more gain single photons were counted. The multiplier tube has an extremely low background counting rate. Because a pressure of 10^{-6} mm of Hg is maintained in the counter, it can be connected directly to the vacuum system through which the electrons or positive ions are accelerated. The absence of a thin window between the counter and the vacuum system should be a great advantage in experiments dealing with low energy positive ions or electrons.

INTRODUCTION

IN RECENT years many of the problems of modern physics have required the measurement of very small currents of positive ions or electrons in a vacuum system. Various types of electrometers and electrometer tube amplifiers have been used to measure the small ion or electron currents collected by a Faraday cage within the vacuum tube. In this manner intensities as low as 10^{-17} ampere have been detected. However, if lower intensities are to be used, it becomes necessary actually to count the individual ions or electrons. The Geiger-Mueller tube, proportional counter, ionization chamber and Wilson cloud chamber have been used for this purpose. Since the operation of all these instruments depends upon the ionization produced in a suitable gas by each particle, they must be separated from the vacuum tube by a window capable of withstanding a difference of pressure of at least a few cm of Hg. Moreover, this foil must also transmit a large proportion of the particles without a great loss of their energy. These two requirements prove to be serious whenever the ions have energies less than a few hundred thousand electron volts and the electrons energies less than a few thousand electron volts.

For over thirty years it has been known that, whenever a beam of electrons having energies of a few hundred electron volts strikes a metal plate in a vacuum, secondary electrons are ejected. Recently, it has been shown that the secondary to primary ratio is about ten for certain surfaces. Zworykin[1] and others have used this fact in designing secondary electron multiplier tubes. These tubes usually have the sensitive surfaces covered with a thin layer of Cs-Cs_2O-Ag and, depending upon the number of electrodes, are capable of amplifying the initial current of photoelectrons by a factor of 10^6 or more. Zworykin has found that the signal-to-noise ratio of such a tube is 60 to 100 times that of the conventional photo-tube plus a thermionic amplifier. In a secondary electron multiplier tube this ratio is essentially determined by the shot noise of the photoelectric and thermionic current from the first electrode. If this emission could be reduced to a few electrons per minute, the noise contributed by this factor would be exceedingly small. The only other important source of noise would be that caused by microphonic vibrations of the electrodes and electrical leads. This can be greatly reduced by careful design. It has been shown that the lower limit of the current that can be amplified by this type of tube is determined by the thermionic current from the photoelectric surface. At room temperature this current is approximately 10^{-12} ampere per cm^2 for Cs

[1] V. K. Zworykin, G. A. Morton and L. Malter, Proc. I. R. E. **24**, 351 (1936).

cells and correspondingly less for surfaces with higher work functions. In attempting to measure still smaller currents it is most important to use metals that have essentially zero thermionic emission at room temperature.

Since it is well known that positive ions as well as electrons are able to eject secondary electrons from metals, a secondary electron multiplier should be capable of multiplying the original number of secondaries sufficiently to form a pulse large enough to be easily amplified by a conventional thermionic amplifier. This would enable individual ions or electrons to be counted in a vacuum.

The electrodes of a tube to be capable of detecting single particles should have the following characteristics: a large work function, a secondary electron to primary electron ratio much greater than unity, a melting point sufficiently high that the surface can be outgassed by heating in a vacuum. The first requirement is necessary to insure both an extremely small thermionic emission at room temperature and also a surface that is not sensitive to light in the visible region. In addition, the surface should be sufficiently stable as to be unharmed by a short exposure to air. In the hope of finding such a surface the secondary electron to proton ratio for a number of metals was investigated.[2] Beryllium was found to satisfy all the requirements exceedingly well. This metal has a secondary electron to proton ratio of about eight, can be heated to a red color in a good vacuum without melting and oxidizes slowly when it is exposed to the air. Mann[3] has found the photoelectric work function to be 3.92 electron volts. Consequently, a Be surface will not be sensitive to light in the visible region.

Bay[4] has given a short report of an attempt to count single photons with a secondary electron multiplier tube having electrodes coated with Cs. In order to reduce the extremely large background current it was necessary to immerse the tube in liquid air. This reduced the background to 40 electrons per minute. Single photons could be counted when a light source was placed near the tube. It is evident that the necessity of using liquid air with this type of tube would be a serious disadvantage in many experiments. He has also described an experiment with a tube having nickel electrodes covered with a layer of barium oxide. The use of this surface reduced the thermionic emission sufficiently so that at room temperature the background counting rate was about five electrons per minute. It was possible to count the individual electrons emitted from the cathode when it was illuminated with a very weak beam of light or when it was heated.

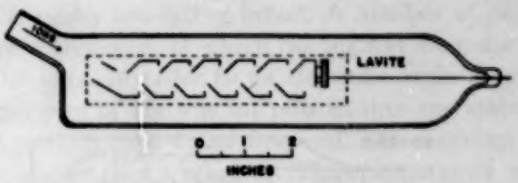

FIG. 1. The electrode arrangement of the secondary electron multiplier tube.

THE SECONDARY ELECTRON MULTIPLIER TUBE

The design chosen for the secondary electron tube is similar to that used by J. R. Pierce.[5] Since this type of tube uses two-dimensional electrostatic fields, the electron optical system can be represented by a mechanical model. A thin rubber sheet is held in a horizontal plane by a metal frame. If small sections of this sheet are given vertical displacements, it can be shown that the relative heights of these areas correspond to the difference of the potentials of similar electrodes in an electron optical system. Then the slope of the sheet will correspond to the electrical field strength. A suitable electrode design was found by constructing a model which was covered with a stretched rubber sheet. The electron paths were traced by allowing small steel balls to roll from one electrode to the succeeding one at a lower elevation. The electrode shape was altered until a ball leaving any point on the inner surface of an electrode arrived at the corresponding point on the next.

A diagram of the actual tube is shown in Fig. 1. The electrodes are of thin nickel sheet with the inner surfaces covered with Be. It was found that the best method of preparing these surfaces was to form the electrodes in a suitable press and then place them in a vacuum furnace. After they

[2] J. S. Allen, Phys. Rev. **55**, 336 (1939).
[3] M. M. Mann, Phys. Rev. **51**, 120 (1937).
[4] Z. Bay, Nature **141**, 284 (1938); **141**, 1011 (1938).
[5] J. R. Pierce, Bell Lab. Record **16**, 305 (1938).

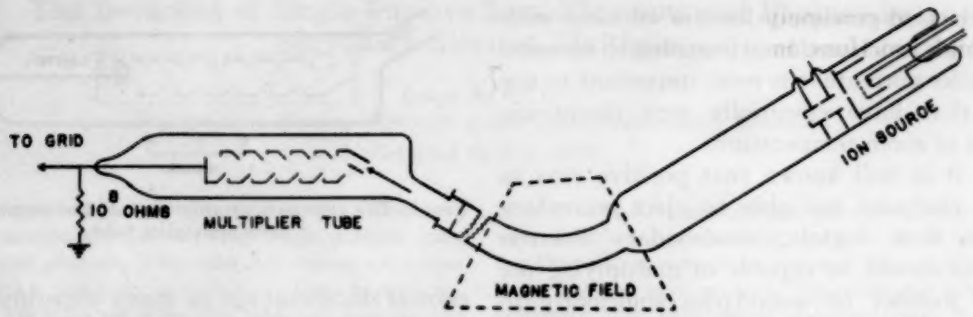

FIG. 2. The electron multiplier tube connected to the end of a magnetic spectrograph.

had been heated to a high temperature for several hours they were placed immediately in another vacuum system and a thin layer of Be was evaporated on them from a tantalum wire. The Be surfaces probably became covered with a thin layer of oxide when they were exposed to the air. Since the oxide has a very high melting point it was not removed when the electrodes were outgassed in the completed tube. The electrode system was held firmly in place between two slabs of fired lavite shown by the dotted lines. The final collecting electrode was supported on a small bar of lavite between the two flat lavite sheets. This electrode as well as the wire through the end of the tube was completely shielded from the other electrodes by guard ring insulation and by an electrostatic shield on the inner surface of the glass tube. The leads to the other eleven electrodes were brought out separately through glass tubes sealed to the main tube. The tube was evacuated continually by means of a small, three-stage, oil diffusion pump. A pressure lower than 10^{-6} mm of Hg was maintained in the tube for most of the measurements. Each electrode was kept about 300 volts positive with respect to the preceding one by taps from a potential divider of eleven 0.3-megohm resistors in series. The necessary voltage was supplied by a stabilizer of the Evans[6] type with the positive side at ground potential.

In order to measure the amplification factor of this tube it was connected to the end of a proton accelerating tube and a beam was allowed to hit the first electrode. The positive ion current to the first electrode was measured with a galvanometer and the final electron current was read on a microammeter. With 330 volts per section an output of 200 microamperes was obtained for an input of 2×10^{-9} ampere of 100-kev protons. This represents a multiplication factor of 10^5. This factor is consistent with a gain of about ten for the first and between two and three for the ten succeeding electrodes. According to the author's data[2] for the secondary electron to proton ratio and the recent value of Kollath[7] for the secondary electron to primary electron ratio for Be, the maximum gain for the first electrode should be 16 and about 4.5 for the others. Thus, the tube is about 60 to 70 percent efficient. Since the electron optical system has essentially two-dimensional electrostatic focusing, some of the electrons must be lost at the edges of the electrodes near the lavite sheets. It was found that the full amplification was not obtained until the tube had been thoroughly outgassed by heating with an induction furnace. The background current of this tube could not be detected with a galvanometer having a sensitivity of 5×10^{-10} ampere per mm deflection. Later experiments showed that the output could be connected directly to the floating grid of a W. E. 259 B tube without changing the plate current. This indicated an extremely small background current.

In order to test the spectral sensitivity of the tube a quartz window was waxed over the opening. When a quartz Hg arc was placed about three feet from the window an output 10^{-7} ampere was obtained. No output current could be measured when a 60-watt tungsten lamp was placed directly in front of the quartz window.

[6] R. D. Evans, Rev. Sci. Inst. **5**, 371 (1934).

[7] R. Kollath, Ann. d. Physik **33**, 285 (1938).

Positive Ion Counting

Figure 2 shows the arrangement used for the counting of positive ions and electrons. The secondary electron multiplier was waxed to the end of a simple mass spectrograph. The lead from the final collecting electrode was connected to the grid of the first W. E. 259 B tube of a Dunning type amplifier. A grid leak of 10^8 ohms was used. The ions were produced by the ionization of the residual gas in the ion source of the magnetic spectrograph. Usually an electron current of 10 to 20 microamperes was sufficient to produce a large number of ions. Only a small fraction of this current actually was effective in producing the ions in the immediate region of the slits. The voltage used for accelerating the ions was obtained from a power supply capable of producing 20 kv.

Since a pressure less than 10^{-6} mm of Hg was maintained in the vacuum system, it was necessary to outgas the multiplier tube very infrequently. This was done by disconnecting the first stage of the linear amplifier from the tube. An induction coil could then be slipped over it and the electrode system heated to a dull red color for several minutes. After the tube had been outgassed it was possible to operate it without further heating even after the system had been exposed to the air for several hours.

When the ions were accelerated by a few thousand volts and the magnet current adjusted so as to allow ions of mass one to enter the counting tube large pulses were seen on the oscillograph screen. These were of about the same magnitude as those observed when alpha-particles entered an ionization chamber one cm deep connected to the linear amplifier. Since the counting rate could be reduced to a few per minute by decreasing the electron current in the ion source, it seemed evident that the multiplier tube was counting single ions. In order to see if this tube was equivalent to the conventional method of measuring the ion current in a mass spectrograph, several spectral curves were obtained by measuring the counting rate as a function of the current through the magnet. The energy of the ions was about three kev. Three such curves are shown in Fig. 3. Since the final slit in the mass spectrograph was three mm wide, the peaks are rather broad. A number of peaks were observed, of which the highest were due to O_2^+ ions. In order to fix the mass scale a small quantity of He was introduced into the system. A peak at mass 4 was observed. This disappeared in about thirty minutes. There apparently was little difference in the height of the pulses due to ions of different masses. A most useful characteristic of this tube is its exceedingly low background counting rate. This was less than one count in five minutes.

It is important to determine the minimum energy that a positive ion may have and still produce sufficient secondaries to be counted. Since the first electrode of the secondary electron tube was always about three kv negative with respect to ground, it was necessary to insulate the mass spectrograph and connect it to this electrode. By suitable adjustment of the accelerating voltages the energy with which the ions hit the first electrode could be varied from a few volts up to 20 kv. The gain of the linear amplifier was calibrated by placing known voltages from a 1000-cycle oscillator on the grid of the first tube. The magnet current was adjusted so as to allow ions of mass 2 to enter the secondary electron tube and then the negative grid bias of the first pair of thyratrons in the scale-of-eight counter was increased until the counting rate decreased to zero. This bias corresponded to the height of the largest pulses produced by molecular hydrogen ions of a given energy. This should also correspond to the maximum number of electrons ejected from the first electrode by an ion. Fig. 4 shows the variation of the maximum pulse height with the energy of the ion. The maximum height of the pulses was also observed visually on the

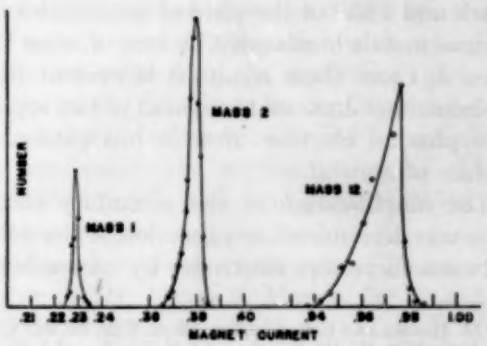

Fig. 3. The peaks due to ions of mass 1, 2 and 12.

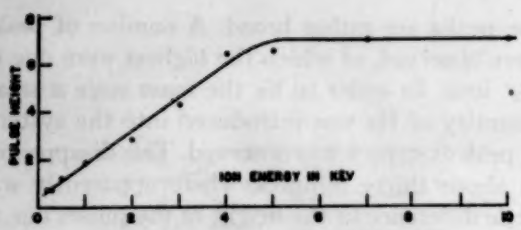

FIG. 4. The variation of the maximum pulse height with the energy of the positive ion. The height of a pulse is proportional to the number of secondary electrons ejected from the first electrode by a positive ion.

oscillograph screen for energies up to 20 kev. The results indicated that the yield of secondaries does not change much from 5 to 20 kev. The slope of the lower part of the curve is approximately equal to that of the curve obtained by Healea and Chaffee[8] for the secondary electron yield from hot Ni bombarded by molecular hydrogen ions having energies from 400 to 1600 electron volts.

It was noticed that the pulses due to ions of mass 1 and mass 2 had very nearly the same height. The mass 2 pulses should be about twice the height of those due to mass 1 ions if the molecular ion dissociates at the metal surface into two atomic ions of half the energy plus an electron. In order to find the reason for this discrepancy the secondary electron to positive ion ratio of a copper plate was measured in the usual manner. This plate was bombarded with mass 1 and mass 2 ions having energies from 25 to 75 kev. At 75 kev it was found that a molecular ion produced only 1.7 times as many secondaries as an atomic ion of the same energy. This ratio decreased with the energy to a value of 1.4 at 25 kev. The value at 75 kev is in agreement with the recent measurements of Hill, Buechner, Clark and Fisk[9] of the yield of secondaries from various metals bombarded by ions of mass 1 and mass 2. From these results it is evident that a molecular ion does not always act as two separate ions plus an electron after it has entered the surface of a metal.

The amplification of the secondary electron tube was determined as a function of the voltage between successive electrodes by measuring the heights of the largest pulses seen on the screen of the oscillograph. The ion-accelerating voltage and the current through the magnet were kept constant. Fig. 5 shows the variation of the pulse height with the secondary electron tube voltage. It is evident that the multiplication of the tube increases rapidly with the voltage per stage. This is due to the fact that the secondary electron to primary electron ratio for Be increases with the energy of the primaries and reaches a maximum at about 450 volts. When the voltage per stage was 135 the pulses were only about twice the height of the noise level due to the combined thermionic and secondary electron amplifiers. This determines the lower limit of the secondary electron tube voltage. During these measurements the gain of the thermionic amplifier was approximately linear.

ALPHA-PARTICLE AND PROTON COUNTING

The following experiment was performed in order to compare the operation of the multiplier tube with that of the ion chamber so widely used for counting alpha-particles and protons. A thin mica window was placed over the end of the multiplier tube and then it was placed near the target of a proton accelerating tube. Alpha-particles of approximately 8.6 cm range were obtained by bombarding a LiOH target with 200-kev protons. These entered the multiplier tube after passing through an absorption tube. Protons of approximately 15 cm range were obtained by bombarding a NaOD target with deuterons. Fig. 6 shows the range numbers curves determined in this manner. Curves A and B were obtained with the multiplier tube while C and D were taken from a paper by Oliphant,

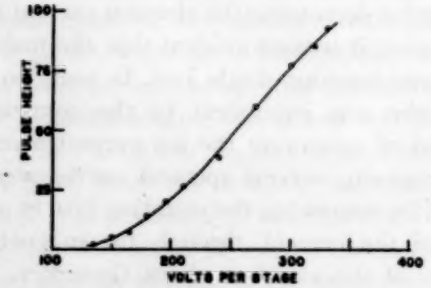

FIG. 5. The variation of pulse height with the voltage per stage of the multiplier tube.

[8] M. Healea and E. L. Chaffee, Phys. Rev. 49, 925 (1936).
[9] A. G. Hill, W. W. Buechner, J. S. Clark and J. B. Fisk, Phys. Rev. 55, 463 (1939).

Kempton and Rutherford.[10] In this case an ionization chamber was used. It is evident that the curves taken with the multiplier tube are entirely similar to those obtained with a conventional integral ion chamber.

Electron Counting

The secondary electron tube was waxed onto the end of the mass spectrograph as before and the accelerating voltages and magnet current reversed so as to allow electrons to enter the counting tube. Since the electrons were retarded after they left the mass spectrograph by the voltage of the first electrode, they were accelerated by voltages greater than three kv. When the filament in the ion gun was heated to a dull red a high counting rate was observed. The tube was able to count single electrons having energies from a few hundred to six thousand electron volts. The background counting rate was still practically zero. The maximum height of the pulses due to electrons was approximately one-seventh that of those due to positive ions of energies greater than five kev.

Photon Counting

When the gain of the linear amplifier was sufficiently high so that a positive ion would produce large pulses on the oscillograph screen and a source of gamma-rays was placed near the multiplier tube, very small pulses could be seen. These were less than one-tenth the height of the positive ion pulses. However, when the gain of the linear amplifier was increased large pulses were obtained without the background noise becoming serious. The background counting rate still had the same low value as before. Since a photon can eject only one electron from the first electrode while a positive ion or an electron can eject a number, the photon pulses will always be much smaller than those due to the ions or electrons.

Conclusion

A secondary electron multiplier tube has been developed and has proved to be a reliable instrument for counting single positive ions, electrons and photons. Since the counting rate does not depend on the voltage across the tube, reproducible results should be obtained. The necessity of separating the counter from the vacuum system by one or more thin windows has been eliminated.

The magnitude of the pulses produced by the multiplier tube when counting ions was obtained by placing known voltages of 60 and 1000 cycles across the 10^8-ohm grid lead of the first tube of the amplifier. An input of 0.05 volt was needed to produce an output of the same magnitude as that of the ion pulses. Because of this relatively large voltage special tubes are not necessary to amplify the pulse from the multiplier tube. An amplifier of the type used to amplify the pulses from a Geiger-Mueller tube should be sufficient.

In conclusion, the author wishes to thank Professors John T. Tate and John H. Williams for many helpful suggestions and for the apparatus used in these experiments. Thanks are also due to Mr. James F. Marvin for his aid in taking some of the observations.

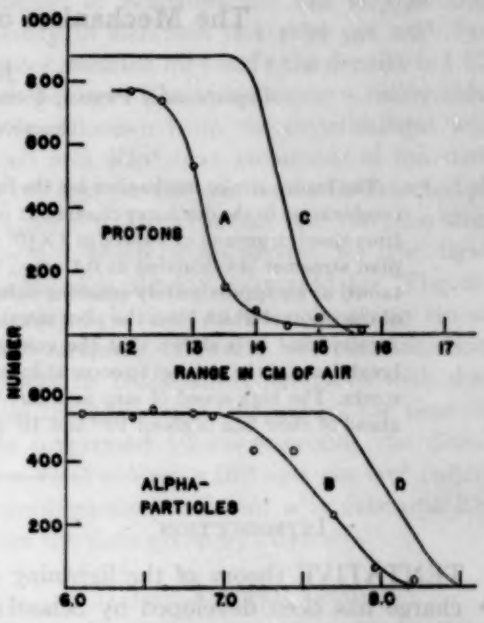

Fig. 6. Range numbers curves for alpha-particles and protons. Curves A and B were taken with the multiplier tube while C and D were taken with an ionization chamber. Curves A and B have been displaced to the left in order to compare them with C and D.

[10] M. L. E. Oliphant, A. R. Kempton and Lord Rutherford, Proc. Roy. Soc. 149, 406 (1935).

The Mechanism of the Lightning Discharge

J. M. MEEK*
Department of Physics, University of California, Berkeley, California
(Received March 28, 1939)

The leader stroke mechanism for the lightning discharge is explained on the basis of ion recombination in the discharge channel. It is assumed that a pilot streamer advances continuously from cloud to ground at a speed of 2×10^7 cm per sec. The current which flows into the tip of the pilot streamer is calculated as 0.1 amp., and it is considered that this current must be maintained at an approximately constant value for the pilot streamer to propagate. The resistance of the channel which joins the pilot streamer to the cloud is then calculated in terms of the ion density, and it is shown that the voltage gradient increases sufficiently to cause successive breakdown of the channel to occur at intervals of some 50 microseconds, i.e., the stepped leader stroke. The high speed of step and dart leaders is explained by the fact that the ion density ahead of their tips is about 10^{13} and 10^7 per cm^3, respectively.

INTRODUCTION

A TENTATIVE theory of the lightning discharge has been developed by Schonland[1] on the basis of his Boys camera studies.[2, 3] The latter show that individual strokes consist of a discharge process, or leader stroke, which develops from a negative cloud to ground and is followed by a return, or main, stroke which develops from ground to cloud along the preionized channel. The initial leader stroke usually proceeds as a series of steps separated by time intervals of some 50 microseconds; each step extends the ionized channel by about 10 meters. The leader process as a whole advances towards ground with a velocity of 2×10^7 cm/sec., while the velocity of propagation of the individual step leaders lies between 1×10^9 and 5×10^9 cm/sec. In order to account for this stepped development Schonland assumed that the leader mechanism is preceded by a pilot streamer, which travels in virgin air at the speed of 2×10^7 cm/sec. This speed is shown by Schonland to be in close agreement with the electron drift velocity v_e, which is given by $v_e=(2E_e\lambda/\pi m)^{\frac{1}{2}}$, on the assumption that the collisions between electrons and molecules are inelastic. Schonland was not able to account for the remarkable uniformity of the stepped process. However, on plausible assumptions, he indicated that the high velocity of the step leaders could be accounted for on the basis of the Cravath-Loeb mechanism[4] if a fairly uniform density of residual ionization of 10^3 ions per cm^3 is present.

His theory does not explain the exact character of stepping and its uniformity, nor does it describe the exact mechanism of the leader stroke.

A study of the rate of ion recombination in both the pilot streamer and in the step leader has been made in terms of the roughly known conditions in the lightning discharge. It is found that the resistance of the leader channel after 50 microseconds is such that for the estimated current which must be maintained in the pilot streamer the potential gradient increases sufficiently to cause the channel to break down again; the breakdown occurs from the cloud end of the channel. On this basis a fairly clear and complete picture of the lightning discharge can be presented in quantitative agreement with experimental observation.

THE PILOT STREAMER

For simplicity we may consider the discharge path to consist of a cylindrical channel of ions and electrons with a hemispherical tip. Ahead of the tip the high field causes ionization by collision of existing electrons or of photoelectrons produced by the ultraviolet light emitted from the streamer tip, as indicated by Loeb.[5] A current

* Commonwealth Fellow.
[1] B. F. J. Schonland, Proc. Roy. Soc. **A164**, 132 (1938).
[2] B. F. J. Schonland and H. Collens, Proc. Roy. Soc. **A143**, 654 (1934).
[3] B. F. J. Schonland, D. J. Malan and H. Collens, Proc. Roy. Soc. **A152**, 595 (1935).
[4] A. Cravath and L. B. Loeb, Physics **6**, 125 (1935).
[5] L. B. Loeb, Rev. Mod. Phys. **8**, 267 (1936).

then flows up the channel from the advancing tip. Rudenberg[6] has estimated this current in relation to the velocity of propagation v, the field strength E and the radius r. Schonland uses the resulting equation in his calculations and Jehle[7] has deduced a similar expression. Unfortunately, because of a confusion in the interpretation of symbols, the equation given by Rudenberg is dimensionally incorrect. In this paper we will use the expression as it is given by Schonland, *viz.*, $i=\frac{1}{2}Evr$ e.s.u., where E is the electric field at the tip in e.s.u., v is the speed of advance of the streamer and r is the radius of the tip.

The field strength is considered as 30,000 volts per cm. This is the generally accepted breakdown strength of air, and it has been shown by Loeb and Kip[8] to be the field at which streamer propagation is important in the breakdown process. The average speed v of the pilot streamer is known from the observations of Schonland to be 2×10^7 cm per sec. This is about the velocity of electron avalanches observed by White[9] and Raether[10] in fields of 30,000 volts per cm.

We still require to know the value of r before the current can be determined. Some measure of its value can be obtained from the experiments of Raether,[10] who has shown that an electron avalanche spreads laterally to a radius $r=(2Dt)^{\frac{1}{2}}$ where t sec. is the time of travel and D is the coefficient of diffusion. For $X/p=40$ the value of D is 500 and thus $r=(1000t)^{\frac{1}{2}}$. The average time-interval between step leaders has been observed by Schonland to be 50 microseconds and for this value of t the radius $r=0.23$ cm. In our calculations we will take $r=0.3$ cm, for which the current in the pilot streamer is 0.1 amp. by the equation given above. The value so chosen for r is not unreasonable since observations indicate the diameter of the main channel to lie between 1 and 10 cm.[11]

The number of electrons which flow into the tip of the pilot streamer per second may be obtained by dividing the current by the electronic charge and is therefore i/e. Whence the number of electrons per cm is i/ev and the density of electrons is $i/\pi r^2ev$ per cm^3. For the values assumed for i and r the density is 1.1×10^{11} ions per cm^3. The value seems a reasonable one, as it is known from the experimental work of Loeb and Kip[8] that streamers of ion densities of 10^{12} ions per cm^3 can barely be detected photographically. Thus the fact that the pilot streamer has not been photographed for the lightning discharge is simply accounted for. The density calculated is that at the advancing tip of the pilot streamer. Because of recombination the density in the channel decreases with distance from the advancing tip, and by the time the tip has progressed 50 microseconds the density is $N=N_0/(1+N_0\alpha t)=10^{10}$ ions per cm^3 (where the recombination coefficient α is taken as 2×10^{-6} from the data given by Sayers[12]).

The Stepped Leader

The tip of an individual step leader, as it travels down the pre-ionized path, is only weakly recorded on the photographs given by Schonland. Experiments by Loeb and Kip[8] show that a cluster of 50 streamers one cm long can be photographed when the total number of ions produced per streamer is 10^9; the streamer diameter is given to be about 0.01 cm and so

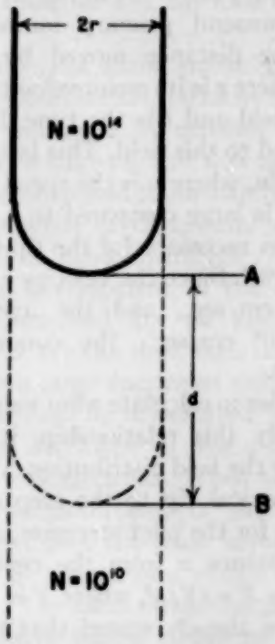

FIG. 1. Diagram to illustrate step leader development.

[6] R. Rudenberg, Wiss. Veröff Siemens-Konz. 9, part 1 (1930).
[7] H. Jehle, Zeits. f. Physik **82**, 784 (1933).
[8] L. B. Loeb and A. F. Kip, J. App. Phys. **10**, 142 (1939).
[9] H. J. White, Phys. Rev. **46**, 99 (1934).
[10] H. Raether, Zeits. f. Physik **107**, 91 (1937).
[11] B. F. J. Schonland, Phil. Mag. **23**, 503 (1937).
[12] J. Sayers, Proc. Roy. Soc. **A169**, 83 (1938).

the ion density is of the order of 10^{14}. We will thus consider that the ion density in the tip of the step leader is 10^{14} ions per cm^3, though the calculations are not materially affected if a value of 10^{13} or 10^{15} is adopted. The ionization decays rapidly with time, and after 50 microseconds, when the subsequent step leader occurs, its value is only 10^{10} ions per cm^3. This is the ion density ahead of the tip of the step leader. As the step leader progresses it eventually encounters a maximum density of 10^{11} ions per cm^3, when it catches up with the pilot streamer. It will later be shown that when the value of ion density of 10^{10} per cm^3 is reached the resistance of the path is so great that the potential gradient is sufficient to cause further breakdown of the channel.

The high velocity of the step leader can now be explained in terms of the ion densities given on the basis of the Cravath-Loeb mechanism as modified by Schonland. Consider the densely ionized tip of the streamer to have reached the position A, as shown in Fig. 1, and that the field strength at B, a distance d ahead of the tip, is 30,000 volts/cm. The distance x moved by the electron originally at B in the direction of the field must be such that by the time it is enveloped by A it must have produced the necessary 10^4 additional electrons to increase N from 10^{10} to 10^{14}, i.e., $e^{\alpha x}=10^4$, or $\alpha x=9.2$, where α is the Townsend primary ionization coefficient. Now the distance moved by the electron is $x=vt$ where v is its mean velocity in the direction of the field and t is the time during which it is subjected to this field. This latter time t is given by $t=d/u$, where u is the speed of the advancing tip and is large compared to v. We then have a condition necessary for the tip to propagate, *viz.* $\alpha vd/u=9.2$. Since the velocity v is approximately 2×10^7 cm/sec., and the average velocity u is 2×10^9 cm/sec., the condition reduces to $\alpha d=920$.

In order to calculate what value of d is required to satisfy this relationship, it is necessary to consider the field distribution. We will consider a hemispherical tip to the step streamer, as was the case for the pilot streamer, and that the field at a distance x from the center of the tip is given by $X=rV/x^2$, where V is the tip potential. We have already stated that the field strength is 30,000 volts per cm when $x=d+r$, and so we may write $X=3\times10^4(d+r)^2/x^2$, or $X/p=39.5(d+r)^2/x^2$. If we plot such a field for $r=0.3$ cm and different values of d, and then plot the corresponding values of α, we find that $\alpha d=920$ for $d=0.8$ cm. The potential at the tip A of the step leader is then 400 kilovolts with reference to B. Thus the high speed of the step leader can be explained without the introduction of an excessively high potential gradient at the tip.

The necessity of stepped leaders can be explained by the fact that the current flowing into the pilot streamer must be maintained at an approximately constant value in order that it may advance in its evidently continuous manner. It is thus reasonable to suppose that a second step streamer will be initiated when the voltage gradient along the channel is sufficient to cause it to break down. Now the specific resistance of a gas which contains N ions per cm^3 is given from the well-known mobility equation as $R=2mc/Ne^2\lambda$ e.s.u. $=(1.3\times10^{15})/N$ ohms per cm^3, where e is the electronic charge, m the electronic mass, λ the mean free path (5.4×10^{-5} cm) and c is the average thermal velocity (10^7 cm/sec.). The resistance of the channel is then $(1.3\times10^{15})/\pi r^2N=(4.6\times10^{15})/N$ ohms per cm. After a time interval of 50 microseconds since the previous step leader we have shown that the ion density in the channel decays to 10^{10} ions per cm^3 and thus the resistance is 4.6×10^5 ohms/cm. The voltage gradient is then 46,000 volts per cm if we consider the pilot streamer current to be maintained at its value of 0.1 amp. This gradient is more than sufficient to cause breakdown; the usually considered breakdown voltage of 30,000 volts per cm would be reached after a time interval of 33 microseconds since the previous step, which is consistent with observed values.

On this basis we can present the following picture of the stepped leader process. The latter is initiated in the form of a pilot streamer by a suddenly occurring local voltage gradient of about 30,000 volts per cm. The possibility of such intense local gradients is most likely in view of the experiments of Simpson and Scrase,[13] who have shown that local concentration of

[13] G. C. Simpson and F. J. Scrase, Proc. Roy. Soc. **A161**, 309 (1937).

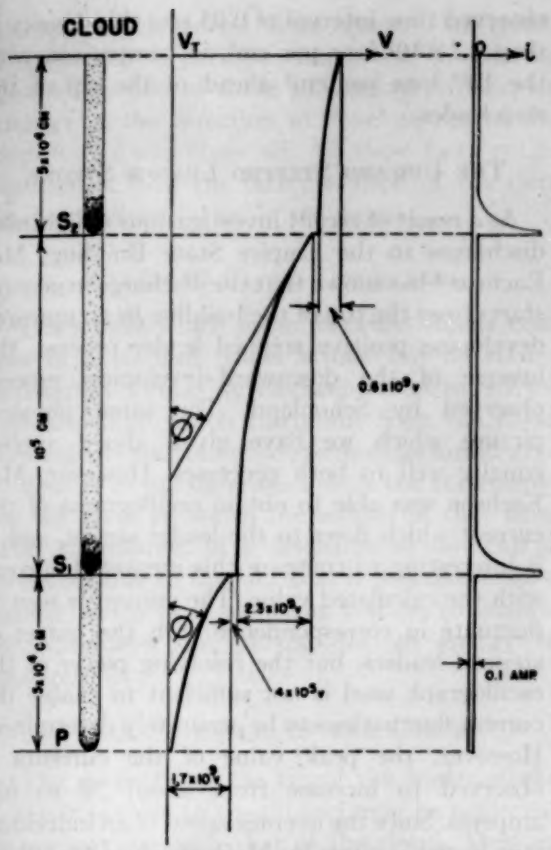

FIG. 2. Voltage and current curves for a stepped leader stroke of length 2 km, when the first step leader S_1 is 5×10^4 cm from the pilot streamer P. The voltage gradient 30,000 volts per cm is given by tan ϕ.

positive charge frequently occurs in the otherwise negatively charged cloud base. When the pilot streamer has traveled for a time of 50 microseconds or so the voltage gradient of the ionized channel at the cloud end increases to such a value that a further breakdown of the channel is initiated, the breakdown proceeding from the cloud end. This breakdown procedure is the step leader observed by Schonland. Since the density of ions ahead of its tip is 10^{10} ions per cm^3, its high speed of 2×10^9 cm per sec. or so can simply be explained. The current which flows in the tip of the step is about 2000 amp., if we consider a tip density of 10^{14} ions per cm^3 and the speed 2×10^9 cm per sec. Thus a high current flows in the cloud end of the channel when a step leader develops. This high current causes the potential of the cloud in the vicinity of the cloud end of the channel to drop immediately, and thus the current is not maintained at its high value, i.e., we can consider an attenuated current pulse to travel down the pre-ionized channel. When the step leader overtakes the advancing tip of the pilot streamer the latter is re-energized and proceeds to advance.

The procedure of successive breakdown, or stepping, is illustrated in the schematic diagram given in Fig. 2. Two step leaders S_1 and S_2 are shown to travel down the pre-ionized channel at the same instant; this occurs when the total length of the path traced out by the pilot streamer P is in excess of the distance traveled by a step leader in 50 microseconds, *viz.* 10^5 cm. The fall in potential from V_c at the cloud to V_T at the tip, and also the current pulses, are represented.

THE MAIN STROKE

When the stepped leader stroke approaches within a few meters of the ground the field intensity is sufficient to cause an upward-developing positive streamer to occur. This positive streamer, which forms the main stroke, travels up the pre-ionized path at a speed of 10^9–10^{10} cm per sec. The speed is observed to decrease as the main stroke develops. Such a decrease in speed can be explained by the fact that the density of ions ahead of the tip falls off as it advances.

The reason why the main stroke does not develop from the cloud is that the latter has such a high internal resistance (it consists of pure water vapor) that a large current flow along the channel from the cloud end immediately causes a decrease in potential in that vicinity. However, the ground is of comparatively low resistance, and the development of the positive streamer is accompanied by no appreciable change in potential. We can thus liken the cloud-ground system to a large condenser only one of whose electrodes can be considered as conducting, and the discharge of the condenser takes place from this electrode. When the main stroke reaches the cloud end of the ionized channel the current does not cease immediately when the charge in the vicinity of the channel has been drained. The main stroke continues to develop as a positive leader stroke to remove further charge from other regions of the cloud.

Malan and Collens[14] have investigated the fine structure of the main stroke and show that steps occur from the ground, in particular when the main stroke reaches a branching point. The stepping may be accounted for in a similar fashion to that described for the leader stroke development, i.e., that breakdown occurs successively from the ground end of the channel due to the increase of voltage gradient. When the main stroke reaches a branching point the current increases suddenly, to maybe double its previous value, and thus it is reasonable to suppose that a step will be initiated.

The Dart Leader

After the first main stroke of the discharge as many as forty further strokes may take place along the same ionized path; the average time interval between such strokes is given by Schonland as 0.03 sec. These subsequent strokes are not preceded by a stepped leader but by what Schonland has termed a dart leader. This dart leader usually travels continuously from cloud to ground at an average speed of 2×10^8 cm per sec.; occasionally, when the time interval since the previous stroke is exceptionally long, the dart leader is stepped as it approaches the ground. Dart leaders and the corresponding main strokes are found to follow the path of the original main stroke in detail.

The initiation of dart leaders is different to that of step leaders. We can consider that no current is flowing in the ionized channel for some time before the dart leader occurs; thus the ionized channel now forms an extended point of potential approximately that of the ground. When the cloud voltage has built up sufficiently in the region of this point breakdown will occur to the point and a dart leader will then develop down the channel from cloud to ground and will be followed by a main stroke in the reverse direction.

The speed of the dart leader can be explained in the same manner as that for the step leader, since it travels down a pre-ionized channel. The ion density ahead of the tip of the dart leader is given by $1/\alpha l$, since N_0 the original ion density in the previous main stroke is high. For the usually observed time interval of 0.03 sec. this density is then 1.7×10^7 ions per cm^3, in comparison with the 10^{10} ions per cm^3 ahead of the tip of the step leader.

The Upward Stepped Leader Stroke

As a result of recent investigations of lightning discharges to the Empire State Building, McEachron[15] has shown that the discharge in general starts from the top of the building in an upward-developing positive stepped leader process, the inverse of the downward-developing process observed by Schonland. The same physical picture which we have given above applies equally well to both processes. However, McEachron was able to obtain oscillograms of the current which flows to the leader stroke, and it is interesting to compare this measured current with the calculated value. The current is seen to fluctuate in correspondence with the outset of stepped leaders, but the resolving power of the oscillograph used is not sufficient to enable the current fluctuations to be accurately determined. However, the peak value of the currents is observed to increase from about 50 to 650 amperes. Since the average speed of an individual step leader is given by McEachron as 6×10^9 cm per sec., the current which flows into its tip is $i=N\pi r^2ev$ e.s.u. $=2.7\times10^{-10}N$ amp., where N is the ion density in the tip and $r=0.3$ cm is the channel radius. Now the minimum value of N is set by the ion density in the tip of the pilot streamer, or else stepped propagation would not occur. We have calculated this ion density as 1.1×10^{11} ions per cm^3, and from this we obtain a minimum current of 30 amp. The higher value of 650 amp. for the leader current, as given by McEachron, can be accounted for if $N=2.4\times10^{12}$ ions per cm^3, which seems a reasonable value in view of the fact that the step leaders are so weakly recorded in the photographs.

The upward-developing stepped leader is not followed by a return stroke from the cloud, for reasons given in the section on the main stroke.

The succeeding strokes of a discharge are of the same type as observed by Schonland for discharges to open country, i.e., downward-developing dart leader strokes followed by main

[14] D. J. Malan and H. Collens, Proc. Roy. Soc. **A162**, 175 (1937).

[15] K. B. McEachron, J. Frank. Inst. **227**, 149 (1939).

strokes which travel from ground to cloud. Occasionally a positive charge was lowered to ground by one of these succeeding strokes; no change in the direction of development of the dart leader was observed. All these facts are in agreement with the interpretation of the dart leader as given earlier in the paper.

Cloud to Cloud Discharges

Discharges which occur between clouds consist of a stepped leader stroke but no return stroke.[3] A similar development is observed for the discharge which starts out from the cloud towards ground, but which terminates in mid-gap.

This is in full agreement with the statements on the main stroke in the section of that title. The termination of a discharge in mid-gap is probably due to the fact that it proceeds from a source which is of sufficient voltage to initiate the discharge but of too low an energy to maintain it.

The Potential of the Cloud

The potential of the tip of the leader stroke when it is close to the ground may be neglected in comparison with that of the cloud. Thus an estimate of the potential of the latter may be obtained by integrating the potential gradient along the leader stroke channel.

Reference to Fig. 2 will show that when the distance between cloud and ground exceeds 10^5 cm two step leaders can be traveling along the channel simultaneously. Now the usually estimated height of a cloud is 2 km, i.e., 2×10^5 cm. Hence the total potential gradient along a channel of such length is

$$2\int_0^{10^5} R_x i\,dx,$$

where R_x is the resistance per cm at a section of the channel distant x from the tip of the step leader. The time interval since the tip passed x is $t=x/u$, where $u=2\times10^9$ cm per sec., the average speed of the step leader. Now the resistance of the channel has been given earlier in the paper as $(4.6\times10^{15})/N$ ohms per cm, so that $R_x=(4.6\times10^{15})(1+N_0\alpha x/u)/N_0$ ohms per cm. The current in the leader channel is 0.1 amp. and therefore the potential V_c of the cloud is given by

$$V_c=2\times0.1\int_0^{10^5}\frac{4.6\times10^{15}}{N_0}\left(1+N_0\alpha\frac{x}{u}\right)dx$$
$$=9.2\times10^{14}(10^5/N_0+5\times10^{-6})\text{ volt.}$$

In our calculations for the step leader mechanism we have considered $N_0=10^{14}$, so that the potential of the cloud is 4.6×10^9 volts.* This value is only changed by one percent if we take $N_0=10^{12}$.

The Spark Discharge in the Laboratory

The leader/main stroke sequence has been observed by Allibone and Meek[16, 17] for sparks between different types of electrodes separated by gap lengths between 25 and 200 cm. It is found that the development of the leader stroke is slowed down by the inclusion of resistance between the voltage source and the discharge gap, and that stepping can be produced if the resistance is sufficiently high. The fact that series resistance has such a marked effect on the development of the leader stroke to a spark substantiates the theory which has been put forward for the lightning discharge, where the high resistance is provided by the leader channel itself.

Preliminary calculations indicate that many of the phenomena of spark breakdown can be accounted for on the basis of ion recombination, and the results of these calculations will be published shortly. It is considered that stepped development of the spark will be observed when the latter occurs over gap lengths greater than ten meters or so, even though there is low resistance between the discharge gap and the voltage source.

In conclusion the author wishes to thank Professor L. B. Loeb for his continual interest and valuable suggestions in the development of the theory, and in particular for his most helpful criticism.

* *Note added in proof.*—Further calculations, based on an oscillographic study of the voltage required to break down a pre-ionized gap in the laboratory, now indicate that propagation of a lightning discharge can occur for an average voltage gradient between cloud and ground of only 600 volts/centimeter. Details of these calculations will be given in an article on the electric spark which will shortly be published.

[16] T. E. Allibone and J. M. Meek, Proc. Roy. Soc. **A166**, 97 (1938).

[17] T. E. Allibone and J. M. Meek, Proc. Roy. Soc. **A169**, 246 (1938).

LETTERS TO THE EDITOR

Prompt publication of brief reports of important discoveries in physics may be secured by addressing them to this department. Closing dates for this department are, for the first issue of the month, the eighteenth of the preceding month, for the second issue, the third of the month. Because of the late closing dates for the section no proof can be shown to authors. The Board of Editors does not hold itself responsible for the opinions expressed by the correspondents.

Communications should not in general exceed 600 words in length.

On the Interpretation of β-Disintegration Data

The interpretation of β-disintegration data by the existing theories (Fermi and Konopinski-Uhlenbeck) is attended by serious difficulties.

The main difficulty of the Fermi theory is that it does not explain the experimentally observed asymmetry of the β-spectrum.

The shape of the β-spectrum given by the Konopinski-Uhlenbeck theory is in far better agreement with experiment, but there is still a sharp discrepancy between theory and experiment at the upper limit, resulting in the disturbance of the energy balance of the disintegration.

Bethe, Hoyle and Peierls[1] in a letter recently published in *Nature* have pointed out the above fact and also other difficulties of the Konopinski-Uhlenbeck theory. They therefore attempt to interpret experimental evidence in connection with β-disintegration while keeping within the limits of the Fermi theory.

To explain the asymmetry of the β-spectrum the authors assume that the experimentally observed spectra are complex and consist of a number of elementary spectra, corresponding to the transition to the various levels of the product nucleus and having the shape predicted by the Fermi theory.

The above assumption however meets with insurmountable difficulties and leads to a direct contradiction with experimental data.

(1) There are known some β-radioactive elements, the disintegration of which is not accompanied by any noticeable γ-radiation,[2] such as P^{30}($\tau\sim 2.5$ m) and RaE. According to the above hypothesis it might have been expected that the β-spectra of these elements would be described by the Fermi formula. Accurate measurements[3] of the P^{30} and RaE spectra, however, show a sharp contradiction to the Fermi spectra and a better agreement with the K-U formula.

(2) The presence of γ-radiation does not in itself warrant the assumption that transition occur to the various levels of the product nucleus. The disintegration of ThC″ may serve as an example of this. While it gives rise to an intensive γ-radiation, the excitation energy of the product nucleus is always the same, i.e., 3.2×10^6 ev.

Proceeding from the well-known level sheme[4] of the ThD nucleus and the upper limit of the ThC″ β-spectrum we ought to consider the ThC″ β-spectrum as an elementary one. This is in contradiction with the above hypothesis, since the ThC″ spectrum cannot be brought into agreement with the Fermi spectrum.[5] This can also be proved by the ThB spectrum the disintegration of which in 95 cases out of a hundred happens to the same excitation level—0.238×10^6 ev. It may be also noted that the ThB and ThC″ disintegration is of the "allowed" type.

(3) The experimental data given by the above-mentioned authors cannot be regarded as conclusive evidence in favor of their hypothesis, since there are no accurate data on the excitation levels of the product nucleus.

We have made an attempt to plot the N^{13} β-spectrum from the Fermi distribution and the Richardson[6] data on γ-rays emitted by the C^{13} nucleus.

The K-U plot of the constructed β-spectrum of N^{13} nucleus differs appreciably from the experimental K-U plot obtained by Fowler, Delsasso and Lauritsen.[7]

(4) Bethe, Hoyle and Peierls have pointed out that the difference between some β-spectra and that of Fermi may be explained by the fact that the transitions corresponding to them are of the "forbidden" type. This explanation seems to be unsatisfactory. Because of the complete symmetry of the interaction term of the Fermi theory as regards the electron and the neutrino, the latter cannot explain the experimentally observed asymmetry of the β-spectrum. Thus, for transitions involving variations of the nuclear moment by one unit, the calculation made for light nuclei gives, for the spectrum, an expression differing from that for the allowed type by the factor:

$$W_0^2+\tfrac{1}{3}(P_e^2+P_\nu^2)-\tfrac{2}{3}W_0\left(\frac{P_e^2}{E_e}+\frac{P_\nu^2}{E_\nu}\right)-\frac{2P_e^2P_\nu^2}{gE_eE_\nu},$$

which has an asymmetry only insofar as the electron and neutrino masses differ from each other.

In conclusion we may point out that, apart from the difficulties mentioned above, it would be hard to imagine such a peculiar distribution of nuclear levels of various elements, as would invariably give rise to an identical shape of the β-spectrum, similar to that of the Konopinski-Uhlenbeck spectrum.

A. I. Alichanian
V. Berestezky

Physico-Technical Institute,
Leningrad, U. S. S. R.,
January 31, 1939.

[1] Bethe, Hoyle and Peierls, Nature **143**, 200 (1939).
[2] C. D. Ellis and W. I. Henderson, Proc. Roy. Soc. **152**, 714 (1935).
[3] A. Alichanian, A. Alichanow and B. Dzelepow, Physik. Zeits. Sowjetunion **11**, 204 (1937).
[4] G. Gamow, *Atomic Nuclei* (Oxford, 1937).
[5] A. Alichanian and A. Zawelsky, Comptes rendus Acad. Sci. U. S. S. R. **9**, 463, 465 (1937).
[6] I. R. Richardson, Phys. Rev. **53**, 610 (1938).
[7] Fowler, Delsasso and Lauritsen, Phys. Rev. **49**, 569 (1936).

X-Ray Emission from the Isomers of Radioactive Bromine

It has recently been shown that the radioactive transformations of the isomeric bromine-nuclei are accompanied by a soft radiation.[1] If the soft radiation is really caused by conversion electrons, the disintegration of the radioactive bromine should be accompanied by the emission of characteristic x-rays.

The following procedure was adopted for the experimental detection of the x-rays. Radioactive bromine was prepared by exposing ethyl bromide to slow neutrons, and the active bromine extracted by chemical methods. The target was placed between the poles of an electromagnet. The radiation was measured by means of a Geiger-Müller counter filled with A at a pressure of 400 mm. With the magnetic field on, no electrons resulting from the disintegration of the radioactive bromine should enter the counter. In actual conditions, however, a great number of impulses could be observed in the counter. Some preliminary experiments had shown that, in addition to the γ-rays accompanying the β-disintegration of the bromine, the radioactive target emitted an electromagnetic radiation with low energy which could be completely absorbed by 1 mm Pb. Further experiments showed that the intensity of the x-ray emission decayed with a four-hour period. The x-rays are therefore emitted by the radioactive Br_{II}-nucleus undergoing conversion.

In order to increase the accuracy of the wave-length determination, the method of selective absorbers was used. The x-ray spectrum of bromine is known to contain two strong lines: the K_{α_2} line ($\lambda = 1041.60$ x.u.) and the K_{α_1} line ($\lambda = 1037.59$ x.u.). A marked change in the absorption coefficient of the K radiation (6.9 times) must be observed when arsenic absorbers are replaced by selenium absorbers.[2] The value of μ/ρ for the K radiation of bromine is 199.0 in As and 28.1 in Se.

As may be seen from Fig. 1, in As and in Se absorbers, with the same mass per unit surface, the x-rays emitted by radioactive bromine are absorbed to a different extent. The experimental values coincide with the calculated values of the absorption coefficients. In As the absorption of the rays is five times greater than in Se. The observed change in the absorption coefficient is somewhat less than might be expected from calculation, but this may be due to the fact that, with the given experimental arrangement, secondary x-rays arising in the As absorber could not be completely eliminated. The influence of this secondary emission was shown by special experiments.

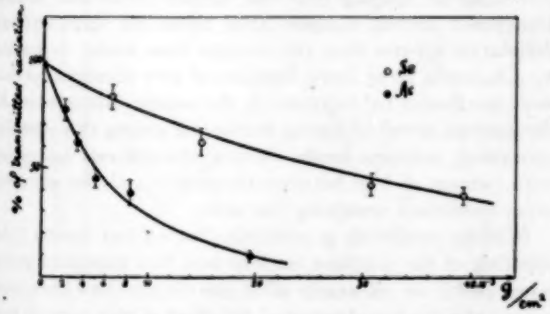

FIG. 1. Absorption of x-rays from radioactive bromine.

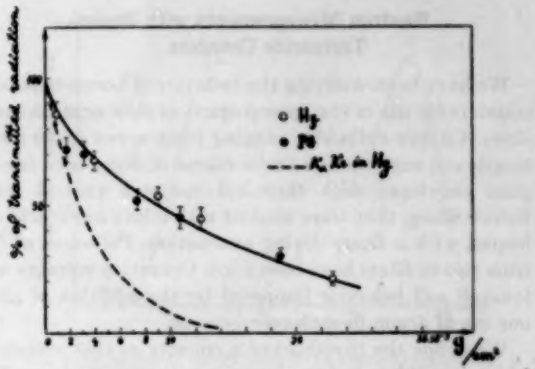

FIG. 2. Absorption of x-rays from radioactive bromine in lead and mercury and of the K line of krypton in mercury.

The observed x-rays cannot be ascribed to a capture of the K electron by the Br nucleus, since, in this case, the x-rays would be emitted by the Se atoms. For selenium, the wave-length K_{α_2} is 1106.52 x.u. and K_{α_1} − 1102.48 x.u. These wave-lengths cannot produce the fluorescence of the As atoms, and their absorption in As and Se must give similar curves. On the basis of the above results, an attempt was made to develop a scheme for the transformation of isomeric Br nuclei. In principle, no objection can be made to the view that the metastable Br nucleus first passes to the ground state by internal conversion, after which β-disintegration sets in. Another scheme is equally possible: the metastable Br nucleus might first emit β-rays, transforming into krypton, after which the excited Kr nucleus passes to the ground state. In this case it would be the Kr nucleus which undergoes internal conversion. The absorption measurements in As and Se do not permit one to decide between the two schemes, since the lines K_{α_2}Kr − 982.1 x.u. and K_{α_1}Kr − 978.1 x.u. also lie within the limits of absorption of Se and As. We therefore measured the absorption of the x-rays in mercury and lead. The absorption-limit L_{III} has a wave-length of 1007.5 x.u. in Hg and of 949.2 x.u. in Pb.

While the x-rays from bromine are unable to excite the fluorescence of the Pb and Hg atoms, the krypton-rays can produce fluorescence in Hg. For the K line of bromine, calculation yields values of μ/ρ equal to 75.3 in Pb and 254 in Hg. Thus, should the conversion take place in krypton, the mass absorption coefficient should decrease 3.4 times upon replacing Pb by Hg.

The corresponding results are shown in Fig. 2. It is easily seen that the absorption in Pb is the same as in Hg, the experimental coefficients of absorption coinciding with those obtained by calculation. It is clear that we have to deal with the first of the two schemes, namely the conversion of the Br nucleus during nuclear isomerism.

In conclusion we wish to thank Professor I. V. Kourtschatow for valuable advice.

L. I. ROUSSINOW
A. A. YUSEPHOVICH

Physico-Technical Institute,
Leningrad, U. S. S. R.,
January 31, 1939.

[1] L. I. Roussinow and A. A. Yusephovich, Comptes rendus Ac. Sc. U. S. S. R. **20**, 9 (1938). See also M. H. Hebb and G. E. Uhlenbeck, Physica **7**, 7 (1938).
[2] M. Siegbahn, *Spektroskopie der Röntgenstrahlen.*

Neutron Measurements with Boron-Trifluoride Counters

We have been studying the behavior of boron-trifluoride counters for use in the measurement of slow neutron intensities. Copper cylinders, ranging from seven to 40 cm in length and one to seven cm in diameter, have been used in glass envelopes with three-mil tungsten central wires. Before filling, they were washed with dilute nitric acid and heated with a flame during evacuation. Pressures of BF_3 from two to 20 cm have been tried. Operating voltages were lowered and behavior improved by the addition of about one cm of argon in each case.

We define the threshold of a counter as that voltage at which it will break down into a continuous discharge if no quenching resistance is used. Below this threshold voltage, the ions formed in the tube are swept by the field to the central wire without starting a self-perpetuating discharge. The average number of ions so swept will be proportional to the number produced in the counter by the passage of the ionizing ray. As the ions travel toward the wire, they produce additional ions by collision, and the number of additional ions will be a function of the voltage. In most counters, such as those filled with argon or air, there is a small voltage range, generally less than five volts below the threshold, within which pulses greater than 0.01 volt are produced on the wire. The boron-trifluoride counters have the property of producing large pulses over a considerably greater voltage range.

A slow neutron entering a counter filled with boron trifluoride produces an alpha-particle by disintegration of the boron nucleus. This alpha-particle will produce a large amount of ionization in the counter, as compared to that produced by cosmic-ray particles or gamma-ray secondaries. By setting the recording amplifier to record only the larger pulses, it is possible to count the alpha-particles to the exclusion of beta- or gamma-counts.

The alpha-particle pulses produced by such counters can be as large as several tenths of a volt when the counter is operated at some 200 volts below the point where gamma-ray pulses of similar size are produced. No high quenching resistance is needed. The counter wire may be connected directly to the grid of the tube and a grid resistor of the order of one megohm is satisfactory.

In Fig. 1 is presented the counting rate of such a counter as a function of the applied voltage, when a radium-beryllium neutron source was nearby. As the voltage applied to the counter increases, the average pulse size increases. The counting rate of the recorder, therefore, rises with voltage until even the smallest pulse produced by the alpha-rays is large enough to record. Further increase of voltage results in no change in the counting rate until that voltage is reached at which the largest of the gamma-ray pulses becomes large enough to operate the recorder. The threshold of this particular counter (11 cm pressure, cylinder 20 cm long, 1.8 cm diameter) was 2080 volts.

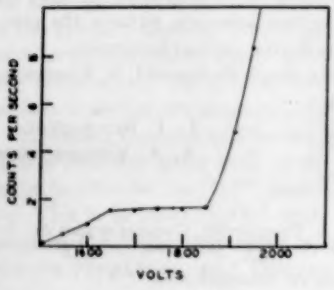

FIG. 1. Counting rate near a beryllium source as voltage applied to the counter is increased.

The limiting neutron intensity which may be measured is that which is small compared to the natural background due to alpha-rays arising from contamination of the cylinder of the counter.

The efficiency of the counters was calculated from the boron cross section to be about 0.3 percent for the counters filled to 11 cm pressure. The order of magnitude of this figure was verified experimentally by comparing the counting rate of a BF_3 counter with that arising from induced radioactivity in a silver (argon-filled) counter.

These counters have been used for about six months, in measuring the neutron intensity in the cosmic radiation in the stratosphere, as well as that due to sources in the laboratory. Stratosphere flights using automatic radio transmission of data with these counters indicate an increase of the neutron counting rate with elevation which is more rapid than the increase in the total radiation. At an elevation of three meters of water equivalent below the top of the atmosphere, the neutron intensity in the cosmic radiation is of the order of 100 times the sea level neutron intensity.

The work on these counters has been partly supported by the Carnegie Institution of Washington. The authors are indebted to M. D. Whitaker of New York University for the loan of the neutron source, and to W. F. G. Swann, T. H. Johnson, C. G. Montgomery and R. D. Fowler for helpful advice and assistance.

S. A. KORFF
W. E. DANFORTH

Bartol Research Foundation,
The Franklin Institute,
Swarthmore, Pennsylvania,
April 27, 1939.

The Detonation of Nitrogen Iodide by Nuclear Fission

Small samples of nitrogen iodide mixed with black uranium oxide were exposed to a 200-mg Ra-Be neutron source surrounded by six cm of paraffin. About half of the exposed samples exploded during exposure after periods of irradiation ranging from one minute to several hours. Unexposed control samples gave times for spontaneous detonation greater than the average time under exposure by a factor of 20 or more. Samples of pure nitrogen iodide were unaffected by exposure to the source. Altogether 32 detonations occurred during irradiation among the *samples* containing uranium oxide. Several detonations occurred with two cm of lead between the source and the sample, other conditions remaining the same.

It seems reasonable to conclude that nuclear fission (the splitting of the uranium nucleus into two approximately equal parts) set off nearly all of the detonations observed among the irradiated samples. An effect of this type is not

surprising when one considers the possibility of intense local heating resulting from the large amount of kinetic energy dissipated in a small space by the slowing down of the fission products. From the activity of an ionization chamber lined with uranium oxide[1] the number of fissions per gram of uranium oxide was estimated to be 60 per minute. A typical sample contained ½ g uranium oxide, while, under favorable conditions, the average exposure time required to produce detonation was 40 minutes. These figures give 1200 fissions per detonation or an efficiency of 0.1 percent.

The writer is indebted to his colleagues in the Physics Department and to Professor W. West and Mr. W. Miller for assistance and advice.

EUGENE FEENBERG

Washington Square College,
New York University,
New York, New York,
April 24, 1939.

[1] Data kindly supplied by W. A. Schneider, R. C. Waddel and D. Callihan.

Energy Distribution of Uranium Fission Fragments*

The energy distribution of the fragments resulting from uranium fissions produced by slow neutrons has been further investigated[1-3] under better defined conditions.

Uncollimated chamber.—A thin layer of uranium oxide (1 mm air equivalent) was electrolytically deposited on gold and served as the central portion of the high voltage electrode in a parallel plate ion chamber which contained argon at a pressure sufficient to absorb the total range of the fission particles. A collecting potential of 2200 v minimized recombination of ions in the 0.6-cm deep chamber.

The ionization pulses from this chamber when exposed to neutrons from the cyclotron were amplified and recorded by an amplifier oscillograph system, of tested linearity. The results obtained (Fig. 1) with the uncollimated chamber show that the fission fragments are divided into at least two major energy groups. The maximum energies in each group were determined by comparison with the U II alpha-particles to be approximately 100 Mev and 72 Mev, respectively.

If these two maximum energies are associated with a single fission process, the total kinetic energy would be about 175 Mev, and the ratio of the masses of the two fragments would be approximately 96/140.

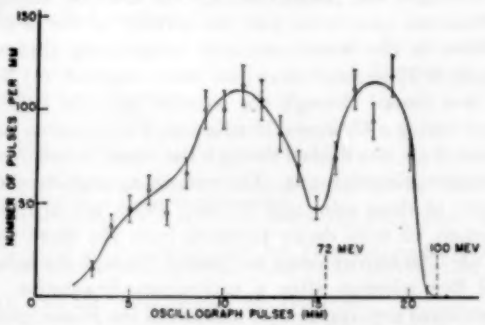

FIG. 1. Total ionization of fission particles in argon.

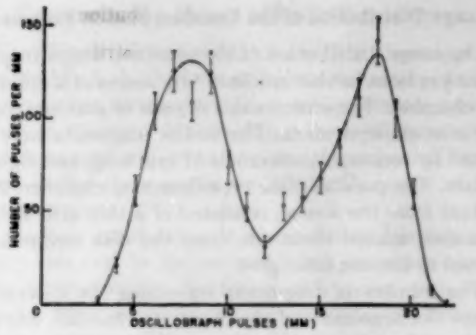

FIG. 2. Ionization of fission particles in argon (collimated).

The difference between this and 200–210 Mev predicted for this process may be accounted for by excitation of the fragments, resulting in beta-, gamma- and neutron emission[4-6] and possibly in part by incomplete collection of ions from the densely ionized tracks.

Collimated chamber.—In order to obtain higher resolution of the energy distribution, and to reduce the effect of energy losses within the uranium target for particles emerging obliquely, a 6-mm deep chamber was constructed for the fission fragments, which employed collimating channels 1 mm long, 0.6 mm diameter. The results obtained with it are shown in Fig. 2. On account of the energy loss within the collimating channels the distance between the peaks is increased and the true origin is displaced to the left of that indicated.

The fission fragments here are clearly divided into two approximately equal major groups, and the widths are considerably less than with the uncollimated chamber. The asymmetry of the low energy group in Fig. 1 has disappeared in Fig. 2, showing that this was probably due to large energy loss suffered by oblique particles. Fine structure within each group may be present, but is not definitely resolved in these experiments.[7, 8]

It should be noted that if fine structure is present in the distribution, then the sum of the kinetic energies of the two fragments would, on the average, be appreciably less than 175 Mev. This could be true if there were high excitation of the fragments, or if collection of the ions were less complete than expected.

The aid of the Research Corporation in this work is gratefully acknowledged.

E. T. BOOTH
J. R. DUNNING
F. G. SLACK

Pupin Physics Laboratories,
Columbia University,
New York, New York,
May 1, 1939.

* Publication assisted by the Ernest Kempton Adams Fund for Physical Research of Columbia University.

[1] Anderson, Booth, Dunning, Fermi, Glasoe and Slack, Phys. Rev. **55**, 511 (1939).
[2] Booth, Dunning and Slack, Bull. Am. Phys. Soc. April 27, 1939.
[3] Frisch, Nature **143**, 276 (1939).
[4] Von Halban, Joliot and Kovarski, Nature **143**, 470 (1939).
[5] Anderson, Fermi and Hanstein, Phys. Rev. **55**, 797 (1939).
[6] Szilard and Zinn, Phys. Rev. **55**, 799 (1939).
[7] Thibaud and Moussa, Comptes rendus **208**, 744 (1939).
[8] Jentschke and Prankl, Naturwiss. **27**, 134 (1939).

Range Distribution of the Uranium Fission Fragments*

The range distribution of the uranium fission fragments in air has been further studied[1, 2] by means of a differential ion chamber. The source was a deposit of uranium oxide of one mm air equivalent. The fission fragments were collimated by rectangular channels 17 mm long, and eight mm square. The parallel plate type detecting chamber, 2.1 cm distant from the source, consisted of a thin grill six cm in diameter, spaced three mm from the disk electrode connected to the amplifier grid.

The number of fragments traversing the distance between the uranium and the detection chamber was measured as a function of the pressure of the air in the chamber. The results are shown in Fig. 1. Two major groups are

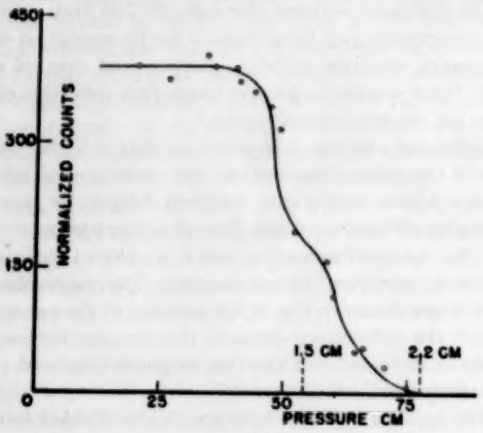

FIG. 1. Range of uranium fission particles in air.

indicated, one with a range of 2.2±0.1 cm and the other with a range of approximately 1.5 cm. The two groups have approximately equal intensity.

The aid of the Research Corporation in this work is gratefully acknowledged.

E. T. BOOTH
J. R. DUNNING
G. N. GLASOE

Pupin Physics Laboratories,
Columbia University,
New York, New York,
May 1, 1939.

* Publication assisted by the Ernest Kempton Adams Fund for Physical Research of Columbia University.
[1] Anderson, Booth, Dunning, Fermi, Glasoe and Slack, Phys. Rev. 55, 511 (1939).
[2] Booth, Dunning and Slack, Bull. Am. Phys. Soc. April 27, 1939.

Fission Products from Uranium*

Further experiments[1, 2] have been performed to study the radioactivity of the fission products from uranium irradiated with slow neutrons. The experiments have been of two types (1) using solid uranium oxide and collecting the products in Cellophane and (2) removing and collecting the gaseous products from uranium in solution. In the first case the uranium oxide, electrolytically deposited on thin copper sheets, was mounted in an evacuated aluminum

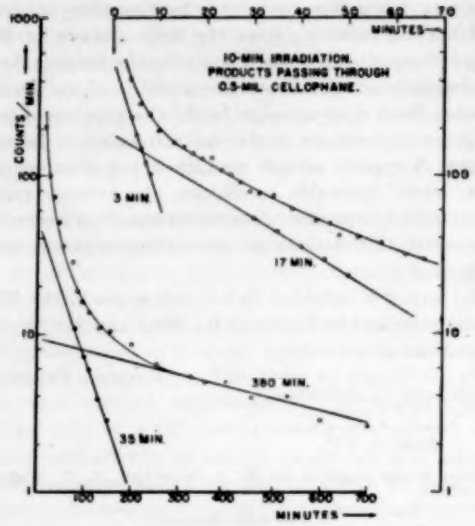

FIG. 1. Decay curves of products which pass through a 0.5-mil Cellophane sheet.

cylinder together with the collecting Cellophane. This cylinder was placed in paraffin near the cyclotron for an irradiation after which the Cellophane was removed and wrapped around a G-M counter for measurement of the radioactivity. With an irradiation of ten minutes the initial activity four minutes later was about 1500 counts/minute and the decay was followed for 24 hours. An analysis of the decay curves is consistent with periods of ~9 hr., 80 min., 32 min., 17 min., and 10 min. (shorter periods unresolved) in agreement with periods reported by others previously.[3, 4]

In order to eliminate one major group of fission products with a range of about 1.5 cm[5] the collecting foil was covered with a 0.5-mil Cellophane sheet which had an air equivalent of 1.4 cm as calculated from its mass and chemical composition. The products which passed through this thin foil showed periods of ~6 hr., 35 min., 17 min., and 3 min., as indicated in Fig. 1. The 10-min. and 80-min. periods are quite definitely absent.

The gaseous products were collected by passing nitrogen through an irradiated uranyl nitrate solution into a glass vessel designed to fit over the G–M counter and having a thin inner wall. Three different procedures were followed: (1) Nitrogen was passed through the solution during an eight-second irradiation and the activity of the products collected in the vessel measured immediately thereafter. Periods of 35 sec. and three min. were observed. (2) Nitrogen was passed through the solution into the collecting vessel during a 45-second irradiation. Two minutes later a stream of air was flushed through the vessel to remove any residual radioactive gas. The remaining activity showed periods of three min. and 20 min. which are attributed, therefore, to solid decay products from the short period gas. (3) The nitrogen was not passed through the solution until five minutes after a one-minute irradiation. The collection of any appreciable amount of the 35-sec. gas was avoided in this manner. This procedure yielded a radio-

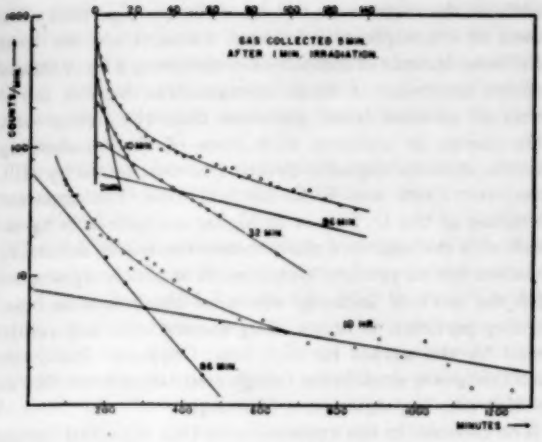

FIG. 2. Decay curves of gaseous products.

active product with a period of five min. A stream of air blown through the vessel 10 minutes after collection removed practically all trace of activity. It is therefore concluded that the product collected in this manner is a gas. A similar experiment was performed in which the activity was followed for 24 hours and the decay curve, Fig. 2, showed periods of 10 hr., 86 min., 32 min., 10 min., and 5 min.

The complete correlation of these data with those from other laboratories[2, 4, 6] cannot be made without further chemical separations and identifications, but some general conclusions may be drawn. There is evidence from these experiments that there are two gaseous products from uranium, one with a period of 35 sec., and the other with a five-min. period, the latter being much longer than indicated in previous reports. The 86-min. period has been quite definitely ascribed to Ba[3, 4] and here appears to be associated with the longer period gas. The 17-min. period has been ascribed to Rb[3, 4] and in these experiments comes from the shorter period gas. The decay of the products collected in Cellophane includes the periods arising from both gases whereas only the products associated with the gas with the shorter period pass through the 0.5-mil foil. The longer range fission products, therefore, may be assigned to a sequence Kr-Rb-Sr rather than to a Xe-Cs-Ba series.

The aid of the Research Corporation in this work is gratefully adknowledged.

G. N. GLASOE
J. STEIGMAN

Pupin Physics Laboratories,
Columbia University,
New York, New York,
May 1, 1939.

* Publication assisted by the Ernest Kempton Adams Fund for Physical Research of Columbia University.

[1] Anderson, Booth, Dunning, Fermi, Glasoe and Slack, Phys. Rev. **55**, 511 (1939).
[2] G. N. Glasoe and J. Steigman, Bull. Am. Phys. Soc., April 27, 1939.
[3] O. Hahn and F. Strassmann, Naturwiss. **27**, 11 (1939) and **27**, 163 (1939).
[4] Heyn, Aten and Bakker, Nature **143**, 516 (1939).
[5] Booth, Dunning and Slack, Phys. Rev. (in process of publication).
[6] Savitch, Comptes rendus **208**, 646 (1939).

Concerning the Nature of Radio Fade-Out

In *The Physical Review* of March 15, 1939, there appears a paper by Mr. L. V. Berkner under the above title. In this paper the author advances evidence and arguments against the view of Martyn, Munro, Higgs and Williams[1] that bright chromospheric eruptions are accompanied by a decrease in the electron density of the F_2 region of the earth's ionosphere.

Mr. Berkner spent some six weeks during January and February this year in Sydney and I had numerous opportunities of thoroughly discussing this point with him personally. After examining all our evidence, Mr. Berkner and I (on February 20th) prepared a joint report on the subject for the information of the Australian Radio Research Board, and of the Department of Terrestrial Magnetism of the Carnegie Institution, Washington. I quote herewith the part of the report which bears on this subject:

"We have made a detailed examination of the radio effects associated with bright chromospheric eruptions. The observations of the Department have been directed mainly towards the examination of ionospheric effects at the time of fade-out, those of the Board mainly to the effect over the whole period of the eruption.

"(*a*) We are agreed that a fade-out is best defined as an abnormal increase in the absorption of radio waves, and appears as an increase in the low frequency (or absorption) limit at which echoes return.

"(*b*) We find that fade-outs as just defined, do not always commence at the beginning of the solar eruption, but may appear during a later phase of the eruption.

"(*c*) F_2 changes are found which changes coincide with the commencement of the eruption. The changes so found consist of a decrease in the penetration frequency of the F_2 region, usually of amount less than one megacycle per second.

"(*d*) It follows that the fade-out does not always occur simultaneously with the change in the F_2 region. We have actually found one case[2] where the F_2 change (and the commencement of the eruption) preceded the fade-out by about two hours.

"The elucidation of the above points, which are not yet generally appreciated, has resulted in reconciling the apparent divergence of our views with regard to the experimental observations."

On the same date (February 20th) Mr. Berkner expressed his intention of withdrawing his paper and rewriting it. It now appears that, unknown to the author, his paper was already in the last stages of publication.

The purpose of this letter is to prevent unnecessary confusion meantime in the minds of other workers on this subject. No doubt the matter will be further elucidated by the author himself when he returns from New Zealand.

D. F. MARTYN

Australia House,
London, W. C. 2, England,
April 21, 1939.

[1] Martyn, Munro, Higgs and Williams, Nature **140**, 603–605 (1937).
[2] This case is illustrated by Fig. 8 in Mr. Berkner's paper, the eruption and F_2 change beginning together at 13.15 hours; the fade-out does not become evident until two hours later, and all three phenomena disappear in about 16.45 hours.

Comparison of the Secondary Electron Emission Due to H_2^+ and D_2^+ Ions

Results of experiments on the secondary electron emission due to bombardment of a hot Ni target by H_2^+ ions have been previously reported.[1] The values obtained ranged from four percent to 22 percent for ions having energies from 300 to 1500 ev.

The same method has now been used to compare the relative emission due to H_2^+ and D_2^+ ions of about the same energy range. The secondary emission, as shown in the accompanying graph, (Fig. 1) is markedly less for D_2^+ than for H_2^+ ions. To obtain these results a Ni target was again used, but after six weeks of continuous heating of the target, when the emission due to H_2^+ had been reduced nearly to the values formerly obtained, the fore pump of the vacuum system suddenly failed to produce the necessary fore vacuum, so that a small amount of air was admitted to the hot target. It was not thereafter possible to reduce the emission to the previous low value. However, reproducible values were obtained and the comparison of the emission due to two ions having so great a relative difference in mass is significant, especially in view of the fact that hydrogen always contaminates a Ni surface and makes impossible the determination of absolute values of emission from a clean Ni surface.

The emission varied approximately linearly from 13.1 percent to 44.7 percent for H_2^+ ions and from 12.2 percent to 35.7 percent for D_2^+ ions over the range of energies used. To be sure that the difference in the effect of the two isotopes was real, the emission for H_2^+ was measured again after the data for D_2^+ were taken and it was found to repeat as closely as before. All points on the curve are averages of a good many values. The deviations in the middle of the curve were not more than two percent. The values at the highest and lowest voltages are the least reliable on account of difficulties in obtaining a large steady positive ion beam at these voltages. The heavier ion is found to produce fewer electrons than the lighter one. This change in emission with mass of the bombarding particle is in the opposite direction to that found by Hill, Buechner, Clark and Fisk[2] for fast ions. The apparent flattening of the D_2^+ curve at higher energies is in agreement with the results of many measurements on secondary emission due to primary electrons. It is also in agreement with the work of Jackson[3] who used alkali ions as bombarding particles. It is not in agreement with any results found by the author for H_2^+ ions. Oliphant[4] found two such changes in slope in the energy range from 80 to 1000 ev for He^+ ions impinging on a Mo target.

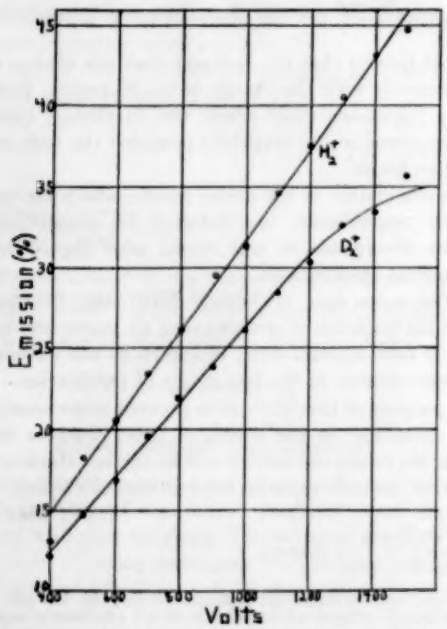

FIG. 1. Relation to energy of secondary electron emission due to H_2^+ and D_2^+ ions.

The increase in the emission over that obtained before, for a Ni surface that is as clean as possible in a hydrogen atmosphere, may be due either to a thin NiO film on the surface or to roughnesses produced by unusual heating of the target in an effort to clean it after its contamination. Güntherschulze and his co-workers[5] report such an increased emission from oxide surfaces over that for pure metals for various metals and gases. Their conclusions were drawn from calorimetric measurements made on the cathode of an anomalous glow discharge.

MONICA HEALEA

Vassar College,
Poughkeepsie, New York,
April 28, 1939.

[1] Monica Healea and E. L. Chaffee, Phys. Rev. **49**, 925 (1936).
[2] A. G. Hill, W. W. Buechner, J. S. Clark and J. B. Fisk, Phys. Rev. **55**, 463 (1939).
[3] W. J. Jackson, Phys. Rev. **28**, 524 (1926); **30**, 473 (1927).
[4] M. L. E. Oliphant, Proc. Roy. Soc. **127**, 373 (1930).
[5] A. Güntherschulze, W. Bär and A. Winter, Zeits. f. Physik 111, 208 (1938).

Interaction of Fast Neutrons with Protons

The interaction of neutrons with protons, as shown by the scattering by protons of neutrons of not too inhomogeneous velocities, has been confined hitherto to neutrons of three Mev or less. We have measured the neutron-carbon and neutron-proton cross sections for higher energies and present here the results of measurements with neutrons of about 15 Mev.

The neutrons from a lithium target bombarded by 0.9-Mev deuterons were all of energies less than 16 Mev (calculated from the mass data of Allison[1]); the threshold of copper, the detector used, is, according to Sagane,[2] between 12 and 13 Mev. Experiments on the angular distribution of the neutrons from the target lead us to believe that the activity of the copper (10.3-minute period) was due predominantly to the neutrons in the higher portions of the 12–16-Mev range.

The scattering was measured by the reduction in intensity of the neutron beam when it traversed paraffin and graphite, cut into truncated cones just large enough to intercept all the neutrons traveling from target to detector. The observed transmissions ranged from 40 to 80 percent, with paraffin 0.54 and 0.84 g/cm² and graphite 0.49 and

0.73 g/cm². The intensity of the neutron beam was calibrated each time by a copper monitor, whose activity was measured with a pressure ionization chamber; the activity of the detector was measured with a Geiger-Mueller counter. No noticeable scattering from the room could be detected.

The results of these measurements were: neutron-carbon cross section 1.13×10^{-24} cm², neutron-proton cross section 0.61×10^{-24} cm².

The theoretical neutron-proton cross section was then evaluated from the phase shifts, according to the theory of Faxen and Holtsmark,[3] with 2.17 Mev for the binding energy of the deuteron, a rectangular well and a range of 2.81×10^{-13} cm. The contribution of the antiparallel spin orientations was calculated with a depth of well 11.7 Mev, obtained by Breit (private communication) from the scattering of slow neutrons. The contribution of the parallel spins was calculated with 20.4 Mev for the depth of the well. The total calculated cross section came out to be 0.61×10^{-24} cm², in satisfactory agreement with the measured value.

The details of these and other measurements will be given later.

E. O. Salant*
R. B. Roberts†
P. Wang‡

Department of Terrestrial Magnetism,
Carnegie Institution of Washington,
Washington, D. C.,
April 25, 1939.

* Washington Square College, New York University.
† Carnegie Institution Fellow.
‡ China Foundation Fellow.

[1] S. K. Allison, Phys. Rev. **55**, 625 (1939).
[2] R. Sagane, Phys. Rev. **53**, 492 (1938).
[3] Faxen and Holtsmark, Zeits. f. Physik **45**, 307 (1927).

Phenomenon of Secondary-Electron Emission

Recently published results on secondary-electron emission indicate that the high secondary-to-primary ratios, δ's, previously reported for electropositive metals are characteristic of contaminated rather than clean surfaces. Bruining and de Boer[1] report that for uncontaminated surfaces the maximum δ is very low while for oxidized surfaces it is very high. Thin oxidized films of Ba and Li on a metal base, for instance, give maximum values of δ of 4.8 and 4.2, respectively.[1]

It has occurred to the writer that the existence of a positive charge in surface films of this type may be an important factor influencing their secondary-electron emission characteristics. A positive charge produced in the insulating layer as a result of the primary-electron bombardment may give rise to an intense electric field through the film. Though the dielectric strength of this type of film is not great enough to support fields of sufficient intensity to give rise to thin-film field emission,[2] it may support fields strong enough to increase materially the probability of escape of the secondary electrons produced within the layer and in the base metal.

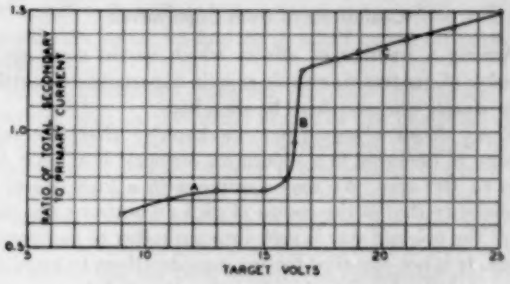

FIG. 1.

In accordance with the hypothesis advanced above, it is to be expected that a curve of δ as a function of primary-electron velocity for the type of surface under consideration should show a definite break in the region of low potentials corresponding to a transformation from negative to positive charge in the insulating film. The film should be negatively charged as long as the δ for its outermost layers remains less than unity and it should become positively charged when this δ becomes greater than unity as the velocity of the primary electrons is increased. When the δ becomes greater than unity, a sudden increase in the secondary emission should result.

An experiment, therefore, was performed to determine δ as a function of the velocity of the primary electrons in the region of low potentials for a film of MgO on Nichrome. The film (about 1000 angstroms thick) was evaporated onto the Nichrome surface in vacuum from a MgO-coated platinum filament. The total secondary emission (true secondaries plus reflected electrons) was determined as a function of the voltage of the MgO-Nichrome target, when the electric field drawing the secondaries from the surface was 100 volts per cm. The curve shows definitely three regions *A*, *B* and *C* corresponding, respectively, to conditions where the charge is negative, where the charge changes from negative to positive, and where the charge is positive and in a state of equilibrium. In regions *A* and *C* the secondary-electron emission remains substantially constant with time while in region *B* it increases with time when readings were taken from low to high potentials and decreases with time when readings were taken in the opposite sense. At the beginning of region *B*, a regenerative action evidently sets in. A positive charge is produced in the outermost layers of molecules which assists the escape of a greater fraction of the secondaries generated within the films, more positive charge is produced, and in turn more secondaries escape, and so on until an equilibrium condition is produced.

At higher voltages, δ varied normally with the potential. A maximum δ of 5.4 was reached at about 400 volts. Neither instability nor thin-film field effects were observed.

Herbert Nelson

Research and Engineering Department,
RCA Manufacturing Company, Inc.,
Harrison, New Jersey,
April 12, 1939.

[1] H. Bruining and J. H. de Boer, Physica **5**, 17 (1938).
[2] L. Malter, Phys. Rev. **50**, 48 (1936).

Cosmic Rays from Supernovae

Among a number of effects which would seem to be capable of generating cosmic rays in supernovae a particularly simple one may here be sketched.

From direct observations we know[1, 2] that the total energy E_t liberated in a supernova outburst is at least 10^{48} ergs to 10^{49} ergs. We may assume with a high degree of probability that in the course of such an outburst the mass M of the original star is split into a number of component parts. It is not essential for our considerations to know the exact details of this fission. For the sake of definiteness we picture M to be divided into a stellar remnant M_1 and an expanding shell of gases of mass M_2, where $M_1+M_2 \leqq M$ and $M_2=\gamma M$ with, presumably, $\gamma \geqslant 10^{-4}$.

Since M is made up of electrically charged particles, the two parts M_1 and M_2 cannot be expected to emerge uncharged from the fission. All distributions of atoms, ions and electrons must be admitted as equally probable, as long as the electric potential energy characteristic for these distributions is small compared with E_t. We set $M=Nm_p$ and $M_1=N_1m_p$ where m_p is the mass of a proton. For simplicity we assume that all of the atoms involved are singly ionized. The numbers of the positively and negatively charged particles in the stellar remnant will be, respectively, $n_1^+=Np_1+\delta_1^+$ and $n_1^-=Np_1+\delta_1^-$ where $Np_1=NM_1/M$ is the most probable value of n_1^+ or n_1^-, and δ_1^+, δ_1^- are the actual deviations in a given distribution. The stellar remnant then carries a total charge $(\delta_1^- - \delta_1^+)e$, where e is the charge of an electron. Setting $\Delta=\delta_1^- - \delta_1^+$ we are consequently interested in the value of Δ^2 averaged over all possible distributions of positively and negatively charged particles e over M_1 and M_2. A simple calculation shows that

$$\langle\Delta^2\rangle_{Av}=4Np_1(1-p_1). \tag{1}$$

The most probable charge on M_1, or on M_2, is therefore

$$\bar{E}=e\langle\Delta^2\rangle_{Av}^{\frac{1}{2}}=2e[Np_1(1-p_1)]^{\frac{1}{2}}, \tag{2}$$

which has its maximum for $p_1=1/2$, $(M_1=M_2)$, namely

$$\bar{E}_{max}=eN^{\frac{1}{2}}. \tag{3}$$

With $\gamma=10^{-4}$ we may expect to get a lower limit for E, namely

$$\bar{E}_{min}=eN^{\frac{1}{2}}/50. \tag{4}$$

If the stellar remnant has a radius R_1, the electric potential between it and the shell of ejected gases is of the order

$$\Phi \geqslant \bar{E}_{min}/R=e(M/m_p)^{\frac{1}{2}}/50R. \tag{5}$$

We write $M=\mu M(\odot)$ and $R=rR(\odot)$, where $M(\odot)=2\times10^{33}$g and $R(\odot)=7\times10^{10}$ cm are the mass and the radius of the sun, and we obtain

$$\Phi=4.7\times10^{8}\mu^{\frac{1}{2}}/r \tag{6}$$

or in volts, for $\mu=1$ and $r=1$

$$\Phi \geqslant 300\times4.7\times10^{8}=1.4\times10^{11} \text{ volts}. \tag{7}$$

The breakdown of these potentials will take place at an advanced stage of the supernova outburst when the expanding gaseous shells are of a density sufficiently low to permit the free escape of the initially trapped excess charges. The total electric potential energy $\bar{E}\Phi/2$ turns out to be very small compared with E_t and our assumption regarding equally probable distributions is therefore justified.

Although considerations of the above type appear sufficient to demonstrate that cosmic-ray particles are generated in supernovae, the fact that $e\Phi/2 \ll E_t$, in combination with previously derived results,[1] indicates that the numbers of cosmic-ray particles produced in this way fall far short from accounting for the total observed intensity of the cosmic rays. The discussion of processes in supernovae which can produce a sufficient number of cosmic-ray particles will be given in a more detailed paper.

F. ZWICKY

Norman Bridge Laboratory of Physics,
California Institute of Technology,
Pasadena, California,
April 27, 1939.

[1] W. Baade and F. Zwicky, Proc. Nat. Acad. Sci. **20**, 254 (1934) and **20**, 259 (1934); Phys. Rev. **46**, 76 (1934).
[2] W. Baade and F. Zwicky, Astrophys. J. **88**, 411 (1938).

On the Structure of Solid Solutions

During the last few years quantitative x-ray investigations of crystals have been carried out at the Physical Institution of the University of Helsingfors, Finland. Certain results have been achieved which are of interest with regard to the present theories for mixed crystals and alloys. A short communication of these results is given below.

We consider a mixed crystal (KCl+KBr). An analysis of the experimental results regarding the intensities of the x-ray reflections from different faces of the crystal shows that the actual mean distances of the ions from the theoretical positions in a face-centered lattice cannot be entirely explained by thermal vibrations. Consequently, the actual positions of equilibrium of the ions do not agree with the theoretical lattice points. The mean square of the displacements of the ions, i.e., of the distances from the actual positions of equilibrium to the theoretical lattice points is greater for K than for Cl and Br. The negative results of similar earlier investigations are easily explained. By means of such more or less qualitative investigations it was indeed impossible to detect the displacements in question.

The experimental results may be explained as follows. The structure of the mixed crystal can be realized through the exchange of Cl and Br ions in an originally completely ordered reference lattice, with alternating Cl and Br ions in the directions of the crystal axes. Because of the differences between the forces K-Cl and K-Br, every such exchange causes a displacement of the surrounding K ions and this displacement is transmitted to all ions in the lattice as a waning long distance disturbance. This long distance disturbance results in a certain average displacement of the ions, the mean square of which may be denoted by $\langle s^2\rangle_{Av}$. However, a K ion is surrounded partly by Cl and partly by Br ions. This asymmetry among the neighbors causes a local displacement, s, of the K ions, which appears also in the completely ordered reference lattice, where $\langle s^2\rangle_{Av}=0$. As regards direction, this local displacement is independent of the long distance disturbance. The total mean square of

the displacement of the K ions is thus $\langle s^2\rangle_{Av}+\langle s^2\rangle_{As}$, the corresponding quantity for Cl and Br ions is only $\langle s^2\rangle_{Av}$.

The indicated microdeformation is of essential importance. A mixed crystal (AB+AC) may be characterized by a certain degree of order. Let the nearest neighbors of the B and C atoms be A atoms. Should an exchange of B and C not cause any displacement of the neighboring A atoms, these A atoms would completely conceal such an exchange from the surroundings. Thereby every correlation between the location of the different B and C atoms in the lattice would disappear. If, on the contrary, a displacement of the surrounding A atoms takes place in consequence of the different "sizes" of the B and C atoms, such a microdeformation would, in the neighborhood of the point under consideration, automatically increase the probability of an exchange contrary to that which has already taken place, thereby provoking a higher or lower degree of order.

Want of knowledge concerning the microdeformation can certainly to some extent be compensated by general assumptions, which implicitly make allowance for the effect of the actual displacements of the atoms. It seems likely however, that such a microdeformation forms the physical background for various assumptions regarding lattice energies, probabilities and ordering forces, which in different papers have been used as the basis for various theories of solid solutions.

J. A. WASASTJERNA

The Physical Institution,
University of Helsingfors,
Finland,
April 20, 1939.

On the Splitting of Heavy Nuclei by Slow Neutrons*

A theory of the disintegrations produced in U and other heavy nuclei by neutron capture by Hahn[1] has been developed by using the "drop" model of the nucleus. According to this model the energy of a heavy nucleus may be considered as due to a *surface energy* $U=\delta A^{\frac{2}{3}}$ ($\delta\sim 9.6$ Mev) and a *volume energy* $E=3(Ze)^2/5r=\epsilon Z^2A^{-\frac{1}{3}}$ because of the Coulomb repulsion of the protons. The radius of the nucleus is related to the value of A by the approximate empirical formula $r\approx 1.4\times 10^{-13}$ cm.

The mutual repulsion between the protons tends to disrupt the nucleus, and this can occur spontaneously as soon as the corresponding increase in the surface energy becomes smaller than the resulting decrease in the electrical volume energy.[2] If the nucleus breaks up into two nuclei corresponding to the values (Z_1, A_1) and (Z_2, A_2), the energy change is

$$\Delta W=E\left[1-\left(\frac{Z_1}{Z}\right)^2\left(\frac{A}{A_1}\right)^{\frac{1}{3}}-\left(\frac{Z_2}{Z}\right)^2\left(\frac{A}{A_2}\right)^{\frac{1}{3}}-\frac{5}{3}\frac{Z_1Z_2}{Z^2}\frac{A^{\frac{1}{3}}}{A_1^{\frac{1}{3}}+A_2^{\frac{1}{3}}}\right]-U\left[\frac{A_1^{\frac{2}{3}}+A_2^{\frac{2}{3}}-A^{\frac{2}{3}}}{A^{\frac{2}{3}}}\right],$$

where the last term in the first bracket represents the Coulomb repulsion of the two resulting nuclei at the separation $r=r_1+r_2$, while $Z=Z_1+Z_2$, $A=A_1+A_2$.

The condition for instability is $\Delta W+\Delta W_1\geqslant 0$ where ΔW_1 is the excitation energy of the nucleus due to the capture of the neutron ($\Delta W_1\approx 8$ Mev). If we omit ΔW_1 and set $Z_1=Z_2=\frac{1}{2}Z$ and $A_1=A_2=\frac{1}{2}A$, for which ΔW has a maximum value, we find $E/U\geqslant 2.17$ as the criterion for instability.

This approximate criterion can also be derived by assuming that in the initial stages of the deviation from the spherical form, the nucleus assumes the form of an ellipsoid or an oblate spheroid. It seems possible that if the ratio E/U is not too large, a stable nonspherical form may be assumed, which proceeds to disrupt into two separate nuclei on increase of this ratio, but a complete proof of this supposition has not been found. The spheroidal and ellipsoidal forms do not appear satisfactory in this respect. If this view should prove correct, the electrical quadrupole moments of the heavier nuclei should be abnormally large.

A theory can also be given of the oscillations which may be set up in the nucleus in the form of surface waves. Such oscillations have been discussed by Bohr on the assumption that they are determined by the surface energy alone, but it is found that actually the electrical volume energy also has an important effect on their behavior. We find for the changes in energy due to the fundamental oscillation

$$\Delta U=2U_0\beta;\quad \Delta E=-E_0\beta,$$

where β is a constant, and U_0, E_0 are the surface and volume energies of the undistorted (spherical) nucleus. Again we find for the criterion of instability $E_0/U_0\geqslant 2$. Instability in the higher types of oscillation requires higher values of this ratio.

This suggests the following three different ways of viewing the explosive rupture process.

(1) The impinging neutron excites the fundamental mode of oscillation of the nucleus, which may be unstable if the ratio E_0/U_0 is sufficiently large, and the nucleus, having started to expand in some direction, may continue to do so until it has completely separated into two nuclei. From this point of view the process is purely "classical," either not occurring at all, or taking place immediately after the capture of the neutron.

(2) A somewhat different possibility consists in assuming the existence of an "activation energy" preventing the immediate rupture even when possible from the energy balance. Rupture would then be impossible on classical theory, but might occur by a quantum-mechanical "tunnel-effect."

(3) If the mean life of the excited nucleus with respect to explosive rupture is large compared with the "relaxation-time" during which the excitation energy is distributed over the different degrees of freedom of the nucleus, then the surface energy might decrease with the excitation energy. Such a decrease might lead to explosive rupture in the absence of an excitation energy.

J. FRENKEL

Industrial Institute,
Leningrad, U.S.S.R.,
March 12, 1939.

* A more complete exposition of the theory will be published in the new journal "Annales Physical, etc." (Russian). The theory was practically completed before the considerations of Bohr were known to the author. (The present letter is an abstract of the manuscript, made at the author's request by E. Hill.)

[1] O. Hahn and F. Strassmann, Naturwiss. **27**, 11 (1939); L. Meitner and O. R. Frisch, Nature **143**, 471 (1939); N. Bohr, Phys. Rev. **55**, 419 (1939).

[2] Similar considerations have been advanced by E. Feenberg, Phys. Rev. **55**, 504 (1939). (Note added by E. H.)

Angle Dependence and Range of Nuclear Forces

The discovery[1] of the electric quadrupole moment of the deuteron has indicated that the specific nuclear interaction between neutrons and protons must contain a considerable angle-dependent term coupling spin and orbit[2] (as suggested by the meson theory), so as to make the ground state of the deuteron a mixture of $^3S_1$ and $^3D_1$. Without this new term, the ground state would be an S state, and the D states would lie in the continuum. The admixture of D to S depresses the final state below the original S state,[3] down to the observed level $-\epsilon=-4.1mc^2$. The spherically symmetric terms (principally the space-exchange term suggested by Majorana) will thus have to account for less deuteron binding than previously. The range of nuclear forces has been determined mainly by the necessity of reconciling the small deuteron binding with the much greater alpha-binding, Wigner having showed that a short range and great depth of interaction favor the stability of the alpha-particle.[4] The angle-dependent term would probably cause comparatively little admixture of higher states (mainly $^3P_0$) to the very deep $^1S_0$ in the ground state of the alpha-particle, because of its isolation so we may tentatively assume that the spherically symmetric terms account for practically all of the alpha-binding. If they are to account for a smaller deuteron binding than previously, we are even more dependent on Wigner's device and require a still shorter range of the forces. Since analysis[5] of the new and rather extensive proton-proton scattering data shows that the earlier determination of the range[6] was correct for the like-particle interactions, a considerably reduced range may well be assumed only for the different-particle interactions.

How much the range might be reduced depends on what part ($\delta\epsilon$) of the deuteron binding (ϵ) is due to D admixture. It would be simplest to assume that the $^3S_1$ and $^1S_0$ are originally degenerate at about zero energy, and that their entire separation (ϵ) is due to D admixture, or $\delta\epsilon\approx\epsilon$, for one could thus completely eliminate the space-spin-exchange and the spin-exchange terms suggested by Heisenberg and by Bartlett.[2] Writing the wave function of the ground state as $\psi_0=(\psi_S+c\psi_D)/(1+c^2)$ and taking a rough average energy $\bar{E}$ of the admixed D states, one has by perturbation theory $\delta\epsilon\approx c^2\bar{E}$. If $\bar{E}$ were about $20mc^2$ or less, as seems consistent with recent computations of Christy and Kusaka,[7] a value $c^2\approx\frac{1}{2}$ or more would be required to make $\delta\epsilon\approx\epsilon$.

For the quadrupole moment $Q=(3\cos^2\theta-1)r^2$ of the proton (about the center of mass of the deuteron) we may write

$$(O|Q|O)=\{2c(D|Q|S)+c^2(D|Q|D)\}/(1+c^2)\approx-0.02(O|r^2|O)$$

the latter experimentally,[1] taking $(O|r^2|O)\approx10^{-25}$ cm. Without calculation based on further specification of the forces, it may at least be considered plausible that the diagonal matrix element $(D|Q|D)$ is larger than the nondiagonal element $(D|Q|S)$, and that neither is much smaller than $(O|r^2|O)$ in order of magnitude. The coefficient c is then approximately either $-0.01(O|r^2|O)/(D|Q|S)$ or $-2(D|Q|S)/(D|Q|D)$. The first root is probably too small, but the second quite large enough to be compatible with putting $\delta\epsilon\approx\epsilon$.

For the magnetic moment corresponding to ψ_0 we may write

$$\{\mu_S+(3\mu_N-2\mu_S)c^2/4\}/(1+c^2)\approx0.85\mu_N,$$

where the latter member is experimental, μ_N is the nuclear magneton and μ_S the sum of the neutron and proton spin moments.[2] For simplicity in a field theory of the forces and spin moments,[8] one would like to have μ_S about equal to or slightly less than μ_N, which implies $c^2\approx\frac{1}{2}$. This also agrees with the possibility that $\delta\epsilon\approx\epsilon$.

To estimate the possible change of range, we therefore assume that the interaction responsible for the alpha-binding gives no deuteron binding. Writing this interaction $J_d=-B_d\exp(-\alpha_d r^2)P^q$ between different particles (proton and neutron), where P^q indicates space exchange, and similarly J_l between like particles, which should also give rise to a state near zero, we then have approximately[9]

$$B_i=2.7\alpha_i, \qquad i=d,\ l.$$

The binding energy of the alpha-particle is[6]

$$E_{\mathrm{He}^4}=(9/4)\alpha_d\sigma-4B_d[\sigma/(\sigma+2)]^{\frac{3}{2}}-2B_l[\sigma/(\sigma+2\alpha_l/\alpha_d)]^{\frac{3}{2}}$$

(in the units of references 6 and 9, neglecting Coulomb energy and the second-order corrections to the central model, which are almost equally small and of opposite sign,[6] even if $\alpha_l\ll\alpha_d$), minimized by variation of σ. Eliminating the B_i,

$$E_{\mathrm{He}^4}/\alpha_d=(9/4)\sigma-10.8[\sigma/(\sigma+2)]^{\frac{3}{2}}-5.4(\alpha_l/\alpha_d)[\sigma/(\sigma+2\alpha_l/\alpha_d)]^{\frac{3}{2}}.$$

If we assume a symmetrical interaction with $\alpha_l=\alpha_d=\alpha$, this has a minimum -1.23 at $\sigma=1.9$. Since E_{He^4} is -55 in units mc^2, we have $\alpha=55/1.23=45$, about twice as large as in previous theory. The range is thus reduced by a factor $2^{-\frac{1}{3}}$, to a value $\alpha^{-\frac{1}{2}}=0.15\hbar/[(mM)^{\frac{1}{2}}c]=0.48e^2/mc^2=1.35\times10^{-13}$ cm. If, instead, we assume $\alpha_l=22$, as determined by proton-proton scattering,[5] we find that the value $\alpha_d\approx130$ gives the correct minimum energy (at $\sigma\approx1.0$). This corresponds to a proton-neutron range of 0.8×10^{-13} cm. The range is thus so sensitive to $\delta\epsilon$ that range measurements may help to delimit the possible spin and angle dependence of the interactions.

D. R. Inglis

Rowland Physical Laboratory,
The Johns Hopkins University,
Baltimore, Maryland,
April 22, 1939.

[1] J. M. B. Kellogg, I. I. Rabi, N. F. Ramsey and J. R. Zacharias, Phys. Rev. **55**, 318 (1939).
[2] J. Schwinger, Phys. Rev. **55**, 235 (1939).
[3] As kindly mentioned in conversation by Professors Teller and Bethe.
[4] E. Wigner, Phys. Rev. **48**, 252 (1933).
[5] G. Breit, H. M. Thaxton and L. Eisenbud, Phys. Rev. **55**, 603 (1939), based on data of Tuve, Heydenberg, Hafstad; Herb, Kerst, Parkinson and Plain.
[6] D. R. Inglis, Phys. Rev. **51**, 531 (1937), Eqs. (19) and (11).
[7] R. F. Christy and S. Kusaka, Phys. Rev. **55**, 665 (1939). We see that $(O|Q|O)\ll(O|r^2|O)$ does not necessarily justify perturbation methods.
[8] G. C. Wick, Acad. Lincei **21**, 170 (1935); W. E. Lamb and L. I. Schiff, Phys. Rev. **53**, 651 (1938).
[9] E. Feenberg and S. S. Share, Phys. Rev. **50**, 253 (1936), footnote 12.

Penetrating Beta-Particles from Uranium Activated by Neutrons

We have looked for penetrating beta-rays and hard gamma-rays coming from U after irradiation by fast neutrons (~3 Mev) from a D−D source, using two counters with a circuit for recording coincidences. The two glass-walled counters were placed horizontally side by side with a 2-mm layer of uranium oxide beside each counter, all as close to the target as possible (~5 cm from target to center of U). A beam of D^+ ions of 40 μA at 350 kv was run onto a target of frozen D_2O. This is known to give about $1.4 \cdot 10^8$ neutrons per sec. (~7 g Ra-Be equivalent). The geometry of the arrangement did not permit the effective use of paraffin.

The number of coincidences was reducible to practically zero by the introduction of 5.2 mm of Al between the U and the counters, showing the activity observed to be attributable to primary beta-rays rather than to secondary particles ejected by hard gamma-rays. Some coincidences were found with 3.9 mm of Al between the U and the counters, the particles having had to penetrate 3.9 mm of Al, 3.6 mm of glass, and 0.12 mm of Cu, thus having had an energy greater than 4.2 Mev. The following measurements of half-lives were made with 1.3 mm of Al between the U and the counters (for keeping out UX_2 beta-rays) and are attributable to particles of energy above 2.9 Mev. Check experiments of two sorts showed the coincidences to be genuine ones, not chance ones resulting from high initial counting rates.

The coincidences were photographically recorded by an oscillograph after stopping the bombardment. Only about 100 counts were found in each run, so it was necessary to repeat the experiment many times. From the record was found the count for each interval of 4 cm (1.93 sec.). The totalled results of 47 such experiments for which the time of bombardment was 5 sec. are shown at A in the accompanying figure. The straight line A', giving the best fit to the later points (averages of 3) corresponds to a half-life of 12.8 sec. The points at B give the differences between the original points and A', the line at B giving a half-life of 3.5 sec. The high value for the first point suggested the presence of an activity of still shorter half-life. Accordingly, the films were re-studied, and the number of counts for each 1-cm interval (0.48 sec.) tabulated. The results are plotted at C after taking off the 13-sec. activity, the line having the slope determined at B (changed scale of abscissae). The circled points show the averages of the neighboring four points. Again taking differences one gets the points at D. The line drawn here corresponds to a half-life of 0.6 sec. It is impossible, of course, to determine accurate values of half-lives from such meager data. Nevertheless, it is fairly certain that at least three must be present, and that the values obtained are of the right order of magnitude. The three half-lives may be given as 11–15 sec., 3.0–4.0 sec., 0.3–0.9 sec. The calculated values of the activities for equilibrium are roughly equal for all three half-lives.

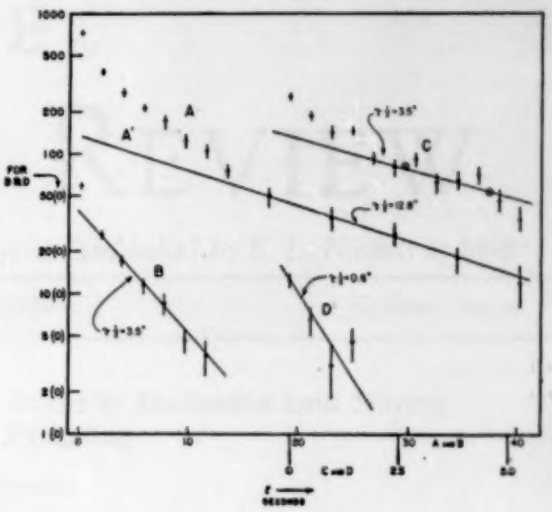

FIG. 1.

Runs made with bombardments of 30 sec. show an increase of the initial activity of the longer period consistent with the above half-lives. With bombardments of 90 sec. a larger apparent value for the longer half-life was obtained, indicating the presence of another activity of still longer half-life, making it probable that the value of 11–15 sec. is too large. It is of interest that our two longer half-lives are nearly the same as those reported for the delayed emission of neutrons.

We also looked for coincidences while the beam was running. Coincidences from beta-rays having an energy >3.3 Mev were found, but the introduction of more Al cut the number down to one inappreciably different from a high background. This result merely shows the absence of very penetrating beta-rays in any quantity comparable with that of these slower ones.

It is a pleasure to acknowledge our indebtedness to Professor Niels Bohr for stimulating discussions which led us to undertake this work, and for many subsequent ones.

This work was done with the high voltage equipment which was purchased with the aid of a grant from the Rockefeller Institute to Professor Ladenburg.

H. H. BARSCHALL
W. T. HARRIS
M. H. KANNER
LOUIS A. TURNER

Palmer Physical Laboratory,
Princeton University,
Princeton, New Jersey,
April 26, 1939.